



# THE UNIVERSITY *of* EDINBURGH

This thesis has been submitted in fulfilment of the requirements for a postgraduate degree (e.g. PhD, MPhil, DClinPsychol) at the University of Edinburgh. Please note the following terms and conditions of use:

This work is protected by copyright and other intellectual property rights, which are retained by the thesis author, unless otherwise stated.

A copy can be downloaded for personal non-commercial research or study, without prior permission or charge.

This thesis cannot be reproduced or quoted extensively from without first obtaining permission in writing from the author.

The content must not be changed in any way or sold commercially in any format or medium without the formal permission of the author.

When referring to this work, full bibliographic details including the author, title, awarding institution and date of the thesis must be given.

**Molecular mechanisms  
underlying Retinitis pigmentosa  
type 2**

**Rodanthi Lyraki**

**Thesis submitted for the degree of Doctor of Philosophy**

**University of Edinburgh**

**2017**

## **Declaration**

I declare that this thesis is my own work, and that the experiments described here were conducted by me except where explicitly stated. This work has not been submitted for any other degree or professional qualification.

Rodanthi Lyraki, August 2017

## **Preface**

*“Photoreceptors sit on a knife edge separating function and survival from dysfunction and death, and almost any defect seems capable of tipping them towards cell death.”*

- Alan F. Wright et al., *“Photoreceptor degeneration: genetic and mechanistic dissection of a complex trait”*

## Acknowledgements

I feel very fortunate to have carried out my PhD in the Institute of Genetics and Molecular Medicine in Edinburgh, where I had the opportunity to interact with first-class scientists on a daily basis. First of all, I would like to thank my supervisor Toby Hurd who welcomed me in his team, entrusted me with such an interesting project and always considered all my ideas and suggestions carefully. I am also grateful to Ian Jackson, Elizabeth Patton and Pleasantine Mill, together with all their group members. Their valuable suggestions and criticisms during lab and committee meetings have decisively helped to shape my thesis.

The work presented here would not be possible without the contribution of our collaborators Dinesh Soares and Jimi Wills who laid the foundations for my subsequent analysis. Dinesh conducted all the structural and biophysical analyses which guided the identification of the RP2-OSTF1 interaction interface, and Jimi carried out all the mass spectrometry experiments which are mentioned at several points during my thesis. I would also like to thank Wei Qing and Witek Rybski for contributing to the generation of *rp2* null zebrafish by helping with zebrafish husbandry and embryo injections.

Thanks to my co-workers Matthieu Vermeren, Abigail Little and Eliza Parish, the friendly faces of the nearby benches, for always being happy to provide a protocol or help each other out in the lab.

I owe special thanks to brilliant budding scientists and close friends, the dream team: Nwamaka Idigo, Jilly Hope, Marion Bonneau and Elena Pérez, for their support. I will miss our endless conversations contemplating life choices and trying to figure out why the fish don't lay eggs and why there are so many unspecific bands in our western blots. Moreover, I would like to thank Mina Pantazi for being my flatmate and friend and a source of continuous encouragement.

Although working towards a PhD degree can be hard at times, having my partner Georgios Koutsovoulos by my side made my journey much easier and more fun. I owe a big thank you to Georgios who not only cared enough for me to listen to my

endless lab stories but also substantially contributed to this thesis by proofreading my drafts and helping with proteomic analysis.

I will always be grateful to my family, especially my parents Eleni and Costis and my sister Maria, for their unconditional love and support of all my choices. Moreover, I would like to mention my grandma Maria, who once taught me, without realising it, the number one rule of a wet lab scientist: if you fail, just try again!

## Lay summary

Diseases of the retina, the layer of the human eye which is responsible for detecting light and relaying that signal to the brain, are a leading cause of blindness, especially in younger ages. One such disease, called “Retinitis pigmentosa” (RP), is characterised by the death of the light-detecting cells, the photoreceptors. The cause of RP is exclusively genetic, meaning that it is caused by DNA alterations that run in families and not environmental or external factors. One subtype of RP (type 2) is known to be caused by alterations in the DNA region which contains instructions for the production of a protein molecule called RP2. Currently, there is no therapy for RP; it is, therefore, important to understand why the function of RP2 in the retina is so crucial that photoreceptors die when it is lost, as this will lead to the identification of more effective treatments. The present thesis reports novel information on how RP2 interacts with other protein molecules in cells and how its activity might be regulated. In particular, molecular biology techniques have been used to show that RP2 forms a complex with other proteins that participate in fundamental cellular processes like cell movement and repair of DNA damage. Moreover, this project has led to the identification of two sites on RP2 where a phosphate group might be added to control the protein’s activity. Finally, a major goal in disease research is finding animal models which can be used to screen and test potential therapies, as it is not possible to perform these procedures directly on human patients. To this end, a novel genome manipulation technique has been used to generate zebrafish with targeted DNA alterations in the region responsible for producing the zebrafish version of RP2. The presence of retinal degeneration has been shown by histological examination in one of these fish lines that lack RP2 function. Overall, this thesis provides new data that expand the knowledge on the molecular mechanisms that cause inherited blindness.

## Abstract

The term “Retinitis pigmentosa” (RP) represents a group of inherited, late-onset diseases characterised by progressive retinal degeneration due to photoreceptor death. Mutations in the *RP2* gene are found in 7-18% of patients with X-linked RP, one of the most severe forms. The *RP2* gene product is a membrane-associated protein which encompasses two distinct domains. The N-terminal domain is well characterised as possessing GTPase-activating protein (GAP) activity towards the small GTPase ARL3 and thus regulate the transport of lipid-modified proteins within the photoreceptor cell. However, it is not known if the loss of this particular function of RP2 is the sole reason that causes the disease, while the role of the protein’s C-terminus remains unknown. This thesis focuses on the characterisation of two novel protein-protein interactions of RP2 with the aim to investigate novel roles of the protein. Firstly, evidence is provided that a highly-conserved cluster of RP2 residues that span both the N- and C-terminus participate in direct interaction with Osteoclast-stimulating factor 1 (OSTF1). Two hypotheses are explored about the potential role of the complex in SRC-mediated RP2 phosphorylation and the regulation of cell motility. Secondly, the catalytic subunit of DNA-dependent protein kinase (DNA PK) is identified as a novel interaction partner of RP2 in cultured cells. The two proteins are shown to co-localise in the nuclear and membrane compartments of a retinal-derived cell line and might engage in a kinase-substrate relationship. So far, no evidence was found that RP2 participates in the canonical function of DNA PK which is the regulation of DNA double-stranded breaks. Finally, the CRISPR/Cas9 genome editing method was applied on zebrafish embryos to generate a novel vertebrate animal model for the loss of RP2 function. One out of three different zebrafish lines with *rp2* mutations was shown by histology to have mild late-onset thinning of the photoreceptor outer segments. The present thesis reports previously unexplored aspects of RP2’s function and will, therefore, contribute to understanding the molecular mechanisms that underlie RP. Moreover, this thesis will contribute to the discussion about the usefulness of zebrafish as an RP model.



# Table of Contents

<b>Declaration</b> .....	<b>ii</b>
<b>Preface</b> .....	<b>iii</b>
<b>Acknowledgements</b> .....	<b>iv</b>
<b>Lay summary</b> .....	<b>vi</b>
<b>Abstract</b> .....	<b>vii</b>
<b>List of figures</b> .....	<b>xi</b>
<b>List of tables</b> .....	<b>xiv</b>
<b>Abbreviations</b> .....	<b>xv</b>
<b>Chapter 1. Introduction</b> .....	<b>1</b>
<b>1.1 General principles of photoreceptor structure and function</b> .....	<b>1</b>
<b>1.2 Retinitis pigmentosa and other forms of inherited retinal degeneration</b> .....	<b>4</b>
1.2.1 Molecular genetics and pathways leading to photoreceptor death in RP .....	8
1.2.2 X-linked RP .....	12
<b>1.3 Functional significance of RP2 in the retina</b> .....	<b>15</b>
1.3.1 The RP2 protein .....	15
1.3.2 Suggested roles of the RP2-ARL3 complex in protein trafficking within the photoreceptors .....	16
1.3.3 Mouse models of RP type 2.....	18
1.3.4 Alternative roles of RP2 .....	20
<b>1.4 Questions and aims of the thesis</b> .....	<b>22</b>
<b>Chapter 2: Materials and methods</b> .....	<b>24</b>
<b>2.1 DNA methods</b> .....	<b>24</b>
2.1.1 Agarose gel electrophoresis .....	24
2.1.2 PCR .....	24
2.1.3 Plasmid isolation from bacterial cultures.....	25
2.1.4 Genomic DNA isolation from zebrafish embryos and adult fish.....	26
2.1.5 DNA sequencing .....	26
2.1.6 Site-directional mutagenesis .....	26
2.1.7 Insertion of constructs into expression vectors by recombination .....	27
2.1.8 Other cloning strategies .....	27

<b>2.2 RNA methods .....</b>	<b>29</b>
2.2.1 Isolation of total RNA from human cells.....	29
2.2.2 Isolation of total RNA from zebrafish embryos.....	30
2.2.3 Quantification of nucleic acid concentration and estimation of quality .....	30
2.2.4 cDNA synthesis.....	30
2.2.5 Reverse transcription quantitative real-time PCR (RT-qPCR) .....	31
2.2.6 <i>In vitro</i> transcription.....	32
<b>2.3 Protein and Proteomics methods .....</b>	<b>41</b>
2.3.1 Protein isolation from human cells, zebrafish and mouse tissues .....	41
2.3.2 Quantification of protein concentration.....	43
2.3.3 Protein separation by SDS-PAGE.....	43
2.3.4 Western blotting .....	44
2.3.5 Stripping membranes.....	48
2.3.6 Production and purification of recombinant proteins .....	48
2.3.7 Kinase assays .....	50
2.3.8 Immunoprecipitations.....	50
2.3.9 Pulldown assays .....	51
2.3.10 Mass spectrometry.....	52
2.3.11 Fractionations.....	53
<b>2.4 Mammalian tissue culture.....</b>	<b>54</b>
2.4.1 Cell culture.....	54
2.4.2 Transient transfections.....	55
2.4.3 Growth curves.....	55
2.4.4 Cell motility experiments .....	56
2.4.5 Immunofluorescence .....	57
<b>2.5 Animal methods.....</b>	<b>57</b>
2.5.1 Fish husbandry .....	57
2.5.2 Generation of zebrafish mutant lines by CRISPR/Cas9 .....	58
2.5.3 Histology of retinal sections .....	59
<b>2.6 Databases, online resources, 3D protein analysis and statistics .....</b>	<b>61</b>
<b>Chapter 3: Characterisation of the interaction between RP2 and OSTF1.....</b>	<b>63</b>
<b>3.1 Introduction.....</b>	<b>63</b>
<b>3.2 Results.....</b>	<b>68</b>
3.2.1 OSTF1 binds a strictly conserved area on RP2 spanning both the N-terminal and C-terminal domains.....	68

3.2.2 Investigation of RP2 tyrosine phosphorylation and the potential role of OSTF1	73
3.2.2.1 c-SRC potentially phosphorylates RP2 on Y27	74
3.2.2.2 Overexpression of c-SRC does not markedly affect binding of RP2 to its interaction partners	84
3.2.2.3 Total tyrosine phosphorylation of RP2 is not due to OSTF1-mediated phosphorylation by c-SRC	86
3.2.3 RPE1 cells lacking RP2 expression are less motile	90
<b>3.3 Discussion</b>	<b>97</b>
3.3.1 Mapping the OSTF1 interaction interface on RP2: conclusions	97
3.3.2. RP2 tyrosine phosphorylation analysis: conclusions	98
3.3.3 A potential role for RP2 in cell motility regulation	100
3.3.4 A potential role for RP2 in cell death	103
<b>Chapter 4: Characterisation of the interaction between RP2 and DNA PKcs and implications for DNA damage repair in the retina</b>	<b>104</b>
<b>4.1 Introduction</b>	<b>104</b>
4.1.1 The importance of DDR mechanisms for retinal development and viability	104
4.1.2 DNA PKcs is a multi-functional kinase	106
<b>4.2 Results</b>	<b>115</b>
4.2.1 RP2 co-precipitates with DNA PKcs from HEK293T cells	115
4.2.2 Plasma membrane localisation of RP2 might be important for its interaction with DNA PKcs	118
4.2.3 RP2 is a novel substrate of DNA PKcs <i>in vitro</i>	127
4.2.4 <i>RP2</i> null cells respond normally to DNA damage with respect to H2AX activation	135
<b>4.3 Discussion</b>	<b>139</b>
4.3.1 Characterisation of the RP2-DNA PKcs interaction	139
4.3.2 Potential roles of the RP2-DNA PKcs complex	141
4.3.3 Conclusions and future directions	142
<b>Chapter 5: Generation of a zebrafish model for the genetic loss-of-function of <i>rp2</i> and examination of its effect on retinal lamination</b>	<b>143</b>
<b>5.1 Introduction</b>	<b>143</b>
5.1.1 The use of zebrafish in retinal research	143
5.1.2 Zebrafish <i>Rp2</i>	145
<b>5.2 Results</b>	<b>146</b>
5.2.1 Generation of <i>rp2</i> null zebrafish lines via the CRISPR/Cas9 method	146

5.2.2	Characterisation of retinal structure in adult <i>rp2</i> mutant fish by histology .....	152
5.2.3	Generation of <i>rp2</i> knockout/eGFP knock-in zebrafish model .....	161
<b>5.3</b>	<b>Discussion .....</b>	<b>163</b>
5.3.1	The discrepancy between gene editing approaches for targeting <i>rp2</i> in zebrafish and morpholino-mediated knockdown.....	163
5.3.2	Comparing the phenotype of adult zebrafish <i>rp2</i> mutants to other reported animal models of RP2 disease .....	165
5.3.3	Potential use of <i>rp2</i> null embryos for studying the role of Rp2 in DNA damage repair .....	167
<b>Chapter 6.</b>	<b>Conclusions and future directions .....</b>	<b>169</b>
<b>6.1</b>	<b>The importance of basic research for the identification of novel therapies for RP .....</b>	<b>169</b>
<b>6.2</b>	<b>Studying the RP2-OSTF1 interaction: future directions .....</b>	<b>171</b>
<b>6.3</b>	<b>A potential role of DNA damage-associated signalling in RP type 2: future directions .....</b>	<b>172</b>
<b>6.4</b>	<b>Convergence of the OSTF1- and DNA PKcs-associated pathways.....</b>	<b>175</b>
<b>6.5</b>	<b><i>rp2</i> null zebrafish as models of retinal degeneration .....</b>	<b>175</b>
<b>6.6</b>	<b>Final remark.....</b>	<b>178</b>
<b>Appendix</b>	<b>.....</b>	<b>181</b>
<b>References</b>	<b>.....</b>	<b>192</b>

## List of figures

Figure 1.1	Basic organisation of the human retina and hallmarks of disease (A-C). Crystal structure of human RP2 (D).....	7
Figure 1.2.	A schematic summary of the suggested roles of RP2 and ARL3 in the cell (numbers 1-4) and their localisation. ....	22
Figure 3.1.	Background information on OSTF1 and its identification as a binding partner of RP2. ....	68
Figure 3.2 .	Mapping the interaction interface between RP2 and OSTF1 on a conserved patch on RP2.....	72
Figure 3.3.	RP2 is phosphorylated by c-SRC in vitro.....	76

Figure 3.4. <b>Overexpression of c-SRC results in tyrosine phosphorylation of RP2 in HEK293T cells.</b> .....	77
Figure 3.5. <b>Y27 is a potential phosphorylation site on RP2, but is not the only site of endogenous phosphorylation in HEK293T cells.</b> .....	81
Figure 3.6. <b>Tyrosine residues on RP2 that are good candidates for phosphorylation.</b> .....	83
Figure 3.7. <b>Overexpression of c-SRC mildly stabilises the binding of RP2 to ARL3.</b> .....	85
Figure 3.8. <b>Binding to OSTF1 is not essential for the endogenous phosphorylation of RP2 in HEK293T cells.</b> .....	87
Figure 3.9. <b>Phosphorylation of RP2-V5 in HEK293T cells is not dependent on endogenous c-SRC activity.</b> .....	89
Figure 3.10. <b>G and I CRISPR clones lack RP2 expression but this is not responsible for the growth defect observed in clone G.</b> .....	93
Figure 3.11. <b>RP2 knockout leads to migration defects in RPE1 cells.</b> .....	96
Figure 4.1. <b>Protein structure of DNA PKcs and schematic overview of NHEJ.</b>	111
Figure 4.2. <b>RP2 interacts with DNA PKcs.</b> .....	117
Figure 4.3. <b>Membrane localisation of RP2 might be important for the interaction with DNA PKcs.</b> .....	121
Figure 4.4. <b>RP2 and DNA PKcs co-localise at the nuclear and the membrane compartments of RPE1 cells: fractionation method 1.</b> .....	125
Figure 4.5. <b>RP2 and DNA PKcs co-localise at the nuclear and the membrane compartments of RPE1 cells: fractionation method 2.</b> .....	126
Figure 4.6. <b>Threonine phosphorylation of RP2 at the DNA PK consensus motif might disrupt binding to ARL3, but could not be detected after DDR induction.</b> .....	130
Figure 4.7. <b>RP2 is a potential substrate for DNA PKcs-mediated phosphorylation in vitro.</b> .....	134
Figure 4.8. <b>RP2 knockout does not result in defects in H2AX activation and repair of double stranded breaks induced by X-rays.</b> .....	138

Figure 5.1. <b>Ensembl annotation of the rp2 gene in zebrafish and the position of CRISPR- induced mutations.</b> .....	150
Figure 5.2. <b>Induction of deleterious mutations in the zebrafish rp2 gene.</b> .....	151
Figure 5.3. <b>Ins1 homozygous fish show mild thinning of the photoreceptor layer compared to their wild-type siblings at 9 months.</b> .....	154
Figure 5.4. <b>Del8 homozygous fish show very mild thinning of the photoreceptor layer compared to their wild-type siblings at 9 months.</b> .....	156
Figure 5.5. <b>Del8 homozygous fish show only very mild thinning of the photoreceptor layer compared to their wild-type siblings at 12 months...</b>	158
Figure 5.6. <b>Del4 homozygous fish do not show thinning of the photoreceptor layer compared to their wild-type siblings at 7 months.</b> .....	161
Figure 5.7. <b>Description of the experimental design for the generation of an rp2 knockout/eGFP knock-in zebrafish model.</b> .....	163
Figure 6.1. <b>Schematic representation of suggested roles for the RP2-OSTF1 and RP2-DNA PKcs interactions.</b> .....	179
Appendix figure 1. <b>Multiple sequence alignment of RP2 vertebrate orthologues.</b> .....	181
Appendix figure 2. <b>Peptide coverage of RP2 in MS/MS analysis used to identify sites of tyrosine phosphorylation.</b> .....	182
Appendix figure 3. <b>Expression pattern of RP2 and OSTF1 in the mouse central nervous system by western blot.</b> .....	183
Appendix figure 4. <b>RP2 null cells do not have altered reactive oxygen species (ROS) balance compared to wild-type cells in culture.</b> .....	184
Appendix figure 5. <b>Multiple sequence alignment of human, zebrafish wild-type and zebrafish mutant RP2.</b> .....	185
Appendix figure 6. <b>Agarose gel and Sanger sequencing-based analysis of products and templates of qRT-PCR experiments conducted in order to detect zebrafish rp2 transcript levels.</b> .....	186
Appendix figure 7. <b>Western blotting detection of exogenously expressed zebrafish Rp2-GFP by the anti-RP2 antibody used in Chapter 6.</b> .....	187

## List of tables

Table 2.1. <b>List of primers and oligonucleotides used for the generation of an rp2 null zebrafish model by CRISPR/Cas9 (Chapter 5).</b> .....	35
Table 2.2. <b>List of primers used in the RP2 site-directed mutagenesis experiments (Chapters 3 and 4).</b> .....	37
Table 2.3. <b>List of primers used in real-time qPCR experiments (Chapters 3 and 5).</b> .....	40
Table 2.4. <b>List of buffers that were used for protein isolation.</b> .....	42
Table 2.5. <b>List of antibodies or antibody-conjugated resins.</b> .....	46
Table 3.1. <b>Several missense RP2 mutations found in patients do not affect the stability of the protein or the RP2/ARL3 interaction.</b> .....	66
Table 3.2. <b>Deleterious mutations in the RP2 gene found in the RPE1 clones that are used in this study.</b> .....	92
Table 4.1. <b>A role has been identified for DNA PKcs in most DNA repair pathways</b> .....	112
Appendix Table 1. <b>List of proteins identified by MS/MS in RP2-V5 IPs.</b> .....	188

## Abbreviations

ABCA4: ATP-binding cassette, sub-family A, member 4

AMD: Age-related macular degeneration

APLF: Aprataxin And PNKP-Like Factor

ARF: ADP ribosylation factor

ARL: ARF-like

ATM: Ataxia-telangiectasia mutated

ATP: Adenosine triphosphate

ATR: ATM- and Rad3- related

BB: Basal body

BER: Base excision repair

bp: Base-pairs

BrdU: 5-bromo-2-deoxyuridine

BSA: Bovine serum albumin

CC: Connecting cilium

cGMP: Cyclic guanosine monophosphate

CRISPR: Clustered regularly interspaced palindromic repeats

DAPI: 4', 6-diamino-2-phenylindole

DDR: DNA damage response

DHA: Docosahexanoic acid

DMSO: Dimethylsulfoxide

DNA: Deoxyribonucleic acid

DNA PKcs: DNA-dependent protein kinase, catalytic subunit

Dpf: Days post-fertilisation

DSB: Double-stranded break

DTT: Dithiothreitol

ECL: Enhanced chemiluminescent substrate

EDTA: Ethylene diamine tetra acetic acid

EGFR: Epidermal growth factor receptor

EGTA: Ethylene glycol tetra acetic acid

ER: Endoplasmic reticulum

ERG: Electroretinogram



ERK: Extracellular signal-regulated kinase  
ESC: Embryonic stem cell  
FANC: Fanconi anaemia  
FPR: False-positive rate  
FRET: Fluorescence resonance energy transfer  
GAP: GTPase-activating protein  
GAPDH: Glyceraldehyde 3-phosphate dehydrogenase  
GCL: Ganglion cell layer  
GDP: Guanosine diphosphate  
GEF: Guanine nucleotide exchange factor  
GFP: Green fluorescent protein  
GOLPH3: Golgi phosphoprotein 3  
GRK1: G protein-coupled receptor kinase 1  
GST: Glutathione-S-transferase  
GTP: Guanosine triphosphate  
H2B: Histone 2B  
H&E: Haematoxylin & Eosin  
HEAT: Huntingtin, Elongation factor 3, regulatory subunit A of PP2A, TOR1  
HEK: Human embryonic kidney  
Hpf: hours post-fertilisation  
HR: Homologous recombination  
HRP: Horseradish peroxidase  
HSP90: Heat-shock protein 90  
IF: Immunofluorescence  
IFT: Intraflagellar transport  
INL: Inner nuclear layer  
IP: Immunoprecipitation  
IPL: Inner plexiform layer  
iPSC: Induced pluripotent stem cell  
IPTG: Isopropyl  $\beta$ -D-1-thiogalactopyranoside  
IR: Ionising radiation  
IRD: Inherited retinal degeneration

IS: Inner segment  
KIF: Kinesin family member  
LCA: Leber's congenital amaurosis  
LFQ: Label-free quantification  
MAP: Microtubule-associated protein  
MERTK: MER proto-oncogene tyrosine protein kinase  
MMR: Mismatch repair  
MRN: Mre11, Rad50 and Nbs1 complex  
mRNA: Messenger RNA  
MS: Mass spectrometry  
MS/MS: Tandem mass spectrometry  
mTOR: Mechanistic target of rapamycin  
MYO1E: Myosin 1E  
NDK: Nucleoside diphosphate kinase  
NER, gg/tc: Nucleotide excision repair, global genomic / transcription-coupled  
NFkB: Nuclear factor kappa B  
NHEJ: Non-homologous end joining  
NPHP: Nephronophthisis  
OCDL: Oxidative clustered DNA lesion  
ONL: Outer nuclear layer  
OPL: Outer plexiform layer  
OS: Outer segment  
OSTF1: Osteoclast-stimulating factor 1  
PBS: Phosphate buffered saline  
PBST: PBS-Tween  
PCNA: proliferating cell nuclear antigen  
PCR: Polymerase chain reaction  
PDE: Phosphodiesterase  
PFA: Paraformaldehyde  
PIKK: Phosphatidylinositol 3-kinase-related kinase  
PKD: Polycystic kidney disease  
PL: Photoreceptor layer

PLA: Proximity ligation assay  
PNKP: Polynucleotide Kinase 3'-Phosphatase  
PRKDC: Protein kinase, DNA-dependent, catalytic polypeptide  
PRPF31: Pre-mRNA processing factor 31  
PRPH2: Peripherin 2  
PUFA: Polyunsaturated fatty acid  
PVDF: Polyvinylidene fluoride  
qRT-PCR: Quantitative real-time PCR  
RHO: Rhodopsin  
RIPA: Radioimmunoprecipitation assay  
RNA: Ribonucleic acid  
ROM-1: Retinal outer segment membrane protein 1  
RONs: Reactive oxygen and nitrogen species  
ROS: Reactive oxygen species  
RP: Retinitis pigmentosa  
RPE: Retinal pigment epithelium  
RPGR: Retinitis pigmentosa GTPase regulator  
RS1: Retinoschisin 1  
RSK1: Ribosomal protein S6 kinase A1  
SCID: Severe combined immunodeficiency  
SDS-PAGE: Sodium dodecyl sulfate polyacrylamide gel electrophoresis  
SEM: Standard error of the mean  
SH3: SRC homology 3  
SHH: Sonic hedgehog  
SSA: Single strand annealing  
SSBR: DNA single strand break repair  
STAT3: Signal transducer and activator of transcription 3  
TAE: Tris base / acetic acid / EDTA  
TALEN: Transcription activator-like effector nuclease  
TBCC: Tubulin cofactor C  
TBE: Tris base / borate / EDTA  
TBS: Tris-buffered saline

TBS-T: TBS-Tween

TOPORS: TOP1 Binding Arginine/Serine Rich Protein

UNC119: Uncoordinated 119

UPR: Unfolded protein response

UV: Ultraviolet

WB: Western blot

WRN: Werner Syndrome RecQ-like Helicase

WT: Wild type

XLRP: X-linked Retinitis pigmentosa

XPA: Xeroderma pigmentosum group-A complementing protein

XRCC4: X-ray repair cross-complementing 4

# Chapter 1. Introduction

Inherited retinal degenerations (IRDs) today affect more than 2 million people worldwide (Sahel, Marazova and Audo 2014). IRDs may be constricted to the macula or affect the entire retina, ultimately leading to severe visual impairment and constituting a substantial burden on patients' everyday lives and the whole of society. Although these diseases remain untreatable, significant progress has been made regarding both the research for therapeutic strategies and the development of technological aids and substitutes. These advances go hand-in-hand with the rise of new sequencing technologies which has led to an explosion in the identification of genetic causes for these highly heterogeneous diseases and basic research which sheds light to the molecular pathways leading to disease.

In the following chapter, I will first provide a brief overview of the principles concerning retinal structure in general and photoreceptor biology in particular. I will then describe some of the main types of IRDs and Retinitis pigmentosa (RP), a form of IRD which stems from photoreceptor degeneration. This disease is the focus of the present thesis, which presents research on the molecular mechanisms underlying a specific subtype of X-linked RP caused by mutations in the *RP2* gene. Subsequently, I will summarise all current bibliography concerning the function of protein RP2, and, finally, I will lay out the aims of my PhD research.

## 1.1 General principles of photoreceptor structure and function

The vertebrate retina is laminated in an orderly manner. It consists of an outer monolayer of polarised epithelial cells, the retinal pigment epithelium (RPE), and the inner neural retina, a laminated network of neurons and their connections. The photoreceptor layer, consisting of highly differentiated neurons which generate electrical responses after light stimulation, is found at the outer part of the retina adjacent to the RPE layer. This arrangement means that light must first pass through the inner layers of the retina before reaching the light-sensitive outer segment (Sung

and Chuang 2010) (Figure 1.1A). Rod photoreceptors (rods) are specialised for high-sensitivity photon detection in low-light conditions, while cone photoreceptors (cones) are adapted to high-resolution colour vision. While this basic organisation is common among vertebrates, the distribution of rods and cones across the retina differs among species. For example, humans and other primates have specialised cone-dense areas in the central retina responsible for high-acuity vision, the macula and the fovea (Hendrickson 2005). Because rodents commonly used in retinal research are nocturnal animals, they have a rod-dominant retina and poor colour vision. Zebrafish, another useful small-animal model for the study of retinal diseases, have four different types of cones and, as a result, possess the ability for tetrachromatic colour vision (Malicki et al. 2016, Gregory-Evans 2012). The zebrafish retina is also considered cone-dominant, at least during early larval stages when vision is exclusively dependent on cones (Bilotta, Saszik and Sutherland 2001). However, there are other physiological differences between the zebrafish and the human retina (Lieschke and Currie 2007). These differences in photoreceptor distribution must be considered when interpreting results from animal model studies.

The photoreceptors have a very tight relationship with the adjacent RPE layer which performs many functions essential for photoreceptor viability. For example, the regeneration of the chromophore 11-cis retinal which is exhausted during phototransduction [a reaction known as the visual cycle (Lamb and Pugh 2004, Jin et al. 2005)] takes place in the RPE. Moreover, the RPE cells prevent and repair retinal photooxidative damage, caused by the production of reactive oxygen species due to high levels of light exposure, via their capacity for light filtration and their high antioxidant content (Newsome et al. 1994, Dun et al. 2013). Other functions of the RPE layer include the transport of nutrients and ions between the retina and the choriocapillaris (Adijanto et al. 2009), the secretion of neurotrophic factors, and the secretion of proteoglycans which make up the interphotoreceptor matrix (Tawara, Varner and Hollyfield 1989). Most importantly, the RPE cells are active phagocytes which daily “consume” shed photoreceptor OS (~10% of OS discs in the rat) and assist in their renewal (Kevany and Palczewski 2010, Young and Bok 1969).

Photoreceptors are highly compartmentalised cells divided into the outer segment (OS), a system of tightly-packed membrane stacks where phototransduction takes place, the inner segment (IS) where all biosynthetic reactions take place, the nucleus and the synapse (Pearing et al. 2013) (Figure 1.1B). Phototransduction begins with photon absorption by the visual pigment molecules (rhodopsin or cone opsins), G protein-coupled receptors covalently conjugated to a chromophore. This event initiates a signalling cascade involving the activation of G protein transducin and cGMP phosphodiesterase (PDE) which ultimately leads to the decrease in intracellular cGMP concentration (Arshavsky and Wensel 2013).

The OS is, in fact, the continuation of a modified primary cilium embedded within the photoreceptor cell, called the connecting cilium (CC). The CC functions as a bridge connecting the IS and the OS and permits protein transport between the two compartments in a highly regulated and efficient manner (Figure 1.1B). It has been estimated that ~80 molecules of rhodopsin, the visual pigment of rod photoreceptors, have to be synthesised and delivered to the OS every second in mouse photoreceptors (Williams 2002). The delivery of OS proteins from their site of synthesis to the base of the cilium is regulated by sophisticated mechanisms involving RAB, ARF and ARL GTPases, of which the most mechanistically dissected is the mechanism governing transport of rhodopsin (Deretic and Wang 2012, Deretic et al. 1995, Mazelova et al. 2009). In general, transmembrane or membrane-associated OS proteins are delivered either as transport vesicles assembled at the Golgi apparatus or with the help of trafficking chaperones which recognise lipid-modified cargo (Pearing et al. 2013). Once in the ciliary apparatus, the transport of proteins up and down the microtubule-based structure, the ciliary axoneme, is carried out by molecular motors and the intraflagellar transport (IFT) protein complexes. This has been shown in primary cilia and is most likely applicable to photoreceptor CC as well (Pearing et al. 2013). Anterograde transport (towards the ciliary tip) is carried out by the IFT-B complex and molecular motors of the kinesin-2 family, while retrograde transport (from the tip to the base of the cilium) is carried out mainly by cytoplasmic dynein-2 and the IFT-A complex. The role of the components mentioned above in ciliary transport has been supported by a multitude of mouse and zebrafish studies showing that mutations in motor proteins or

IFT proteins lead to mislocalisation phenotypes and defective photoreceptor development (Pazour et al. 2002, Marszalek et al. 2000, Zhao et al. 2012, Krock, Mills-Henry and Perkins 2009, Tsujikawa and Malicki 2004b).

A disruption in ciliary trafficking is bound to affect all outer segment functions, from phototransduction to phagocytosis by the RPE, and therefore compromise photoreceptor function and viability. The strict requirement for efficient protein transport through the CC is only one of the reasons that the photoreceptors are so vulnerable to the slightest compromise of their functional state. Another factor that contributes to the vulnerability of photoreceptors and stems from their unique cellular organisation is the susceptibility to light-induced damage and lipid oxidation (Wright et al. 2010, Hollyfield et al. 2008). The combination of photoexcitation of molecules, such as retinoids, and high oxygen content in the retina can readily lead to the generation of reactive oxygen species and oxidative damage in biomolecules, especially if genetic mutations lead to increased accumulation of by-products of the visual cycle (Sun and Nathans 2001). Besides, the susceptibility of photoreceptors to oxidative damage is multiplied by their very high lipid content, especially regarding long-chain polyunsaturated fatty acids, readily oxidised to highly reactive compounds which can initiate free radical chain reactions. Indeed, the potential of so many stressors to tip the balance towards cell death is reflected in the fact that photoreceptor degeneration is considered one of the most genetically heterogeneous disorders in humans (Wright et al. 2010).

## **1.2 Retinitis pigmentosa and other forms of inherited retinal degeneration**

Several types IRDs exist which stem from photoreceptor degeneration but differ from each other by the kind of photoreceptors involved, the age of onset and the clinical characteristics. Some examples are:

- Leber congenital amaurosis (LCA) [reviewed in (den Hollander et al. 2008)] is the most severe non-syndromic retinal dystrophy, characterised by



early (infantile onset) visual loss and non-detectable electroretinogram (ERG) responses. Mutations in more than 20 genes can cause the disease (Retinal Information Network, RetNet) and can manifest as cone-rod or rod-cone degeneration, depending on which photoreceptor type is primarily affected.

- Cone-rod dystrophies [reviewed in (Michaelides et al. 2006)] are types of retinal dystrophies characterised by cone degeneration preceding rod degeneration. Early manifestations include loss of visual acuity, photophobia, and the appearance of macular pigment deposits, while late stages are characterised by arteriolar attenuation and optic disc pallor. More than 30 genes have been identified today to cause the various forms of the disease (RetNet), such as *ABCA4* (autosomal recessive form), *UNC119* (autosomal dominant form) and even *RPGR*, one of the major causative genes for X-linked RP.
- X-linked retinoschisis [reviewed in (Molday, Kellner and Weber 2012)] stems from the splitting of the inner layers of the neurosensory retina, leading to foveal “schisis” (breaking) and vision loss. It is diagnosed in infancy or early childhood and usually follows a mild disease progression course. It is caused by mutations in the *RS1* gene.
- Stargardt disease [reviewed in (Tanna et al. 2017)] is bilateral macular atrophy accompanied by subretinal deposition of lipofuscin-like material. It is juvenile-onset and usually diagnosed as impaired central and detailed vision and decreased visual acuity. Typical Stargardt disease is associated with mutations in the *ABCA4* gene.
- **Retinitis pigmentosa (RP)** is a clinically and genetically heterogeneous group of IRDs, characterised by progressive bilateral dysfunction of predominantly rod photoreceptors followed by secondary degeneration of cone photoreceptors (therefore, a rod-cone degeneration) and the RPE. The disease in its typical form initially manifests with problems in night vision (nyctalopia) and progressive restriction of the peripheral vision field (tunnel vision), characteristic of rod photoreceptor loss. The central retina (the macula) is usually preserved until the latest stages of the disease. However, the patients are often already considered legally blind due to

severely constricted visual fields. In late stages, RP is characterised by a classic clinical triad of changes in fundus appearance: retinal blood vessel attenuation, retinal pigmentary changes (often hyperpigmentation in the form of bone spicule deposits), waxy pallor of the optic nerve head (Sahel et al. 2014) (Figure 1.1C). Other symptoms/ocular manifestations of the disease include fatigue and decline in contrast sensitivity, scotomas in the mid-periphery, early development of cataracts, refractive errors including myopia and astigmatism, cells in the vitreous as well as cystoid macular oedemas (Hartong, Berson and Dryja 2006). RP is an exclusively genetically determined form of retinal degeneration, meaning that there are no known risk factors other than genetic predisposition. The age of onset is very variable among the different types, ranging from early childhood to mid-30s to -50s (Tsujikawa et al. 2008).

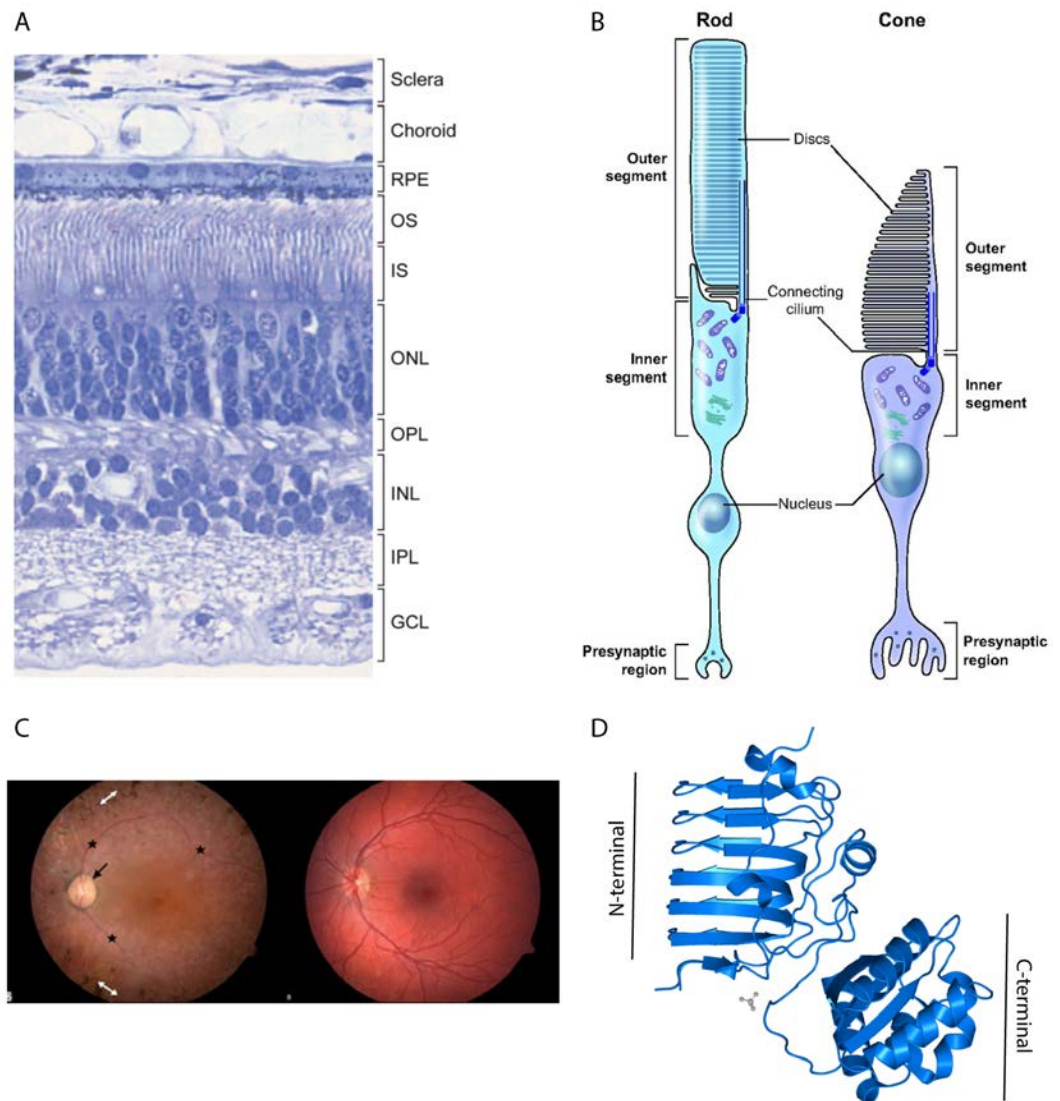


Figure 1.1 **Basic organisation of the human retina and hallmarks of disease (A-C). Crystal structure of human RP2 (D).**

A) Transverse section of the human retina visualised with H&E staining which makes its laminated layers visible, reproduced from (Sung and Chuang 2010). The OS, IS, ONL layers represent different parts of the photoreceptor cells. The INL and GCL layers contain the nuclei of the second-order neurons that process the light signals generated by the photoreceptors and transmit them through the optic nerve to the brain. The OPL and IPL layers are formed by neuronal synaptic terminals and processes. B) A schematic representation of rod and cone photoreceptors reproduced from (Veleri et al. 2015). Photoreceptors are highly compartmentalised neurons, consisting of the photosynthetic OS with its membranous discs containing phototransduction components, the IS which contains the biosynthetic machinery, the nucleus and the presynaptic region where docking of synaptic vesicles takes place. C) Picture of the internal surface of the eye (fundus) from a Retinitis pigmentosa patient (left) compared to a healthy person (right). The characteristic clinical manifestations of RP are marked on the picture, namely the bone spicule

pigment deposits (white arrows), retinal vessel attenuation (star) and waxy pallor of the optic disc head (black arrow). The picture is taken from the National Eye Institute website. D) Crystal structure of human RP2 (Kuhnel et al. 2006). The N-terminal has homology to Tubulin cofactor C (TBCC) and the C-terminal domain is homologous to Nucleoside diphosphate kinases (NDK).

RPE: retinal pigment epithelium, OS: outer segment, IS: inner segment, ONL: outer nuclear layer, OPL: outer plexiform layer, INL: inner nuclear layer, IPL: inner plexiform layer. GCL: Ganglion cell layer.

### **1.2.1 Molecular genetics and pathways leading to photoreceptor death in RP**

The average worldwide prevalence of RP ranges from 1:3000-1:7000, an estimation which differs between populations but argues for the labelling of this disease as a leading cause of inherited blindness worldwide (Sahel et al. 2014). About 20-30% of RP patients suffer from the syndromic or systemic form of the disease, meaning that retinal degeneration co-exists with other manifestations affecting multiple organs or with system-wide pathological features. For example, RP constitutes the ocular manifestation of ciliopathy syndromes such as Usher syndrome (RP and hearing impairment), Bardet-Biedl syndrome (RP associated with polydactyly, obesity, diabetes type 2, hypogonadism, cognitive impairment and renal abnormalities) or Joubert syndrome (RP associated with hypotonia progressing to ataxia, global developmental delay, breathing dysregulation, renal and liver abnormalities). Non-syndromic RP can be inherited as autosomal dominant (20-25% of non-syndromic, non-systemic cases), autosomal recessive (15-20%) or X-linked trait (10-15%) (Ferrari et al. 2011). In addition, rare cases of digenic and mitochondrial inheritance have been reported (Kajiwara, Berson and Dryja 1994), while a significant percentage of patients are referred to as isolated or simplex cases, meaning that an inheritance pattern is not immediately recognisable (Bravo-Gil et al. 2017).

The enormous genetic complexity of RP is highlighted by the fact that to date, mutations in more than 60 genes have been found to account for the non-syndromic forms of the disease only (Retinal information network, RetNet). Moreover, genotype-phenotype correlations are not always possible, as many distinct genes are

linked to the same phenotype, while mutations in the same gene can cause different diseases. As a striking example, mutations in the *RPGR* gene which account for the majority of recessive and dominant X-linked RP cases (depending on whether female carriers are affected) have also been blamed for X-linked recessive atrophic macular degeneration, cone-rod degeneration and extra-ocular ciliopathies like recurrent respiratory infections, deafness, and primary ciliary dyskinesia, in different patients (Sharon et al. 2003, Pelletier et al. 2007).

Disruptions in various molecular pathways and functions can cause RP. However, common stressors and photoreceptor death pathways, as well as secondary responses of the retina to photoreceptor degeneration, seem to be remarkably similar regardless of the mutant gene (Bramall et al. 2010). For example, one of the main factors that seem to contribute to photoreceptor cell death in a large group of RP forms is elevated oxygen levels in the retina, probably due to energy-demanding procedures, such as phototransduction, and the inability of the choroidal blood vessels for autoregulation in response to external oxygen levels (Bramall et al. 2010). Several rodent models of retinal degeneration display abnormal increases in oxygen concentration in the outer retina (Yu et al. 2004). Moreover, light exposure is a common stressor which can be translated to oxidative stress in mutant retinæ displaying accumulation of all-trans-retinal and toxic bis-retinoid byproducts of the visual cycle, which are easily oxidised (Organisciak and Vaughan 2010). Mutations that disturb outer segment phagocytosis or disc turnover fall into this category.

Below are some examples of the most common RP causative genes:

- Mutations in the gene encoding for rhodopsin (*RHO*), the visual pigment of rod photoreceptors and a G protein-coupled receptor, are found in 26.5% patients with autosomal dominant RP, while they also account for autosomal recessive RP and congenital stationary night blindness when they lead to constitutively active protein (Ferrari et al. 2011). Rhodopsin forms over 90% of the total protein in the rod OS (Basinger, Bok and Hall 1976, Ferrari et al. 2011). Mutations in this protein, known to impair binding of 11-cis retinal, cellular trafficking, or the ability for G protein coupling and

activation, lead to impairment of the phototransduction cascade which is essential for normal vision (Malanson and Lem 2009). Another big class of rhodopsin mutations lead to impaired protein folding, resulting in rhodopsin being trapped in the endoplasmic reticulum (ER) (Kunte et al. 2012). Because rhodopsin is very abundant in rod photoreceptors, the accumulation of misfolded proteins in the ER leads to ER stress and the activation of the unfolded protein response (UPR).

- Mutations in other proteins of the phototransduction cascade are also common, such as PDE6A, PDE6B or PDE6G, the subunits of the tetrameric phosphodiesterase complex which regulates intracellular cGMP levels by hydrolysing cGMP in response to light activation of G protein-coupled receptors (Tsang et al. 2008). Responsible for more than 8% of cases, mutations in *PDE6A* and *PDE6B* are the second most identifiable cause of autosomal recessive RP (Ferrari et al. 2011).
- Notable examples of how disruption in the visual cycle can lead to RP are mutations in the *RPE65* gene, responsible for ~2% of autosomal recessive RP as well as 16% of LCA (Ferrari et al. 2011). *RPE65* encodes for an isomerohydrolase expressed in the RPE layer which catalyses regeneration of 11-cis retinal (Moiseyev et al. 2005). Mouse models of *RPE65* knockout have no 11-cis retinal and no detectable rhodopsin in their retinae; instead, they display an accumulation of retinoid intermediates of the visual cycle in their RPE layer (Samardzija et al. 2008). Due to the abundance of naturally occurring and genetically engineered animal models, the effects of lack of *RPE65* have been extensively studied, and patients have participated in gene therapy clinical trials which have so far positive results in terms of visual reactions but did not slow down retinal degeneration (Cideciyan 2010, Cideciyan et al. 2013). Importantly, this example highlights the stringent functional cooperation of the photoreceptors and the RPE layer which is required for retinal viability. Mutations in other genes that are exclusively expressed in the RPE are also responsible for RP and other forms of retinal degeneration (among others, *ABCA4* and *MERTK*).

- Molecular pathways required for retinal viability are not restricted to the visual cycle but are very diverse. Some causative genes participate in maintaining photoreceptors' structure. For example, the *PRPH2* gene which is found mutated in 5-10% of patients with autosomal dominant RP (Ferrari et al. 2011), encodes for an integral membrane glycoprotein, Peripherin-2, located in the outer segment discs of rods and cones. This protein forms homomeric and heteromeric complexes with ROM1 which are important for disc morphogenesis and stabilisation (Loewen, Moritz and Molday 2001).
- On the other hand, RP can also be caused by metabolic stress due, for example, to defects in protein synthesis. *PRPF31* encodes for one out of three pre-mRNA splicing factors which are found mutated in RP and accounts for up to 8% of autosomal dominant RP in various cohorts (Audo et al. 2010). Interestingly, the proteins encoded by these genes are essential for splicing in all cell types; it is, therefore, unknown why rod photoreceptors are exclusively affected by their mutations.
- Finally, an important group of genes whose mutations are often connected to retinal degenerations are genes encoding for structural or functional components of the CC. Because of this, and the fact that RP constitutes the ocular manifestation of several syndromic ciliopathies, non-syndromic RP is also characterised as a ciliopathy. A notable example is *RPGR*, the causative gene for the majority (70-90%) of X-linked RP cases (Pelletier et al. 2007, Prokisch et al. 2007). Two of the protein isoforms encoded by this gene, a constitutive ( $RPGR^{Ex1-19}$ ) and a retinal-enriched ( $RPGR^{ORF15}$ ) one, localise to the base of the photoreceptor connecting cilium, where they have been attributed roles in the regulation of protein trafficking to the connecting cilium and cytoskeletal regulation (Lyraki, Megaw and Hurd 2016).

## 1.2.2 X-linked RP

X-linked inheritance pattern characterises about 10-20% of families with RP. X-linked RP (XLRP) cases are among the most severe due to early onset leading to significant visual loss before the fourth decade (Pelletier et al. 2007). Linkage analyses indicate at least five XLRP loci, but only three genes have been identified to date. Mutations in *RPGR* (Roepman et al. 1996) and *RP2* (Schwahn et al. 1998) genes together account for the vast majority of all XLRP [over 80%, as estimated in (Sharon et al. 2003)], but have also been identified in patients previously characterised as simplex cases (Branham et al. 2012). Different studies have estimated that the percentage of patients with *RP2* mutations in XLRP cohorts ranges from 7 to 18%, while *RPGR* mutations have been identified in 70-90% of the cases (Sharon et al. 2003, Pelletier et al. 2007, Jayasundera et al. 2010). A hypomorphic intronic variant in *OFDI*, the causative gene for severe syndromes such as Joubert and orofaciodigital syndrome-1, which is male lethal, has been identified in one XLRP family (locus RP23); this report is an example of how reduced expression of a syndromic ciliopathy gene can lead to RP (Webb et al. 2012).

The present thesis focuses on the molecular mechanisms that result in disease in response to *RP2* mutations. More than 70 pathogenic mutations in *RP2* have been identified to date (Retinal information network, RetNet). These include variable changes like premature stop codons leading to truncated proteins, splice site changes, small in-frame deletions and missense mutations. According to an estimation based on a French cohort of 127 families, the majority of identified *RP2* mutations were expected to result in null alleles or highly truncated proteins (Pelletier et al. 2007). Nonetheless, even mutations that are not initially predicted to be deleterious, like small in-frame deletions, have been proved to severely affect protein expression when assessed from a structural point of view. For example, a recent *in vitro* and *in silico* study of the expression levels of different mutated forms of *RP2* found that more than half of the missense mutations or small in-frame deletions lead to misfolded or destabilised proteins (Liu et al. 2017a). On the other hand, there is a smaller subset of missense mutations that are not predicted to affect the folding of the protein and are expressed at wild-type levels. These mainly affect solvent-



exposed residues which are very likely mediators of protein-protein interactions: E138, R211, R118, T87 (Liu et al. 2017a). Non-destabilising missense mutations are very informative from a research point of view and will be discussed in more depth in Chapter 3. Finally, another category of non-destabilising missense RP2 mutations, affecting residues of the extreme N-terminal, are known to impair protein targeting to the plasma membrane (Chapple et al. 2000). Overall, these are the main effects of pathogenic mutations on RP2 protein which are known so far: 1) Nonsense mutations early in the gene lead to mRNA degradation by nonsense-mediated decay (NMD) [e.g., The R120\* mutation (Mears et al. 1999, Schwarz et al. 2015)] 2) Destabilising mutations result in protein misfolding and degradation through the proteasome pathway [e.g., C67Y (Breuer et al. 2002), pLys323fs (Neidhardt et al. 2008)] 3) Non-destabilising missense mutations affect protein-protein interactions or catalytic functions [e.g., E138G (Miano et al. 2001), R211L (Villaverde-Montero et al. 2007), R118H (Breuer et al. 2002)] 4) Mutations of the extreme N-terminus lead to loss of membrane association [e.g.,  $\Delta$ S6, G2A, C3S (Jayasundera et al. 2010)].

RP2 mutations generally lead to a distinct and recognisable phenotype characterised by early manifestations of cone degeneration in the form of macular atrophy and declining visual acuity. In one study (Jayasundera et al. 2010), the majority of male patients had early-onset (before 12 years of age) of macular atrophy and low visual acuity combined with high myopia. This characteristic is in contrast with typical forms of RP, where cone degeneration is only secondary to rod degeneration and, therefore, the macula is spared until very late in the disease course. Macular atrophy was not associated with a particular type of mutation but rather manifested in patients with different kinds of RP2 changes [deletion leading to protein instability, frameshift, splice site change and missense mutation (R118C)]. ERG data confirmed the conclusion of cone degeneration in the early stages. Despite the unusually early involvement of cone degeneration, it should be noted that RP2 disease is still labelled as a rod-cone degeneration because rods are affected first in most patients (only one case was described with clear cone-rod dysfunction). Interestingly, another study (Dandekar et al. 2004) has also associated a small deleterious deletion with an atypical phenotype of macular and peripapillary retinal atrophy.

Other atypical phenotypes have been reported, adding to the complexity of RP2 disease. These mainly include RPE and choroid involvement in the form of RPE and choroidal atrophy and depigmentation reminiscent of typical choroideremia (Jayasundera et al. 2010). Mutations associated with a choroideremia-like phenotype fall in the N-terminal  $\beta$ -helix domain and include both deleterious mutations (e.g. R120\*, W150\* nonsense mutations) and missense mutations (e.g. R118C).

In general, it has been reported that *RP2* mutations lead to one of the most severe forms of RP. Apart from the early onset of macular atrophy, all patients under 16 presented with severe constriction of visual fields (Jayasundera et al. 2010). In another study, patients with *RP2* mutations had on average significantly lower visual acuity than patients with *RPGR* mutations for the same age and across all ages (Sharon et al. 2003).

Predictable genotype-phenotype correlations are not possible when studying RP type 2, because even *RP2* mutations that are not predicted to be deleterious sometimes lead to severe phenotypes. In general, most mutations are thought to lead to severe phenotypes such as declining visual acuity from an early age (a sign of macular dysfunction) (Jayasundera et al. 2010). This category includes all premature truncations as well as some missense mutations that are predicted to be non-destabilising (Liu et al. 2017a) such as R118H and R211H. Only three mutations have so far been associated with a less severe phenotype, characterised by relatively older age at onset of macular dysfunction: C3S, S6del and T87I (Jayasundera et al. 2010). C3S and  $\Delta$ S6 affect the protein's localisation to the plasma membrane, while T87I is a missense mutation which is not predicted to destabilise the protein structure and is thought to affect yet unknown protein-protein interactions of RP2 (Liu et al. 2017a).

Overall, mutations in the *RP2* gene result in severe retinal disease whose spectrum reaches beyond typical RP and involves both rod and cone degeneration.

## 1.3 Functional significance of RP2 in the retina

### 1.3.1 The RP2 protein

The *RP2* gene, which was first identified as an XLRP gene in 1998 by linkage analysis (Schwahn et al. 1998), encodes for a protein product of 350 residues. At the RNA level, *RP2* expression was detected at several human fetal and mouse tissues including the brain, the kidney and the liver (Schwahn et al. 1998). At the human retina, RP2 was detected at the intracellular face of the plasma membrane of both rod and cone photoreceptors, the RPE and other cell types (Grayson et al. 2002). Numerous other studies in cultured cells and mouse models have also reported pools of RP2 in the Golgi apparatus, the primary cilium axoneme (where it is transported via an Importin  $\beta$ -mediated mechanism) and the basal body of the photoreceptor's CC (Evans et al. 2010, Hurd et al. 2010, Hurd, Fan and Margolis 2011). The N-terminus of RP2 undergoes lipid modifications in the form of myristoylation of G2 and palmitoylation of C3 which are necessary for plasma membrane localisation and cilia targeting and are pathologically relevant (Chapple et al. 2000, Chapple et al. 2002).

Crystallography revealed that RP2 consists of two domains that appear not only structurally but also functionally distinct (Kuhnel et al. 2006) (Figure 1.1 D). The N-terminal domain (residues 1-228) consists of a  $\beta$ -helix with a tightly packed and mainly hydrophobic domain. This part of the protein is homologous (~30% sequence identity) to Tubulin Cofactor C (TBCC), a chaperone in the  $\alpha/\beta$  tubulin heterodimer assembly. TBCC has GTPase activating protein (GAP) activity towards  $\beta$  tubulin, stimulating GTP hydrolysis which causes the release of native tubulin heterodimers from the cofactor complex (Tian et al. 1997). Despite the fact that critical residues of the TBCC catalytic core, such as the catalytic arginine finger R118 and E138, are conserved on RP2, it was shown early that RP2 cannot substitute for TBCC in tubulin folding reactions *in vitro* (Bartolini et al. 2002). While both RP2 and TBCC can partially complement for the loss of their distant yeast homolog CIN2 in restoring hypersensitivity to microtubule poisons (Bartolini et al. 2002), it is believed today that RP2 and TBCC have developed distinct functions in mammals. In

particular, it is now established that the small GTPase Arf-like 3 (ARL3) is a substrate for the GAP activity of RP2. This interaction is highly specific and very efficient: RP2 accelerates the intrinsic GTP hydrolysis rate of ARL3 more than 1000 fold, while it only shows a minor activity towards the closely related ARL2 GTPase (Veltel et al. 2008). The RP2-ARL3 interaction has been the subject of intense research, and its function will be analysed in the next section in further detail.

On the other hand, the C-terminal domain of RP2 (residues 229-350) has a ferredoxin-like fold. It has been described as a three-layered  $\alpha/\beta$  sandwich with an antiparallel  $\beta$  sheet (Kuhnel et al. 2006). This domain is characterised by sequence similarity with Nucleoside diphosphate kinases (~22% identity with the *D. discoideum* NDK). However, because there is no evidence of ADP binding on RP2 and the overall protein structure does not support an NDK-like phosphotransferase activity, it is unlikely that RP2 shares NDK's canonical function (Kuhnel et al. 2006). This RP2 domain is not necessary for GTP hydrolysis (Veltel et al. 2008), and its function has been so far understudied. Only one study has looked comprehensively at this domain, showing that it participates in exonuclease activity against single-stranded DNA *in vitro* (Yoon et al. 2006). One of the aims of the present thesis is to investigate a novel potential role for the C-terminal domain of RP2 (Chapter 3).

### **1.3.2 Suggested roles of the RP2-ARL3 complex in protein trafficking within the photoreceptors**

The small GTPase ARL3 belongs to the ADP ribosylation factor (ARF) family of the Ras superfamily of small GTPases, which includes ARF, ARL and SAR1 proteins. Members of the ARF family participate in membrane traffic and organelle structure (Donaldson and Jackson 2011). Members of the ARL subfamily, in particular, are known to be important for transport of ciliary proteins and cilia maintenance and are associated with human ciliopathies, like Bardet-Biedl syndrome (ARL6) (Chiang et al. 2004) and Joubert's syndrome (ARL13B) (Cantagrel et al. 2008). ARL3 itself is considered a microtubule-associated protein (MAP) and linked to several

microtubule-related processes such as unloading of cargo from dynein motors (Jin et al. 2014), cell morphology and cytokinesis (Zhou et al. 2006), and flagellum biogenesis (Cuvillier et al. 2000). Mouse models of absent or aberrant ARL3 function have established a role of this small GTPase in ciliary processes. For example, an *Arl3* knockout mouse model suffers from abnormal development of renal, hepatic and pancreatic epithelial tube structures reminiscent of human polycystic kidney disease (PKD), alongside severe retinal degeneration post-natally characterised by abnormal OS discs (Schrack et al. 2006). The combination of these defects is reminiscent of human ciliopathies because mechanosensory primary cilia have a central role in regulating renal epithelial cells' proliferation and differentiation, whereas retinal degeneration is often attributed to defective protein transport through the photoreceptor's modified cilium.

Most hypotheses about the function of the RP2-ARL3 complex revolve around protein trafficking within ciliated cells in general and more specifically through the CC to the photoreceptor OS (Figure 1.2). Some studies claim RP2 participates in global vesicle trafficking between the Golgi and the cilium and is essential for Golgi cohesion (Evans et al. 2010, Schwarz et al. 2015). Other studies have suggested that RP2 participates in the subcellular targeting of specific lipid-modified protein cargo. Structural approaches have uncovered an allosteric mechanism by which GTP-bound ARL3 displaces lipid-modified cargo from chaperones UNC119 and its homolog PDE6 $\delta$ , which solubilise and assist the cargo mentioned above in its transport through the cytosol (Ismail et al. 2011, Ismail et al. 2012). UNC119 regulates the ciliary targeting of acylated proteins, while PDE6 $\delta$  binds prenylated cargo; known cargoes of specific interest to phototransduction that need to be delivered to the OS through the CC are myristoylated T $\alpha$  transducin subunit, and prenylated cGMP phosphodiesterase PDE6 and rhodopsin kinase GRK1 (Zhang et al. 2011, Zhang et al. 2012). The role of RP2 in this process would be to keep ARL3 in an inactive, GDP-bound state by stimulating GTP hydrolysis, and therefore to render it unable to displace cargo from UNC119 and PDE6 $\delta$ . It is also possible that RP2 is more directly involved in trafficking of phototransduction proteins by interacting with the protein cargo. Specifically, RP2 has been found to interact with G $\beta$  transducin and facilitate its trafficking to the membrane compartment (Schwarz et al. 2012).

Besides, RP2 interacts with ciliary kinesins KIF17 and KIF7 and regulates their trafficking to the ciliary tip of cultured immortalised RPE cells (Schwarz et al. 2017).

The exact location in the cell where RP2 and ARL3 interact remains a mystery, although (Gotthardt et al. 2015) recently suggested an intriguing hypothesis by identifying ARL13B as having guanine exchange factor (GEF) activity towards ARL3, meaning it can exchange GDP for GTP and activate the protein. Because ARL13B is almost exclusively localised within the ciliary axoneme, this study suggested that ARL3 exists in an active state (which is capable of releasing lipid-modified cargo) only within the ciliary axoneme, while it is inactive outside the cilium due to the action of RP2 on the basal body and other cellular locations (Figure 1.2). However, this hypothesis is counteracted by other studies which have detected RP2 within the ciliary axoneme in cultured cells (Schwarz et al. 2017, Hurd et al. 2010).

### **1.3.3 Mouse models of RP type 2**

Genetically engineered mouse lines have been generated to test some of the hypotheses mentioned above *in vivo*. At first, a mouse model for the absence of *Rp2* expression was generated by exon 2 deletion and was found to suffer late-onset, slowly progressive photoreceptor degeneration which affected both types of photoreceptors with the effect on cones being more prominent (Li et al. 2013a). One of the most important phenotypes of these mice was mislocalisation of cone M-opsin from the OS, where it is normally localised, to the inner nuclear layer (INL) and synaptic layer. Interestingly, no mislocalisation of other cargoes that are proposed to undergo RP2-mediated transport, such as transducin subunits, was observed. Later studies have also reported reduced cone PDE6 expression (Mookherjee et al. 2015) and abnormal elongation of the axoneme and membrane of the cone CC (Li et al. 2015).

A second mouse model for the complete absence of *Rp2* expression was later generated by a gene trap strategy. Contrary to the first study, the phenotype of these

mice corroborates the hypothesis that RP2 participates in the targeting of lipid-modified proteins cone and rod PDE6 and GRK1, as these proteins are mislocalised from the OS to the synaptic region<sup>1</sup> (Zhang et al. 2015). However, no mislocalisation of cone opsins or transducin subunits was observed in retinal sections from these mice. The differences between the two mouse models could be attributed to the different knockout strategies or could simply reflect the phenotypic variation which is characteristic of the disease and is often observed in human RP2 patients. On the other hand, the possibility that the mislocalisation phenotypes are secondary manifestations of a more fundamental defect that is yet unknown, must not be excluded. Finally, it is important to stress the common points of both studies, as both mouse models present with late-onset, slowly progressive retinal degeneration that affects the cone function more prominently.

Apart from the genomic *ARL3* null model (Schrack et al. 2006), other mouse models have been generated to analyse the function of *ARL3* in the retina further. These have been genetically manipulated to model rod-specific and retina-specific lack of *ARL3* expression (Hanke-Gogokhia et al. 2016), or to mimic accumulation of activated *ARL3* (Wright et al. 2016). The conclusions drawn from these studies generally corroborate a role for the RP2-*ARL3* complex in the trafficking of lipid-modified phototransduction proteins in mammals; however, lack of *ARL3* produces a more severe phenotype than lack of RP2. For example, the absence of *ARL3* expression leads to developmental phenotypes (like improper basal body formation) and mistrafficking of transducin subunits, which is not observed in the *Rp2* null mouse models. This discrepancy means that the complete lack of *ARL3* does not cause the same effects as the accumulation of the active form, which occurs in the absence of the GAP (RP2). Also, it might mean that there is another GAP protein for *ARL3* in addition to RP2.

---

<sup>1</sup> It is important to note that contrary to the earlier study, Zhang et al (2015) report mislocalisation of PDE6 rather than reduced expression, as was confirmed by western blotting of whole retinal lysates. However, this technique could potentially mask a cone-specific reduction in PDE6 expression.

### 1.3.4 Alternative roles of RP2

Although the function of RP2 in the photoreceptor CC is often almost exclusively focused upon, alternative roles have been proposed for RP2 and ARL3 in different tissues and different cellular contexts. For example, RP2 expression has been detected in the ciliary axoneme and other cellular locations in mouse kidney tubules, where it is proposed to regulate retrograde transport of the ciliary PKD protein, polycystin 2 (PC2) (Hurd et al. 2010). In addition, several studies using zebrafish embryos have reported a role of *rp2* in early vertebrate development, not only because it is a maternally provided transcript which is present throughout early embryo development, but also because knockdown leads to developmental malformations (curved tail, microphthalmia (small eyes), and laterality defects-situs inversus) (Hurd et al. 2010, Shu et al. 2011, Desvignes et al. 2015). The role of protein Rp2 in zebrafish will be discussed in a detailed fashion in Chapter 5.

Finally, roles for RP2 in the nucleus, such as in DNA processing and the regulation of transcription, have emerged. The authors of an earlier study (Yoon et al. 2006) have biochemically characterised RP2 as a DNA-binding protein with 3'-5' exonuclease activity against single-stranded DNA. Furthermore, a recent study has implicated ARL3 in STAT (signal transducer and activator of transcription) signalling. ARL3-GTP is a direct interaction partner of STAT3 transcription factor and is involved in its activation by tyrosine phosphorylation and nuclear translocation which allows the regulation of gene expression (Togi et al. 2016). The presumed role of RP2 in this pathway would be to shut down STAT3 activation by ARL3-GTP through GTP hydrolysis. Interestingly, a recent study has established STAT3 as a cell-autonomous neuroprotective factor in mouse models of retinal degeneration (Jiang et al. 2014).



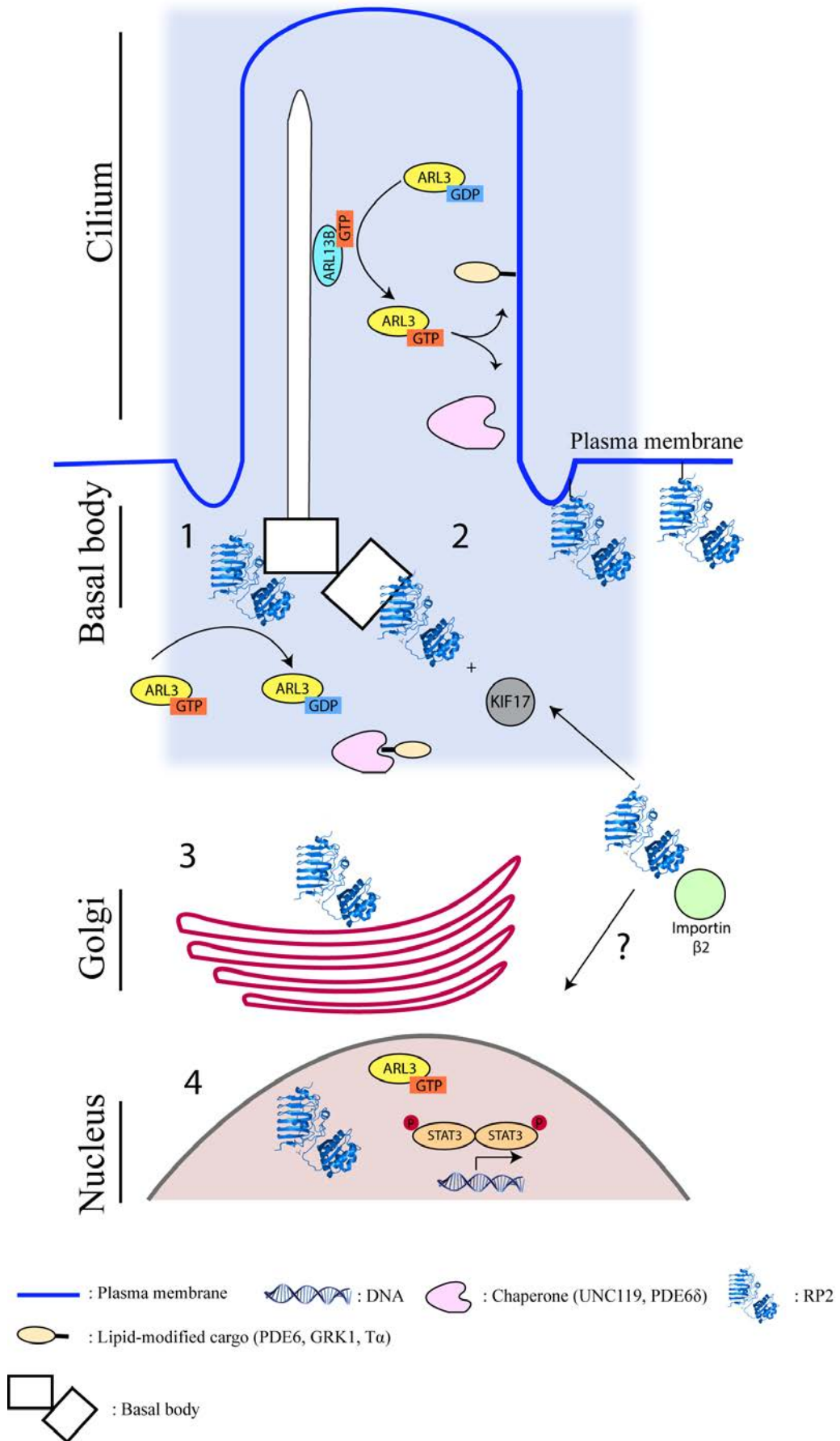


**Figure 1.2. A schematic summary of the suggested roles of RP2 and ARL3 in the cell (numbers 1-4) and their localisation.**

While many of the suggested roles of RP2 and ARL3 have been based on studies using cultured cells forming primary cilia, they are likely applicable to the photoreceptors as well. Pools of RP2 have been detected at the periciliary ridge and the basal body of the primary and the connecting cilium (CC), the Golgi complex (Evans et al. 2010) and the plasma membrane (Grayson et al. 2002) (anchored thanks to dual lipid modification) of vertebrate photoreceptors and other cell types. In cultured cells, RP2 has also been detected in the nucleus (Yoon et al. 2006) and the axoneme of the primary cilium (Hurd et al. 2010, Schwarz et al. 2017). RP2 interacts with Importin- $\beta$ 2 which assists trafficking to the cilium (Hurd et al. 2011) and potentially to the nucleus as well. 1) ARL3-GTP displaces lipid-modified cargo (such as prenylated GRK1, PDE6, or acylated T $\alpha$ ) from retinal chaperones UNC119 and PDE6 $\delta$  within the ciliary axoneme. RP2 activity at the basal body and possibly other cellular locations prevents ARL3 from acting as a displacement factor in the wrong locations (Zhang et al. 2015, Gotthardt et al. 2015). 2) RP2 interacts with the molecular motor KIF17 (and KIF7, not shown in this figure) and regulates its localisation to the ciliary tip (Schwarz et al. 2017). RP2 and KIF17 have both been found at the basal body of photoreceptors, but the exact location of the interaction is not established yet. 3) RP2 is localised to the Golgi and is essential for Golgi cohesion as well as Golgi-to-cilium vesicle transport of proteins such as IFT20 (Evans et al. 2010). 4) ARL3-GTP directly interacts with transcription factor STAT3 and regulates its activation and nuclear translocation (Togi et al. 2016). The exact location of the interaction is not known.

#### **1.4 Questions and aims of the thesis**

The function of RP2 in protein transport pathways to and within the ciliary apparatus is established and well characterised, although the discrepancies among animal studies regarding the identity of the transported cargo mean that the relationship between protein mislocalisation and disease is still obscure. Similarly, the importance of the RP2-ARL3 complex in RP is well established, not only because pathogenic RP2 mutations exist which specifically destabilise the interaction (Kuhnel et al. 2006) but also since ARL3 itself has been identified as a retinal degeneration gene (Strom et al. 2016).

On the contrary, much fewer studies have focused on other roles that RP2 might have outside the cilium. For example, RP2 displays a uniform plasma membrane localisation and has been reported to localise to the nucleus, but its role in these

compartments is not clear. Moreover, it is not known if the RP2-ARL3 interaction is exclusively relevant for the disease, or if other RP2 interactions also play a role. A whole domain on RP2 protein (the C-terminal domain) is still devoid of functional significance, although studies have often speculated that it forms the interface for unknown protein-protein interactions (Liu et al. 2017a). Lastly, modes of RP2 regulation, such as post-translational modifications, have not yet been investigated, except for the well-known lipid modifications of the N-terminus. Answering these questions will undoubtedly contribute to the development of a safe and efficient therapeutic option for patients with RP type 2. Another hallmark that would potentially contribute to the development of a –pharmacological- treatment option would be the generation of a whole-organism platform that can be used for screening chemical compounds to identify modifiers of phenotypes caused by the lack of RP2.

My PhD had two main aims.

1. To identify novel functions and modes of regulation for RP2 via the characterisation of novel protein-protein interactions. In Chapters 3 and 4 of the present thesis, I describe the work conducted in order to achieve this aim. Chapter 3 refers to the characterisation of the novel interaction between RP2 and Osteoclast stimulating factor 1 (OSTF1), via mapping the interaction interface on the surface of RP2 and investigating the potential function of the complex in regulating tyrosine phosphorylation of RP2 and cell motility. Chapter 4 refers to the proteomic analysis of RP2 complexes in cultured cells and the verification of the DNA-dependent protein kinase (DNA PKcs) as a novel RP2 interaction partner. The interaction is then characterised by examining co-localisation in cultured cells, its potential effect on serine/threonine phosphorylation of RP2 and the involvement of RP2 in the cell's response to DNA double-stranded breaks.
2. To generate a genomic *rp2* null zebrafish (*Danio rerio*) model and examine if it presents with a retinal degeneration phenotype. The use of CRISPR (Clustered Regularly Interspaced Short Palindromic Repeats)/Cas9 for genome editing in zebrafish and the examination of retinal lamination in adult fish is described in Chapter 5.

## **Chapter 2: Materials and methods**

### **2.1 DNA methods**


#### **2.1.1 Agarose gel electrophoresis**

Nucleic acids were separated according to molecular weight by agarose gel electrophoresis. The gel was made by dissolving agarose (Ultrapure agarose, Invitrogen) in the appropriate buffer: 1% agarose in Tris-acetate-EDTA (TAE) buffer (40 mM Tris base, 20 mM acetic acid, 1 mM EDTA) was used for standard applications, while 2-3% agarose in Tris-borate-EDTA (TBE) buffer (89 mM Tris-base, 89 mM boric acid, 2 mM EDTA) was used for the separation of small DNA fragments (<100 bp). Agarose was fully dissolved in the buffer by heating in a microwave oven and then left to set in a cast with combs for the formation of wells, after mixing with 10% v/v SYBR Safe DNA gel stain for the visualization of DNA (ThermoFisher Scientific). DNA samples were mixed with blue gel loading dye (New England Biolabs), and loaded in the wells of the agarose gel. DNA ladders were loaded on the gel alongside DNA samples (according to the expected molecular weight of the DNA fragments, 1 kb, 100 bp or low molecular weight DNA ladders were used, from New England Biolabs). Voltage of 90-100 V was applied to mobilise the nucleic acids towards the positive electrode in an electrophoresis gel tank. Separated nucleic acids fragments were visualized and pictures were taken using a UV transilluminator (Biorad).

#### **2.1.2 PCR**

DNA amplification was conducted by polymerase chain reaction (PCR) using the Phusion High Fidelity PCR Mastermix (New England Biolabs). The reaction mix contained Phusion DNA Polymerase, deoxynucleotides and reaction buffer including MgCl<sub>2</sub> (all included in the Phusion Mastermix), 0.5 μM primers and DNA template (whose quantity varied according to the application), in a 20-50 μl total reaction volume. PCR reactions were carried out in a BioRad C1000 Touch thermal cycler. A

typical protocol is the following, although parameters like the annealing temperature and extension time were often changed to serve the specific application:

- Initial denaturation 3 minutes 98 °C
  - Denaturation 10 seconds 98 °C
  - Annealing 15 seconds 65 °C
  - Extension 10 seconds 72 °C
  - Final extension 5 minutes 72 °C
  - Hold 4 °C
- 
- X 30

### 2.1.3 Plasmid isolation from bacterial cultures

Isolation of plasmids from bacterial cultures was conducted using the mini-preps (for low-yield extraction) and midi-preps (for higher-yield extraction of plasmid to use in cell culture transfections) kits from Qiagen, following the manufacturer's instructions. Briefly, the outline of the procedure was the following: bacterial cells were lysed and the lysates were cleared by centrifugation. The lysates were loaded onto anion-exchange resin columns, where plasmid DNA selectively binds under appropriate low-salt and pH conditions. The next step involved washes with a medium-salt buffer to remove impurities (RNA, proteins etc). Finally, plasmid DNA was eluted from the columns with a high-salt buffer. During midi-preps, plasmid DNA was further concentrated and de-salted by isopropanol precipitation and washed in 70% ethanol. The DNA pellet was resuspended in TE buffer (10 mM Tris-HCl, 1 mM EDTA •Na<sub>2</sub>) or DNase/RNase-free water and kept at 4°C for immediate use or -20°C for long term storage.

#### **2.1.4 Genomic DNA isolation from zebrafish embryos and adult fish**

Genomic DNA was isolated from pooled embryos or adult fish fin clips using the DNA Release reagent (Nippon Genetics). Fin clips or 10-20 embryos were placed in micro-tubes and covered with 10-20  $\mu$ l of DNA Release. The tubes were placed in a thermal cycler and the following protocol was applied: 20 minutes at 65°C, 2 minutes at 96°C, 4 minutes at 65°C, 1 minute at 96°C, 1 minute at 65°C, 30 seconds at 96°C, 20°C hold. The supernatant contained the genomic DNA, which was kept at -20°C until use.

#### **2.1.5 DNA sequencing**

Sanger sequencing was conducted by the Institute of Genetics and Molecular Medicine (IGMM) core technical services using a 3730 genetic analyser (Applied Biosystems). Primers used for sequencing were either provided by the technical services (generic primers like T7 or M13) or designed and provided by me (listed in Table 2.1). Chromatograms were then analysed using SnapGene Viewer software (version 3.2.1, GSL Biotech).

#### **2.1.6 Site-directional mutagenesis**

Point mutations were introduced in the human RP2 coding sequence using QuikChange II Site-Directed Mutagenesis kit following the manufacturer's instructions. Briefly, pENTR/D-TOPO entry vector (Invitrogen) containing the wild-type human RP2 coding sequence was used as a template in PCR reaction using the high-fidelity PfuUltra DNA polymerase and primers specific for each mutation (primer sequences are found in Table 2.2). After the amplification reaction, the template containing WT RP2 was digested by Dpn I endonuclease which only cleaves methylated and hemi-methylated DNA. Finally, the mutated plasmids were transformed into competent DH5a competent *E. coli* cells by heat shock at 42°C and isolated using the Qiagen midi-preps plasmid isolation kit after propagation by the

bacteria. The existence of the correct insert was confirmed by Sanger sequencing.

To achieve expression of the constructs in mammalian cells, RP2 coding sequences were transferred into the destination vector pCDNA-DEST40 (Invitrogen), which added a C-terminal V5 tag to the construct, by recombination reaction using LR Clonase II (part of the Invitrogen Gateway cloning system).

### **2.1.7 Insertion of constructs into expression vectors by recombination**

Recombination was used to flip mutated RP2 coding sequences from pENTR/D-TOPO (Invitrogen) into mammalian expression vector pCDNA-DEST40-V5 (Invitrogen) and WT RP2 sequence from pENTR/D-TOPO into bacterial expression vector pGEX6P1-Dest-HIS (a gift from Dr Martin Reijns). 70 ng of expression vector were mixed with equal amount of the insert-containing entry vector and LR Clonase II (mix of proteins to catalyse recombination, isolated from  $\lambda$  bacteriophage and *E.coli*, from the Invitrogen Gateway system) in TE buffer (0.5 mM EDTA, 0.3 M NaCl, 50 mM Tris pH 7.5). After incubation for 1 hour at room temperature, Proteinase K (Invitrogen Gateway system) was added to digest the recombinases via incubation for 10 minutes at 37°C. The flip reaction was used to transform DH5a competent *E. coli* cells by heat shock at 42°C. The new plasmids were isolated using the Qiagen midi-preps plasmid isolation kit after being propagated by the bacteria. Plasmids were kept in TE buffer or purified water at -20°C for long term storage or 4°C for short-term storage and regular use.

### **2.1.8 Other cloning strategies**

#### Cloning guide RNA sequences into guide RNA expression vector

For the CRISPR/Cas9 strategy to target zebrafish *rp2* (Chapter 5), guide RNA (gRNA) sequences needed to be *in vitro* transcribed from a gRNA expression vector. Specific gRNA expression vectors were built by cloning a pair of annealed

oligonucleotides (each 26 nucleotides in length and specifically designed for ligation with sticky ends created by BsaI digestion) into a pDR274 vector (Addgene) that has been digested by BsaI endonuclease (New England Biolabs). Oligonucleotides corresponding to the 3 different gRNA sequences were ordered from Sigma-Aldrich (sequences can be found in Table 2.1). 100  $\mu$ M of top and bottom strand oligonucleotides were annealed together by heating at 95°C for 5 minutes in the appropriate annealing buffer (0.01 M Tris-HCl pH 7.5, 0.05 M NaCl, 1mM EDTA) and then slowly cooling down to room temperature. The vector was digested by BsaI in CutSmart buffer (New England Biolabs) for 1 hour at 37°C. After digestion, BsaI needed to be heat inactivated for 30 minutes at 65°C, in order to be released from the DNA. After dephosphorylation by Antarctic phosphatase (New England Biolabs) for 15 minutes at 37°C to prevent the vector from self-annealing, the linearized vector was purified using the Qiagen PCR column purification kit. 10 nM of annealed oligonucleotides were annealed with ~50 ng of linearized and purified pDR274 vector by incubating with 1  $\mu$ l of Quick ligase (New England Biolabs) for 15 minutes at room temperature. DH5a competent E. coli cells were transformed with the ligation mix by heat shock at 42°C. The presence of the correct insert was tested in plasmid DNA isolated from individual transformed colonies by Sanger sequencing using the M13 forward primer. Chosen colonies containing the correct insert were then propagated further, and high- quality plasmid DNA was isolated from them using the midi-preps plasmid isolation kit from Qiagen. These plasmids were further used as templates for the *in vitro* transcription of the gRNA sequences using a T7 promoter.

#### Cloning PCR products in pGEM-T to identify individual mutations in chimaeric animals

Founder fish, the animals that have been injected with CRISPR/Cas9 component RNAs targeting the *rp2* gene, are expected to be chimeric, i.e. different populations of cells will have different mutations or no mutations at all. To identify individual mutations by Sanger sequencing, the targeting site on the *rp2* gene was amplified from founder fish genomic DNA using Phusion High fidelity polymerase-based PCR (New England Biolabs). The PCR product was purified using the Qiagen PCR



column purification kit and poly(A) tailed by incubating with GoTaq Flexi polymerase (Promega) and dATP nucleotides for 30 minutes at 72°C. The addition of 3'A tail fragments to the PCR products aids ligation of one only insert into the vector compared to blunt-ended PCR products which can lead to multiple insertions. Subsequently, the PCR product was ligated into pGEM-T vector (Promega), via incubation with a T4 DNA ligase overnight at 4°C. The ligation reaction was used to transform OneShot TOP10 chemically competent *E. coli* cells (Invitrogen) by heat shock at 42°C. This strain of cells allows for blue/white screening of recombinant clones because of the lacZ deletion mutant (lacZ $\Delta$ M15) gene, by  $\alpha$ - complementation assay. For this reason, 40  $\mu$ g X-gal were plated on the agar plates before plating the transformed cells. Plasmid DNA was isolated from individual white colonies (=have internalised pGEM-T vector containing the insert of interest) and used as a template for Sanger sequencing using the T7 primer.

## **2.2 RNA methods**

### **2.2.1 Isolation of total RNA from human cells**

Total RNA was isolated from hTERT-RPE1 cells grown to confluency in 6-well plates, using the RNeasy Plus Mini kit (Qiagen). This kit preferentially isolates RNA molecules longer than 200 nucleotides, so the resulting sample is enriched in mRNA compared to smaller RNA species. To prepare the cell lysate, cells were harvested from their plate using trypsin. Cell pellet was lysed in RLT buffer with the addition of 40 mM DTT and applied through a Qias shredder column, which reduces viscosity and removes insoluble material (Qiagen), to homogenise. After centrifugation for 2 minutes at 13000 rpm, the flow through was applied on a gDNA eliminator column to remove genomic DNA, and centrifuged for 30 seconds at 10000 rpm. The lysate was then used for RNA isolation according to manufacturer's instructions. Briefly, it was mixed with equal volume of ACS-grade 70% ethanol to ensure appropriate binding conditions and applied on an RNeasy column where RNA molecules are selectively bound on silica-based membranes. After a series of washes to remove contaminants, RNA was eluted in RNase-free water in an RNase-free tube. After

concentration and purity of the generated RNA was estimated, it was aliquoted and stored at 80°C, until use. Freeze-thaw cycles were avoided as they could compromise the integrity of the RNA.

### **2.2.2 Isolation of total RNA from zebrafish embryos**

Total RNA was isolated from 30-40 embryos that were 3 days (post-fertilisation) old, using the RNeasy Plus Mini kit (Qiagen). To prepare the tissue lysate, embryos were released from the chorion manually, anaesthetised in Tricaine and then washed in distilled water. All liquid was removed. Subsequently, embryos were lysed in RLT buffer (Qiagen) with the addition of 40 mM DTT and the tissues were disrupted using pestle and mixer. The lysate was then applied to a Qias shredder homogeniser column, which reduces viscosity and removes insoluble material (Qiagen), and centrifuged for 2 minutes at 13000 rpm. To remove genomic DNA, the flow-through was applied to a gDNA eliminator column (Qiagen) and centrifuged for 30 seconds at 10000 rpm. The lysate was then mixed with 70% ethanol and RNA isolation proceeded as described above.

### **2.2.3 Quantification of nucleic acid concentration and estimation of quality**

The yield and purity of nucleic acids were estimated by measuring optical density at 260 nm using a NanoDrop ND-1000 spectrophotometer (NanoDrop Technologies). 260/280 and 260/230 absorbance ratios indicate the presence of contaminants and were used to assess the purity level of nucleic acids.

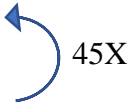
### **2.2.4 cDNA synthesis**

Total RNA isolated from RPE1 cells or zebrafish embryos was used as template to

synthesise cDNA using the Superscript First-strand synthesis system for RT-PCR (Invitrogen). At first, ~0.8-1 µg total RNA was annealed with oligo-dT primers. The mix was incubated with the reverse transcriptase, 5 mM MgCl<sub>2</sub>, 10 mM DTT and 40 units RNase OUT (Invitrogen) for 50 minutes at 42°C followed by 15 minutes at 70°C to terminate the reaction. The mix was finally incubated with RNase H for 20 minutes at 37°C, to digest the RNA template. Negative controls were processed alongside the samples: a control without any reverse transcriptase and one without any RNA template. cDNA was stored at -20°C for future use or used in downstream applications (RT-qPCR).

### **2.2.5 Reverse transcription quantitative real-time PCR (RT-qPCR)**

Primers specific to zebrafish *rp2* and to zebrafish *actb* (*β-actin*, reference gene) were designed so that assays were intron-spanning, to identify any amplification resulting from genomic DNA contamination in the samples. Primer sequences are found in Table 2.3. 1 µl of cDNA was used in a 20- µl reaction containing 0.2 µM primer mix and 10 µl SYBR Select Green Mastermix (ThermoFisher Scientific) in RNase/DNase- free water. SYBR Select mastermix contains Green ER dye, a fluorescence dye that binds to all double-stranded DNA molecules generated during PCR reaction. Assays were conducted in 96-well plates with opaque walls and each reaction was run in triplicates. The negative controls generated during the cDNA synthesis reaction (without RNA/ without reverse transcriptase) were also ran in qPCR reactions alongside the samples, and served to identify any contamination resulting in unspecific amplification. All qPCR experiments were run on a LightCycler 480 Instrument II (Roche) using the replicate methodology below for three biological replicates:

- Denaturation 2 minutes 95 °C
  - Denaturation 15 seconds 95 °C
  - Annealing/extension 15 seconds 56 °C
  - Extension 15 seconds 72 °C
- 

Amplification data were analysed using the LightCycler software (Roche). Only high-quality runs were chosen for further analysis based on the absence of any significant amplification in the negative controls and the amount of variation between the three replicates which is an indication of pipetting errors. Ct values (the number of cycles required to reach threshold fluorescence value upon amplification) were used to approximate the abundance of specific mRNA molecules in the samples and were normalized to the Ct values corresponding to the reference gene for the same cDNA template. Wild-type values were set arbitrarily to one and fold-change was calculated for the mutant samples based on the assumption that transcripts are doubled after each cycle. Melting curve analysis and agarose electrophoresis confirmed that the reactions produced single amplification products.

## **2.2.6 *In vitro* transcription**

### *In vitro* transcription of guide RNAs

gRNA sequences were first amplified from the gRNA expression vector in a PCR reaction using Phusion high fidelity DNA polymerase (New England Biolabs), mix of forward and reverse primers whose sequences are found in Table 2.1, and the gRNA expression vector as template. [60 annealing temp, 10 sec extension, x30 repeats] After a fraction of the PCR product was tested by electrophoresis on 3% agarose in TBE buffer gel, it was purified using the PCR column purification kit (Qiagen) and eluted in DNase/RNase-free water.

~1 µg of the PCR product was used as a template for *in vitro* transcription using the

Ambion MAXIscript T7 kit (Thermo Fisher Scientific). T7 phage RNA polymerase is used to catalyse the transcription step, which was conducted at room temperature for two hours. Subsequently, incubation with Turbo DNase at 37°C for 15 minutes served to digest the template DNA. The gRNAs were then purified using the SigmaSpin sequencing reaction cleanup kit (Sigma Aldrich). They were aliquoted and kept in RNase-free micro-tubes, at -80°C, until use.

#### *In vitro* transcription of nCas9 mRNA

For the CRISPR/Cas9 experiment targeting zebrafish *rp2*, Cas9 mRNA was synthesized from the pCS2-nCas9n vector (Addgene), which contains the coding sequence for a codon-optimised version of Cas9 nuclease that is more appropriate for genome editing in zebrafish (Jao, Wente and Chen 2013) and an SP6 promoter for *in vitro* transcription. First, the vector needed to be linearised in order to be used as template for the transcription reaction. Restriction digestion was conducted using the NotI-HF endonuclease (New England Biolabs), for 1.5 hours at 37°C in CutSmart buffer, followed by purification of the linear vector using the PCR column purification kit (Qiagen). The linearized vector (~370 ng) was used as a template to synthesize the nCas9 mRNA using the SP6 mMACHINE kit (Thermo Fisher Scientific), following manufacturer's instructions. This method serves to produce mRNA molecules that mimic most eukaryotic mRNAs *in vivo* thanks to the presence of a 7-methyl guanosine cap structure at the 5' end. After the transcription reaction and addition of the cap analog, the mRNA was purified using the RNAeasy kit (Qiagen), following the manufacturer's "RNA cleanup" protocol. Subsequently, E-PAP enzyme (E. coli Poly(A) polymerase) from the T7 mMACHINE Ultra kit (Thermo Fisher Scientific) was used to add a poly(A) tail to the mRNA molecules. After poly(A) tailing, the mRNA molecules were purified again as above using the RNAeasy kit (Qiagen) and eluted in RNase-free water. To test the poly(A) tailing reaction efficiency, fractions of the mRNA product pre-tailing and post-tailing were analysed by DNA electrophoresis in 1% agarose in TAE buffer gel (the poly(A)-tailed mRNA runs as a smear rather than one distinct band). Both the 5' cap analog and the poly(A) tail served to enhance stability of the mRNA molecules in the zebrafish zygote and boost translation efficiency, as they favour

correct initiation of protein synthesis. Synthesised nCas9 mRNA was aliquoted and stored in RNase-free micro-tubes at -80°C.

**Table 2.1. List of primers and oligonucleotides used for the generation of an *rp2* null zebrafish model by CRISPR/Cas9 (Chapter 5).**

The sequence of all primers and oligonucleotides used for PCR-based applications or cloning purposes are listed here, together with their specific application and the company that they were ordered from.

<b>NAME</b>	<b>APPLICATION</b>	<b>SEQUENCE (5'-3')</b>	<b>COMPANY</b>
gRNA-DR274F	Amplifying gRNA sequence from pDR274	AACAGCTATGACATCAAGC TGACTAG	Sigma-Aldrich
gRNA-DR274R	Amplifying gRNA sequence from pDR274	AAAAGCACGACTCGGTGC	Sigma-Aldrich
zfRP2crispr1seqF	Sequencing rp2 to check for indels-gRNA1	AGAGCAAAGATCGGCAATC A	Sigma-Aldrich
zfRP2crispr1seqR	Sequencing rp2 to check for indels-gRNA1	CGGCAGTTCACACAGTCAT C	Sigma-Aldrich
zfRP2crispr2seqF	Sequencing rp2 to check for indels-gRNA2	CTGAGCTGGCTTTCCACTTT	Sigma-Aldrich
zfRP2crispr2seqR	Sequencing rp2 to check for indels-gRNA2	CGGCTCCCTTTAGTCAGAG G	Sigma-Aldrich
zfRP2revseq3	Sequencing rp2 to check for indels-gRNA3	GGAAGTCTGACAGGCCA	Sigma-Aldrich
zfRP2crispr1TOP	Cloning gRNA1 into pDR274	[P]TAGGCCTCAAGAATGAG ACCGT	Sigma-Aldrich
zfRP2crispr1BOT	Cloning gRNA1 into pDR274	[P]AAACACGGTCTCATTCTT GAGG	Sigma-Aldrich

zfRP2crispr2TOP	Cloning gRNA2 into pDR274	[P]TAGGACAACAGCATCCT CTGGC	Sigma-Aldrich
zfRP2crispr2BOT	Cloning gRNA2 into pDR274	[P]AAACGCCAGAGGATGCT GTTGT	Sigma-Aldrich
zfRP2crispr3top	Cloning gRNA3 into pDR274	[P]TAGGTTCGGCAACTATT ACCATCG	Sigma-Aldrich
zfRP2crispr3bot	Cloning gRNA3 into pDR274	[P]AAACCGATGGTAATAGT TGCCGAA	Sigma-Aldrich



**Table 2.2. List of primers used in the RP2 site-directed mutagenesis experiments (Chapters 3 and 4).**

The sequence of all primers used for the PCR-based generation of RP2 constructs with missense mutations are listed here, together with their specific application and the company that they were ordered from.

<b>NAME</b>	<b>APPLICATION</b>	<b>SEQUENCE (5'-3')</b>	<b>COMPANY</b>
Y27ATOP	Site-directed mutagenesis	GAGCGGCCAAAGCAGGCCAGCTG GGATCAGCG	Sigma-Aldrich
Y27ABOT	Site-directed mutagenesis	CGCTGATCCCAGCTGGCCTGCTTT GGCCGCTC	Sigma-Aldrich
Y40ATOP	Site-directed mutagenesis	CCTTCAGTCCACTGAACATGGCGT CTTTTGGATCAACCTTCT	Sigma-Aldrich
Y40ABOT	Site-directed mutagenesis	AGAAGGTTGATCCAAAAGACGCC ATGTTCACTGGACTGAAGG	Sigma-Aldrich
K160ATOP	Site-directed mutagenesis	AAGATACTTAGCCCTGCATCTGCG AACTGGAAAGCTAATTCAGG	Sigma-Aldrich
K160ABOT	Site-directed mutagenesis	CCTGAATTAGCTTTCCAGTTCGCA GATGCAGGGCTAAGTATCTT	Sigma-Aldrich
E154ATOP	Site-directed mutagenesis	CATCTTTGAACTGGAAAGCTAATG CAGGATAGTACCATTGAAAACAT	Sigma-Aldrich
E154ABOT	Site-directed mutagenesis	ATGTTTTCAATGGTACTATCCTGC ATTAGCTTTCCAGTTCAAAGATG	Sigma-Aldrich
Y27FTOP	Site-directed mutagenesis	GCGGCCAAAGCAGTTCAGCTGGG ATCAGC	Sigma-Aldrich
Y27FBOT	Site-directed mutagenesis	GCTGATCCCAGCTGAACTGCTTTG GCCGC	Sigma-Aldrich
E205ATOP	Site-directed mutagenesis	TCCTATACCTACTACCGCAGAGCT CAAAGCTGTTC	Sigma-Aldrich

E205ABOT	Site-directed mutagenesis	GAACAGCTTTGAGCTCTGCGGTA GTAGGTATAGGA	Sigma-Aldrich
E206ATOP	Site-directed mutagenesis	TATACCTACTACCGAAGCGCTCAA AGCTGTTTCGTG	Sigma-Aldrich
E206ABOT	Site-directed mutagenesis	CACGAACAGCTTTGAGCGCTTCG GTAGTAGGTATA	Sigma-Aldrich
Y245ATOP	Site-directed mutagenesis	GCTTAGTGGTATTATTTGCTGGTG ATGCCACTATTGCAAATGCCAGA AAAC	Sigma-Aldrich
Y245ABOT	Site-directed mutagenesis	GTTTTCTGGCATTGCAATAGTGG CATCACCAGCAAATAATACCACT AAGC	Sigma-Aldrich
Y245ETOP	Site-directed mutagenesis	GCTTAGTGGTATTATTTGCTGGTG ATGAGACTATTGCAAATGCCAGA AAA	Sigma-Aldrich
Y245EBOT	Site-directed mutagenesis	TTTTCTGGCATTGCAATAGTCTC ATCACCAGCAAATAATACCACTA AGC	Sigma-Aldrich
K208ATOP	Site-directed mutagenesis	CCTACTACCGAAGAGCTCGCAGC TGTTTCGTGTTCCAC	Sigma-Aldrich
K208ABOT	Site-directed mutagenesis	GTGGAAACACGAACAGCTGCGAG CTCTTCGGTAGTAGG	Sigma-Aldrich
R218STOP	Site-directed mutagenesis	TTCCACAGAAGCCAATAGCAGC ATTGTTCCAATATCCC	Sigma-Aldrich
R218SBOT	Site-directed mutagenesis	GGGATATTGGAACAATGCTGCTA TTGGCTTCTGTGGAAA	Sigma-Aldrich
S213ATOP	Site-directed mutagenesis	CTCAAAGCTGTTTCGTGTTGCCACA GAAGCCAATAG	Sigma-Aldrich

S213ABOT	Site-directed mutagenesis	CTATTGGCTTCTGTGGCAACACGA ACAGCTTTGAG	Sigma-Aldrich
E215ATOP	Site-directed mutagenesis	CTGTTTCGTGTTTCCACAGCAGCCA ATAGAAGCATTGT	Sigma-Aldrich
E215ABOT	Site-directed mutagenesis	ACAATGCTTCTATTGGCTGCTGTG GAAACACGAACAG	Sigma-Aldrich
E256ATOP	Site-directed mutagenesis	AAGCCTTTACCAACCATCGCATCA ATTAG	Integrated DNA Technologies (IDT)
E256ABOT	Site-directed mutagenesis	GCAAATGCCAGAAAATAATTGA TGCGA	IDT
K160ETOP	Site-directed mutagenesis	CCTGAATTAGCTTTCCAGTTCGAG GATGC	IDT
K160EBOT	Site-directed mutagenesis	GAAGATACTTAGCCCTGCATCCTC GAACT	IDT
K252ATOP	Site-directed mutagenesis	GGTGATTACACTATTGCAAATGCC AGAG	IDT
K252ABOT	Site-directed mutagenesis	CCAACCATCTCATCAATTAGTGCT CTGGC	IDT
D255ATOP	Site-directed mutagenesis	CTATTGCAAATGCCAGAAAATA ATTGCT	IDT
D255ABOT	Site-directed mutagenesis	CCTTTACCAACCATCTCAGCAATT AGTTT	IDT

**Table 2.3. List of primers used in real-time qPCR experiments (Chapters 3 and 5).**

The sequence of all primers used in real-time qPCR are listed here, together with their specific application and the company of origin.

<b>NAME</b>	<b>APPLICATION</b>	<b>SEQUENCE (5'-3')</b>	<b>COMPANY</b>
ZebACTINBqpcrF	Zebrafish <i>actb</i> primers	CAGCCGAAAGAGAAATTG TCC	IDT
ZebACTINBqpcrR	Zebrafish <i>actb</i> primers	GATACCGCAAGATTCCATA CC	IDT
RT QPCR 3F	Zebrafish <i>rp2</i> primers exons 4-5	AGACTAAAGAGGTTTCCAT GCG	IDT
RT QPCR 3R	Zebrafish <i>rp2</i> primers exons 4-5	TGGCAAAGGATCGACACG	IDT
RT QPCR 1F	Zebrafish <i>rp2</i> primers exons 1-2	GCTGGGACAAACGAGAAA AG	IDT
RT QPCR 1R	Zebrafish <i>rp2</i> primers exons 1-2	GTTACAGTTTTCGCAGTCC TG	IDT
zebRP2qpcrF	Zebrafish <i>rp2</i> primers exons 2-3	GTCTGTTTGTGTTCTTCGCT G	IDT
zebRP2qpcrR	Zebrafish <i>rp2</i> primers exons 2-3	TTATTCTGGAACACTCGGC TC	IDT
hRP2qpcrF	Human <i>RP2</i> primers	GCAAATGCCAGAAAATA ATTGATG	IDT
hRP2qpcrR	Human <i>RP2</i> primers	CAGGACCTTTGTTTCAGAAG AGG	IDT

## **2.3 Protein and Proteomics methods**

### **2.3.1 Protein isolation from human cells, zebrafish and mouse tissues**

Cell pellets, fresh or snap frozen tissues or zebrafish embryos were lysed for 20 minutes in appropriate volumes of a lysis buffer on ice (see Table 2.4 for the compositions). 1 mM PMSF, Protease and phosphatase inhibitor cocktails (Sigma-Aldrich) were added to all lysis buffers just prior to use; tyrosine phosphatase inhibitor sodium orthovanadate ( $\text{Na}_3\text{VO}_4$  1 mM, Alfa Aesar) was also added when examining tyrosine phosphorylation of RP2. Homogenisation using mixer and pestles was employed to aid lysis of tissues. Low-power sonication (3 times for 30 seconds) was used when lysing zebrafish eyeballs. Subsequently, lysates were clarified by centrifugation at 13,000 rpm for 10 minutes at 4°C. The clarification step was repeated twice for mouse tissues. The supernatant was then moved to a new tube and was used immediately or transferred to -80°C for future use.

**Table 2.4. List of buffers that were used for protein isolation.**

The composition of different lysis buffers used for total protein isolation from cells and tissues. Isolated proteins were then used in downstream applications such as pulldown assays, immunoprecipitations (IPs) and western blotting.

<b>LYSIS BUFFER</b>	<b>COMPOSITION</b>	<b>APPLICATIONS</b>
RIPA	50 mM Tris-HCl pH 7.5, 150 mM NaCl, 1 mM EDTA, 1% NP40, 0.1% SDS, 0.5% sodium deoxycholate	<ul style="list-style-type: none"> <li>• Lysis of zebrafish eyeballs for western blot</li> <li>• Lysis of HEK293T cells for RP2-V5 IP designed to detect tyrosine or serine/threonine phosphorylation</li> <li>• Lysis of RPE1 cells to detect RP2 expression levels after X-ray treatment</li> </ul>
Triton lysis buffer	50 mM Tris-HCl pH 7.5, 150 mM NaCl, 1% Triton x100	<ul style="list-style-type: none"> <li>• Lysis of mouse brain tissues for western blot</li> <li>• Lysis of HEK293T and RPE1 cells for RP2-V5/RP2-FLAG and DNA PKcs co-IPs</li> <li>• Lysis of HEK293T cells for RP2-V5 IPs for mass spectrometry</li> <li>• Lysis of HEK293T cells for DNA PKcs and RP2 endogenous co-IPs</li> </ul>

IP lysis buffer	25 mM Tris-HCl pH 7.5, 150 mM NaCl, 1 mM EDTA, 1% NP40, 5% glycerol	• Lysis of HEK293T cells for OSTF1/ARL3 Q71L-GST pulldowns
Co-IP lysis buffer	50 mM Tris-HCl pH 7.5, 150mM NaCl, 0.1 mM EGTA, 2 mM MgCl <sub>2</sub> , 1% Triton X-100, 10% glycerol	• Lysis of RPE1 cells for ARL3 Q71L-FLAG and RP2, DNA PKcs co-IPs

### 2.3.2 Quantification of protein concentration

Protein concentration of lysates was determined using the Biorad DC assay, as per manufacturers' instructions. Dc is a colorimetric assay based on the reaction of the proteins with an alkaline copper tartrate solution and Folin reagent which leads to color development. 20 µl of reagent S were mixed with 1 ml of reagent A to produce A' solution. 125 µl of A' was then mixed with 2 µl of protein sample in a cuvette. Finally, 1 ml of reagent B was added. After mixing well and incubating for 5 minutes at room temperature, colorimetric readings were recorded by measuring absorbance at 750 nm using the BioMate 3 Spectrophotometer (ThermoFisher Scientific). A BSA (bovine serum albumin) reference curve that was always made on the day was used to estimate protein concentration based on the colorimetric readings.

### 2.3.3 Protein separation by SDS-PAGE

Proteins were separated by their molecular weight by SDS-polyacrylamide gel electrophoresis (PAGE) on 4-12% Bis-tris (for standard molecular weight proteins) or 3-8% Tris-acetate (for high molecular weight proteins) pre-cast acrylamide gels (NuPage Novex, Life Technologies), which were inserted in an XCell SureLock electrophoresis chamber (Life Technologies). Before loading on the gel, protein samples were reduced and denatured by the addition of 0.25 volume of NuPage LDS buffer and 0.05 M DTT, and subsequent heating at 70°C for 10 minutes. As a molecular weight marker, 5 µl of Broad Range Color Protein Standard were loaded

alongside the protein samples (New England Biolabs). The protein-loaded gels were run in MOPS (for 4-12% gels) or Tris-acetate buffer (for 3-8% gels) supplied with antioxidant (Life Technologies), by applying 150V for 60-70 minutes until satisfactory electrophoretic separation was achieved.

### **2.3.4 Western blotting**

Proteins that were separated by SDS-PAGE were then transferred onto polyvinylidene fluoride (PVDF) or nitrocellulose membranes (0.45  $\mu\text{m}$  pores, Amersham GE Healthcare) by semi-dry transfer (for standard molecular weight proteins) or wet transfer methods (for very high molecular weight proteins). In both cases, transfer was carried out in Towbin transfer buffer (0.25 M Tris base, 1.92 M glycine, 20% methanol, pH was fixed to 8.1-8.5). For semi-dry transfer, the gel containing the resolved proteins was “sandwiched” with the activated and equilibrated wet membrane between two stacks of three pieces of wet paper each, and inserted into the BioRad Trans-Blot Turbo Transfer system where voltage of 25 V was applied for 30 minutes. For wet transfer, the gel containing the resolved proteins was “sandwiched” with the activated and equilibrated wet membrane between two stacks of three pieces of wet paper each and two sponges and inserted into a cassette that kept the sandwich firmly together. The cassette was then inserted into an electrophoresis chamber filled with transfer buffer and 100 V were applied for 90 minutes in the cold room. An ice pack was also inserted in the chamber to prevent overheating. After transfer was over, transfer success as well as equal loading in all lanes were confirmed by staining the membrane with Ponceau S (Sigma-Aldrich). After removing Ponceau S by TBS washes, the membrane was ready for the blocking stage which was carried out on an orbital shaker at room temperature for 1 hour or overnight in the cold room, in TBS- 0.05%Tween20- 5% dried skimmed milk or in Superblock (ThermoFisher Scientific) if the primary antibody ought to recognize phosphorylated proteins. Primary antibody incubation was similarly carried out on an orbital shaker at room temperature for 1 hour or overnight in the cold room, in blocking buffer. A list of the antibodies used and their



respective dilutions can be found in Table 2.5. This was followed by extensive washes and incubation with horseradish peroxidase (HRP)-conjugated secondary antibodies or Clean Blot reagent for 1 hour at room temperature in blocking buffer. After extensive washes in TBS- 0.05% Tween20 and one last wash in TBS to remove the detergent, protein band detection was achieved by incubating the membrane in Pierce ECL chemiluminescent substrate (Thermo Fisher Scientific) or Pierce ECL Plus for detection of low-abundance signal. The membrane was then inserted in a dark-room cassette and exposed onto a photographic film (Amersham Hyperfilm ECL by GE Healthcare) which was then developed in a medical film processor (SRX 101A, Konica) to visualize the bands.

When needed, the intensity of the protein bands was estimated by densitometry measurements using the “plot gel lanes” feature of Fiji software. Measurements for the protein of interest were normalized to the corresponding measurements for the loading controls ( $\beta$ -actin blots or Ponceau stains for the Glutathione-S-transferase (GST)-tagged proteins that were used as baits for pulldowns). The result was expressed as fold-change compared to the value of one of the samples that was set to 1. This quantification was used as a proxy to estimate protein abundance between the samples. The amount of variation between the samples was expressed as the standard error of the mean (SEM) and t-tests were carried out to estimate significance based on three independent biological repeats of the experiment.

**Table 2.5. List of antibodies or antibody-conjugated resins.**

The antibodies used during the present thesis for western blotting (WB), immunofluorescence (IF) and immunoprecipitation (IP) purposes are listed below, together with the specific dilutions in blocking buffer or the amount used per mg of total protein for immunoprecipitation, and the companies of origin.

<b>ANTIBODY</b>	<b>HOST SPECIES</b>	<b>COMPANY</b>	<b>DILUTION (WB)</b>	<b>DILUTION (IF)</b>	<b>DILUTION (IP)</b>
Monoclonal anti-V5 (R960-25)	Mouse	Life technologies/ Invitrogen	1 in 5000	1 in 1000	
Monoclonal anti-phosphotyrosine clone 4G10 (05-321)	Mouse	Millipore	1 in 1000		
Polyclonal anti-SRC (#2108)	Rabbit	Cell Signaling	1 in 1000		
Monoclonal anti-His tag (#2366)	Mouse	Cell Signaling	1 in 500		
Polyclonal anti-phospho S/T ATM/ATR substrate motif (#2851)	Rabbit	Cell Signaling	1 in 1000		
Polyclonal anti-RP2 (HPA000234)	Rabbit	Sigma Aldrich	1 in 1000		
Monoclonal anti-DNA PK, clone Y393 (ab32566)	Rabbit	Abcam	1 in 1000	1 in 100	
Monoclonal anti-Ku80 (611360)	Mouse	BD transduction laboratories	1 in 1000		
Monoclonal anti-phospho-Histone H2AX(Ser139), clone JBW301 (#05-636)	Mouse	Millipore		1 in 800	

Polyclonal anti-eGFP tag (#CAB4211)	Rabbit	ThermoFisher Scientific	1 in 1000	
Polyclonal anti-OSTF1 (A303-004A)	Rabbit	Bethyl laboratories	1 in 10000	
Monoclonal anti- $\beta$ actin, clone AC-74 (A2228)	Mouse	Sigma-Aldrich	1 in 5000 (zebrafish) 1 in 10000 (human cells)	
Monoclonal anti-histone H3 (10779)	Mouse	Abcam	1 in 1000	
Polyclonal anti-histone H2BB (GTX61374)	Rabbit	GeneTex	1 in 2000	
Monoclonal anti-DNA PKcs, clone 25-4 (#MA5-13244)	Mouse	ThermoFisher scientific		2 $\mu$ g/2 mg total lysate protein
Monoclonal anti-GAPDH, clone 14C10 (#2118)	Rabbit	Cell Signaling	1 in 5000	
Cleanblot IP detection reagent (21230)		ThermoFisher Scientific	1 in 500 to 1000	
Polyclonal anti-RP2	Rabbit	Custom-made	1 in 2000	
Polyclonal anti-Integrin $\beta$ 1 (AB1952)	Rabbit	Millipore	1 in 500	
Monoclonal anti-FLAG (#14793)	Rabbit	Cell Signaling	1 in 2000	
EZ View red anti-FLAG affinity gel (F2426)	Mouse	Sigma-Aldrich		5 $\mu$ l/mg total lysate protein

Anti-mouse and anti-rabbit IgG, HRP-conjugated (#31430, 31460)	Goat	ThermoFisher Scientific	1 in 2000
Anti-mouse and anti-rabbit IgG, Alexa Fluor 594-conjugated (#A-11032, #R37117)	Goat	ThermoFisher Scientific	1 in 2000
Anti-mouse and anti-rabbit IgG, Alexa Fluor 488-conjugated (#32723, #A-11034)	Goat	ThermoFisher Scientific	1 in 2000

### 2.3.5 Stripping membranes

In order to re-probe PVDF membranes for a loading control (V5 or  $\beta$ -actin), primary and secondary antibodies were removed by incubating the membrane in a mild stripping buffer (0.2 M glycine, 0.1% SDS, 0.1% Tween20, pH adjusted to 2.2), twice for 5-10 minutes. The membrane was then washed rigorously several times with PBS and TBS-T before proceeding to the blocking stage.

### 2.3.6 Production and purification of recombinant proteins

For the generation of GST-ARL3 Q71L, GST-OSTF1 and RP2-His recombinant proteins, competent BL21 DE3 *E. coli* cells (Agilent technologies) were transformed by heat shock at 42°C with pGEX4T3 vectors (GE Healthcare) containing the OSTF1 and ARL3 Q71L cDNAs or a modified pGEX6P1vector containing human RP2 cDNA. The pGEX4T3 added an N-terminal GST tag sequence to the constructs. The destination vector for the RP2 construct was a gift from Dr Martin Reijns who modified the pGEX6P1vector to add a C-terminal His tag to the construct, in

addition to the pre-existing N-terminal GST tag. Individual transformed colonies were grown in a shaking incubator at 37°C in liquid broth (LB) supplemented with 50 µg/ml ampicillin, overnight. On the next day, 10 ml of the culture were transferred into fresh LB with 25 µg/ml ampicillin and incubated at 37°C until the optical density of the culture at 600 nm (OD600) reached appropriate levels. Isopropyl β-D-1-thiogalactopyranoside (IPTG) was then added for 4 hours to induce expression of the recombinant protein. After the induction, bacteria were separated from the medium by centrifugation and cell lysis was conducted by incubation with 4 mM DTT, 1 mg/ml chicken lysozyme (Sigma Aldrich), 0.2% NP40 and the addition of PMSF protease inhibitor. Genomic DNA was fragmented by passing the mixture through a small needle several times. Desired recombinant proteins were found at the supernatant after centrifugation at 20,000 g for 20 minutes at 4°C.

GST-tagged recombinant proteins were purified by immobilisation on glutathione-sepharose bead slurry (GE Healthcare).

The presence of the recombinant proteins in the lysates was confirmed by analyzing samples from different steps of the procedure by SDS-PAGE on 4-12% NuPage gels (Life Technologies), alongside BSA standard for roughly estimating protein concentration. The gel was then stained with Coomassie Brilliant Blue.

While GST-tagged OSTF1 and ARL3 remained bound on the bead slurry for the pulldown assays, RP2-His needed to be released from the beads to be used in the kinase assays. To achieve this, the GST tag was cleaved off the protein by incubation with Precision Protease (Sigma Aldrich) for 4 hrs at 4°C. Beads were pelleted down and protein remained at the supernatant, while incubation with fresh beads was employed to remove the protease and any residual GST. Buffer exchange and concentration of the recombinant RP2-His protein was conducted using Corning Spin-X UF concentrator columns.

Recombinant proteins were aliquoted and stored in PBS with 10% glycerol and 1 mM DTT at -80°C.

### **2.3.7 Kinase assays**

#### RP2-SRC kinase assay

Recombinant His-tagged human RP2 (0.8 µg) was mixed with different quantities of recombinant GST-tagged human SRC (Precisio kinase Sigma-Aldrich) (100, 200, 400 ng corresponding to 11, 22 and 44 u) and 2 mM ATP (Thermo Scientific) in the appropriate kinase buffer (25 mM MOPS pH 7.2, 12.5 mM glycerol-2-phosphate, 20 mM MgCl<sub>2</sub>, 12.5 mM MnCl<sub>2</sub>, 5 mM EGTA, 2 mM EDTA, 0.25 mM DTT added just prior to use) and incubated for 15 minutes at 30°C. SRC was diluted in the reaction buffer supplemented with 0.04 mg/ml BSA. The reaction was stopped by the addition of LDS sample buffer (NuPage, Life Technologies) / DTT and the mixture was heated at 70°C for 10 minutes to prepare for SDS-PAGE.

#### RP2-DNA PKcs kinase assay

The Promega DNA PK kinase enzyme system was used which contained the reaction buffer, activation buffer and DNA PK. 100 u of human DNA PK purified from HeLa cells and diluted in 0.1 mg/ml BSA and reaction buffer was mixed with 1 µg of recombinant human RP2-His, 2 mM ATP, Activation buffer (100 µg/ml calf thymus DNA), 1 mM PMSF, phosphatase inhibitor cocktail and 2 mM ATP (Thermo Scientific) in the appropriate reaction buffer (50 mM HEPES pH 7.5, 100 mM KCl, 10 mM MgCl<sub>2</sub>, 0.2 mM EGTA, 0.1 mM EDTA, 1 mM DTT). The mix was incubated for 60 minutes at 30°C. The reaction was either stopped by the addition of LDS sample buffer and DTT, followed by incubation at 70°C for 10 minutes to prepare for SDS-PAGE, or snap-frozen at -80°C for subsequent mass spectrometry analysis.

### **2.3.8 Immunoprecipitations**

Immunoprecipitations (IPs) were performed using cell lysates. V5 IPs with the aim to isolate RP2-V5 and assess phosphorylation were conducted in radioimmunoprecipitation assay (RIPA) buffer cell lysates. 10 µl V5 beads (Sigma-

Aldrich) were incubated with 2-3 mg of total lysate protein for 1 hr on a rotator at 4°C. V5 and FLAG IPs aiming to co-IP RP2-V5 and DNA PKcs and other interaction partners were conducted in Triton lysis buffer lysates. Endogenous DNA PKcs-RP2 co-IPs were conducted in Triton lysis buffer lysates. 2 µg of mouse anti-DNA PKcs antibody (Thermo Scientific, clone 25-4) per 2 mg total lysate protein was incubated with the cell lysate overnight on a rotator at 4°C. A mouse-derived, isotype-matched (IgG2a) antibody was used at equal amounts for IP as the negative control. On the next day, 20 µl protein A-sepharose beads (Abcam) were added for 1 hour at 4°C to collect the antibody-protein complexes. ARL3 Q71L-FLAG IPs aiming to co-precipitate RP2 and DNA PKcs were conducted in Co-IP lysis buffer. 5 µl of EZ View red anti-FLAG M2 agarose affinity gel beads (Sigma-Aldrich) were incubated with ~1 mg of total lysate protein for 2 hours on a rotator at 4°C. After incubation with the antibodies, extensive washes followed in all cases in the respective lysis buffer in order to minimize non-specific protein binding. After washing, the beads were collected at the bottom of the tube by brief centrifugation, immunocomplexes were eluted off the beads by the addition of LDS buffer (NuPage, Life Technologies) / DTT and resolved by SDS-PAGE. Resolved protein mixes were then subjected to western blotting.

### **2.3.9 Pulldown assays**

Fresh HEK293T cell lysates in IP lysis buffer supplemented with 1 mM PMSF, phosphatase and protease inhibitor cocktails were used for the GST pulldown assays, after keeping 10-20% of total protein separately as inputs. GST pulldown assays were conducted in IP lysis buffer by incubating 0.7-1 mg of total cell lysate protein with ~10 µg of GST-tagged protein bound on glutathione-sepharose beads (GST-OSTF1, GST-ARL3 Q71L or RP2-GST) for 2 hours at 4°C under continuous rotation. After the end of the incubation, 10 µl of washed unbound glutathione-sepharose beads (GE Healthcare) were added to the mix to make the bead pellet visible. The bead-bound GST protein complexes were washed at least three times in lysis buffer to remove non-specifically bound proteins. In the end, beads were

collected at the bottom of the tube by brief centrifugation and the GST complexes were eluted off the beads by the addition of LDS buffer (NuPage, Life Technologies) / DTT and resolved by SDS-PAGE. Resolved protein mixes were then subjected to western blotting.

### **2.3.10 Mass spectrometry**

Immunocomplexes concentrated on agarose beads or kinase assay mixes were processed to generate tryptic peptides for mass spectrometry (MS) analysis in the IGMM MS facility, where all subsequent workflow was conducted by Dr Jimi Wills-Bukowski and Dr Alex von Kriegsheim. Resulting peptides were processed for HPLC and tandem MS in a Thermo Scientific 3000 RSLC Nano liquid chromatography system coupled to QExactive Plus mass spectrometer. All samples were analysed in two technical repeats; RP2-V5 interactome analysis was also analysed in three biological repeats. Data were processed in MaxQuant software version 1.5.3.17 (Cox and Mann 2008), searching against Uniprot human reference proteome (UP000005640\_9606, release 2015\_12) using Andromeda search engine (version 1.5.6.0). False discovery rate was set to 0.05 for peptides/post-translational modifications and 0.01 for protein identification. Normalized label-free quantification (LFQ) values were generated with match-between-runs enabled, and used in downstream analysis as described in chapter 4. Initial analysis and quality control was performed with R version 3.2.3 (2015-12-10). The above workflow corresponds to the RP2-DNA PK kinase assay experiment and the proteomic analysis of RP2-V5 IPs (Chapter 4: Figure 4.2, Figure 4.7).

For the identification of RP2 Y27 phosphorylation (Chapter 3: Figure 3.5), data were processed in Peaks software version 7.0.1 (Bioinformatics solutions Inc.), searching against the current Uniprot human proteome dataset (08/2013 version) using Mascot (2.4.0) and X!Tandem (2010.12.01.1) search engines. Scaffold software (version 4.3.4, Proteome Software Inc., Portland, OR) was used to validate MS/MS based peptide and protein identifications with a false discovery rate of 0.05 for peptides and 0.01 for proteins.



### 2.3.11 Fractionations

A detergent-based cell fractionation kit (#9038, Cell Signaling Technology) was used to separate proteins from RPE1 cells according to 3 subcellular fractions (cytoplasmic, membrane/organelle and nuclear/cytoskeletal), following manufacturer's instructions. Protease inhibitor cocktail and 1 mM PMSF were added to the buffers just before use. Confluent hTERT-RPE1 (roughly  $2.5 \times 10^6$  cells per sample) were trypsinised to detach from the flask, and growth medium was added to deactivate trypsin. After isolating 100  $\mu$ l of cell suspension to prepare the whole cell lysate (crudely lysing the cells by applying LDS sample buffer and DTT and sonicating), the rest of the cell pellet was resuspended in 250  $\mu$ l of cytoplasmic isolation buffer (CIB) and incubated for 5 minutes on ice (like all steps from this point on were performed on ice). After centrifugation for 5 minute at 500 g, the supernatant was kept as the cytoplasmic fraction. Subsequently, the pellet was resuspended in 250  $\mu$ l of membrane isolation buffer (MIB) and incubated for 5 minutes on ice. After centrifugation for 5 minute at 8000 g, the supernatant was kept as the membrane and organelle fraction. Finally, the pellet was resuspended in 125  $\mu$ l of cytoskeleton/nucleus isolation buffer (CyNIB) and sonicated 3 times for 5 seconds at low power. This represented the cytoskeletal/nuclear fraction. LDS sample buffer and DTT were added to the samples which were subsequently heated at 70 °C for 5 minutes, to reduce and denature the proteins and prepare the samples for SDS-PAGE and western blotting.

A second method of fractionation was also employed based on (Holden and Horton 2009). Protease inhibitor cocktail was added to the buffers just before use. Confluent hTERT-RPE1 cells were scraped off their plates in isotonic buffer (150 mM NaCl, 25 mM HEPES buffer pH 7.5, 1 mM  $\beta$ -mercaptoethanol, 0.2 mM  $\text{CaCl}_2$ , 0.5 mM  $\text{MgCl}_2$ ) and transferred to Eppendorf tubes. Cell suspensions were then incubated with 20  $\mu$ g digitonin for 30 minutes at 4 °C. This concentration of digitonin is expected to fully extract the cytosol by forming pores on the plasma membrane, without permeabilising intracellular membranes. After centrifugation for 1 minute at 13000 rpm, the supernatant was kept as the cytosolic fraction. Subsequently, the remaining pellet was washed with PBS and then resuspended again in isotonic

buffer. After adding NP-40 to 0.5% final concentration, the suspension was vortexed and centrifuged for 1 minute at 13000 rpm. The supernatant was kept as the membrane fraction, as NP-40 solubilises intracellular membranes. Finally, after washing the pellet in PBS, it was resuspended in RIPA buffer, which solubilizes the nuclear membrane and extracts nuclear residing proteins. After vortexing and centrifuging for 10 minutes at 13000 rpm, the supernatant was kept as the nuclear fraction. The pellet which contained RIPA-insoluble proteins and cell debris was discarded. LDS sample buffer and DTT were added to the samples which were subsequently heated at 70 °C for 5 minutes, to reduce and denature the proteins and prepare the samples for SDS-PAGE and western blotting.

## **2.4 Mammalian tissue culture**

### **2.4.1 Cell culture**

HEK293T and hTERT-RPE1 cells were obtained from the ATCC (American type culture collection) and maintained as adherent cultures at 37 °C and 5% CO<sub>2</sub>. HEK293T were grown in Dulbecco's modified Eagle medium (DMEM) with 4.5g/l L/D glucose and preferably (+) pyruvate (Gibco, Life Technologies), with the addition of 10% v/v fetal serum (bovine or calf) and penicillin/streptomycin cocktail at 1 mg/ml final concentration. hTERT-RPE1 were grown in DME-F12 medium (Hyclone, Thermo Fisher Scientific) with the addition of 10% v/v fetal serum (bovine or calf), penicillin/streptomycin cocktail at 1 mg/ml final concentration and hygromycin (10 µg/ml final concentration). The RPE1 cell lines that were stably expressing ARL3-FLAG or the corresponding empty vectors additionally required the presence of puromycin (2.5 µg/ml) and G418 (250 µg/ml) in the medium, as selection antibiotics. Cells were split regularly using TrypLE trypsin substitute (ThermoFisher Scientific).

Cell aliquots were frozen in regular medium with the addition of 10% dimethyl sulfoxide (DMSO) to prevent formation of water crystals. Freezing took place slowly in cryovials placed in ethanol baths at -80°C. For long term storage, frozen aliquots

were transferred to liquid nitrogen.

### Treatments

All reagents were filtered with 0.22 µm filter before treating the cells, unless they were sterile. HEK293T cells have been subjected to the following treatments: sodium orthovanadate tyrosine phosphatase inhibitor, 100 µM in the pre-existing medium for 30 minutes before cell lysis, when investigating tyrosine phosphorylation of RP2-V5 (Chapter 3). SRC inhibitor treatment (eCF560), 100 and 200 nM in fresh medium for 1.5 hours before lysis (Chapter 3). hTERT-RPE1 cells were subjected to the following treatments to induce DNA damage (Chapter 4): 2,5,10 Gy of X-rays using Faxitron at 1 Gy/min and 130 peak kilovoltage. Cells were incubated for at least 1 hour at normal conditions before lysis or fixation. 50 µM DMSO-dissolved etoposide or respective quantity of DMSO alone, for 4 hours in fresh medium before lysis or fixation.

### **2.4.2 Transient transfections**

HEK293T and hTERT-RPE1 cells were transiently transfected with approximately 0.5 µg purified plasmid DNA containing the relevant constructs per  $0.2 \times 10^6$  cells. The nonliposomal transfection reagent Fugene HD (Promega) was used to deliver the plasmids into the cells.

### **2.4.3 Growth curves**

To produce a growth curve of RPE1 cells, they were plated in 6-well plates at  $1.12 \times 10^4$  cells per well. Every day, cells from 3 biological replicates-wells were split and counted using the Cellometer Auto T4 cell counter (Nexcelom).

#### 2.4.4 Cell motility experiments

Cell motility of RPE1 cells was assessed via two different *in vitro* assays: random migration assay and scratch wound (wound healing) assay.

For the random migration assay, cells were very sparsely plated (1000 cells per well in a 96-well plate) and left overnight in the incubator to adhere to the substrate. 6 technical replicates (wells) were plated for each cell type. On the next day, the plate was transferred to the Incucyte ZOOM live-cell imaging system (Essen Bioscience) where cells were maintained at optimal physiological conditions inside an incubator for 24 hours, during which the plate was imaged every 30 minutes. Wild-type RPE1 cells appear to be very motile when sparsely plated, moving continuously around in response to local gradients of growth factors in the growth medium. The distance covered by individual cells during a specific 10-hour time-frame was analysed blindly using the Manual cell tracking feature in Fiji.

For the scratch wound assay, RPE1 cells were plated on specialized 96-well plates (Essen Bioscience), including 6 technical replicates (wells) for each cell type, and allowed to reach complete confluency. A scratch wound was then introduced in the middle of each well using the 96-well WoundMaker Tool (Essen Bioscience). After carefully washing the wells to remove floating cells, the plate was transferred in the Incucyte ZOOM live cell imaging system (Essen Bioscience), where the cells were maintained at optimal physiological conditions while imaging every 30 minutes for 24 hours. Cells at the edge of the wound moved in a directed manner towards the center of the cell-free zone until the formation of new cell-cell contacts inhibited migration. After 24 hours, the wounds were completely closed. Cell migration was then measured by quantifying cell density as the cells migrated into the cell-free zone. The Incucyte cell migration software module automatically generated a mask of the initial versus later wound width and calculated the relative wound density.

## **2.4.5 Immunofluorescence**

hTERT-RPE1 were grown on sterile coverslips previously treated with HCl to create a rough surface for the adherent cells (12 hours at 55 °C). Cells used in the  $\gamma$ H2AX staining experiment were fixed in 4% paraformaldehyde (PFA) in PBS for 10 minutes at room temperature, washed extensively in PBS to remove PFA and then permeabilised in 0.1% Triton X100 in PBS for 10 minutes. Cells used in the DNA PKcs-RP2-V5 staining experiment were instead treated with ice-cold methanol for 5 minutes at 4 °C, and then extensively washed in PBS to remove methanol. Cells were blocked in goat serum diluted 1:10 in PBS for 1 hour at room temperature or overnight at 4 °C, on an orbital shaker. Primary antibody incubations were performed in the dilutions indicated in table for 1 hour at room temperature in blocking buffer. After washing 3 times in blocking buffer, secondary antibody incubation followed at the indicated dilutions for 1 hour at room temperature. From this stage on the stained cells were protected from light. Before mounting, cells were stained with 4',6-diamidino-2-phenylindole (DAPI) (Sigma-Aldrich) diluted 1:10000 in PBS to show the nuclei, for 5 minutes at room temperature. Finally, stained cells were mounted on Superfrost slides using Prolong Gold mounting medium (Invitrogen), and imaged on a Zeiss upright epifluorescent microscope operating with the Micro-manager open source imaging software (<https://micro-manager.org/>) ( $\gamma$ H2AX staining), or with an A1+ Nikon confocal microscope operating with the NIS Elements software (DNA PKcs-RP2-V5 co-staining).

Image analysis was conducted using the NIS Elements viewer software (for images obtained on the Nikon confocal) or Image J/FIJI open source software.

## **2.5 Animal methods**

### **2.5.1 Fish husbandry**

Zebrafish used during this study were maintained in the MRC Human Genetics Unit (HGU) core fish facility, in a recirculating closed water system (Aquatic Habitats,

UK) at pH 7.4 and 28°C temperature. Light cycle followed a stable 14-hour day/10-hour night pattern. All lines were derived from matings between wild-type AB adults from within the facility. Embryos destined to grow to adulthood were bleached on the first day post-fertilisation (dpf) in alternating 5-minute washes of bleach solution and MilliQ distilled water. Bleached embryos were grown up to 5 dpf in a petri dish with fresh E3 medium, in a 28°C incubator. After five days, the larvae were transferred to static tanks at room temperature and grown until 20-30 dpf. During this period, their diet consisted of paramecium and ZM000 dry food (ZM Systems, UK). Subsequently, the larvae were transferred into the main system and fed a combination of dry food (ZM Systems) and brine shrimp.

All experimental procedures described in the present study were approved by the UK Home Office and complied with the UK Animals (Scientific Procedures) Act 1986. Permission to carry out the experiments was granted to Personal Project Licence (PPL) number 60/4418 and Personal Individual Licence (PIL) number 15CF674A1.

### **2.5.2 Generation of zebrafish mutant lines by CRISPR/Cas9**

The Target Finder tool from Feng Zhang's lab (<http://crispr.mit.edu/>) was used to identify possible gRNA target sequences on zebrafish *rp2* and check for potential off-target binding. To generate *rp2* null zebrafish, 600 ng/μl nCas9 mRNA [codon-optimised for zebrafish genome editing, (Jao et al. 2013)] were mixed 1:1 with the respective gRNA (~80 ng/μl) and micro-injected directly into the cell of 1-cell stage AB zebrafish embryos. Injections were conducted by me and Witold Rybski. On the 3<sup>rd</sup> day post fertilisation, 5-10 embryos were pooled and genomic DNA was isolated from them, in order to determine Cas9 targeting efficiency by Sanger sequencing. All sequencing experiments began with a single PCR reaction using appropriate primers flanking the targeted site on zebrafish *rp2* (termed “*rp2* sequencing PCR” from now on) and Phusion High fidelity DNA polymerase (New England Biolabs) (Table 2.1). When the template was expected to consist of heterogeneous DNA fragments, as in this case of pooled zebrafish embryos, the PCR products were subcloned into pGEM-T vectors and subsequently used to transform *E.coli* competent cells (see full

procedure above). Plasmid DNA from individual transformed colonies was submitted for Sanger sequencing using a T7 primer.

When targeting efficiency was high (as in gRNA1- guided targeting), the rest of the embryos were allowed to grow to ~3 months and total genomic DNA was isolated from their fin clips. Because of the quick developmental rate of zebrafish embryos, it was expected that these fish are chimaeras, meaning that different populations of cells are expected to carry different mutations, if any. For this reason, sequencing to separate the different mutations and determine the degree of chimaerism necessarily included a pGEM-T subcloning step, as described above. When *rp2* mutations were found among the colonies, the fish was considered a potential founder (F0), and was isolated. Because founders were all female, they were crossed with AB males to determine if they could pass *rp2* mutations to their progeny. Total genomic DNA was isolated from pooled embryos produced by the AB x F0 cross, and the *rp2* sequencing PCR product was submitted for Sanger sequencing using both the forward and reverse primers that were used for PCR (“Sequencing primers”, see Table 2.1). Mutations in the heterozygous embryos were identified using the PolyPeak Parser software (Hill et al. 2014). When *rp2* mutations were identified in the pooled embryo sample, the rest of the progeny were allowed to grow to ~3 months, when the fish that were heterozygous for *rp2* mutations were identified by *rp2* sequencing PCR and Sanger sequencing (F1). F1xF1 crosses between fish with identical *rp2* mutations were conducted and the progeny were screened by *rp2* sequencing PCR and Sanger sequencing to identify putative *rp2*-null homozygous fish (F2). Wild-type and heterozygous fish from these crosses were also kept and used in the histology experiments.

### **2.5.3 Histology of retinal sections**

#### Paraffin sectioning

Eyeballs were freshly dissected from adult animals, washed in PBS and then immediately immersed into Davidson’s fix buffer [22% v/v 10% neutral formalin in

phosphate buffer (100 ml/l 40% PFA, 900 ml/L distilled water, 18.6 g/l  $\text{NaH}_2\text{PO}_4$ , 42.2 g/l  $\text{NaOH}$ ), 33% v/v 95% ethanol, 11% v/v acetic acid in distilled water]. Fixation took place overnight at 4 °C. Subsequently, the eyeballs underwent a couple of washes in 70% ethanol and remained in 70% ethanol for another night before the next step. Dehydration of the tissues and embedding in paraffin took place in the Tissue Tek Tissue VIP5 Jr. embedding console system (Sakura). The procedure included the following steps, each one lasting for 40 minutes:

1. 70% ethanol
  2. 70% ethanol
  3. 85% ethanol
  4. 95% ethanol
  5. 100% ethanol
  6. 100% ethanol
  7. 100% ethanol
  8. Xylene
  9. Xylene
  10. Xylene
  11. Paraffin
  12. Paraffin
  13. Paraffin
  14. Paraffin
- 
- 37 °C
- 58 °C

After embedding in molten paraffin, the eyeballs were transferred into casts where they were orientated according to the plane of sectioning required. Paraffin was then allowed to set completely around the specimen and form a block. All samples that would be compared (e.g. age-matched *rp2* null and wild-type siblings) were processed and stained simultaneously using the same settings.

A Leica RM2235 microtome was used to obtain 7  $\mu\text{m}$ -thick sections of the eyes. Sections were obtained orthogonally to the vertical meridian of the eye. Sections were spread out in a water bath at 47°C and then collected on the (+) side of



Superfrost microscopy slides (Menzer-Gläser, Thermo Fisher Scientific). They were subsequently air-dried overnight.

#### Haematoxylin and eosin (H&E) staining

To prepare for staining, eye sections were first de-waxed in xylene. Next, they underwent stepwise rehydration, passing through a reverse series of graded ethanol washes. Sections were subsequently dipped in haematoxylin for 4 minutes, washed in running tap water, differentiated in 1% HCl in 70% alcohol, washed well in running tap water. Next, the sections were dipped in saturated Lithium carbonate solution for a few seconds, washed well in tap water, stained in eosin for 4 minutes, rinsed in water and finally rinsed in 100% ethanol. After staining, the sections were dehydrated again through several 100% ethanol washes. After passing through 3 xylene washes for 5 minutes each, the sections were ready to be mounted with DPX medium (Cell Path). Mounted sections were left to cure overnight.

#### Imaging and analysis

Brightfield microscopy with a Zeiss upright microscope and the Micro-manager open source imaging software (<https://micro-manager.org/>) was used to take pictures of the stained retinal sections. Fiji software was used to measure the thickness of different layers, which were made visible thanks to the H&E stain, along the length of the retina. The mean values from 3 different fish of the same genotype were then plotted on graphs, and GraphPad prism software was used for the statistical analysis.

## **2.6 Databases, online resources, 3D protein analysis and statistics**

Online databases and resources used in this thesis include the Ensembl genome browser (<http://www.ensembl.org/index.html>), National centre for biotechnology information (NCBI) (<https://www.ncbi.nlm.nih.gov/>), Uniprot protein knowledgebase (<http://www.uniprot.org/>), Phosphosite Plus database for post-translational modifications (<http://www.phosphosite.org/homeAction.action>), and the Retinal Information Network (<https://sph.uth.edu/retnet/>).

RP2 3D structure cartoons shown in [Chapter 3: Figure 3.6 and Chapter 4: Figures 4.6,4.7] were made using Pymol software. A publicly available Pymol script (<https://pymolwiki.org/index.php/FindSurfaceResidues>) was employed to show surface exposed residues. The default cut-off value was used (2.5 Å<sup>2</sup>).

Phosphorylation site prediction for RP2 shown in Chapter 3 was conducted using the freely available Group-based prediction system (GPS) 3.0 software (<http://gps.biocuckoo.org/>) using medium threshold settings (9% FPR-false positive rate) which is appropriate for small scale experiments.

Dr Dinesh Soares conducted calculations of RP2 stability upon mutagenesis (Chapter 3: Table 3.1, Figure 3.2, Chapter 4: Figure 4.6) using FoldX software tool (Schymkowitz et al. 2005, Rakoczy et al. 2011). He also conducted sequence conservation analysis on the surface of RP2 (Chapter 3: Figure 3.2) using ConSurf software tool (Ashkenazy et al. 2016) and multiple-sequence alignment of vertebrate RP2 orthologues using MUSCLE (EMBL-EBI tool) (Edgar 2004) (Chapter 3: Figure 3.5, Chapter 4: Figure 4.7).

Statistical analysis was conducted using Graphpad Prism software, except for the analysis of the IP/MS experiment, which was analysed based on an R script provided by Dr Jimi Bukowski-Wills using RStudio version 0.99.903.

During the CRISPR/Cas9 experiment (Chapter 5), the Target Finder tool from Feng Zhang's lab (<http://crispr.mit.edu/>) was used to identify possible gRNA target sequences on zebrafish *rp2* and check for potential off-target binding. EMBL-EBI's tool Clustal Omega (<http://www.ebi.ac.uk/Tools/msa/clustalo/>) was used for multiple sequence alignments to identify *rp2* mutations in Sanger-sequenced samples. PolyPeak Parser software served to separate Sanger sequencing chromatograms with double peaks into wild-type and alternative allele sequences (Hill et al. 2014) (<http://yosttools.genetics.utah.edu/PolyPeakParser/>).

## **Chapter 3: Characterisation of the interaction between RP2 and OSTF1**

### **3.1 Introduction**

Osteoclast stimulating factor 1 (OSTF1) was identified in our group previously as a direct interaction partner of RP2 by a yeast two-hybrid screen approach, and the interaction was subsequently confirmed using Glutathione-S-Transferase (GST) pulldown assays from bovine retinal extracts (Dr Toby Hurd, Figure 3.1B). This interaction was later identified in HEK293T cells by a large-scale study of the human interactome based on mass spectrometry, providing further validation of this interaction (Huttlin et al. 2015). OSTF1 has never been linked to photoreceptor degeneration before, instead it was initially identified as an intracellular polypeptide that indirectly stimulates formation of osteoclast-like multinucleated cells in human bone marrow culture and bone resorption when overexpressed (Reddy et al. 1998).

OSTF1 is 214 residues-long and its main protein domains are a SRC-homology 3 (SH3) domain (which shares 63% sequence homology with Fyn kinase), an N-terminal proline-rich region (which functions as an SH3-binding domain), four ankyrin repeats and a well-conserved cluster of amino acids at the C-terminus (Figure 3.1A). Expression of OSTF1 at mRNA level has been detected in several human tissues including heart, brain, placenta, lung, liver, skeletal muscle, kidney, pancreas and differentiated osteoclasts (Reddy et al. 1998). OSTF1 has twice been reported to form a complex with c-SRC kinase, either directly (Reddy et al. 1998) or indirectly via dimers of c-Cbl (Szymkiewicz et al. 2004). In addition, it co-localises with c-Cbl at podosomes in differentiated osteoclasts and is known to associate with filamentous actin (Szymkiewicz et al. 2004). Hence, it has been considered an adaptor for c-SRC's functions in the actin cytoskeleton. Other interactions that OSTF1 has been implicated in, via its SH3 domain, include the spinal muscular atrophy-determining gene product SMN (Kurihara et al. 2001) and Fas ligand (Voss, Lettau and Janssen 2009). Further, OSTF1 has been independently identified during a screen for molecules that regulate cell motility in HeLa cells. Following up this discovery revealed that OSTF1 is a negative regulator of cell motility under direct

control of the extracellular signal-regulated kinase (ERK)1/2 pathway and that this property is linked to its interaction with Myosin 1E (Tanimura et al. 2016, Tanimura et al. 2011). Finally, OSTF1 is one of the four genes and two open reading frames that are included in a rare 9q21 microdeletion which causes a syndrome of intellectual disability, epilepsy and mild facial dysmorphism. However, loss of OSTF1 is not the most likely cause of these defects (Boudry-Labis et al. 2013).

What makes this novel interaction of RP2 interesting is the fact that it is absent in patients with a particular missense RP2 mutation, according to previous data from our group (Dr Toby Hurd, Figure 3.1C). Several pathogenic missense mutations have been found on RP2 which are not predicted to destabilise the overall folding of the protein or affect its expression (biophysical calculations of structural stability based on the free energy difference upon mutagenesis were conducted by Dr Dinesh Soares, Table 3.1), and are therefore expected to be highly informative about specific interactions/modifications that are important for the disease. Most pathogenic missense mutations are segregated on the interaction interface with small GTPase ARL3 and are experimentally proven to affect the binding (Kuhnel et al. 2006), highlighting the importance of this interaction for the viability of photoreceptors. On the contrary, the RP2-OSTF1 binding is affected by the R211L mutation which lies away from the ARL3 interaction interface on the opposite face of the GAP domain and is not predicted to destabilise the structure of RP2 or the RP2-ARL3 interaction (Table 3.1). These preliminary results suggested that studying the RP2-OSTF1 interaction promises to shed light on a novel function or mode of regulation of RP2 and led to the hypothesis that the opposite face of the GAP domain together with the poorly studied NDK-like C-terminal domain form the binding interface for OSTF1.

In the following chapter, I will describe the steps I took to characterise the RP2-OSTF1 interaction. Firstly, I will map the interaction interface on a strictly conserved (among vertebrates) area on RP2 which spans both the N-terminal and the C-terminal domains. Secondly, I will attempt to identify the function of the complex based on the two prominent hypotheses about the molecular pathways that OSTF1 participates in. In particular, I will test if OSTF1 acts as an adaptor protein to mediate the

phosphorylation of RP2 by c-SRC and I will examine if RP2 is a regulator of cell motility, similar to OSTF1.

**Table 3.1. Several missense RP2 mutations found in patients do not affect the stability of the protein or the RP2/ARL3 interaction.**

Stability calculations of the energy difference between wild-type and mutant RP2 both for the unbound protein and the RP2-ARL3 complex. The result is shown as  $\Delta\Delta G$  free energy expressed in kcal/mol. When  $\Delta\Delta G < 1.6$  kcal/mol, no effect on structural stability is predicted upon mutation, whereas if  $\Delta\Delta G > 1.6$  kcal/mol (shown in red), the mutation is predicted to destabilise the structure [data generated by Dr Dinesh Soares using the FoldX software (Liu et al. 2017a)].

Missense pathogenic mutations on RP2	Stability energy calculation on human RP2 crystal structure (PDB ID: 2BX6)	Stability energy calculation on human RP2-ARL3 crystal structure (PDB ID: 3BH7)
	(mean $\Delta\Delta G$ in kcal/mol)	(mean $\Delta\Delta G$ in kcal/mol)
C67Y	12.81	18.75
C86Y	15.27	20.02
T87I	-0.73	-0.97
P95L	9.25	7.74
C105W	25.68	21.32
C108G	2.35	2.18
C108Y	15.73	11.03
R118H	0.54	2.63
R118L	-0.72	0.60
R118G	2.98	5.67
R118C	1.10	2.76
E138G	0.97	2.77
S140F	22.05	24.32
L188P	2.55	2.34
R211H	0.38	0.61
R211L	-0.27	0.30
L253R	8.74	7.23
L253P	11.03	10.90
R282W	1.21	1.37

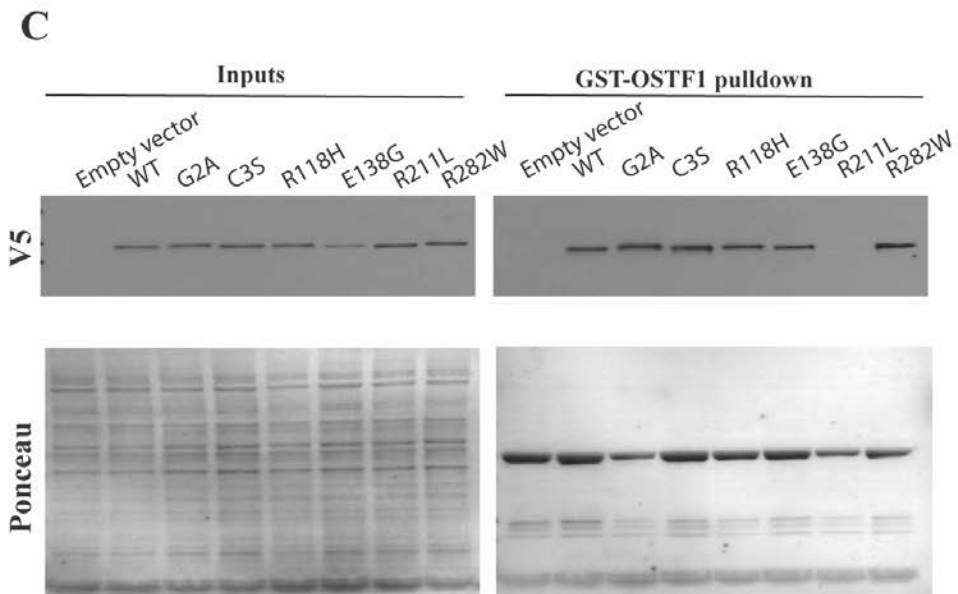
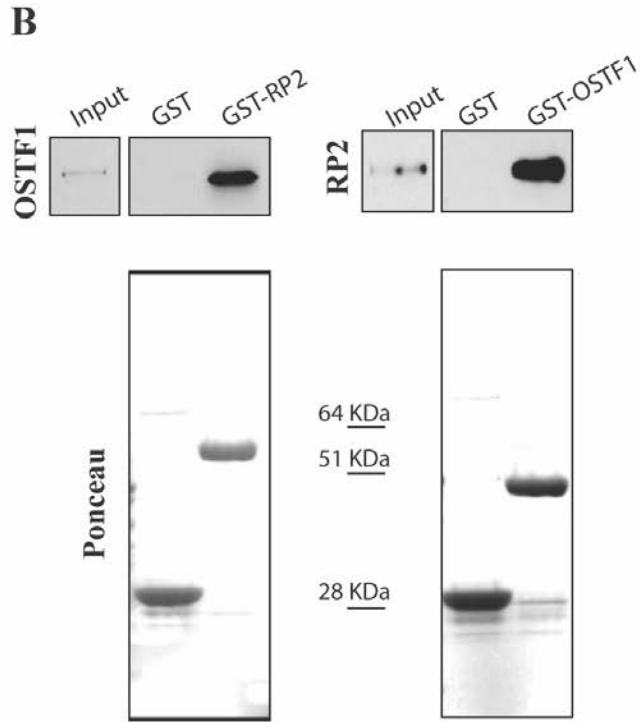


**Figure 3.1. Background information on OSTF1 and its identification as a binding partner of RP2.**

A) Schematic representation of the main protein domains of OSTF1. The 214-residue protein consists of a proline-rich region at the N-terminus (Pro), an SH3 domain, 4 ankyrin repeats and a cluster of acidic amino acids at the C-terminus. B) OSTF1 was confirmed as a binding partner of RP2 by reciprocal GST pulldown assays from bovine retinal extracts. Recombinant GST-OSTF1 can pulldown endogenous RP2 and recombinant GST-RP2 can pulldown endogenous OSTF1. GST-only pulldowns served as negative control. (data generated by Dr Toby Hurd) C) GST-OSTF1 pulldown assays from HEK293 cells transfected with V5-tagged wild-type human RP2 and pathogenic forms of human RP2 with missense mutations. The R211L mutation abolishes the interaction between RP2 and OSTF1 (unpublished data generated by Dr Toby Hurd).

## **3.2 Results**

### **3.2.1 OSTF1 binds a strictly conserved area on RP2 spanning both the N-terminal and C-terminal domains**

Intrigued by the preliminary finding that the R211L pathogenic mutation on RP2 abolishes the interaction with OSTF1, I aimed to map the interaction interface and test the hypothesis that this interaction is independent of ARL3 binding. Identifying more contact sites in addition to R211 has a double purpose. Firstly, it will determine if the OSTF1 and ARL3 binding interfaces overlap on the RP2 surface. Secondly, finding more residues that are important for the RP2-OSTF1 interaction will help to predict the effect of pathogenic mutations, both existing ones and others that will be found in the future.

In order to identify more residues, I followed a PCR-based site-directed mutagenesis approach to mutate individual residues on RP2 and then test for the ability of the mutated protein to interact with OSTF1 (Figure 3.2). The different forms of RP2-coding sequence were inserted in a mammalian expression vector which added a V5-tag to the C-terminus of the protein and were subsequently transiently expressed in HEK293T cells. This cell line was chosen for its high transfection efficiency. The lysates of the transfected cells were then used for pulldown experiments using recombinant GST-OSTF1 as bait. The particular residues to be mutated were chosen



on the basis of advice by Dr Dinesh Soares. His analysis took the following characteristics into account: 1) the position of the residues in relation to R211 2) the conservation status among vertebrates 3) the electrostatic properties and hydrophobicity of the residues and 4) the possibility of post translational modifications. The mutations generated aimed to abolish the charge, the hydrophobicity or the phosphorylation potential of the original residues. Taking into account the electrostatic properties and hydrophobicity of the different residues is important because these factors often mediate molecular recognition by determining the relative orientation of molecules in a complex as well as the binding specificity and affinity. As a result, highly charged and/or exposed hydrophobic residues often participate in protein-protein interactions (Honig and Nicholls 1995).

In addition, structural analyses and biophysical calculations were conducted (Dr Dinesh Soares) to ensure that the resulting substitutions were not predicted to affect the overall structural stability of the protein, an unwanted side-effect which would lead to poor expression or absence of expression of the mutated protein. Indeed, all the RP2 mutants in my experiment were expressed at the same level as the wild-type protein (inputs in Figure 3.2A), confirming that the computational predictions were correct. As an additional control, I conducted pulldowns using recombinant GST-ARL3 Q71L, the ARL3 mutant that stably interacts with RP2 (Veltel et al. 2008), as bait. All the mutations I generated co-precipitated with ARL3 Q71L as efficiently as the wild-type protein, confirming that the mutant RP2 proteins were correctly folded and that any defect observed was specific to the interaction with OSTF1.

Using this approach, I previously tested mutations in 7 RP2 residues and identified Y245 as essential for the RP2-OSTF1 interaction to occur (Rodanthi Lyraki, MSc thesis). During my PhD, I confirmed the previous results and examined 6 more residues. This led to the identification of 2 more residues that affect the interaction when mutated, namely D255 and K160. Figure 3.2 shows only experiments conducted during my PhD. The D255 to A mutation, which abolishes the negative charge, is prohibitive for the RP2-OSTF1 interaction. Mutating K160 to A which eliminates the positive charge, only mildly affects the interaction. However, reversing the charge via a K160 to E mutation eliminates the interaction completely,

leading me to conclude that K160 has an essential role in the binding interface. Moreover, another substitution which affects the RP2-OSTF1 interaction by eliminating the positive charge of the residue is K252A, although its effect is to reduce rather than abolish the interaction (Figure 3.2 C).

It is interesting that four out of the five RP2 residues so far identified as belonging to the OSTF1 binding interface are highly charged and in particular mostly positively charged (K252, R211, K160), whereas the surface of RP2 is predominantly negatively charged (Kuhnel et al. 2006). This observation might reveal that possible oppositely charged interactions are important for the RP2-OSTF1 binding. Identifying the OSTF1 residues that participate in the interaction will be useful to prove if this is the case. In addition, Y245 which has also been identified as participating in the RP2-OSTF1 interaction belongs to an exposed hydrophobic cluster which lies within a noticeable surface cavity [analysis by Dr Dinesh Soares based on the RP2 crystal structure solved by (Kuhnel et al. 2006)]. These characteristics make it a good candidate for participating in a protein-protein interaction.

The residues identified as essential mediators of the RP2-OSTF1 interaction belong to a strictly conserved (among vertebrates) “patch” on RP2 which spans both the N-terminal and C-terminal domains of the protein and is distinct from the interaction interface with ARL3. It is suggested that this “patch” forms the OSTF1 binding interface. The remarkable conservation status of all three residues (Figure 3.2B and Appendix figure 1) suggests that the RP2-OSTF1 interaction occurs in all vertebrates and carries out an important function. Furthermore, my results suggest that OSTF1 probably does not antagonise ARL3 for binding to RP2 and that, in theory, a trimeric complex can be formed between the three proteins. Co-precipitation experiments will need to be conducted in the future to prove whether this complex is actually formed *in vivo*. Finally, this experiment provides one of the first pieces of evidence for a functional role of the NDK-like domain of RP2.

In the future, the binding interface of other interaction partners can be mapped on RP2 using the same approach. Previously identified RP2 binding partners include the

G $\beta$ 1 subunit of transducin (Schwarz et al. 2012), Importin  $\beta$ 2 (Hurd et al. 2011) and Polycystin 2 (Hurd et al. 2010). It should be noted, however, that the site-directed mutagenesis approach that I followed is meaningful only when applied to direct interactions. OSTF1 was known from the beginning to be a direct interaction partner of RP2 because it was identified via a yeast two-hybrid screen (work conducted by Dr Toby Hurd). Moreover, the RP2-ARL3 interaction is well studied and the crystal structure of the structure has been solved, showing direct binding of the two proteins (Kuhnel et al. 2006). On the contrary, the other interaction partners of RP2 have been identified using pull-down and co-IP approaches, which do not ensure that two proteins that are found together in a complex directly bind to each other. As a conclusion, direct binding to RP2 should be shown first before research proceeds to mapping the binding interface.

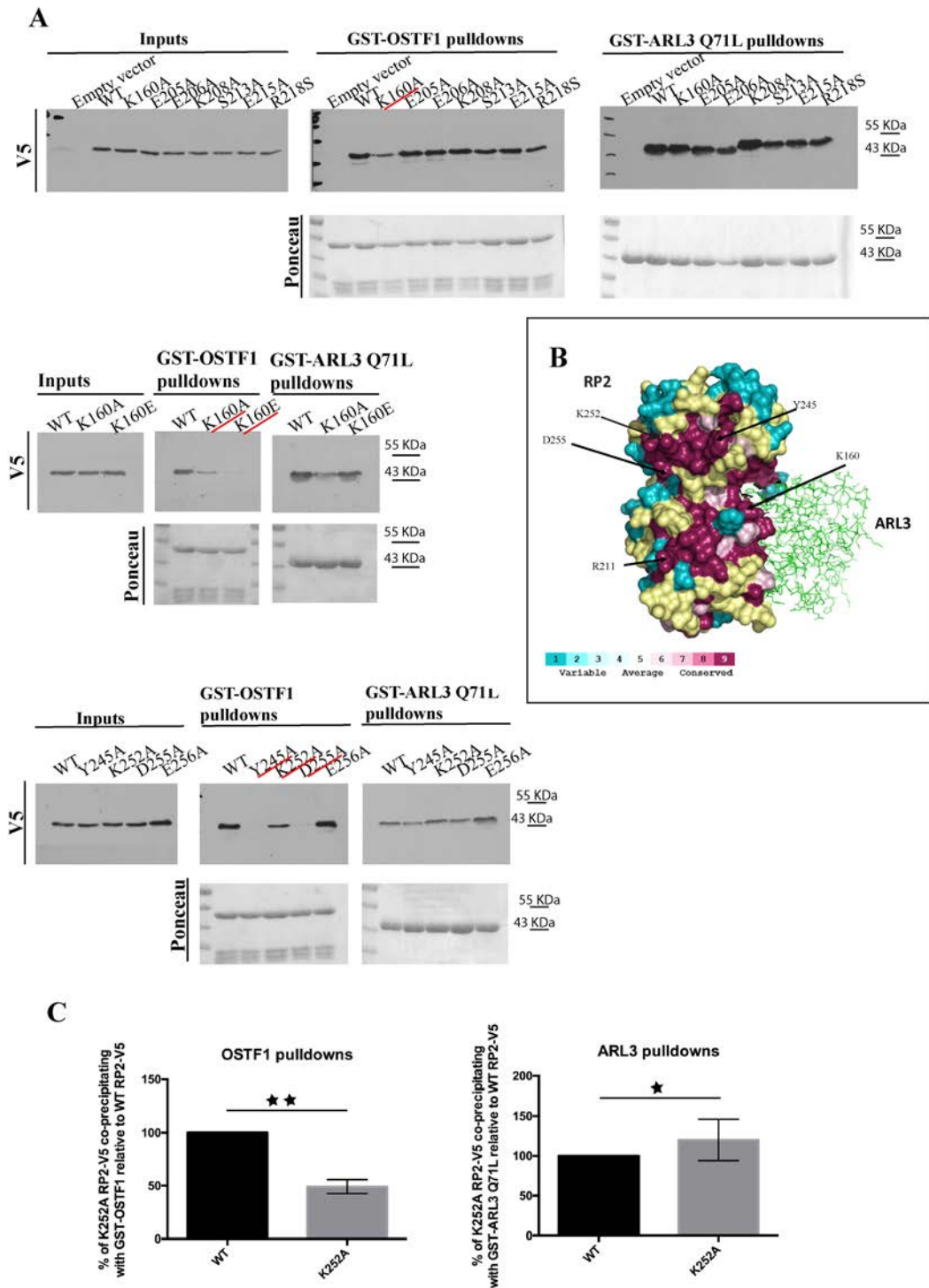


Figure 3.2 . Mapping the interaction interface between RP2 and OSTF1 on a conserved patch on RP2.

A) Critical residues on RP2 surface were mutated by site-directed mutagenesis and the resulting constructs were transiently transfected in HEK293T cells. V5 tagged wild-type (WT) and mutant RP2 proteins were compared for their ability to co-precipitate with GST-OSTF1 in pulldown assays. Pulldown assays using GST-ARL3

Q71L as bait were also conducted as controls for the correct folding of the mutant proteins. Both lysates before pulldown (inputs) and pulldown samples were subjected to SDS-PAGE and western blot using anti-V5 antibody. Staining with Ponceau shows the GST-tagged recombinant proteins that were used as baits. Using this method, four residues were identified as parts of the interaction interface with OSTF1 because mutating them completely abolished the RP2-OSTF1 interaction but not the RP2-ARL3 Q71L interaction (Y245, K160, K252 and D255). (B) Crystal structure of RP2 in complex with ARL3 (PDB ID: 3BH7) where the conservation status among vertebrates of residues on the surface of RP2 is shown in colour code (with dark purple being strictly conserved). Yellow colour represents those residues whose conservation status was assigned with low confidence. Arrows point to the four residues that have been identified to participate in the interaction interface with OSTF1, which are all strictly conserved. It is suggested that RP2 interacts with OSTF1 via the strictly conserved “patch” on the side of the protein that is shown here, which is distinct from the interaction interface with ARL3. Sequence conservation analysis was conducted by Dr Dinesh Soares using the ConSurf software. (C) The K252A mutation on RP2 reduces the interaction with OSTF1 but does not have the same effect on the interaction with ARL3. Relative quantification of the amount of WT and K252A RP2 co-precipitating with recombinant OSTF1 and ARL3 Q71L (mean  $\pm$  S.E.M for densitometry measurements from n=3 separate immunoblots normalised to the inputs). Two-tailed one-sample t-test was used to assess the significance of the observed differences between WT RP2 (value set to 100) compared to K252A RP2 pulldowns. P-value for OSTF1 pulldowns: 0.0162. P-value for ARL3 pulldowns: 0.0444.

### **3.2.2 Investigation of RP2 tyrosine phosphorylation and the potential role of OSTF1**

Protein phosphorylation is the most widespread type of post-translational modification used in signal transduction (Ubersax and Ferrell 2007). Several phosphorylated residues on mouse and human RP2 have been experimentally identified by large-scale phosphoproteomic studies (Figure 3.6A), but these modifications have not been verified or characterised to date and their function remains elusive (Sharma et al. 2014, Moritz et al. , Bershteyn et al. 2010, Kettenbach et al. , Humphrey et al. 2013, Wang et al. 2011, Stuart et al. 2015). Tyrosine phosphorylation is expected to be particularly important for the function of RP2, since previous work in our group has shown that phospho-mimic mutations of Y27 and Y245 disrupt binding of RP2 to its interaction partners ARL3 and OSTF1, respectively (Rodanthi Lyraki, MSc thesis). In order to characterise the role of

tyrosine phosphorylation of RP2, it is important to identify the responsible kinase. Interestingly, the newly identified interaction partner of RP2, OSTF1, is known to interact with the ubiquitous tyrosine kinase c-SRC and has been suggested to act as an adaptor for c-SRC's functions (Szymkiewicz et al. 2004). Based on this, I hypothesised that c-SRC is responsible for tyrosine phosphorylation of RP2 and that OSTF1 mediates this phosphorylation as a "scaffold" molecule, a mechanism for bringing the kinase and the substrate into the same complex that has been described before as an important way to enhance phosphorylation specificity (Ubersax and Ferrell 2007). In addition, I hypothesised that tyrosine phosphorylation influences binding of RP2 to its interaction partners and thus indirectly regulates the GTPase activity of RP2. In Chapter 3.2.2, I will describe the methods I used to verify my hypotheses *in vitro*. I will show that c-SRC is, indeed, a candidate kinase for phosphorylating RP2 on Y27, but other kinases are responsible for the low-level tyrosine phosphorylation of RP2 that is observed in HEK293T cells.

### **3.2.2.1 c-SRC potentially phosphorylates RP2 on Y27**

Firstly, I tested the ability of recombinant human c-SRC-GST to phosphorylate recombinant human RP2-His in an *in vitro* kinase assay. As a readout, I analysed the assay mix by western blot using anti-phosphorylated tyrosine antibody and observed the presence of a phosphorylated band at the same molecular weight as His-tagged RP2. This initial experiment shows that it is possible for RP2 to be directly phosphorylated by c-SRC (Figure 3.3).

Subsequently, I wanted to test if it is possible to induce tyrosine phosphorylation on RP2 by overexpressing c-SRC in cell culture. Because the phosphorylation of endogenous RP2 proved impossible to detect by western blot, I detected phosphorylation of transiently expressed V5-tagged RP2 from HEK293T cells after affinity purification by anti-V5 immunoprecipitation (IP). This cell line was chosen because of its robust transfection efficiency which allowed me to reproducibly detect such a low-level modification. Simultaneous co-expression of c-SRC-GFP induced tyrosine phosphorylation of a band at the same molecular weight as RP2-V5 which was not observed with co-expression of GFP alone (Figure 3.4). This result suggests

that RP2 phosphorylation by c-SRC can occur not only during a kinase assay but also in the cell environment. The experiment could be ameliorated by the addition of a sample transfected with SRC-GFP alone. In the absence of this negative control, there is still a possibility that the observed phosphorylated band does not correspond to RP2-V5 but another protein of similar molecular weight that is strongly phosphorylated by SRC-GFP. If the phosphorylated band indeed corresponds to RP2-V5, then I would expect it to be absent in the sample of cells transfected with SRC-GFP alone.

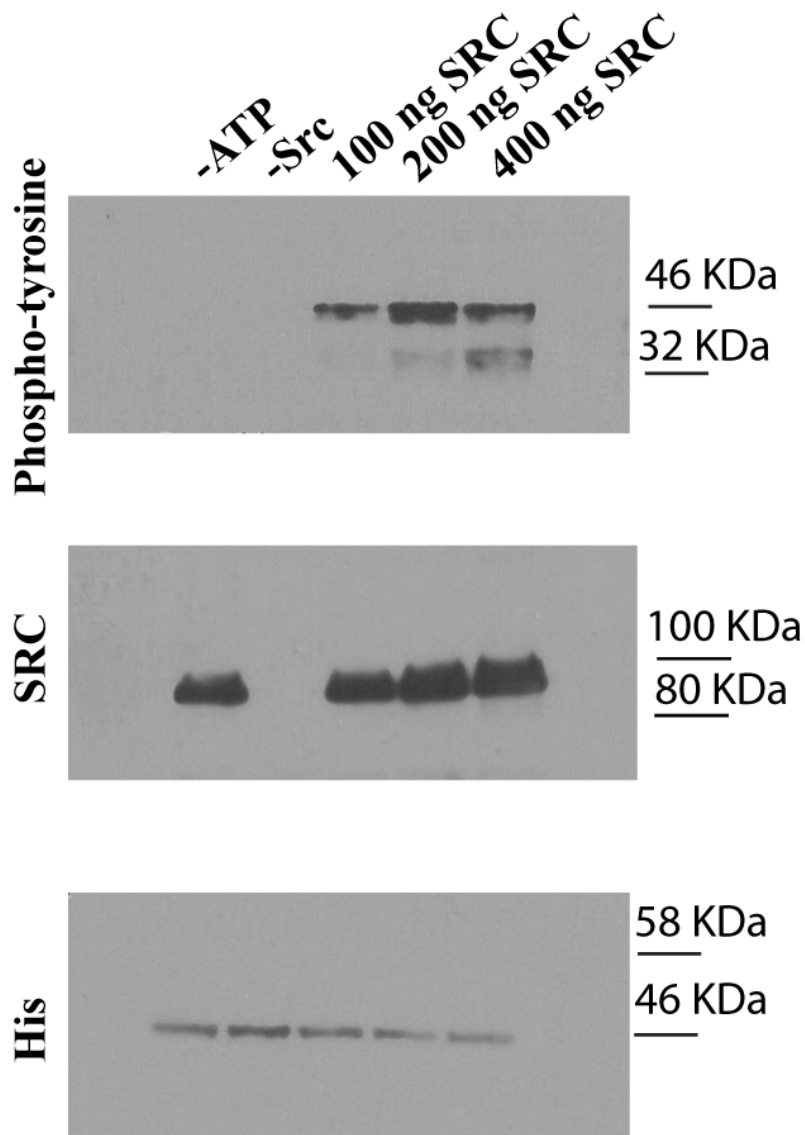
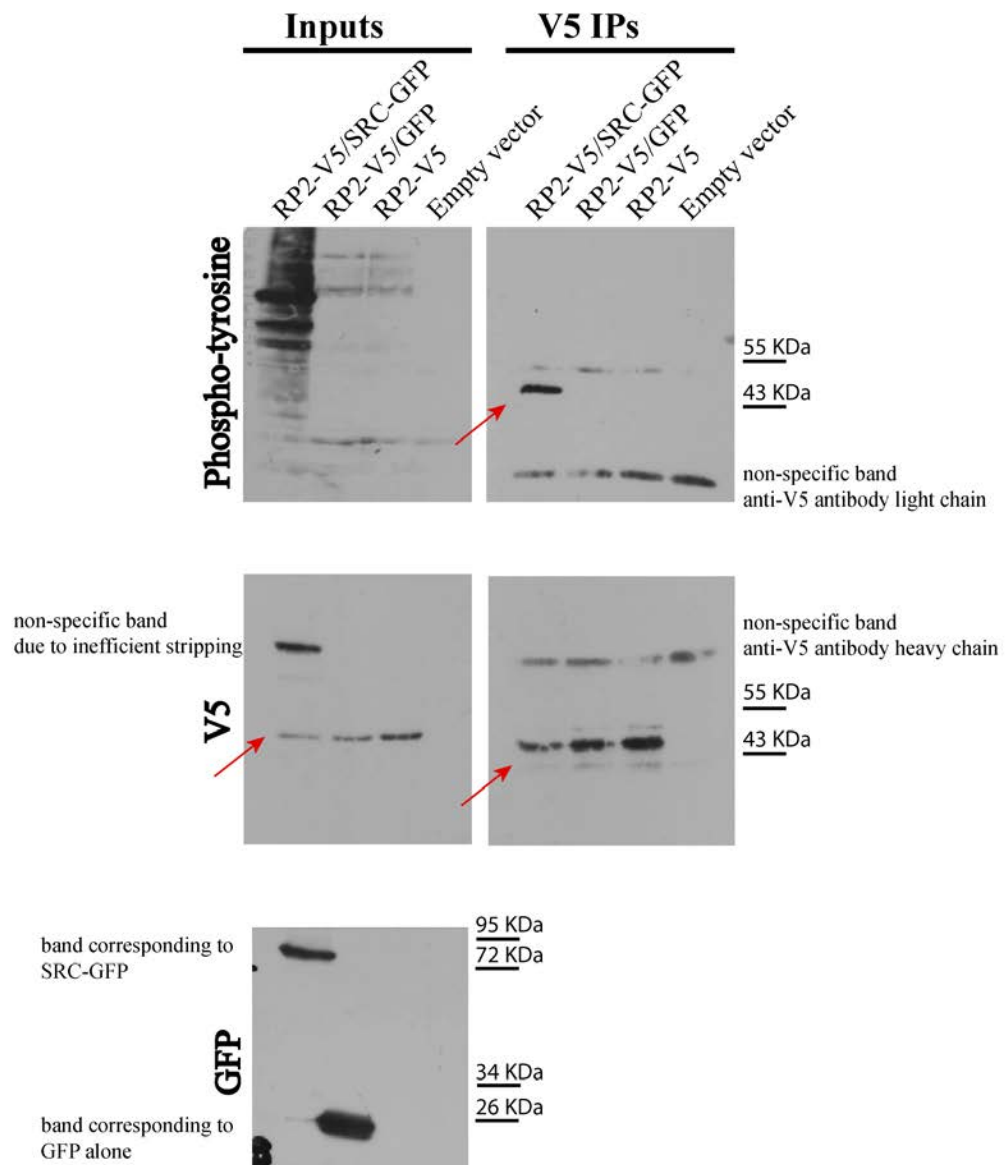


Figure 3.3. **RP2 is phosphorylated by c-SRC *in vitro*.**

Kinase assay was performed *in vitro* using recombinant human RP2 with a C-terminal His-tag and increasing quantities of GST-tagged recombinant human c-SRC kinase. The assay mix was subjected to SDS-PAGE and western blot analysis using anti-phosphorylated tyrosine antibody to detect phosphorylation of the substrate. No phosphorylation is observed in the negative controls, when the assay mix does not contain any kinase (-SRC) or the phosphate donor (-ATP). The blotted membrane was subsequently stripped and re-probed with anti-His antibody to confirm the presence of RP2-His at the same molecular weight as the phosphorylated band, and anti-SRC antibody to confirm the presence of the kinase.





**Figure 3.4. Overexpression of c-SRC results in tyrosine phosphorylation of RP2 in HEK293T cells.**

The phosphorylation status of exogenous human RP2 with a C-terminal V5-tag was examined in HEK293T cells that were transiently transfected with empty pcDNA destination vector, RP2-V5 alone, RP2-V5 and GFP, or RP2-V5 and human c-SRC-GFP. To detect phosphorylation, RP2-V5 was immunoprecipitated from the cells' lysates using anti-V5 antibody conjugated agarose beads. The immunoprecipitates (IPs) as well as the lysates before IP (inputs) were subjected to SDS-PAGE and western blotting using anti-phosphorylated tyrosine antibody. This approach shows that overexpression of c-SRC induces phosphorylation of RP2 that can be detected even when endogenous phosphorylation is undetectable. Subsequent re-probing with

anti-V5 and anti-GFP antibodies confirms correct expression of the constructs. Red arrows point to the RP2 bands. Annotations next to the non-specific bands as well as the two different GFP bands have been added to help the reader.

In order to confirm that the phosphorylated band corresponds to RP2-V5 and to identify the phosphorylated residues, IP samples from the overexpression experiment were subjected to tandem mass spectrometry (MS/MS) analysis in the IGMM MS facility by Dr Andy Finch and Dr Jimi Wills-Bukowski. Protein complexes were immunoprecipitated with RP2-V5 from cell lysates transfected with empty vector (negative control), RP2-V5/GFP and RP2-V5/SRC-GFP and subsequently subjected to in-solution tryptic digest followed by LC-MS/MS. The experiment was conducted in three independent biological replicates. The resulting analysis showed a phosphate on RP2 Y27, as well as the adjacent S28, in the c-SRC overexpression sample only (Figure 3.5A). In addition to identifying post-translational modifications, this experiment provided information about the proteins that co-precipitate with RP2-V5 which I will present in Chapter 4. Both Y27 and S28 have been identified before as phosphorylation sites during large-scale phosphoproteomic studies of cancer cell lines (Sharma et al. 2014, Moritz et al. , Stuart et al. 2015). Y27, which is more relevant to my study of tyrosine phosphorylation, is located on a highly flexible (disordered) region that was not visible on the crystal structure (Veltel et al. 2008) and it is therefore assumed to be surface exposed and a good candidate for phosphorylation. The N-terminal 25-30 residues of RP2 are essential for the interaction with ARL3, and Y27 in particular is engaged in hydrophilic interactions with Q156 and D168 of the small GTPase (Veltel et al. 2008). Not surprisingly, Y27 is strictly conserved among vertebrates according to conservation analysis of diverse RP2 orthologues (conducted by Dr Dinesh Soares, Figure 3.5B). The identification of this particular tyrosine as a site of phosphorylation by c-SRC is further evidence that phosphorylation is a critical mechanism of functional regulation of RP2. It is also worth commenting on the phosphorylation of S28 which was also identified in the MS analysis to occur after SRC overexpression. The relationship between c-SRC activity and phosphorylation of S28 is not known, but it might be a case of “priming”; in other words, previous phosphorylation of RP2 by another kinase might

be required for the ultimate phosphorylation at Y27 (Ubersax and Ferrell 2007) or vice versa. Whether this is true will require separate investigation.

Because overexpressing c-SRC can lead to off-target phosphorylation of substrates and might not reflect the endogenous activity of the kinase, I chose to examine phosphorylation of RP2-V5 by endogenous kinases. In order to confirm if Y27 is a phosphorylation site on RP2, I compared the phosphorylation status of WT RP2-V5 and the non-phosphorylatable mutant Y27F in HEK293T cells. Since the Y27F mutant is expressed at the same levels as the WT protein (Figure 3.5C, inputs), the overall stability of the protein does not seem to be affected by the mutation. In figure 3.5C, a tyrosine phosphorylated band can be seen corresponding to the molecular weight of RP2-V5 in both the WT- and Y27F-transfected cells. This result suggests that Y27 is not a site of endogenous phosphorylation in HEK293T cells, or that other phosphorylation sites also exist on the protein that mask any reduction in Y27 phosphorylation. Figure 3.6B contains a list of residues on RP2 that are computationally predicted to be phosphorylated by SRC-family kinases using the GPS 3.0 prediction software operating on a medium threshold value of 9% FPR (false positive rate) for each kinase (Xue et al. 2008, Xue et al. 2011). Among them, Y27, Y198 and Y40 are strong candidates as they are both computationally predicted and experimentally identified as sites of phosphorylation in human cells (PhosphoSite Plus database). All candidate tyrosine residues are surface exposed and thus appropriate candidates for phosphorylation (Figure 3.6C).

Incomplete coverage of the protein during the MS/MS analysis is one of the reasons that other tyrosine phosphorylation sites were not identified on RP2. As shown in Appendix figure 2, predicted phosphorylation sites such as Y198 and Y245 (Figure 3.6A) are not contained in any of the six unique RP2 peptides identified in the MS/MS experiment. Phosphorylation of Y245, for example, would be particularly interesting to study both because this peptide has been identified before as important for the RP2-OSTF1 interaction (Figure 3.2A) but also because its phosphorylation has been detected before in a large-scale study of tyrosine phosphorylation in gastric carcinoma cells (Moritz et al. 2010). The sequence coverage of RP2 can be improved

in the future by combining the use of trypsin with alternative proteases during the digestion step of the MS workflow.

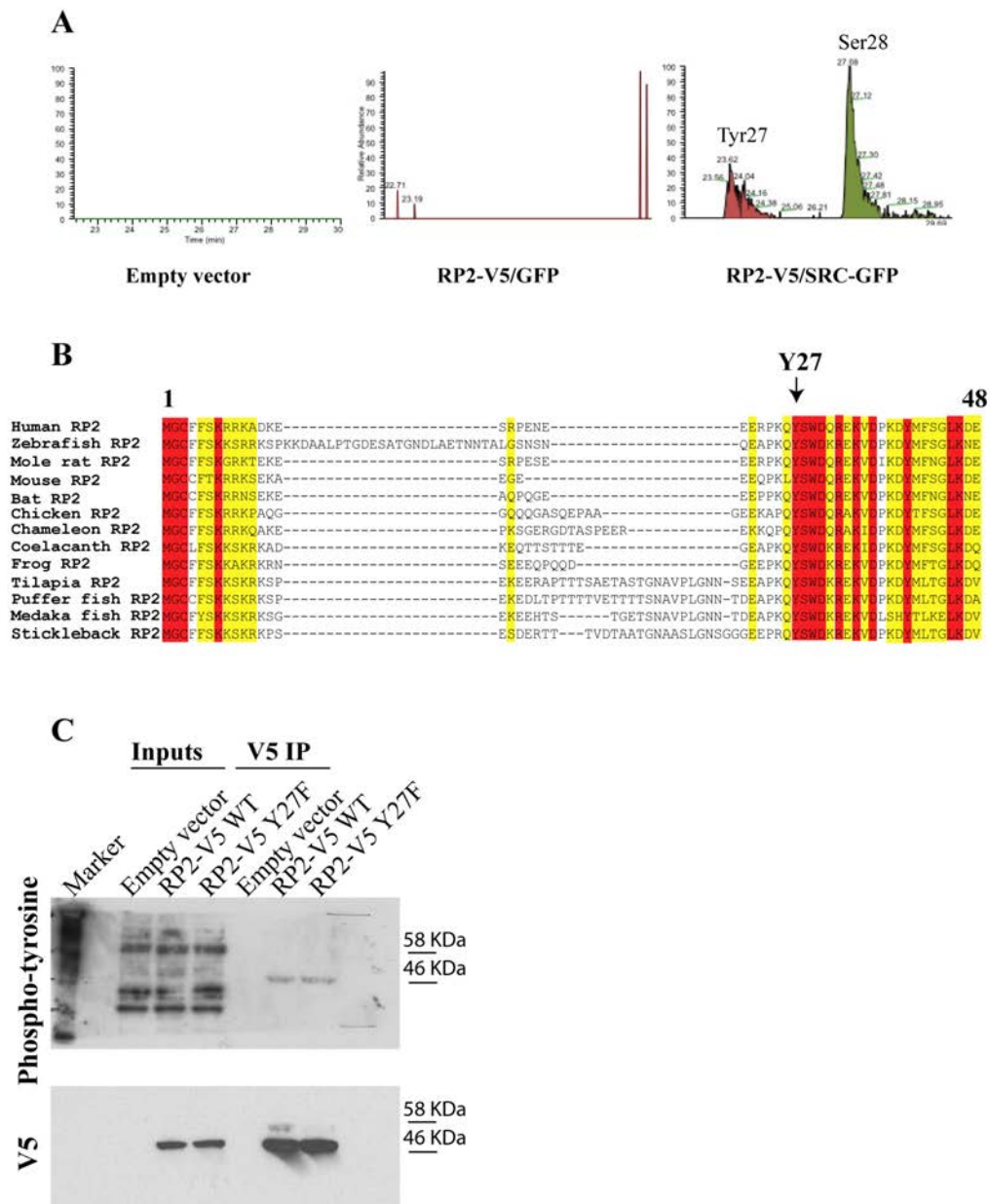
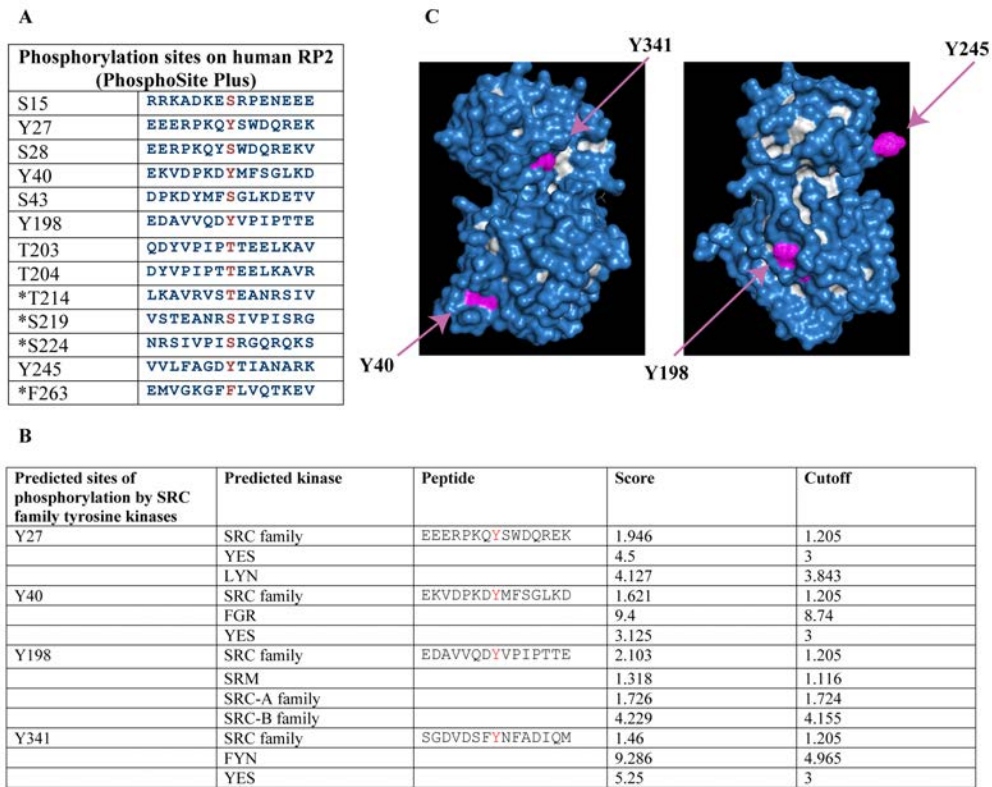


Figure 3.5. Y27 is a potential phosphorylation site on RP2, but is not the only site of endogenous phosphorylation in HEK293T cells.

A) Affinity purification of RP2-V5 from HEK293T cells followed by tandem mass spectrometry (MS/MS) was conducted in order to identify sites of tyrosine phosphorylation when the protein is co-expressed with c-SRC-GFP. Extracted ion chromatograms from one repeat of the experiment show the identification of Y27 as a phosphorylation site only in the RP2-V5/SRC-GFP transfected HEK293T cells but not in the RP2-V5/GFP transfected cells or the empty vector negative control. B) Section of multiple sequence alignment of vertebrate RP2 orthologues, encompassing the Y27 residue. The conservation status of each residue is shown in colour code (red= strictly conserved, yellow= largely conserved/conservatively

substituted, white=non-conserved). Y27 is strictly conserved among vertebrates. (analysis conducted by Dr Dinesh Soares) C) RP2 WT-V5 and RP2 Y27F-V5 were immunoprecipitated from lysates of cells transfected with the respective constructs using anti-V5 antibody conjugated agarose beads. Cells transfected with an empty destination vector were used as negative control. The IPs as well as the lysates before IP (inputs) were subjected to SDS-PAGE and western blotting using anti-phosphorylated tyrosine antibody. The WT and Y27F proteins are equally phosphorylated, suggesting that Y27 is not a site of endogenous phosphorylation in HEK293T cells or that other phosphorylated tyrosines mask any reduction in Y27 phosphorylation. Subsequent re-probing with an anti-V5 antibody confirms the presence of an RP2-V5 band at the same molecular weight as the phosphorylated band in the transfected lysates.



**Figure 3.6. Tyrosine residues on RP2 that are good candidates for phosphorylation.**

A) List of phosphorylated residues on human RP2 that have been identified by large-scale phosphoproteomics (Source: Phosphosite Plus database). Asterisks denote the corresponding human residues, when the phosphorylation site has originally been identified in mouse. Both Y27 and S28, the residues which were identified by mass spectrometry to be phosphorylated after c-SRC overexpression, are in the list of known phosphorylation sites on RP2. B) List of RP2 tyrosine residues which are predicted to be sites of phosphorylation by SRC-family kinases. Predictions were generated by the GPS 3.0 software using medium threshold (=9% False positive rate) (Xue et al. 2011). A “score” value is given to each prediction that should be compared to an individual “cut-off” value to get an idea of the strength of the prediction. Score values were given to the prediction that a site is phosphorylated by SRC-family kinases in general but also by individual kinases. C) Surface representation of RP2 3D structure cartoons (PDB ID: 2BX6) showing the position of RP2 tyrosine residues which were either identified experimentally by large-scale studies (Y40, Y198, Y245) or computationally predicted as possible sites of c-SRC mediated phosphorylation (Y341). Arrows point to the relevant tyrosine residues which are marked in pink colour. Surface exposed residues are shown in blue, while buried residues are white. Y27 is not visible because it belongs to an intrinsically disordered region which was not solved in the crystal structure (Kuhnel et al. 2006).

### 3.2.2.2 Overexpression of c-SRC does not markedly affect binding of RP2 to its interaction partners

The identification of Y27, an important residue for the interaction with the small GTPase ARL3, as a potential phosphorylation site on RP2 further supports the hypothesis that this modification plays a role in the regulation of protein-protein interactions between RP2 and its binding partners. To examine this hypothesis, I conducted pulldowns using recombinant GST-OSTF1 and GST-ARL3 Q71L as bait and RP2-V5 transiently expressed in HEK293T cells as prey. I used the ability of c-SRC overexpression to induce RP2 tyrosine phosphorylation and compared the amount of RP2-V5 that co-precipitated with the GST-tagged proteins between three different conditions, namely co-expression of GFP alone (using an inactive SRC mutant would be a better negative control than GFP alone), WT c-SRC-GFP or the constitutively active mutant of c-SRC, 527F. As shown in Figure 3.7A, overexpression of 527F c-SRC mildly enhances binding of RP2-V5 to its interaction partners, but this effect is not statistically significant for any of the pulldowns (Figure 3.7B). Taking into account the small sample size and the small observed differences, it appears that if RP2 phosphorylation affects binding to its interaction partners, this must be a very mild effect. However, a mild effect can still have an important biological function, especially when it comes to finely tuning the regulation of a GTPase. In order to confirm this finding by enhancing endogenous RP2 phosphorylation, the pulldown assays must be repeated after pre-treatment of the cells with tyrosine phosphatase inhibitors versus mock-treated cells. It must be noted that, while this method is indicative of a crude-qualitative effect of phosphorylation on the interactions of RP2, it is not quantitative because it does not provide information on what fraction of total RP2 is phosphorylated *in vivo*. If the stoichiometry of RP2 phosphorylation is low, this might explain why a bigger effect of phosphorylation on the RP2 interactions is not observed.



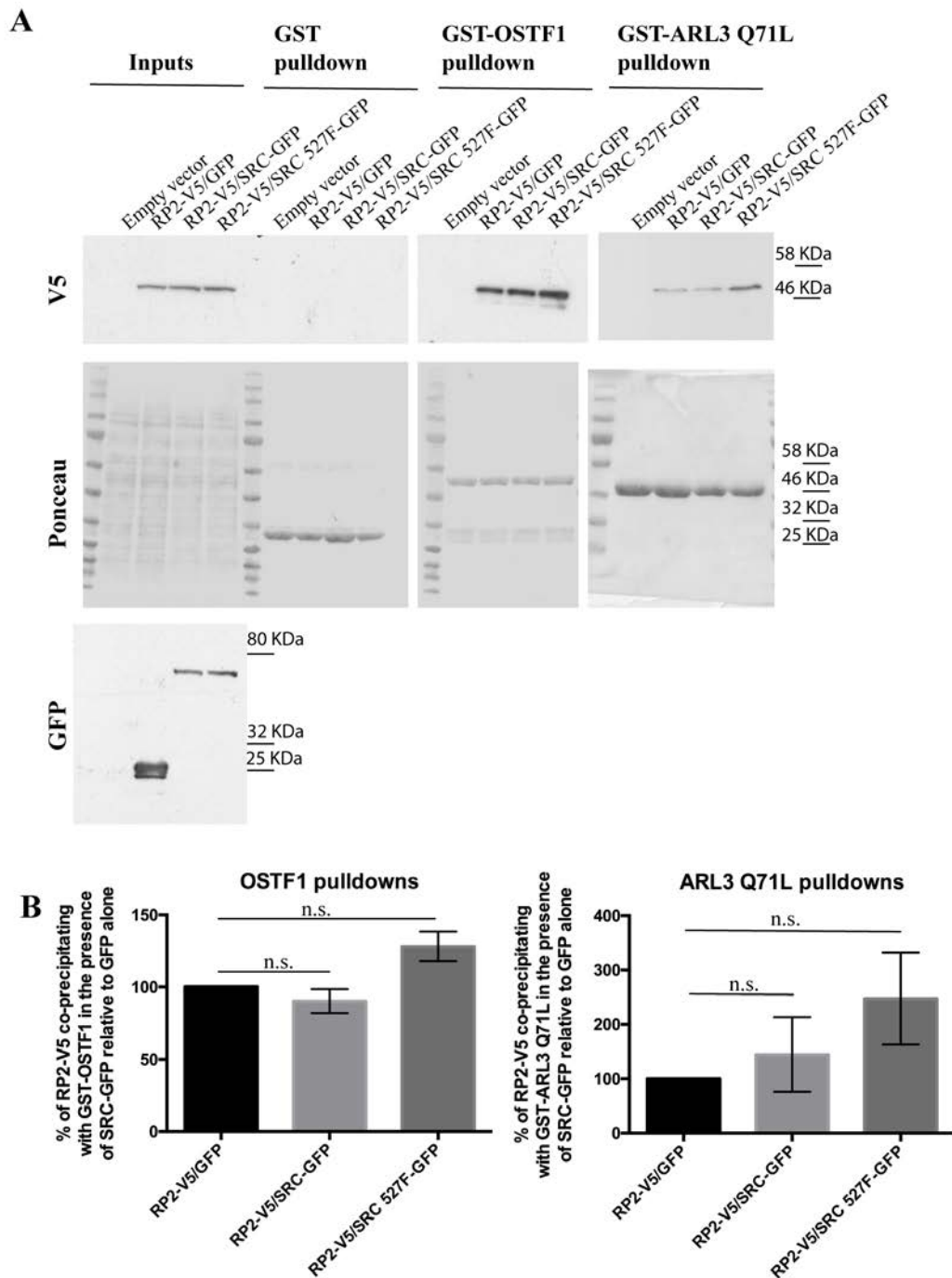


**Figure 3.7. Overexpression of c-SRC mildly stabilises the binding of RP2 to ARL3.**

A) To determine if tyrosine phosphorylation of RP2 affects binding to its interaction partners, recombinant GST-OSTF1 and GST-ARL3 Q71L were used as baits to pulldown RP2-V5 from HEK293T cells transiently co-transfected with RP2-V5/GFP, RP2-V5/c-SRC-GFP, or RP2-V5/c-SRC 527F-GFP (the constitutively active mutant of c-SRC). SDS-PAGE and western blotting analysis with anti-V5 antibody was used to approximate the amount of RP2-V5 found in the cell lysates (inputs) and bound to

the bait proteins. Ponceau staining was used to visualise the GST-tagged protein bands. B) Relative quantification of the RP2-V5 abundance between pull-down samples (mean  $\pm$  S.E.M n=3 densitometry measurements on 3 separate immunoblots normalised to the inputs). Two-tailed one-sample t-test was used to assess the significance of the observed differences between c-SRC-transfected samples compared to the RP2-V5/GFP sample, whose value was set to 100. P-values for GST-OSTF1 pull-downs: RP2-V5/GFP compared to RP2-V5/ c-SRC-GFP: 0.3611, RP2-V5/GFP compared to RP2-V5/ c-SRC 527F-GFP: 0.1092. P-values for GST-ARL3 Q71L pull-downs: RP2-V5/GFP compared to RP2-V5/ c-SRC-GFP: 0.5836, RP2-V5/GFP compared to RP2-V5/ c-SRC 527F-GFP: 0.2239.

### **3.2.2.3 Total tyrosine phosphorylation of RP2 is not due to OSTF1-mediated phosphorylation by c-SRC**

The next point of my hypothesis that I wanted to test is whether OSTF1 acts as an adaptor for bringing RP2 and its kinase to the same complex and if, therefore, it is necessary for RP2 phosphorylation to occur. For this purpose, I decided to test if the RP2 mutants that I previously identified as deficient in interacting with OSTF1 (Y245A, Y245E) can still be tyrosine phosphorylated. In Figure 3.8, a tyrosine phosphorylated band can be seen corresponding to the molecular weight of RP2-V5 in IPs from both the WT and the Y245A/E-transfected cells. In conclusion, interaction with OSTF1 is not an essential prerequisite for the endogenous tyrosine phosphorylation of RP2 in HEK293T cells.

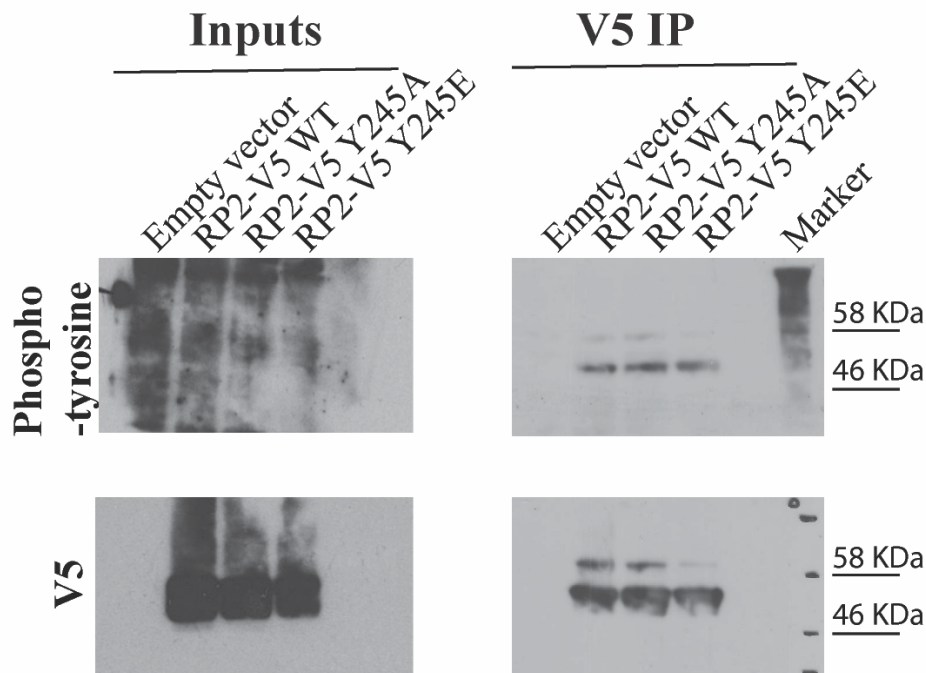


**Figure 3.8. Binding to OSTF1 is not essential for the endogenous phosphorylation of RP2 in HEK293T cells.**

In order to test the hypothesis that OSTF1 acts as an adaptor protein which facilitates the phosphorylation of RP2 by c-SRC, I examined the phosphorylation status of RP2 Y245A- and Y245E-V5 mutants, which do not interact with OSTF1, as shown in Chapter 3.2.1. RP2 WT, Y245A and Y245E-V5 were immunoprecipitated from lysates of cells transfected with the respective constructs using anti-V5 antibody conjugated agarose beads. Cells transfected with an empty destination vector were used as negative control. The IPs were subjected to SDS-PAGE and western blotting using anti-phosphorylated tyrosine antibody. An anti-mouse IgG (kappa light chain) HRP-conjugated secondary antibody was used for the visualisation of the phosphorylated bands. The WT and Y245A, E RP2 proteins are equally phosphorylated, leading to the conclusion that interaction with OSTF1 is not essential for phosphorylation of RP2 to occur in HEK293T cells. Subsequent re-probing with an anti-V5 antibody confirms the presence of an RP2-V5 band at the same molecular weight as the phosphorylated band in the transfected lysates.

Finally, I wanted to examine if endogenous c-SRC activity is linked to tyrosine phosphorylation of RP2 that is observed in HEK293T cells. To achieve this, I treated HEK293T cells with the novel small molecule inhibitor of c-SRC, eCF506 (Fraser et al. 2016). This compound is known to inhibit c-SRC and its related kinase YES and,

to a lesser extent, FYN at subnanomolar levels in vitro and displays exceptional specificity (3 orders of magnitude) against c-Abl. Inhibition of c-SRC kinase activity was confirmed by western blot against phospho-Y416 SRC, the residue where c-SRC is autophosphorylated upon activation. HEK293T cells were transfected with RP2-V5 or empty vector and treated for 1 hr before lysis with DMSO, 100 and 200 nM of the inhibitor (higher concentrations caused complete detachment of the cells from the substrate). 100 and 200 nM treatment caused Y416 phosphorylation on SRC to drop 50% and ~100%, respectively. However, treatment did not have any effect on RP2 tyrosine phosphorylation (Figure 3.9). This experiment suggests that SRC is not the only responsible kinase for total tyrosine phosphorylation of RP2 in HEK293T cells.

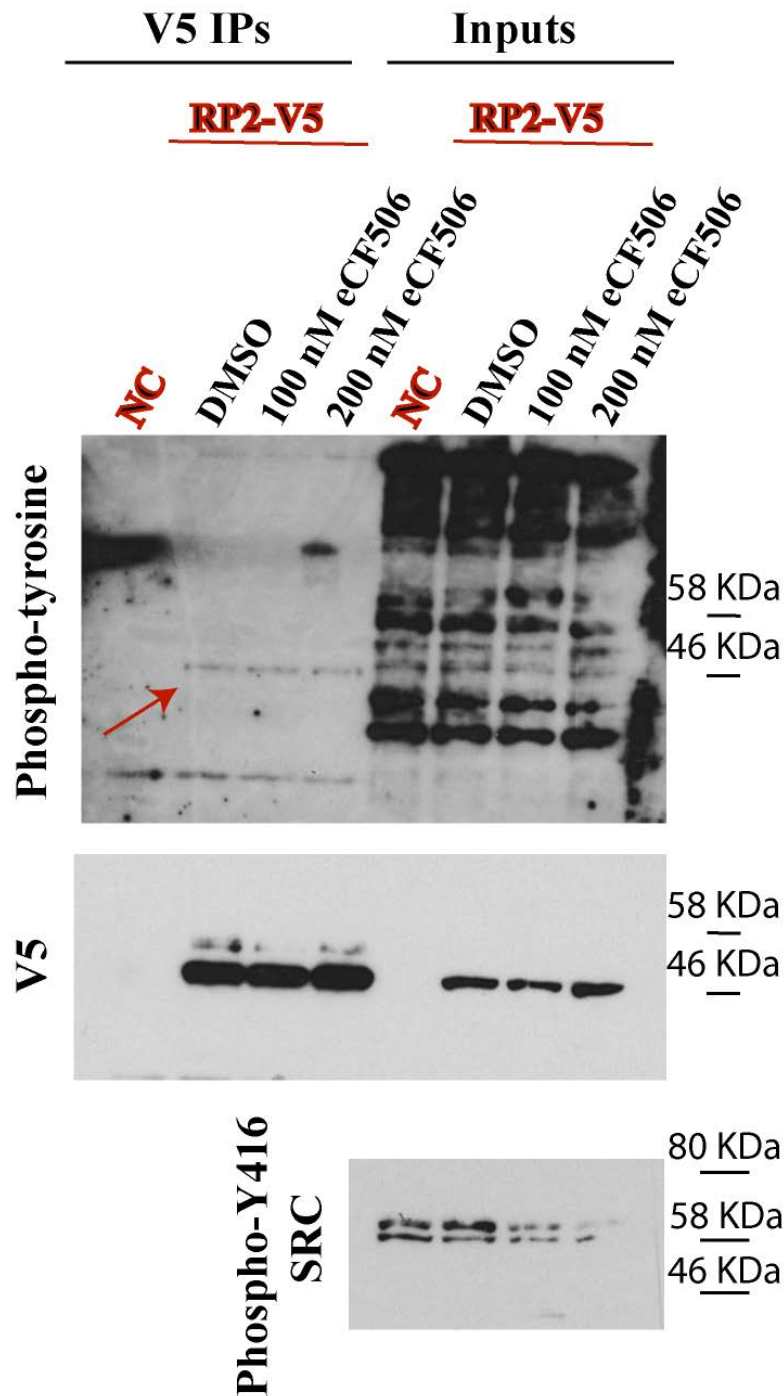


Figure 3.9. Phosphorylation of RP2-V5 in HEK293T cells is not dependent on endogenous c-SRC activity.

In order to determine if c-SRC is indeed responsible for phosphorylating RP2 endogenously, the phosphorylation status of RP2-V5 was tested in HEK293T cells that were treated with DMSO only or the novel small molecule inhibitor of c-SRC, eCF506. To detect phosphorylation, RP2-V5 was immunoprecipitated from the transiently transfected cells' lysates using anti-V5 antibody conjugated agarose

beads. The IPs as well as the lysates before IP (inputs) were subjected to SDS-PAGE and western blotting using anti-phosphorylated tyrosine antibody. Cells transfected with an empty destination vector were used as negative control (NC). This approach shows that phosphorylation of RP2-V5 is not reduced when the cells are treated with the c-SRC inhibitor. Subsequent re-probing with an anti-V5 antibody confirms the presence of a band corresponding to RP2-V5 at the same molecular weight as the phosphorylated band. The inputs were also probed with an antibody against Y416-phosphorylated c-SRC to show that the kinase activity is indeed affected by the inhibitor (Y416 is a site for activating auto-phosphorylation of the kinase).

### **3.2.3 RPE1 cells lacking RP2 expression are less motile**

Two studies have previously identified OSTF1 as an important regulator of cell motility in cancer cell lines. According to Tanimura and colleagues (Tanimura et al. 2011), OSTF1 exerts a negative effect on cell motility which is counteracted by phosphorylation by p90 ribosomal S6 kinase (RSK1) under command of the ERK1/2 signalling pathway downstream of Ras. Indeed, overexpression of OSTF1 in HeLa cells where the ERK pathway is not constitutively active attenuates cell motility, while knockdown of OSTF1 by RNAi has the opposite effect. This role of OSTF1 is attributed to its direct interaction with MYO1E, a long-tail type I Myosin, whose intracellular localisation is regulated by OSTF1 in an ERK pathway-dependent manner. In particular, OSTF1 functions as a “cytoplasmic anchor” for MYO1E and thus prevents it from localising to sites of actin nucleation in lamellipodia, which is essential for their proper formation and for cell motility to occur (Tanimura et al. 2016).

The emergence of these studies led me to examine if the RP2-OSTF1 complex also has a role in cell motility regulation. To achieve this, I performed migration assays on hTERT-RPE1 clonal cell lines that were engineered to be genomic *RP2* null by Dr Toby Hurd using the CRISPR/ Cas9 method (Table 3.2). Initially, I characterised the cell lines as shown in Figure 3.10. Two lines (G, I) were selected for analysis because they were proved to completely lack expression of RP2 both by western blot and real-time qPCR using  $\beta$ -actin as the loading control and reference gene accordingly. qPCR experiments were performed by Cora Harrison under my supervision as part of her Honours thesis. The levels of endogenous ARL3 GTPase,

the most well known interaction partner of RP2, were unchanged in the *RP2* null cells. In order to examine if they cell lines grow normally, I generated growth curves by counting the number of cells in 6-well plates at different time-points. This experiment showed that the G line grows slower than the parental WT cells. However, because this defect was not observed in the I line, it is not considered a specific phenotype caused by the absence of RP2, but rather a product of clonal variation between the cell lines.

**Table 3.2. Deleterious mutations in the RP2 gene found in the RPE1 clones that are used in this study.**

G, I clones are both homozygous for 2-bp deletions, as identified by Sanger sequencing of a PCR product encompassing the targeted sequence of RP2 exon 2. The deletions are predicted to result in premature stop codons and nonsense mediated decay of the mRNA product.

<b>RP2 null clone</b>	<b>Type of mutation</b>	<b>Sequence</b>	<b>Change</b>
<b>G</b>	2 bp deletion	CCACTCAACCCATCATTGAGTCTTCCTCAAATATCAA A--TGGATGTTTTCAATG	F145Wfs8x
<b>I</b>	2 bp deletion	CCACTCAACCCATCATTGAGTCTTCCTCAAATATCAA ATTT--ATGTTTTCAATG	G146Mfs7x



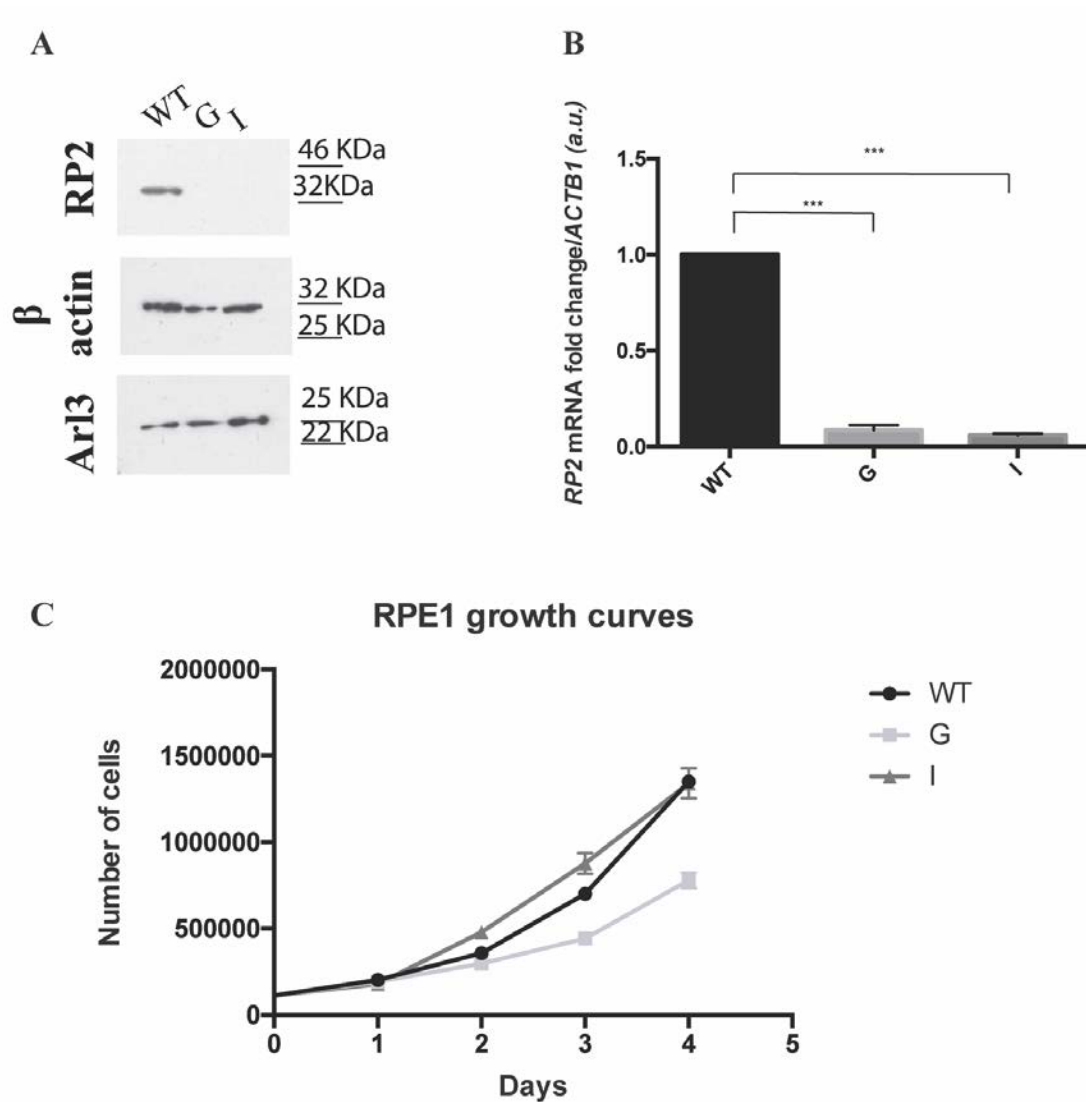


Figure 3.10. **G and I CRISPR clones lack RP2 expression but this is not responsible for the growth defect observed in clone G.**

A, B) Lack of RP2 expression was confirmed in the hTERT-RPE1 clones that I use in this study by western blotting and real-time qPCR. A) Lysates from wild-type, G and I clones were subjected to SDS-PAGE and western blotting using anti-RP2, anti-ARL3 and anti- $\beta$  actin (loading control) antibodies. B) mRNA was extracted from WT parental, G and I RPE1 cells and was used to generate cDNA to serve as template for real-time qPCR. *RP2* transcript levels (normalised to *ACTB1* transcript levels) are greatly reduced in cells from the G and I clones that are homozygous for 2-bp deletions in the *RP2* gene, compared to WT cells. This reduction implies that nonsense mediated decay of the transcripts is taking place (error bars correspond to S.E.M. from 3 biological repeats of the real-time qPCR experiment,  $p < 0.0001$  for

WT vs I and  $p=0.0009$  for WT vs G according to one-sample two-tailed t- test<sup>2</sup>). Au=arbitrary units. qPCR experiments were conducted by Cora Harrison under my supervision as part of her Neuroscience Honours thesis C) Growth rate of parental WT, G and I RPE1 cells was estimated in culture by counting the number of cells at different time points (error bars correspond to SEM from 3 technical repeats).

In order to examine the role of RP2 in cell motility regulation, I compared the motility of WT parental RPE1 cells to the RP2 null RPE1 lines G and I in a random migration assay and a wound healing assay. The random migration assay involves recording the movement of individual sparsely plated cells that are not contact-inhibited, in response to local gradients of growth factors contained in the serum-supplemented growth medium. As shown in Figure 3.11A, *RP2* null cells cover smaller distance compared to WT cells over the same time frame. The difference seems more pronounced when quantifying the absolute migration distance (defined as the distance between starting and ending point), implying that *RP2* null cells are defective in directional migration compared to the WT cells. In addition, while the WT RPE1 cells appear to form well-defined lamellipodia, cells that lack RP2 are rounder in shape. On the other hand, the wound healing assay is performed on cells that form a confluent monolayer and are therefore contact-inhibited. Inducing a scratch wound on the monolayer activates the cells that are on the edges and causes them to move towards the centre of the wound in order to populate it. As shown in Figure 3.11B, cells that lack RP2 expression cover smaller area in the wound compared to WT cells at the same time-points. Taken together, these assays suggest that RP2 is also involved in the regulation of cell motility like its binding partner, OSTF1. Both the *RP2* null cell lines are defective in cell migration compared to the WT cells, but they also display remarkably different behaviour between them, which can be attributed again to the effect of clonal variations like for example the presence of modifiers of the phenotype. Clonal variation is a potential problem because each *RP2* null cell line was grown from a single cell with a specific deleterious mutation. While examining two different lines (G, I) partially circumvents this problem, the

---

<sup>2</sup> Mean reduction of transcript levels between WT and mutant lines: 91.5% and 94% for G and I lines respectively, with 95% confidence intervals: 103.6% to 79.4% and 97.8% to 90.3% for G and I lines respectively.

experiment would benefit from the use of better control lines. For example, clonal cell lines that have undergone the CRISPR procedure but display RP2 expression at WT levels, either because they have retained the WT RP2 sequence or because they encompass silent mutations, could be used for comparison in the place of the parental WT cell line.

It must also be noted that RP2 seems to have an opposite role to OSTF1 in the regulation of cell motility; it can be suggested, therefore, that RP2 is a positive regulator of cell motility. More studies are needed to characterise the phenotype and pinpoint exactly what the role of RP2 is in the process.

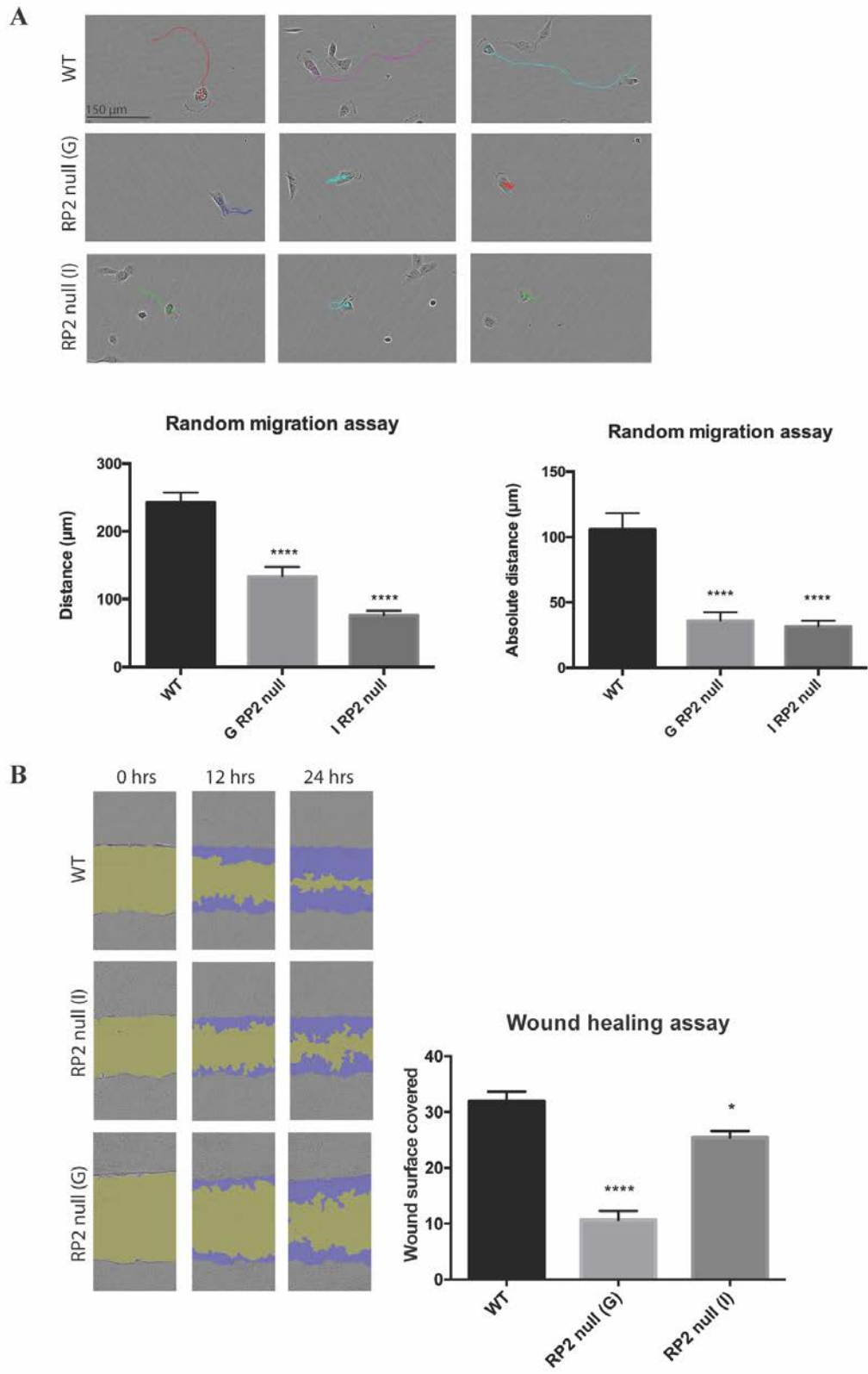


Figure 3.11. *RP2* knockout leads to migration defects in RPE1 cells.

A) Parental WT RPE1 and two clones (G,I) of *RP2* null RPE1 cells were sparsely plated and random migration of individual cells was analysed over a 24-hr period.

Top panels show representative tracks followed by individual cells (during a 9-hr period) as coloured lines. Cells lacking RP2 tend to move in circles rather than towards a specific direction and cover less distance than WT cells. The graph on the left shows distance covered by individual cells over a 9 hr period in  $\mu\text{m}$  (mean  $\pm$  SEM for 40 cells from 4 technical repeats.  $P=0.0006$  for G vs WT,  $P<0.0001$  for I vs WT as calculated by two-tailed t-test and two-tailed t-test with Welch's correction, respectively<sup>3</sup>). The graph on the right shows absolute distance (distance between starting and ending point) covered by individual cells over a 9 hr period in  $\mu\text{m}$  (mean  $\pm$  SEM for 40 cells from 4 technical repeats.  $P<0.0001$  for G vs WT and I vs WT as calculated by Mann-Whitney test). B) Parental WT RPE1 and two clones (G, I) of RP2 null RPE1 cells were subjected to a wound healing assay. Images on the left show the wound across three different time-points. Yellow represents the wound area and purple is the area covered by migrating cells. The graph on the right represents the wound surface that was covered by migrating cells 10 hrs after the scratch was introduced (mean  $\pm$  SEM for 6 technical repeats.  $P=0.0103$  for I vs WT,  $p<0.0001$  for G vs WT as calculated by two-tailed t-tests<sup>4</sup>).

### 3.3 Discussion

#### 3.3.1 Mapping the OSTF1 interaction interface on RP2: conclusions

In this chapter, I characterised the recently identified protein-protein interaction between RP2 and OSTF1. By mapping the interaction interface between the two proteins on a patch of RP2 that is strictly conserved among vertebrates, I showed that OSTF1 is a specific interaction partner of RP2 whose function may underlie the etiology of retinal degeneration caused by mutations in the *RP2* gene. Therefore, studying the role of the complex is important and could provide the scientific community with novel ways of therapeutic intervention for Retinitis pigmentosa type 2. For example, it is worth noting that peptoid inhibitors were recently designed which display high affinity for the SH3 domain of human OSTF1 (Han et al. 2016),

---

<sup>3</sup> Mean difference in distance covered by WT vs mutant cells: 96.6  $\mu\text{m}$  and 175.6  $\mu\text{m}$  for G and I lines, respectively, with 95% confidence intervals: 148.6 to 44.5  $\mu\text{m}$  and 219.1 to 132.0  $\mu\text{m}$  for G and I lines, respectively.

<sup>4</sup> Mean difference in percentage of wound area covered by WT vs mutant cells: 21.3% and 6.5 % for G and I lines, respectively, with 95% confidence intervals: 26.6% to 16.0 % and 11.1% to 1.9% for G and I lines, respectively.

the domain which mediates the interaction with c-SRC and SMN (Szymkiewicz et al. 2004, Kurihara et al. 2001). In the future, mapping of the RP2 binding interface on OSTF1 will provide a complete structural profile of the interaction and will help investigate if the SH3 domain is important. Importantly, the present study is one of the first to suggest a function for the C-terminal domain of RP2, namely to provide a binding interface for the interaction with OSTF1. The other such study was by (Yoon et al. 2006), who suggested that RP2 has exonuclease activity via its C-terminus.

### **3.3.2. RP2 tyrosine phosphorylation analysis: conclusions**

To identify the function of the RP2-OSTF1 interaction, I formed two hypotheses based on previous evidence about the protein complexes that OSTF1 participates in. Initially, I investigated if OSTF1 is an adaptor for the c-SRC mediated tyrosine phosphorylation of RP2. In particular, I hypothesised that OSTF1, which has been suggested before to be an adaptor for SRC's functions, might act as a "scaffold" for the phosphorylation of RP2. Binding of OSTF1 to the SH3 domain could activate the kinase by inducing phosphorylation of Y416 and lifting of the activation loop (Ubersax and Ferrell 2007). I used *in vitro* methods (kinase assay) and MS analysis to support the suggestion that c-SRC directly phosphorylates RP2 at Y27. Because this tyrosine residue directly participates in the interaction between RP2 and ARL3, one of the ramifications of this finding is the possibility that phosphorylation serves to regulate the protein-protein interactions of RP2. However, site-specific mutagenesis and western blotting showed that the non-phosphorylatable Y27F mutation does not alter total tyrosine phosphorylation levels on RP2 in HEK293T cells. This suggests that there are other phosphorylatable tyrosine residues on RP2 which might mask Y27 phosphorylation. To confirm Y27 phosphorylation, the specificity of detection can be enhanced by the development of a phospho-specific antibody against phosphorylated Y27, instead of the generic anti-phosphotyrosine antibody. Finally, a different method, such as two-dimensional phosphopeptide mapping (Nagahara 2016), could be used to investigate if there are other phosphorylated tyrosines on RP2.

Despite the initial findings, further analysis of endogenous RP2 phosphorylation after treatment of HEK293T cells with a highly specific SRC inhibitor shows that c-SRC may not be the endogenous tyrosine kinase that phosphorylates RP2. The responsible kinase could be identified in the future by screening a library of known tyrosine kinase inhibitors for any effect on RP2 phosphorylation. However, the hypothesis that c-SRC phosphorylates RP2 *in vivo* should not be entirely rejected based on the present study, but should be investigated further using different experimental methods. First of all, c-SRC may be only partly responsible for the total tyrosine phosphorylation of RP2 and other kinases might be involved which could have masked any reduction in total tyrosine phosphorylation after treatment with c-SRC inhibitors. For this reason, the development of a phospho-specific antibody is again the way forward. Secondly, I had to rely on HEK293T that display very high transfection efficiency, as the low level of RP2 tyrosine phosphorylation meant that I did not manage to detect it in a cell line that is more physiologically relevant to the retina (such as RPE1 cells or 661W mouse cone retinoblastoma cells). Therefore, it is possible that I failed to detect c-SRC-mediated phosphorylation of RP2 because it is tissue- and cell line- specific. After all, c-SRC is known to participate in various retinal-specific processes: it has been reported to co-localise with rhodopsin at the cell body and the outer segment of photoreceptors and is linked to phosphorylation of phototransduction proteins (Ghalayini et al. 2002, Berta et al. 2011); c-SRC activity has also been associated with health and pathogenesis of the RPE (Rohrer et al. 2014, Law et al. 2009). Moreover, phosphorylation of RP2 by c-SRC might occur in a cilia-dependent manner. Ectopic c-SRC activity during G1 inhibits ciliogenesis, possibly via local regulation of actin polymerisation (Bershteyn et al. 2010). Finally, it is possible that RP2 phosphorylation by c-SRC is found downstream of specific signalling pathways and might need to be stimulated. In a recent large-scale study of the human phosphoproteome, tyrosine phosphorylation was found at exceptionally low stoichiometric levels in the absence of specific signalling events (Sharma et al. 2014). As a conclusion, it might be necessary to use a different cell line and stimulate c-SRC activity in order to detect c-SRC-dependent endogenous phosphorylation of RP2.

### 3.3.3 A potential role for RP2 in cell motility regulation

In the last part of the chapter, I find that RP2 might play a role in cell motility regulation, similarly to its interaction partner OSTF1. In particular, it seems that RP2 is a positive regulator of cell motility, while the opposite is true for OSTF1. Future work will characterise this phenomenon in more detail and must focus on the exact molecular pathways that regulate the role of RP2 in cell motility. Because OSTF1 exerts its negative effect on cell motility via its interaction with MYO1E, which OSTF1 prevents from associating with F-actin at sites of actin nucleation (Tanimura et al. 2016), future experiments could begin by investigating if RP2 also associates with MYO1E or if it competes with MYO1E for binding to OSTF1, which would explain the positive effect it has on cell migration. Site-directed mutagenesis and deletion approaches can be used for the identification of the exact domains on OSTF1 that interact with RP2. This approach could help investigate if they overlap with MYO1E's binding sites. Another interesting area of study that I would like to investigate in the future is the role of ARL3 in cell motility regulation. It is already known that knockdown of ARL3 reduces cell motility in HeLa cells and this is associated with STAT3-mediated signalling (Togi et al. 2016). Moreover, (Wright et al. 2016) have linked overexpression of constitutively active ARL3 (Q71L mutant) with defective migration of rod photoreceptors to the ONL during early post-natal development.

A point that is important to elucidate in future experiments is the relationship between cell motility and retinal degeneration. For my experiments, I used immortalised human retinal pigment epithelial cells (hTERT-RPE1), which are behaving as migratory cells in cell culture. The RPE are known to have a strong interdependence with the photoreceptors and other layers of the retina. Many forms of RP arise from RPE genes such as *RPE65* or *MERTK* which affect the visual cycle and OS phagocytosis, respectively. Moreover, progressive degeneration of RPE cells play a central role in the development of age-related macular degeneration (Nowak 2006). However, it is important to stress that RPE should not behave as migratory cells *in vivo*. In fact, cell transformation of the RPE, a phenomenon when they regain their proliferative and migratory capacity, leads to loss of contact with the



photoreceptors and the adjacent RPE, retinal detachment and proliferative retinopathies such as proliferative vitreoretinopathy (PVR) (Ruiz-Loredo and Lopez-Colome 2012).

On the other hand, a dynamically regulated acto-myosin cytoskeleton is a prerequisite for many of the function of the RPE *in vivo* (Ruiz-Loredo and Lopez-Colome 2012). Several myosin classes are expressed in the RPE, including I, II, III, V, VI, VII, IX and X. Some of them are associated with important RPE functions, such as phagocytosis (Myosin II, Myosin Va, Myosin VIIa which is mutated in Usher syndrome (Kevany and Palczewski 2010)), vesicular trafficking (Myosin VI) (Kitamoto et al. 2005) and melanosome aggregation (Myosin II) (Barsoum and King-Smith 2007). The function of class I Myosins in the RPE and the retina in general is unknown and should be a focus of future studies.

To find out if the RP2-OSTF1 complex has a role in retinal biology, it is important to investigate if the two proteins are co-expressed in the retina. Data from our group concerning expression analysis in mouse tissues based on  $\beta$ -gal staining suggest that OSTF1 is expressed in the RPE but not the photoreceptor layer in mice (Vermeren et al. 2017). Preliminary expression analysis by western blotting in various mouse tissues of the central nervous system (Appendix figure 3) suggests that OSTF1 and RP2 are both expressed in the RPE. This finding is preliminary and requires further corroboration by more detailed experiments that will examine OSTF1 expression in the retina, such as *in situ* hybridisation and immunostaining for the endogenous protein on retinal sections. Based on the data that is available so far, I hypothesise that OSTF1 is a negative regulator of cell motility processes in the RPE. OSTF1-mediated regulation of cytoskeletal processes might serve to prevent RPE migration, an unwanted effect of cell transformation that is related to retinal detachment and other diseases, as mentioned above (Ruiz-Loredo and Lopez-Colome 2012). Alternatively, the regulatory activity of OSTF1 might be required for other motility-related RPE functions, such as the extension of motile processes into the photoreceptor OS layer, or their phagocytic activity. These possibilities are discussed further in the next paragraph.

Therefore, it is suggested here that, while previous research on X-linked RP has focused almost entirely on the photoreceptors, future research should carefully examine any potential involvement of the RPE in the pathogenesis of RP type 2. An RPE-related process that requires extensive cytoskeletal reorganisation that could be reflected in the cell motility defect that I observed *in vitro* is the daily phagocytosis of shed photoreceptor OS. In order to assess if the loss of RP2 function leads to phagocytosis defects, I suggest that purified RPE cells from animal models of RP type 2 should be used in future experiments including phagocytosis assays of OS.

Furthermore, another interesting aspect of cell motility in the retina are the apical microvilli that the RPE cells project into the interphotoreceptor matrix. These projections, which interact with the OS tips, are reported to be motile (Bonilha 2014) and to contain a filamentous actin core as well as several types of myosins and other actin-associated proteins (Gu et al. 2012). Because the RPE microvilli are thought to mediate key processes such as visual pigment transport and regeneration, transport of nutrients to the photoreceptors and removal of waste (Bonilha 2014), it would be interesting to study them in relation to RP type 2.

In order to determine whether the death of photoreceptors in X-linked RP is due to intrinsic (cell-autonomous) defects or is caused by a dysfunction of neighbouring cells such as the RPE, the mosaic analysis method can be used which relies on the use of zebrafish as *in vivo* model. According to this method, zebrafish with chimeric retinæ can be generated via the transplantation of dextran-labelled blastomeres from a donor to a host embryo (WT donor to mutant host or the opposite). It has been shown that a fraction of donor blastomeres will then contribute to the retinal neuroepithelium (Tsujikawa and Malicki 2004a, Pujic and Malicki 2001, Goldsmith, Baier and Harris 2003). It can thus be examined whether mutant photoreceptors surrounded by WT RPE can be rescued from degeneration, or, conversely, whether WT photoreceptors degenerate when their environment is composed of mutant RPE. Chapter 5 of the present thesis is dedicated to the generation and characterisation of *rp2* null zebrafish lines generated using the CRISPR/Cas9 method, which would provide ideal platforms to apply the mosaic analysis method.

### 3.3.4 A potential role for RP2 in cell death

If it is proved that the death of photoreceptors in RP type 2 is not a secondary effect of defects in other cell types, the hypothesis can be formed that RP2 mutations directly affect cell death pathways. In Figure 3.10C, it was shown that the growth rate of the G *RP2* null line is slower than the WT parental cells. Although this observation might not be due to loss of RP2 function but simply represent a result of clonal variation, it must be investigated in the future if RP2 mutations lead to increased cell death. This can be tested directly on retinal sections of *RP2* knockout animal models by TUNEL assay or acridine orange staining, showing DNA fragmentation and apoptotic cells, respectively. In addition, immunostaining for cell death markers, either apoptosis-specific or encompassing different cell death pathways (e.g. cleaved Caspase 3 or Annexin V) (Galluzzi et al. 2009) can be used on the *RP2* null RPE cell lines that I have described.

## **Chapter 4: Characterisation of the interaction between RP2 and DNA PKcs and implications for DNA damage repair in the retina**

### **4.1 Introduction**

One of the prominent methods for discovering novel biological roles for a protein is the identification of novel interaction partners. In chapter 3, I referred to the LC/MS-MS analysis we conducted aiming to identify phosphorylation sites on immunoprecipitated V5-tagged RP2. Apart from this original purpose, my experiment had the additional benefit of providing information about the interactome of RP2 when transiently expressed in HEK293T cells. In the present chapter, I will present the proteomic analysis of the MS results from three independent biological replicates. Among the proteins that were significantly enriched in the RP2-V5 IPs compared to the negative controls, there is an enzyme which plays a central role in numerous processes important for neuronal maintenance in general and retinal viability in particular: the catalytic subunit of the DNA damage repair (DDR) enzyme, DNA-dependent protein kinase (DNA PKcs, product of the *PRKDC* gene).

#### **4.1.1 The importance of DDR mechanisms for retinal development and viability**

DDR mechanisms are core components of all cells' survival strategies. As shown in Table 4.1, different molecular pathways are employed to repair different types of DNA lesions. Among them, DNA double-stranded breaks (DSBs) are the most severe insults to DNA. They can be caused by ionising radiation (IR), chemical agents, oxidative stress or during DNA replication. Importantly, "programmed DSBs" are also introduced in eukaryotic organisms during physiological processes such as meiosis and development of the immune system. DSBs affect chromatin structure and will lead to cell death or trigger genomic instability and cancer if left unrepaired (Jackson and Bartek 2009). Moreover, selective generation of DSBs has been observed during neural development, and is linked to the early phase of

programmed cell death that occurs physiologically in the developing nervous system (Boya and de la Rosa 2005). For example, correct function of the DSB repair machinery and DNA PKcs is essential for the survival of young neurons in the developing mouse retina. It is worth noting that DNA PKcs has a specific role in this process which is not shared with other kinases of the same family that also participate in DSB repair, such as ataxia telangiectasia mutated (ATM) kinase (Baleriola, Suarez and de la Rosa 2010).

The mature retinal photoreceptors and the retinal pigment epithelium (RPE) have extremely stringent requirements for efficient DNA repair mechanisms due to their susceptibility to oxidative stress, which is not only damaging DNA and other biomolecules, but is also the main mediator of light-induced photoreceptor death (Cortina et al. 2003, Gordon et al. 2016, Gordon et al. 2002). One of the reasons for this vulnerability is the extremely high lipid content of the photoreceptor outer segment (OS) compared to other tissues. In particular, polyunsaturated fatty acids (PUFAs) are readily oxidised to highly reactive compounds that initiate free radical chain reactions. In addition, reactive oxygen and nitrogen species (RONs) are produced by the activation of photosensitising molecules and by-products of the visual cycle (Wright et al. 2010). Therefore, it is not surprising that Retinitis pigmentosa (RP) is one of the clinical features of DNA damage-related conditions Cockayne syndrome and xeroderma pigmentosum, which stem from impaired repair of UV-induced DNA damage and oxidative lesions, mostly due to defects in enzymes of the nucleotide excision repair (NER) pathway (Ramkumar et al. 2011, Brooks et al. 2013, Gorgels et al. 2007).

The link between retinal degeneration and defective DNA damage repair has not been extensively studied. However, reports have accumulated recently that link retinal degeneration and ciliopathies in general to DDR protein components. For example, mutations in the gene encoding for the centrosomal protein Cep164 have been identified in patients with retinal degeneration and other Nephronophthisis (NPHP)-related ciliopathies (Chaki et al. 2012); Cep164 co-localises with DDR proteins in nuclear foci upon UV irradiation and interacts with ATM and ATM- and Rad3-related (ATR) kinases, which are key DDR signalling mediators, and XPA

which is a core component of the NER pathway (Sivasubramaniam et al. 2008, Pan and Lee 2009). *SDCCGA8* is another protein that was recently linked to NPHP and retinal degeneration in patients suffering from syndromes of the Bardet-Biedl spectrum (Otto et al. 2010). Renal degeneration in the *Sdccga8* gene trap mouse model is underlined by increased DDR signalling activity and hyperactivation of  $\gamma$ H2AX, a chromatin marker of DNA damage; the protein itself has been related to replication stress and cell cycle progression through the S-phase (Airik et al. 2014). Furthermore, (Valdes-Sanchez et al. 2013) report the existence of severe retinal degeneration in a mouse model of Seckel syndrome harboring a humanized pathogenic mutation in the gene encoding for ATR kinase, a DNA damage sensor protein which is activated by replication stress. Nevertheless, the authors of the study suggest that the retinal phenotype is not due to DNA damage defects but a result of a non-canonical function of the kinase at the photoreceptor connecting cilium (CC). Furthermore, it was recently found that retinal degeneration in the rd10 mouse model is underlined by abnormal localization of Sirt1, an MRN DNA damage sensor protein with neuroprotective function, from the nucleus to the cytoplasm (Jaliffa et al. 2009). Finally, mutations in the topoisomerase I-binding RS protein (TOPORS), an E3 ubiquitin ligase, have recently been linked to autosomal dominant RP (Chakarova et al. 2007). TOPORS is not only a nuclear protein which participates in DNA damage signalling but also a component of the photoreceptor CC (Chakarova et al. 2011). Collectively, the studies mentioned above all point to a relationship between DDR proteins and retinal viability. Therefore, I hypothesised that RP type 2 might also be associated with defective DDR signalling and I aimed to characterise the potential novel interaction between RP2 and DNA PKcs further.

#### **4.1.2 DNA PKcs is a multi-functional kinase**

The catalytic subunit of DNA PK is a widely expressed (Proteomics DB, <http://www.proteomicsdb.org/>) large (469,089 Da) Ser/Thr kinase. It belongs to the phosphatidylinositol 3 kinase-like family of protein kinases (PIKK) and it shares amino acid and protein architecture similarities, as well as overlapping functions, with the other members of the PIKK family and DDR proteins ATM and ATR. The

DNA PK holoenzyme refers to the catalytic subunit in complex with the Ku 70/80 heterodimer. Ku has the property of binding to DNA ends with high affinity and in a sequence-independent manner. One of its main functions is to recruit DNA PKcs to DSBs and stimulate its kinase activity (Jette and Lees-Miller 2015).

The main protein domains of DNA PKcs are: an N-terminal region composed of HEAT (Huntingtin, Elongation factor 3, regulatory subunit A of PP2A, TOR1) repeats and other  $\alpha$ -helical regions, and a C-terminal region containing the kinase domain as well as FAT (FRAP, ATM, TRRAP) and FAT-C domains, required to stabilize the kinase domain. The HEAT repeats region forms the “arms” that surround a central cavity, a formation that is thought to accommodate DNA (Jette and Lees-Miller 2015, Sibanda, Chirgadze and Blundell 2010) (Figure 4.1A). These crude structural characteristics already give a clue about the main functions that this DNA-binding holoenzyme has been associated with. Its most well-studied role has been in the repair of DSBs via the non-homologous end joining pathway (NHEJ). This pathway is employed not only for the repair of random exogenously-induced DSBs, but also for the physiological processes of V(D)J recombination and class-switch recombination which are essential for the development and maturation of lymphocytes and immunoglobulin rearrangement (Malu et al. 2012). It is therefore not surprising that radiosensitivity (due to defects in repairing IR-induced DSBs) and severe combined immunodeficiency (SCID) are prominent characteristics among patients with DNA PKcs deficiencies (Mathieu et al. 2015, Woodbine et al. 2013, van der Burg et al. 2009), similar to deficiencies in other NHEJ proteins (Woodbine, Gennery and Jeggo 2014). Figure 4.1B shows an overview of the role of DNA PK in NHEJ (Davis and Chen 2013). The Ku heterodimer is the first complex to bind to free DNA ends and act as a scaffold to recruit the other NHEJ components, including scaffold proteins and enzymes required to process DNA ends and catalyze re-ligation: DNA PKcs, XRCC4, DNA ligase IV, XLF, APLF, the DNA polymerases  $\mu$ ,  $\lambda$  and WRN helicase, among others. In this first stage of NHEJ, the cooperative action of Ku and DNA PKcs is required to stabilize the DSB complex and protect the free DNA ends from unspecific processing. Most of the NHEJ component proteins have also been suggested to be substrates of DNA PKcs-mediated phosphorylation: PNKP, Artemis endonuclease, XRCC4, DNA Ligase IV, XLF, WRN, Ku70/80 and

DNA PKcs itself. The cooperative action of the enzymes mentioned above is required for processing DNA ends to make them ligatable and filling any gaps. One notable role for DNA PKcs which has been studied extensively and has pathological importance is the activation of Artemis, which is necessary for its endonucleolytic activity (Ma et al. 2005, van der Burg et al. 2009). Finally, the last step is ligation of the broken DNA ends by DNA ligase IV. Finally, the NHEJ complex is released; in the case of DNA PKcs, dissociation from DNA is facilitated by a conformational change induced by autophosphorylation at the so-called ABCDE cluster (T2609, S2612, T2620, S2624, T2638 and T2647) (Jette and Lees-Miller 2015).

DNA PKcs has a dual role in DSB repair, because it is also implicated in phosphorylating histone H2AX, a central event in sensing and signalling the presence of a DSB in the context of chromatin. Nevertheless, DNA PKcs is not the only kinase capable of doing so, and its specific role in the process is still debated (Kinner et al. 2008).

Although its role in NHEJ is the most well documented, DNA PKcs has been shown to participate in other pathways of repairing DNA lesions. These can be seen in Table 4.1, which summarises known pathways of DDR and highlights which ones have been linked to the function of DNA PKcs. For example, DNA PKcs co-precipitates in a complex with most essential components of the base excision repair (BER) pathway from HeLa cells, independently of DNA damage (Parlanti et al. 2007). BER is responsible for resolving most single-stranded DNA lesions induced by oxidative damage. Another study has found that absence of DNA PKcs from cells reduces their viability and DNA repair capacity after H<sub>2</sub>O<sub>2</sub> treatment. Interestingly, cells deficient in other NHEJ components do not display this vulnerability to H<sub>2</sub>O<sub>2</sub>, strongly arguing for an NHEJ-independent role of DNA PKcs in the cellular defense against oxidative stress (Li et al. 2014). In addition, (An et al. 2011) have argued that DNA PKcs depletion causes over-sensitivity to UV irradiation and defective transcription-coupled nucleotide excision repair (tcNER), the pathway that preferentially repairs DNA lesions caused by UV irradiation in the transcribed strand of a transcriptionally active gene. Finally, far from being an exclusive NHEJ factor, it seems that DNA PKcs actively regulates the choice of DSB repair pathway (NHEJ



or HR) in cooperation with ATM (Shrivastav, De Haro and Nickoloff 2008). Reports have contradicted each other regarding the exact effect DNA PK exerts on pathway choice and it seems more possible that this depends on its phosphorylation status and which exact residue is phosphorylated (Neal et al. 2011, Serrano et al. 2013).

Among the multitude of processes that have been linked to DNA PKcs activity, there are also basic cellular functions such as mitosis and transcription. During mitosis, DNA PKcs is phosphorylated at multiple sites and localizes to centrosomes, mitotic spindle and the midbody (Douglas et al. 2014), while it mediates phosphorylation of checkpoint kinase 2 (Chk2) and  $\gamma$ H2AX in a mitosis-dependent manner (Tu et al. 2013). Lack of DNA PKcs causes multiple mitotic defects (Lee et al. 2011). Interestingly, these phenomena are independent of Ku and DNA damage (Douglas et al. 2014). Furthermore, DNA PKcs plays a major role in telomere protection (Le et al. 2013). This prolific kinase has even been implicated in transcriptional activation of lipogenic genes in response to feeding/insulin (Kong et al. 2011).

Apart from its nuclear roles, reports have emerged recently that DNA PKcs participates in a number of cytoplasmic pathways, including EGFR signaling (Dittmann et al. 2008) and Golgi cohesion (Farber-Katz et al. 2014). Therefore, a more pivotal role is emerging for DNA PKcs not only in the cross-talk between different repair pathways and cell survival, but also in relaying DNA damage signals outside the nucleus and orchestrating the general cellular response, in addition to several other, non-DNA damage related, functions. It is not by chance that decreased activity and/or expression of DNA PK has been associated with diseases outside the typical spectrum of NHEJ deficiencies, in particular with cancer susceptibility (Goodwin and Knudsen 2014), neurodegeneration (Woodbine et al. 2013) and Alzheimer's (Kanungo 2016).

In the present chapter, I characterise the potential interaction between RP2 and DNA PKcs and provide the basis for further studies that will prove if photoreceptor survival can be added to the long list of physiological pathways that DNA PKcs has been associated with. I will provide evidence that DNA PKcs co-precipitates with exogenous and endogenous RP2 from HEK293T and RPE1 cells, and that this interaction is abolished by a pathogenic missense RP2 mutation which affects

palmitoylation of the protein. I will characterize the interaction further by showing where the proteins co-localise within RPE1 cells, and suggest that RP2 is a potential substrate for DNA PKcs-mediated phosphorylation at a non- S/T-Q site *in vitro*. Finally, I will provide evidence that cells lacking RP2 expression do not display compromised DSB repair after IR, and will suggest that the newly identified RP2-DNA PKcs complex is likely associated with a non-canonical function of the kinase outside the NHEJ pathway.

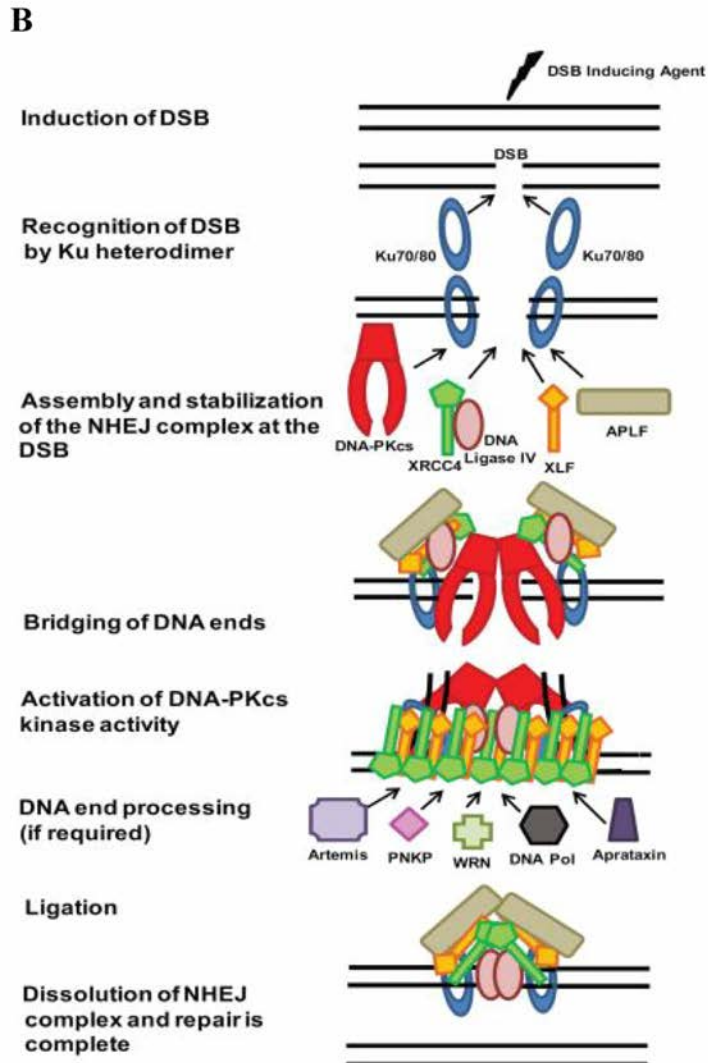
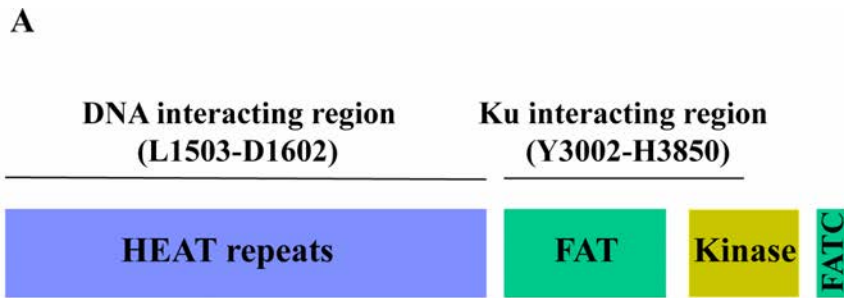


Figure 4.1. **Protein structure of DNA PKcs and schematic overview of NHEJ.**

A) Cartoon showing the main protein domains of DNA PKcs. The N-terminal HEAT repeats form the DNA-containing structure. The FAT and FATC domains are required for the stability of the kinase domain (Jette and Lees-Miller 2015). B) The basic steps of NHEJ are shown here. DNA PKcs has a central role which includes stabilising the DSB complex, protecting free DNA ends, and phosphorylating other protein components of the complex [reproduced from (Davis and Chen 2013)].

**Table 4.1. A role has been identified for DNA PKcs in most DNA repair pathways**

Adaptation of the table from (Jackson and Bartek 2009), where the main pathways for the repair of DNA lesions in higher eukaryotes are listed. The original table has been complemented with newer information and the pathways where DNA PKcs has been shown to be involved are summarised.

<b>DDR mechanism</b>	<b>DNA lesions under repair</b>	<b>Key protein components</b>	<b>DNA PKcs involvement</b>
<b>Direct lesion reversal</b>	O <sup>6</sup> alkylguanine	O <sup>6</sup> -methylguanine methyltransferase	
<b>Mismatch repair (MMR)</b>	Mismatches and insertions/deletions occurring during DNA replication.	Sensors MSH2–MSH6 and MSH2–MSH3 plus MLH1–PMS2, MLH1–PMS1, PLH1–MLH3, EXO1, polymerases δ and ε, PCNA, RFC, RPA, ligase I	
<b>Base excision repair and SSB repair (BER/SSBR)</b>	Abnormal DNA bases, simple base adducts, single-stranded breaks caused by oxidative damage or by abortive topoisomerase I activity.	DNA glycosylases (sensors), APE1 endonuclease, DNA polymerases (β, δ,ε) and associated factors, flap endonuclease FEN1, ligase I or ligase III. SSB repair can also involve polymerase β lyase activity, XRCC1, PARP1, PARP2, polynucleotide kinase and aprataxin.	<ul style="list-style-type: none"> <li>• DNA PK interacts with essential BER protein components (Parlanti et al. 2007, Levy et al. 2006).</li> <li>• DNA PKcs-deficient cells have trouble repairing H<sub>2</sub>O<sub>2</sub>-induced DNA damage (Li et al. 2014) and IR-induced oxidatively induced clustered DNA lesions (OCDLs) (Peddi et al. 2010).</li> </ul>
<b>Global genomic nucleotide excision repair (ggNER)</b>	Lesions that affect the double helix, such as the bulky base adducts,	Sensors elongating RNA polymerase, XPC-HR23B and	

<b>Transcription-coupled nucleotide excision repair (tcNER)</b>	pyrimidine dimers and crosslinks caused by UV irradiation.	DDB1/2, plus XPA, XPE, XPF/ERCC1, XPG, CSA, CSB, TFIIH (containing helicases XPB and XPD), DNA polymerases including polymerase $\kappa$ and associated factors, PCNA, RPA, ligase I and III	<ul style="list-style-type: none"> <li>• Depletion of DNA PKcs enhances sensitivity to UV and causes defects in tcNER (An et al. 2011).</li> </ul>
<b>Non-homologous end joining (NHEJ), DNA PKcs-dependent</b>	Double-stranded breaks (DSBs) induced by ionizing radiation, chemical agents and oxidative stress. Programmed DSBs during V(D)J recombination and class-switch recombination.	Sensors Ku and DNA-PKcs plus XRCC4, XLF/Cernunnos and ligase IV. Can also use the MRE11–RAD50–NBS1 complex, Artemis nuclease, polynucleotide kinase, aprataxin and polymerases $\mu$ and $\lambda$ .	<ul style="list-style-type: none"> <li>• Key role for DNA PKcs. It is recruited to DSBs by Ku and phosphorylates/activates most protein components of the NHEJ complex. Also required for DNA end protection from unspecific processing during NHEJ (Davis and Chen 2013). DNA PKcs inactivation/ absence causes defective DSB repair reflected clinically as radiosensitivity and immunodeficiency, among others (Woodbine et al. 2014).</li> </ul>
<b>Non-homologous end joining (NHEJ), DNA PKcs-independent</b>	DSBs, operating in cells of higher eukaryotes when DNA PKcs-dependent NHEJ is defective (Rosidi et al. 2008).	PARP-1/DNA Ligase III/ XRCC1 module, facilitated by linker histone H1	

<b>Homologous recombination (HR)</b>	DSBs caused by stalled replication forks and meiosis or exogenous agents, inter-strand DNA crosslinks.	RAD51, RAD51-related proteins (XRCC2, XRCC3, RAD51B, RAD51C, RAD51D, DMC1), RAD52, RAD54, BRCA2, RPA, FEN1, DNA polymerase and associated factors. Promoted by MRN, CtIP, BRCA1 and the ATM signaling pathway.	<ul style="list-style-type: none"> <li>• DNA PKcs participates in DSB repair pathway choice via its kinase activity. It can either favour or inhibit HR dependent on its autophosphorylation status (Shrivastav et al. 2008, Neal et al. 2011, Serrano et al. 2013).</li> </ul>
<b>Single-strand annealing (SSA)</b>	DSBs	ATM (sensor), MRN complex, RPA, Rad52, ERCC1/XPF (Bhargava, Onyango and Stark 2016).	
<b>ATM-mediated DDR signalling</b>	DSBs	ATM, MRN and CHK2. Promoted by mediator proteins such as MDC1, 53BP1 MCPH1/BRIT1, and by ubiquitin ligases RNF8, RNF168/RIDDLIN and BRCA1.	<ul style="list-style-type: none"> <li>• Possible.</li> <li>• ATM signaling is hyperactivated by oxidative stress in DNA PKcs deficient cells (Li et al. 2014).</li> <li>• Like ATM and ATR, DNA PKcs can also phosphorylate H2AX to initiate DDR signalling (Kinner et al. 2008).</li> </ul>
<b>ATR-mediated DDR signalling</b>	ssDNA, resected DSBs, UV-induced DNA damage.	Sensors ATR, ATRIP and RPA plus the RAD9–RAD1–HUS1 (9-1-1) complex, RAD17 (RFC1-like) and CHK1. Promoted by MRN, CtIP and mediator proteins	

		such as TOPBP1, Claspin, MCPH1/BRIT1 and BRCA1
<b>Fanconi anaemia (FANC) pathway</b>	Inter-strand DNA crosslinks.	FANCA, FANCC, FANCD1/BRCA2, FANCD2, FANCE, FANCF, FANCG, FANCI, FANCI, FANCL, FANCM, FANCN plus factors including PALB2 and HR factors.
<b>Trans-lesion bypass mechanisms</b>	Base damage blocking replication fork progression.	Error-prone DNA polymerases, including polymerases $\eta$ , $\iota$ , $\kappa$ , REV3 and REV1.

## 4.2 Results

### 4.2.1 RP2 co-precipitates with DNA PKcs from HEK293T cells

The catalytic subunit of the DNA-dependent protein kinase (DNA PKcs) was among the top proteins that co-precipitated with V5-tagged RP2 from HEK293T cells in our experiment of MS/MS analysis following affinity purification of V5-tagged RP2 from HEK293T cells. Figure 4.2A shows the analysis of MS hits presented as a volcano plot with the y-axis representing significance and x-axis representing enrichment. Quantitative analysis of proteins (fold change) was calculated by the label-free quantitation feature of the MaxQuant software which was used to analyse the MS datasets. This analysis resulted in 58 proteins that were enriched ( $p > 0.1$ ) in the RP2-V5 IPs compared to the negative controls (V5 IPs from empty vector-transfected cells). RP2 itself is, as expected, by far the most enriched protein in the IPs of RP2-V5 –transfected compared to empty vector-transfected cells. Among the proteins that co-precipitate with RP2 with high statistical significance is OSTF1, a recently identified interaction partner of RP2 which is referred to in detail in Chapter 3, and Transportin-1 (Importin  $\beta$ 2) which has been identified before as an interaction

partner of RP2 that mediates its targeting to cilia (Hurd et al. 2011). The identification of known interaction partners in complex with RP2 is important because it confirms the validity of the experiment. Another interesting hit among the potential interaction partners of RP2 is the PIKK-family kinase mTOR; since the involvement of mTOR-mediated pathways in retinal neuroprotection has been shown before (Faghiri and Bazan 2010), this is an interesting result that can be followed-up in the future.

For the reasons described in the introduction, this study has focused on the characterisation of the potential interaction between RP2 and DNA-repair enzyme DNA PKcs. Initially, I confirmed the interaction by IP and western blotting in HEK293T cells under mild lysis conditions. I showed that endogenous DNA PKcs co-precipitates with exogenous, tagged RP2 and this is independent of the nature of the tag, as it occurs both with V5- and FLAG- tagged RP2 (Figure 4.2B). Subsequently, I wanted to show the interaction between the endogenous proteins. To this end, I immunoprecipitated DNA PKcs and confirmed that a fraction of the total RP2 co-precipitates with the anti-DNA PKcs antibody, but not with another antibody of the same class that is produced in the same species (“control IP”- Figure 4.2C). In addition, I was interested in testing if DNA PKcs co-precipitates with ARL3, the most well-characterised interaction partner of RP2. To achieve this, I made hTERT-RPE1 cells that were retrovirally transduced to express FLAG-tagged ARL3 Q71L, the constitutively active mutant, after induction by doxycycline. ARL3 Q71L was used in this particular experiment because it stably binds RP2, contrary to the wild-type protein which only transiently interacts with the GAP (Velzel et al. 2008). FLAG IPs from ARL3 Q71L cells, but not cells transduced with an empty vector, were enriched in endogenous RP2 compared to the inputs. However, DNA PKcs is not present in the complex (Figure 4.2D). This result is a first indication that RP2, ARL3 and DNA PKcs may not form a stable trimeric complex. It is possible that the RP2-DNA PKcs interaction takes part in a pathway that is separate to the regulation of ARL3. If the RP2-DNA PKcs is a direct interaction, it is also possible that ARL3 and DNA PKcs antagonise each other for binding to RP2. This hypothesis must be tested in the future using a structure-based approach which will determine if the same RP2 domains participate in ARL3 and DNA PKcs binding.



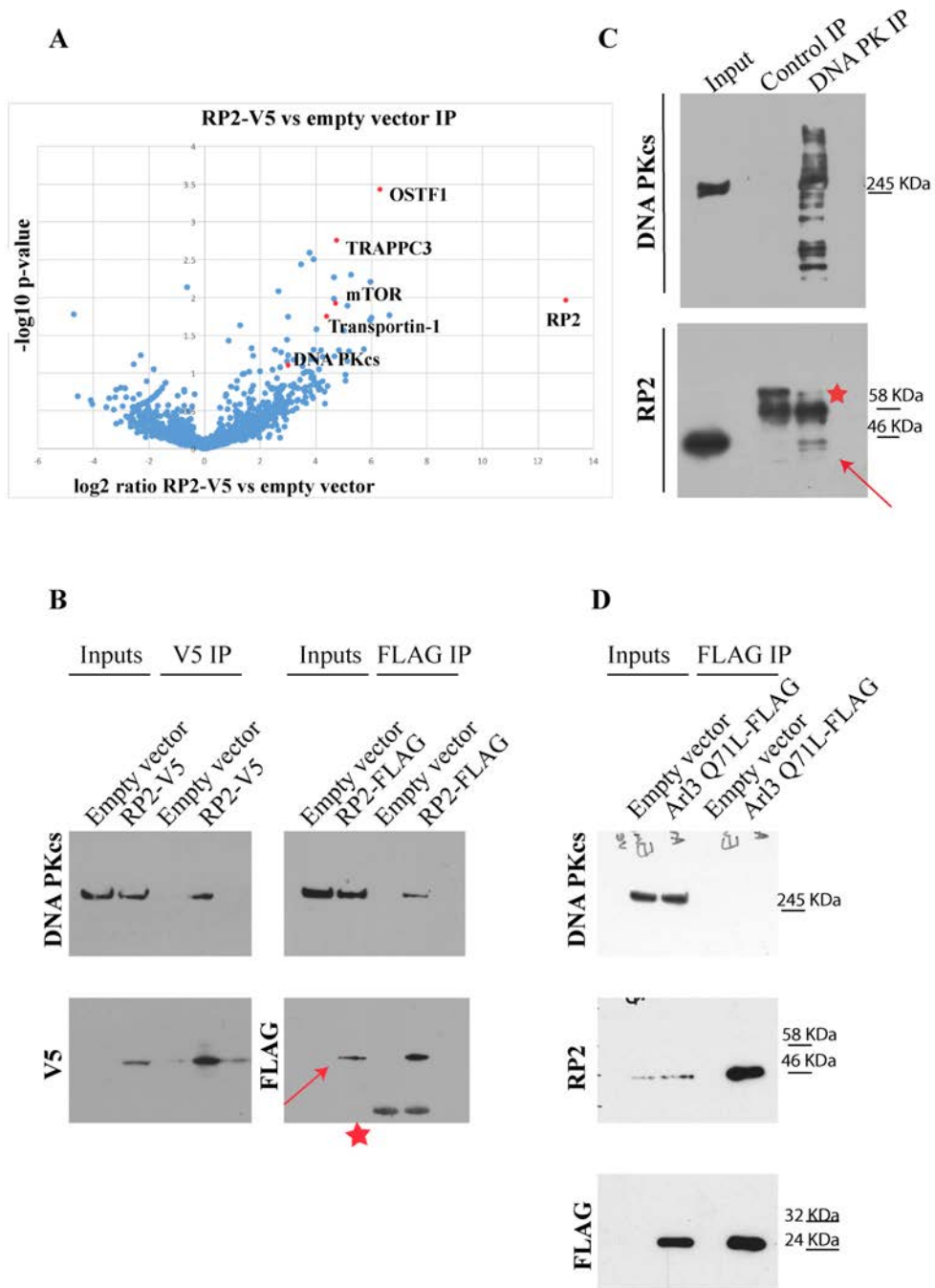


Figure 4.2. **RP2 interacts with DNA PKcs.**

A) Volcano plot of MS/MS data comparing anti-V5 immunoprecipitates (IPs) from RP2-V5-transfected HEK293T cells vs empty vector-transfected (negative control). Each datapoint in the graph represents a unique protein ranked and plotted on the x-axis according to fold enrichment (log2 transformed) in the RP2-V5-transfected cells (+ve x axis) over the negative control (-ve x axis). On the y-axis, proteins were ranked according to significance represented as  $-\log_{10} p$  value calculated by

unpaired two-tailed t-tests (n=3 independent biological repeats of the IP experiment and MS runs). Points representing the bait protein (RP2) and top-ranked proteins that immunoprecipitated with it, including DNA PKcs which was chosen for further analysis, are shown in red. B) V5- or FLAG- tagged RP2 was immunoprecipitated from HEK293T cells, transiently transfected with empty vector or tagged RP2-containing vector, using agarose beads-conjugated anti-V5 or anti-FLAG antibody, respectively. The IPs as well as the lysates before IP (inputs) were subjected to SDS-PAGE and western blotting using anti-DNA PKcs antibody. Subsequent re-probing with anti-V5 and anti-FLAG antibodies confirms correct expression of the constructs. The red arrow indicates the RP2-FLAG band, while the asterisk indicates the light chain of the antibody used for IP. C) Endogenous RP2 was co-immunoprecipitated with endogenous DNA PKcs from HEK293T cells' lysates using a mouse monoclonal anti-DNA PKcs antibody. An anti-V5 mouse monoclonal antibody was used for IP as negative control. The IPs and the inputs were subjected to SDS-PAGE and western blotting using anti-DNA PKcs and anti-RP2 antibodies. The red arrow indicates the RP2 band and the asterisk indicates the heavy chain of the antibody used for IP. D) Anti-FLAG IP was conducted in lysates from RPE1 cells that stably express constitutively active ARL3 Q71L-FLAG after doxycycline induction, as well as cells retrovirally transduced with an empty vector as negative control. The IPs and the inputs were subjected to SDS-PAGE and western blotting using anti-DNA PKcs, anti-RP2 and anti-FLAG antibodies.

#### **4.2.2 Plasma membrane localisation of RP2 might be important for its interaction with DNA PKcs**

After confirming that DNA PKcs is in a complex with RP2, I wanted to characterise the interaction further and assess the importance of the complex in RP. For this purpose, I tested several missense RP2 mutations initially identified in RP patients for any potential effect on the interaction with DNA PKcs (Figure 4.3A). The mutations that I chose to examine are not predicted [for R118H, R211L this fact is also experimentally proved by us and others (Veltel et al. 2008)] to destabilise the overall structure and folding of the protein based on biophysical calculations conducted by Dr Dinesh Soares [see Chapter 3, Table 3.1 and (Liu et al. 2017a)]. As a consequence, I did not expect the expression levels of the mutant proteins to be altered compared to the wild-type. R118H, one of the first RP2 mutations identified in RP patients (Schwahn et al. 1998), is known to severely affect the RP2-ARL3 binding (Kuhnel et al. 2006). R211L (Pelletier et al. 2007) disrupts the RP2-OSTF1 binding, as was shown recently by our group (Chapter 3, Figure 3.1). T87I is a non-destabilising missense pathogenic mutation (Jayasundera et al. 2010) with no known

effect on the function of RP2; therefore, the mechanism by which this mutation causes retinal degeneration is yet unknown.

Finally, my experiment included the N-terminal pathogenic mutations G2A (Neidhardt et al. 2008) and C3S (Jayasundera et al. 2010), which alter the sites of dual acylation on RP2, namely myristoylation at G2 and palmitoylation at C3. Attachment of myristate increases the hydrophobicity of the protein and is sufficient to exclude GFP from the nucleus and associate it with intracellular membranes (McCabe and Berthiaume 1999), but it is not sufficient to stably anchor the modified protein to the plasma membrane. This typically requires a second signal, for example a polybasic domain (as in c-SRC) or a second fatty acid, for example palmitate (Aicart-Ramos, Valero and Rodriguez-Crespo 2011, Resh 2016). This is the case for RP2, as dual acylation of the N-terminus is required for targeting and anchoring RP2 to the plasma membrane (Chapple et al. 2002, Chapple et al. 2000). For this reason, the G2A and C3S mutants do not display the characteristic plasma membrane localisation of the wild-type protein; Instead, G2A RP2 is localised throughout the cytoplasm in a diffuse pattern and abnormally accumulates to the nucleus, while C3S RP2 is trapped in intracellular membranes (Chapple et al. 2000).

After transiently expressing V5-tagged RP2 in its wild-type and mutant forms in HEK293T cells, western blotting for the V5 tag confirms that all proteins are equally expressed (Figure 4.3A, inputs). Subsequent anti-V5 immunoprecipitation and western blotting for endogenous DNA PKcs shows that none of the R118H, R211L, T87I and G2A mutations affect the RP2-DNA PKcs interaction. On the contrary, RP2 C3S has completely lost the ability to interact with DNA PKcs (Figure 4.3A, V5 IPs), as was consistently shown in three independent repeats of the experiment. Importantly, this finding supports the suggestion that the RP2-DNA PKcs interaction is authentic and not a product of non-specific binding. Because C3 is a palmitoylation site, there are two possible explanations about the effect of the C3S mutation on the interaction. Firstly, that the residue is structurally important for the interaction to occur. Secondly, that the interaction is lost due to lack of co-localisation and not because of a structural defect. However, the second hypothesis fails to explain why the C3S mutation abolishes the RP2-DNA PKcs interaction but

the G2A mutant fully co-precipitates with DNA PKcs despite the fact that it does not localise to the membrane either. One possible explanation for this phenomenon could be that abnormal accumulation of RP2 in the nuclear compartment leads to ectopic binding to DNA PKcs, which makes up in the IP assays for the loss of membrane interaction.

Therefore, a hypothesis can be formed that RP2 and DNA PKcs interact at the plasma membrane. In order to test this hypothesis, it is necessary to examine where the two proteins co-localise in the cell. To achieve this, I switched to hTERT-RPE1 cells which are more physiologically relevant than HEK293T cells for studying the cell biology of the retina and conducted immunofluorescence experiments. Using this method, I showed that although DNA PKcs is predominantly localised to the nucleus, a pool of the protein can also be observed in a punctate pattern along the periphery of the cell, where it co-localises with exogenous RP2-V5 (Figure 4.3B). Although DNA PKcs is predominantly referred to as a nuclear protein in the literature, lipid raft localisation has been shown before using biochemical methods (Lucero, Gae and Taccioli 2003).

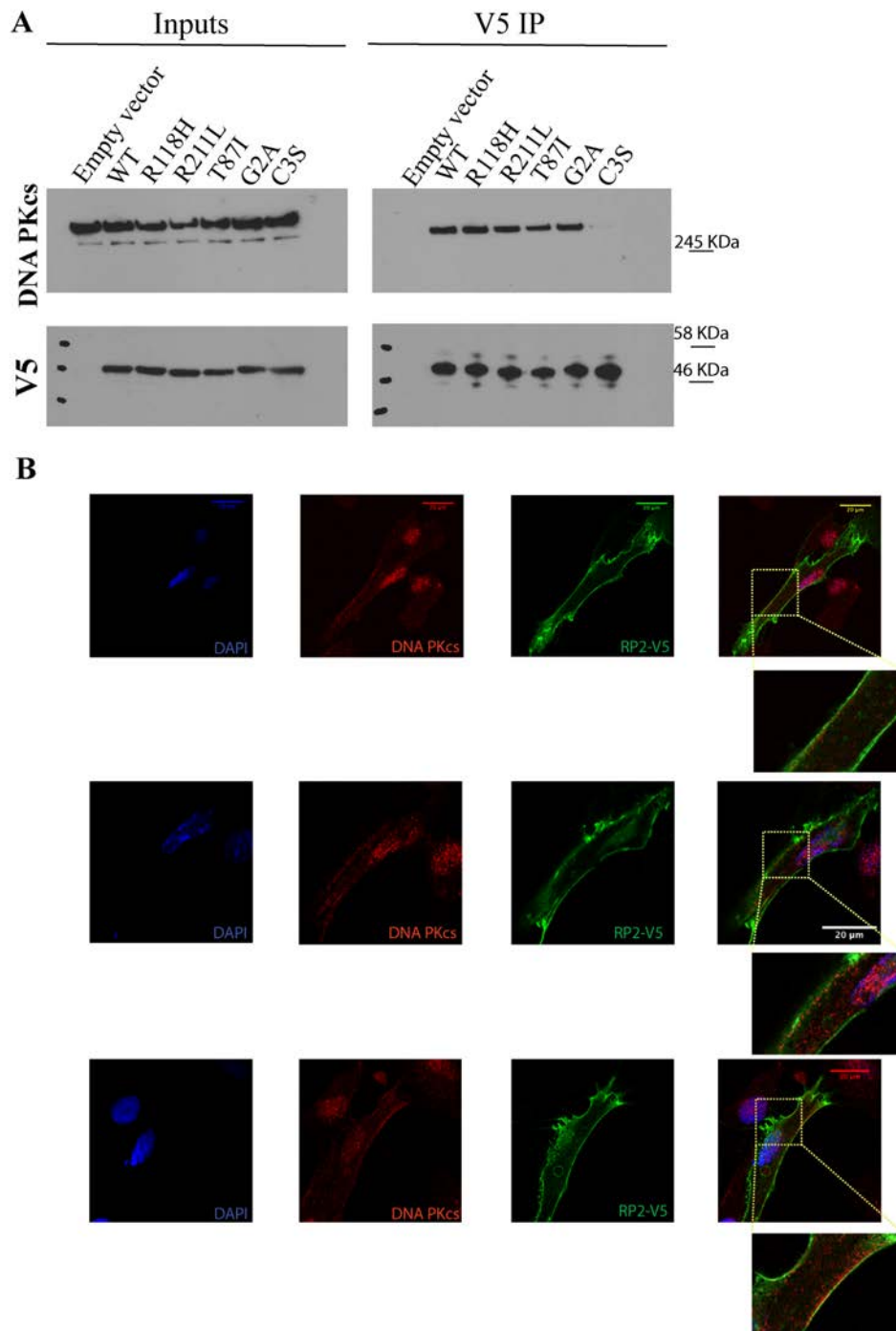


**Figure 4.3. Membrane localisation of RP2 might be important for the interaction with DNA PKCs.**

A) Several missense pathogenic mutations on RP2 which do not affect the expression levels of the protein were tested for their effect on the interaction with DNA PKCs. HEK293T cells were transiently transfected with V5-tagged WT and mutant forms of RP2, lysed and subjected to anti-V5 IP. The IPs as well as the lysates before IP (inputs) were subjected to SDS-PAGE and western blot using an anti-DNA PKCs antibody. Subsequent re-probing with an anti-V5 antibody confirms correct

expression of the constructs. C3S RP2, which has lost the palmitoyl anchor to the plasma membrane, does not interact with DNA PKcs. B) Immunofluorescence staining of fixed RPE1 cells using anti-DNA PKcs and anti-V5 antibodies shows a pool of DNA PKcs at the periphery of the cell in addition to the main nuclear localisation, and suggests that DNA PKcs co-localises with RP2-V5 at the plasma membrane. The part of the image denoted by a white box is magnified on the right.

Because of the possibility that the staining observed at the periphery of the cell is due to non-specific binding of the anti-DNA PKcs antibody, I aimed to confirm this finding using a biochemical method. To show that DNA PKcs is not exclusively nuclear but can also localise to the membrane compartment of the cell, I conducted subcellular fractionations on wild-type and genomic *RP2* null hTERT- RPE1 cells, followed by western blotting using antibodies against the endogenous proteins. The *RP2* null cell lines have deleterious mutations in the *RP2* gene that were introduced by the CRISPR/Cas9 method and are described in more detail in Chapter 3 (Figure 3.10). At first, I utilised a detergent-based commercial subcellular fractionation kit to generate a cytoplasmic fraction, a fraction for the plasma membrane and organelles, and a nuclear /cytoskeletal fraction, which is further disrupted by sonication (Figure 4.4). This approach showed that DNA PKcs, as well as its regulatory subunit Ku80, is present not only in the nuclear/cytoskeletal fraction but also in the membrane/organelle fraction. In addition, DNA PKcs is present in the cytoplasm although presumably in smaller quantities. As expected based on the literature, endogenous RP2 is more abundant in the membrane compartment; however, I show here for the first time that it is also present in the cytoplasm and the nuclear/cytoskeletal compartment. Moreover, I observed that DNA PKcs is absent (clone I) or reduced (clone G) from the nuclear compartment of *RP2* null cells compared to the wild-type RPE1, as observed in three independent repeats of the experiment. Because of the significant potential ramifications of this observation, I wanted to confirm it by using a different fractionation method. To this end, I repeated the crude subcellular fractionations using home-made buffers based on (Holden and Horton 2009). This protocol exploits the property of digitonin to bind to the plasma membrane and form pores on its surface to extract cytosolic proteins without permeabilising intracellular membranes. Subsequently, membrane

complexes are solubilised using NP40. Finally, the nuclear membrane and nuclear-residing proteins are extracted using RIPA buffer (Figure 4.5). RIPA/NP40 insoluble proteins are then pelleted down by centrifugation and are not extracted with this method. This approach confirmed the cytoplasmic, membrane and nuclear localisation of DNA PKcs, as well as the membrane and nuclear localisation of RP2 (Figure 4.5). However, it did not confirm that nuclear DNA PKcs levels are reduced when RP2 is absent. Therefore, this is considered an artefact of the first method and may not be a real phenotype. It is possible that the sonication step of the first protocol is responsible for introducing some degree of unspecific variability among the samples. There is also a possibility that the reduced amount of DNA PKcs in the last fraction in Figure 4.4 is an effect linked to the insoluble protein fraction which is not extracted using the second method. Finally, it is worth commenting on the fact that GAPDH, a widely used cytosolic marker, is present both in the cytosolic and membrane fractions in both experiments (Figures 4.4,4.5). Although this observation might mean that cytosolic proteins were not completely extracted during the first fractionation step, recent studies have identified GAPDH as a membrane localised protein (Ghosh et al. 2010). Therefore, it is possible that GAPDH is not an appropriate cytosol-only marker for RPE1 cells.

Lastly, other fractionation methods could be used to confirm my results and also to resolve the question of DNA PKcs localisation in *RP2* null cells. One common method to obtain pure preparations of different subcellular organelles is density-gradient centrifugation, based on the separation of organelles according to their size and density via ultracentrifugation through a density gradient of a medium such as sucrose (Lee, Tan and Chung 2010). Although more time-consuming, this method has higher resolution power than detergent-based fractionation and could help determine the specific organelles where RP2 and DNA PKcs co-localise, rather than generally isolating the membrane-associated fraction of the cells.

In conclusion, I conducted immunofluorescence and subcellular fractionation experiments and showed that DNA PKcs and RP2 co-localise at the membrane and nuclear compartments of RPE1 cells. In theory, both these cellular compartments are potential sites of interaction. Because abolition of the plasma membrane localisation

of RP2 via the C3S mutation is prohibiting for the interaction, the hypothesis that they interact at the plasma membrane is more likely based on experimental evidence.



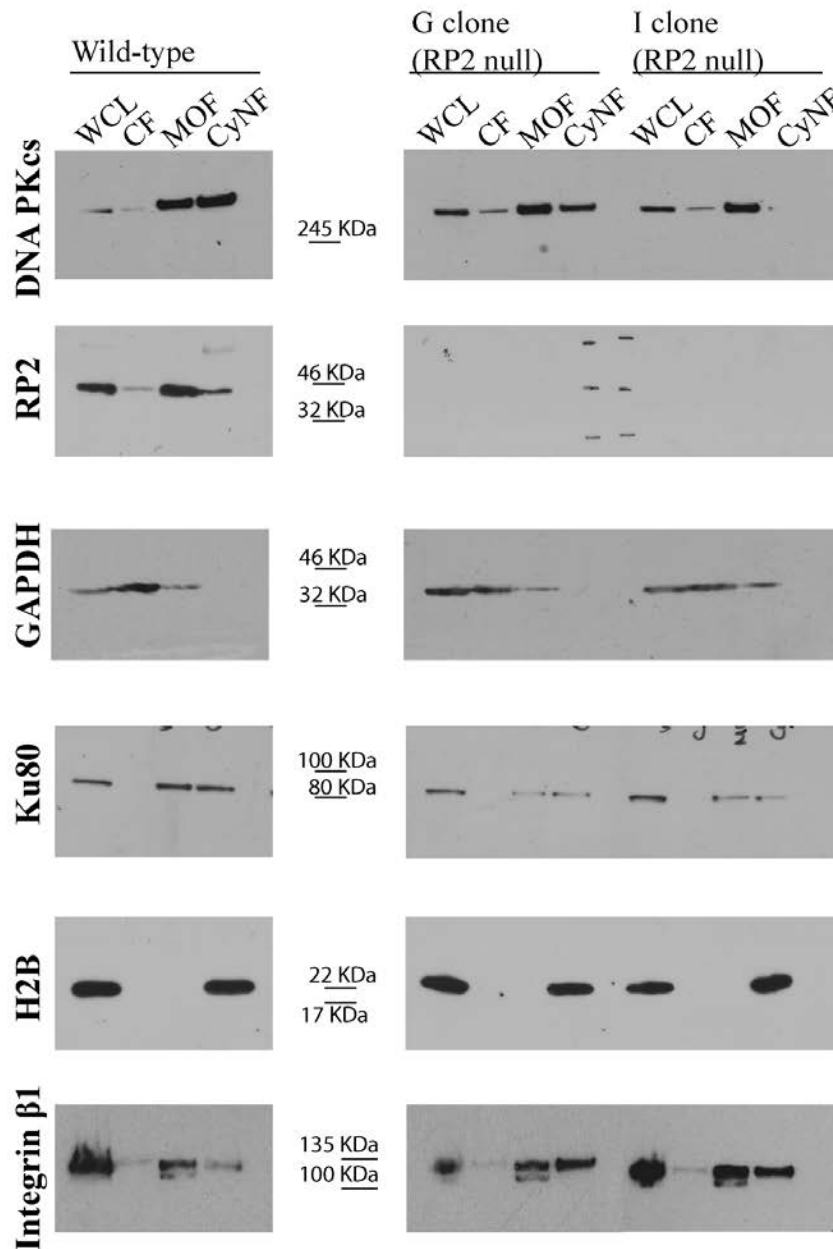


Figure 4.4. **RP2 and DNA PKcs co-localise at the nuclear and the membrane compartments of RPE1 cells: fractionation method 1.**

Parental WT and two clones (G,I) of *RP2* null hTERT-RPE1 cells, generated by the CRISPR-Cas9 method, were subjected to subcellular fractionation using the Cell Signalling fractionation kit. Cell lysates (WCL) and the different fractions-cytoplasmic (CF), membranes and organelles (MOF) and cytoskeleton and nucleus (CyNF)- were subjected to SDS-PAGE and western blotting using antibodies against endogenous DNA PKcs, RP2 and one the regulatory subunits of DNA PK, Ku80. H2B, GAPDH and Integrin β1 blotting were used as markers for the nuclear, cytoplasmic-membrane fractions, membrane-cytoskeletal fractions, respectively.

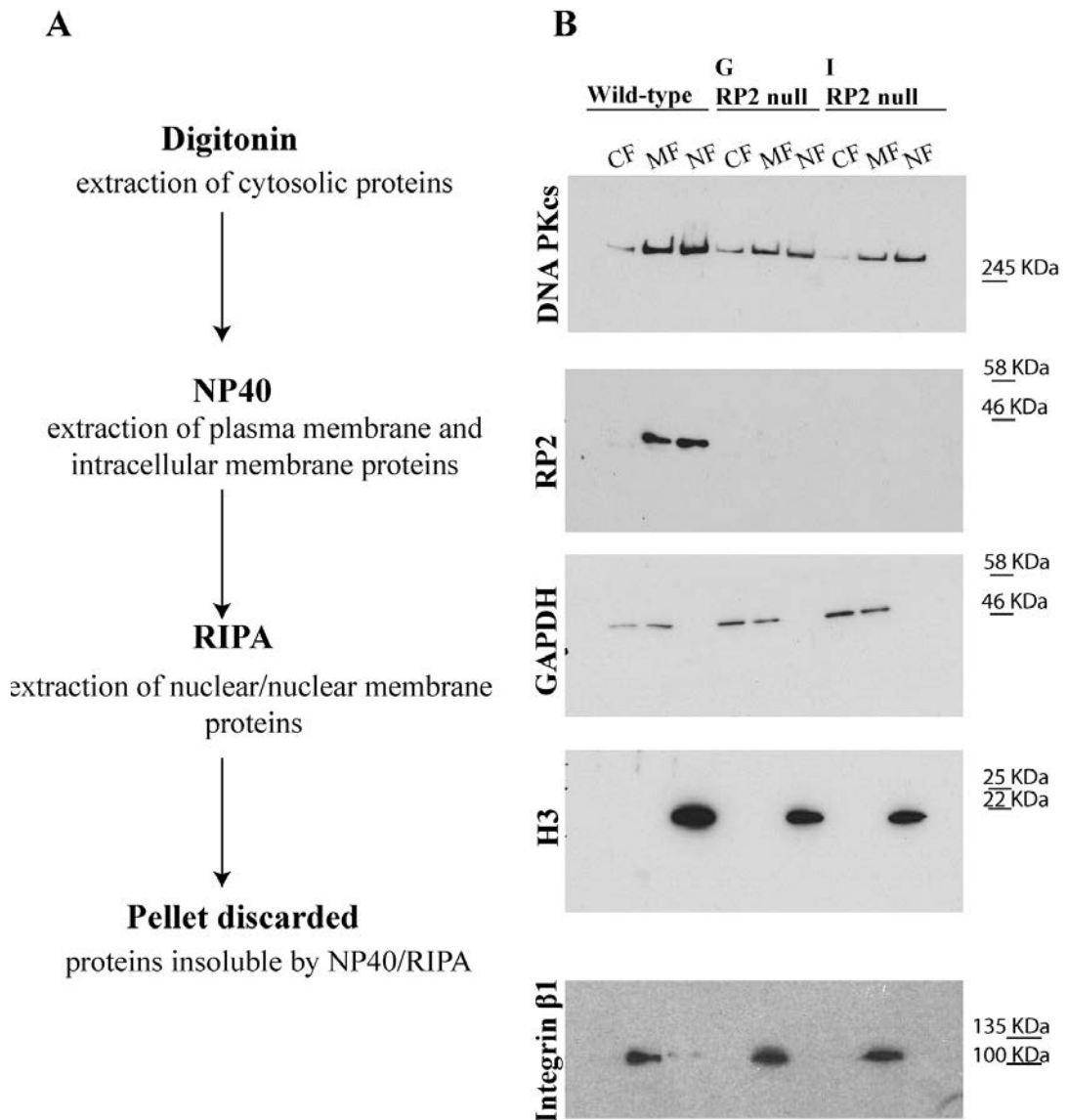


Figure 4.5. **RP2 and DNA PKcs co-localise at the nuclear and the membrane compartments of RPE1 cells: fractionation method 2.**

Parental WT and two clones (G,I) of *RP2* null hTERT-RPE1 cells, generated by the CRISPR-Cas9 method, were subjected to subcellular fractionation using a crude fractionation method which included the stepwise use of digitonin, NP40 and RIPA buffer to solubilise cytoplasmic (CF), membrane (MF) and nuclear proteins (NF) respectively. (A) Diagram summarising the experimental steps of the fractionation protocol. (B) Subcellular fractions were subjected to SDS-PAGE and western blotting using antibodies against endogenous DNA PKcs and RP2. H2B, GAPDH and Integrin  $\beta$ 1 blotting were used as markers for the nuclear, cytoplasmic-membrane and membrane fractions, respectively.

#### 4.2.3 RP2 is a novel substrate of DNA PKcs *in vitro*

DNA PKcs is a prolific kinase with many of its substrates belonging to the NHEJ complex. The highly purified catalytic subunit has weak kinase activity on its own, which can be stimulated 5-10 fold in the presence of double-stranded DNA and the Ku heterodimer. Inactivation of its kinase activity results in radiosensitivity and defects in DSB repair, highlighting the importance of DNA PKcs-mediated phosphorylation of substrates for NHEJ to occur normally (Kurimasa et al. 1999). Apart from phosphorylating other proteins, DNA PKcs itself undergoes autophosphorylation, which can exert important effects on the protein such as inducing conformational changes which lead to the dissociation from the DNA damage sites (reviewed in (Jette and Lees-Miller 2015)).

Apart from phosphorylating substrates in the nucleus, DNA PK is known to phosphorylate numerous cytoplasmic targets, including Hsp90 (Quanz et al. 2012), the NFkB inhibitor Ikb- $\beta$  (Bottero et al. 2001) and Akt kinase (Li et al. 2013b). Activation of DNA PK by small DNA molecules mimicking DSBs leads to phosphorylation of the intermediate filament protein Vimentin, and it is suggested that this phosphorylation regulates cell migration and adhesion (Kotula et al. 2013). Another recent study showed evidence for the phosphorylation of GOLPH3, a protein that participates in the application of tensile forces to the Golgi, by DNA PK. This event ultimately leads to a dramatic reorganization of the Golgi upon DNA damage which appears to be crucial for cell survival (Farber-Katz et al. 2014). Thus, evidence is accumulating that DNA PK is responsible for transmitting signals via its kinase activity that ultimately lead to a cytoplasmic response to DNA damage.

DNA PKcs is shown to have the highest selectivity for its consensus motif S/T-Q. However, a study involving screening of peptide libraries suggested that its substrate requirements are modestly flexible with respect to the critical +1 position. For example, there exists an additional tendency to prefer a hydrophobic residue, for example a Y, nearby the targeted S/T (O'Neill et al. 2000). Since then, multiple other DNA PKcs phosphorylation sites have been found on potential substrates that do not conform to the S/T-Q consensus (Jette and Lees-Miller 2015).

Due to the close links between the kinase activity of DNA PKcs and its numerous functions, I was interested in testing whether the novel interaction between RP2 and DNA PKcs is linked to a kinase-substrate relationship. Interestingly, the RP2 amino acid sequence encompasses a classic DNA PKcs consensus phosphorylation motif around T133 (LCCATQPIIE). T133 is a good candidate for phosphorylation because it is surface exposed on the unbound RP2 (Figure 4.6A). Moreover, it is strictly conserved among vertebrates, suggesting an important role in the protein's core functions. In addition, the T133 residue is located very close to the ARL3-GDP interface on the RP2-ARL3 complex (Figure 4.6A). Neighbouring residues A132 and Q134 are both involved in hydrophilic interactions with ARL3 residues (Veltel et al. 2008), while the R118 and E138 residues which are critical for the catalytic activity of RP2 towards ARL3 and sites of missense pathogenic mutations (Kuhnel et al. 2006) are also found in close proximity to T133. Because of the position of this residue, I hypothesised that the addition of a phosphate group, possibly as a result of the RP2-DNA PKcs interaction, could affect binding to ARL3 and, as a result, serve as a way to regulate the catalytic activity of RP2. To test this hypothesis, I generated the V5-tagged phospho-mimic (T133E) and phospho-dead (T133A) mutants of RP2 and used them to transiently transfect HEK293T cells. Both these mutations were not predicted to destabilise the secondary structure of the protein (stability calculations by Dr Dinesh Soares, unpublished) and were indeed expressed at the wild-type levels, as the inputs show in Figure 4.6B. Subsequently, I conducted pulldown assays using recombinant GST-ARL3 Q71L (the constitutively active mutant which stably associates with RP2) as bait, testing for its ability to associate to the V5-tagged proteins. Lysates expressing R118H RP2 were also included in the pulldown assays as a negative control, since it has been shown before that this mutation abrogates the RP2-ARL3 interaction (Kuhnel et al. 2006). The amount of RP2-V5 that associated with ARL3 was approximated by western blot and densitometry measurements of the V5 band intensity normalised to the total GST-tagged protein band intensity in the sample for 3 independent repeats of the experiment. This approach revealed that the phospho-mimic T>E mutation reduces the RP2-ARL3 binding efficiency, although its effect is not as pronounced as the one exerted by the R118H mutation which completely abolishes the interaction (Figure 4.6B). On the contrary, the phospho-

dead T>A mutation does not influence the binding of the two proteins. To ensure that the observed changes are not due to an effect of the mutations on the overall folding of the protein, pulldown assays were conducted using GST-OSTF1 as bait, because the mutations mentioned above are found away from the RP2-OSTF1 interaction interface. Indeed, I found that the mutant proteins bind to OSTF1 as efficiently as the wild-type RP2. Overall, this experiment suggests that T133 is important for the RP2-ARL3 interaction, and that the hypothetical addition of a negative charge at this position, similarly to the addition of a phosphate group, would downregulate the RP2-ARL3 interaction.

Subsequently, I aimed to test if RP2 is indeed phosphorylated at the DNA PKcs consensus motif under conditions of DNA PKcs activation in a retinal cell line. To this end, I transiently expressed V5-tagged human RP2 or empty vector (as negative control) in hTERT-RPE1 cells. The transfected cells were treated with different doses of IR (2, 5 and 10 Gy of X-rays) or etoposide (50  $\mu$ M for 4 hrs), a topoisomerase II inhibitor, to induce DNA damage and, as a result, activation of DNA PKcs. DMSO- treated cells were also included in the experiment as a vehicle-only control. To detect any potential phosphorylation of RP2-V5, I immunoprecipitated RP2-V5 and conducted western blot with an antibody against the phosphorylated S/T-Q motif. As shown in the inputs lanes in Figure 4.6C, the antibody detects novel phosphorylated bands in the etoposide- and X-ray-treated inputs compared to the untreated ones. Because the phosphorylation of S/T-Q motifs is a general marker of DNA damage and response of the PIKK family kinases, this confirms that my treatments were effective in inducing DNA damage response in the cells. However, no S/T-Q phosphorylation was detected in the IP samples, despite RP2-V5 being efficiently expressed and immunoprecipitated, as shown by the anti-V5 loading control blot (Figure 4.6C). This result suggests that RP2 is not detectably phosphorylated in an S/T-Q consensus motif after treatment of the cells with DSB-inducing agents.

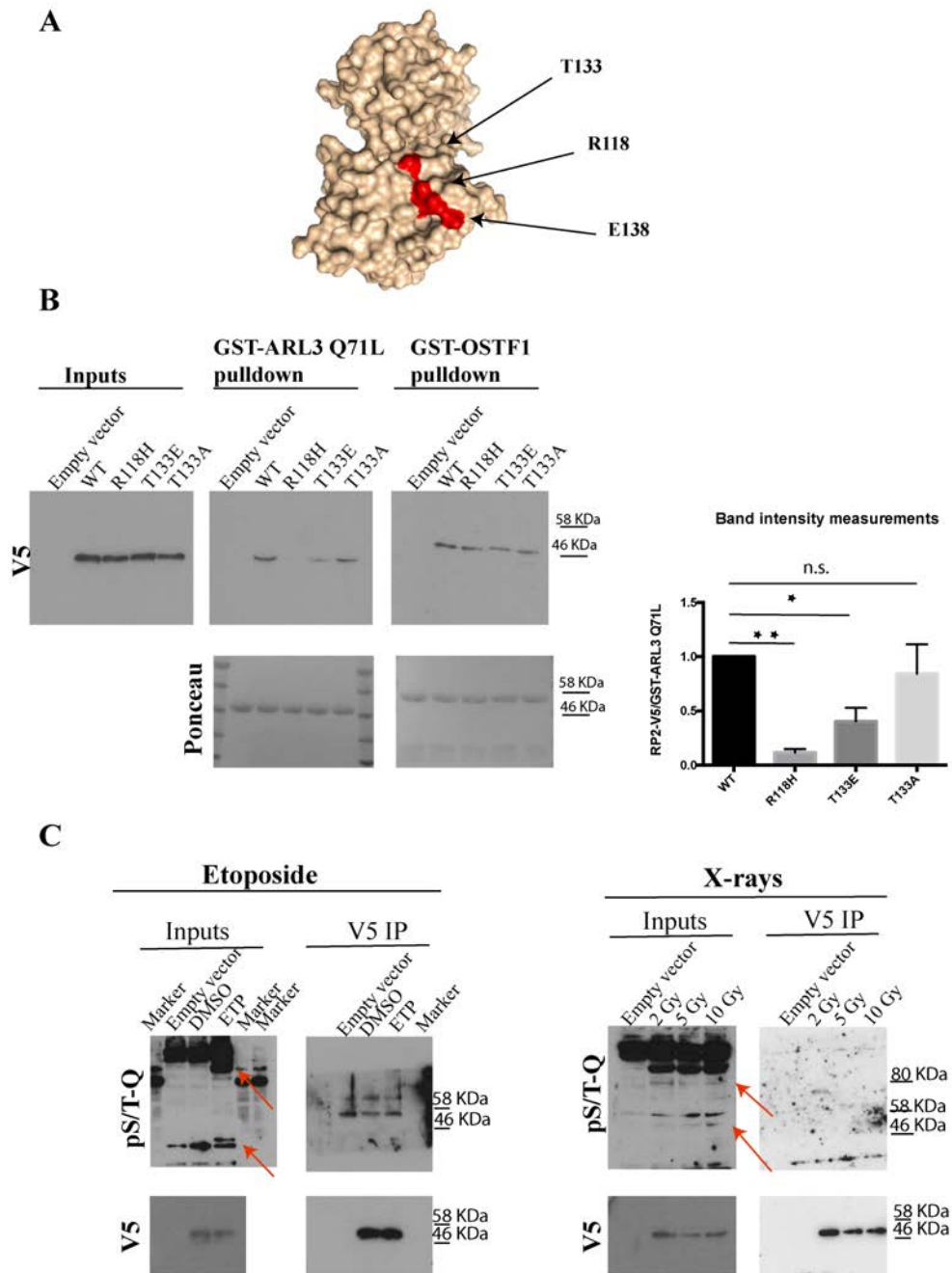


**Figure 4.6. Threonine phosphorylation of RP2 at the DNA PK consensus motif might disrupt binding to ARL3, but could not be detected after DDR induction.**

A) Surface representation of human RP2 crystal structure (PDB ID: 2BX6) where T133, which corresponds to the DNA PK consensus motif (S/T-Q), is highlighted in red. The other two highlighted residues correspond to R118 and E138, which are both critical for the catalytic activity of the protein towards ARL3. B) Recombinant GST-ARL3 Q71L was used as bait in pulldown assays from HEK293T cells transiently transfected with different forms of RP2-V5. GST-OSTF1 pulldowns are used to control for the mutant proteins' correct folding. SDS-PAGE and western

blotting analysis with anti-V5 antibody was used to approximate the amount of RP2-V5 found in the cell lysates (inputs) and bound to the bait proteins. Ponceau staining was used to visualise the GST-tagged protein bands. Band densitometry measurements were used as a relative quantification of the RP2-V5 abundance between pulldown samples (mean +/- S.E.M n=3 densitometry measurements on 3 separate immunoblots normalised to GST-tagged ARL3 Q71L bands). Two-tailed one-sample t-test was used to assess the significance of the observed differences between the mutant RP2 bands' intensities compared to that of the WT protein whose value was set arbitrarily to 1. As expected, the interaction between RP2 R118H and ARL3 Q71L is almost completely abolished ( $p=0.0013$ ), while the phospho-mimic T133E mutation also affects the interaction ( $p=0.0420$ )<sup>5</sup>. The phospho-dead T133A mutation does not significantly affect the RP2-ARL3 interaction. C) RP2-V5 was immunoprecipitated from RPE1 cells transfected with the corresponding construct or empty vector and treated with 2,5 and 10 Gy X-rays (right) or 50  $\mu$ M etoposide for 4 hrs (left) to induce DNA double stranded breaks. DMSO-treated cells were also used as a vehicle-only control. IPs and lysates before IP (inputs) were subjected to SDS-PAGE and western blotting using an anti-pS/T-Q antibody as well as anti-V5 antibody to confirm correct expression of the constructs. However, no band corresponding to RP2 phosphorylation was observed. Red arrows point to bands that become S/T-Q phosphorylated after treatment with etoposide and X-rays.

Since I could not detect S/T-Q phosphorylation of RP2 after DNA damage, I hypothesised that this modification could occur under an entirely different context, possibly related to a non-canonical function of DNA PKcs that is independent of its role as a DNA damage signal-relaying kinase. To investigate the possibility of RP2 phosphorylation with a different approach, I conducted a kinase assay using commercially available DNA PK, purified from HeLa cells' nuclei, and recombinant His-tagged human RP2. Subsequently, I analysed the assay mix by western blot using the anti-phosphorylated S/T-Q motif antibody. As shown in Figure 4.7A, multiple phosphorylated bands can be observed in the kinase assay mix as opposed to the negative controls (no ATP and no DNA PK), which most likely correspond to autophosphorylation of the DNA PK catalytic subunit and the regulatory Ku subunits, as inferred by the molecular weight. As expected, overall S/T-Q phosphorylation in the mix is stimulated multiple fold by the addition of double-stranded DNA, which activates the activity of the catalytic subunit. However, the

---

<sup>5</sup> Mean reduction in densitometry measurements for WT vs mutant RP2: 88.5% and 59.9% for R118H and T133E, respectively, with 95% confidence intervals: 102.4% to 74.6% and 114.4% to 53.7% for R118H and T133E, respectively.

study of RP2 phosphorylation using this method is impeded by the presence of a phosphorylated band at the expected molecular weight for RP2-His, even in the “no RP2” negative control (marked by a red arrow in Figure 4.7A). Since the kinase I used in this assay is not recombinant but purified from human cells, the band possibly corresponds to another protein that co-purifies with the DNA PK complex. In order to circumvent this problem, the kinase assay mix was analysed by LC-MS/MS in the IGMM Mass Spectrometry facility by Dr Jimi Wills-Bukowski and Dr Alex von Kriegsheim. This analysis revealed a modified RP2 peptide corresponding to phosphorylation at positions 213/214 (because of their proximity it was not possible to distinguish which of the two residues was phosphorylated) (Figure 4.7B). Intensity values, corresponding to the summed up extracted ion current of all isotopic clusters associated with the identified sequence (used here to loosely estimate quantification), show that the phosphorylated version of the corresponding RP2 peptide was only detected in the kinase assay sample. At the same time, the unmodified peptide could be detected in all samples, including the negative controls (without ATP or without DNA PK). In addition, the identification of several sites of DNA PKcs autophosphorylation, which can only be detected in the full kinase assay and not the negative controls, provides further confirmation that the kinase used in the assay was active and the experiment was valid. All the identified autophosphorylation sites have been previously reported by other groups (Ma et al. 2005, Douglas et al. 2002, Chen et al. 2007).

It is important to note that the sequence context of the identified modified residues S213, T214 does not conform to the classical S/T-Q motif that is preferentially phosphorylated by DNA PK. However, it has already been mentioned that only a fraction of the many DNA PK substrates is phosphorylated at this canonical motif. In fact, a similar phosphorylation site where the targeted residue is followed by E as the critical +1 position has been identified before on human Artemis (Ma et al. 2005). On the contrary, my experiment did not detect phosphorylation on T133 which is the site of the canonical motif. Before the possibility of DNA PK-mediated phosphorylation at this site is excluded, the experiment should be repeated and another method should be tried, such as TiO<sub>2</sub> enrichment of phosphopeptides. The absence of phosphorylation at this site could explain why I did not detect any RP2



phosphorylation after the induction of DSBs in RPE1 cells, since the method I used was only appropriate for detecting phosphorylation at an S/T-Q site (Figure 4.6C).

My studies have led to the emergence of S213/T214 as novel potential sites of DNA PK-mediated phosphorylation on human RP2. T214 and S213 appear mostly conserved among diverse classes of vertebrates, according to multiple sequence alignment of RP2 vertebrate orthologues conducted by Dr Dinesh Soares. T214 is strictly conserved among amniota and the coelacanth, but it is replaced with A in ray-finned fish and the frog. On the contrary, S213 is strictly conserved among vertebrates. T211 on mouse RP2, which is homologous to T214 on the human protein, was found to be phosphorylated specifically under neurite growth conditions in a large-scale study of the neurite phosphoproteome (Wang et al. 2011) (See Chapter 3: Figure 3.6A). It is also worth mentioning that S213 and T214 are both surface exposed and therefore assumed good candidates for phosphorylation. In order to further confirm this result, the experiment should be repeated including treatments with DNA PK-specific small molecule inhibitors. This will ensure that DNA PK, and not some other kinase present in the purified complex, is the responsible kinase for phosphorylating RP2 in the kinase assay. Further, the next step for this study is naturally the development of phospho-specific antibodies for phosphorylated S213/T214 on RP2. The development of these antibodies will provide the final confirmation that these RP2 residues are authentic phosphorylation sites and will open the way for a multitude of new experiments discussed at the end of this chapter.

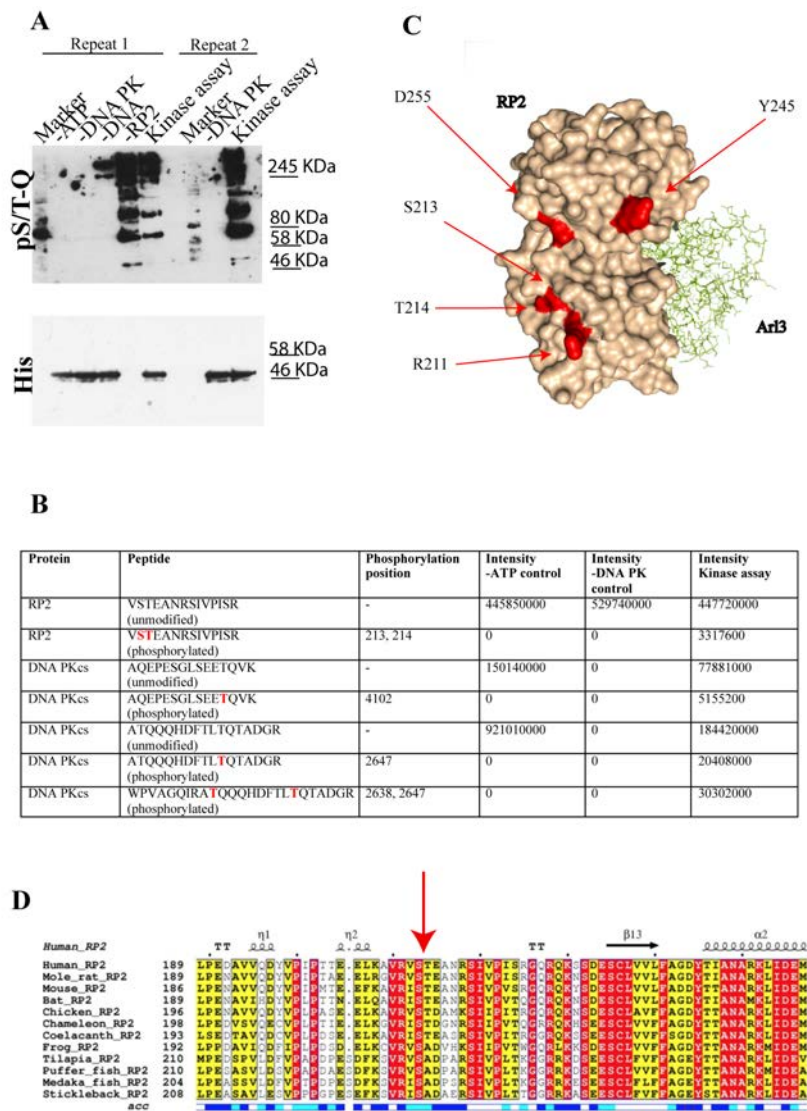


**Figure 4.7. RP2 is a potential substrate for DNA PKcs-mediated phosphorylation *in vitro*.**

A) Recombinant human RP2-His and purified commercial DNA PK were mixed in an *in vitro* kinase assay. The assay mix was analysed by western blotting using an anti-His antibody for recombinant RP2 and anti-phospho S/T-Q motif antibody, which is the preferred consensus motif for phosphorylation by DNA PK, as a phosphorylation marker. The more intensely phosphorylated bands marked with red arrows likely correspond to the catalytic subunit and the regulatory subunits Ku70 and Ku80, based on the molecular weight. B) Table summarising key findings of the LC-MS/MS analysis of the kinase assay. It shows the modified RP2 and DNA PKcs peptides identified (phosphorylated residues marked in red) and the summed up extracted ion current of all isotopic clusters associated with the identified sequences as Intensity values. C) Surface representation cartoon of the RP2-ARL3 complex 3D structure (PDB ID: 3BH7), where the newly identified potential phosphorylation

sites on RP2 are marked in red (S213, T214). These adjacent residues are found in close proximity to residues R211, D255 and Y245 (also in red) which are critical for the RP2-OSTF1 interaction to occur, as shown in Chapter 3. D) Section of the multiple sequence alignment of vertebrate RP2 orthologues, encompassing residues S213 and T214. The conservation status of each residue is shown in colour code (red=strictly conserved, yellow= largely conserved/ conservatively substituted, white=non-conserved). S213 is strictly conserved among vertebrates, while T214 is only largely conserved (analysis conducted by Dr Dinesh Soares).

#### **4.2.4 *RP2* null cells respond normally to DNA damage with respect to H2AX activation**

A fundamental question concerning the RP2-DNA PKcs binding is the function of this interaction. The most well characterized role of DNA PK is in the repair of DNA DSBs, primarily by NHEJ but also by HR, as previously discussed. Therefore, it is imperative to start investigating any potential role of RP2 in the same pathways, especially since the slightest defect in DNA damage repair could be fatal for the neural retina. The photoreceptor's function is characterized by extremely high metabolic rates and constant threat by DSB-inducing DNA damaging agents, including reactive oxygen species and UV irradiation. To achieve this, I compared the response of *RP2* null hTERT-RPE1 cells that were previously generated in our group using the CRISPR-Cas9 method (Dr Toby Hurd) (characterization of these cell lines in Chapter 3: Figure 3.10) to the parental wild-type line after DNA DSB induction by low-dose IR (2 Gy X-rays). As a readout, I chose the formation and disappearance pattern of  $\gamma$ H2AX foci, which is generally considered a consistent and quantitative marker for DNA DSBs (Kinner et al. 2008). The H2AX variant of histone H2A is readily phosphorylated at S139 at the vicinity of DNA DSBs to generate  $\gamma$ H2AX. All three major kinases of the PIKK family (ATM, DNA PKcs and ATR) have the potential to phosphorylate H2AX; there is evidence for overlapping functions of the three kinases and it is still not clear which one is chiefly responsible for the initial H2AX phosphorylation (Kinner et al. 2008). After repair,  $\gamma$ H2AX foci are removed from chromatin and phosphatase PP2A is largely responsible for the de-phosphorylation in mammalian cells (Chowdhury et al. 2005). Notably, cells with compromised DNA PKcs activity display abnormally retained  $\gamma$ H2AX levels because of the persistence of unrepaired DNA breaks (Zhao et al. 2006, Koike et al.

2008, Woodbine et al. 2013). Figure 4.8A shows the emergence of the characteristic  $\gamma$ H2AX foci in the nuclei of sub-confluent, IR-treated cells at 1 hr after treatment, which gradually disappear at later time-points as the DNA breaks undergo repair. Quantification of the number of  $\gamma$ H2AX foci per nucleus (Figure 4.8B) shows that there is no obvious defect that is consistent among both the *RP2* null lines in the  $\gamma$ H2AX activation-deactivation pattern, while any differences that are not observed in both the *RP2* null clones are considered as clonal variation and not a result of the absence of *RP2* function.

In order to further investigate any potential involvement of the *RP2*-DNA PK complex in DNA damage signalling or repair, I examined if their interaction is upregulated after DNA damage. To this end, I immunoprecipitated transiently expressed V5-tagged *RP2* from DMSO (vehicle-only control) or etoposide-treated hTERT-RPE1 cells. Subsequently, I conducted western blot using an antibody against endogenous DNA PKcs. As shown in Figure 4.8C, the amount of DNA PKcs that co-precipitates with *RP2* is not affected by DNA damage. In addition, I examined if the expression of endogenous *RP2* is regulated in response to DNA damage in RPE1 cells. Figure 4.8D shows that the levels of endogenous *RP2* remain unchanged 1 hr after treatment of hTERT-RPE1 cells with IR (This time-point was chosen because I have observed maximum  $\gamma$ H2AX activation at 1 hr). Therefore, these experiments provide evidence that *RP2* does not have an essential function in the DNA DSB signalling and repair machinery after IR and DSB-inducing drugs, but rather point towards a non-canonical function of the DNA PK complexes in cell biology.

However, it is important to note that my  $\gamma$ H2AX activation experiment is by no means conclusive about the role of *RP2* in DSB response. Importantly, this experiment was planned to examine the cells' response to DNA damage rather than survival, hence the repair of DNA breaks and the observed resumed proliferation and cell growth confirm that the 2 Gy dose that I used is sub-lethal. Assessing survival of the cells after DNA damage would be better approximated by other methods, such as cleaved caspase-3 staining (a marker of potentially increased apoptosis in the *RP2* null lines), and clonogenic survival assays after higher doses of X-rays. Further, it

should be noted that the cells were sub-confluent at the time of treatment. Therefore, DSB repair in my experiment could theoretically occur via both NHEJ and HR pathways. While this experiment is useful to give an overview of DSB repair in general, it could also be necessary to repeat this experiment by using fully confluent (synchronous) cells that can only repair their DSBs by NHEJ, in order to separate the two pathways.

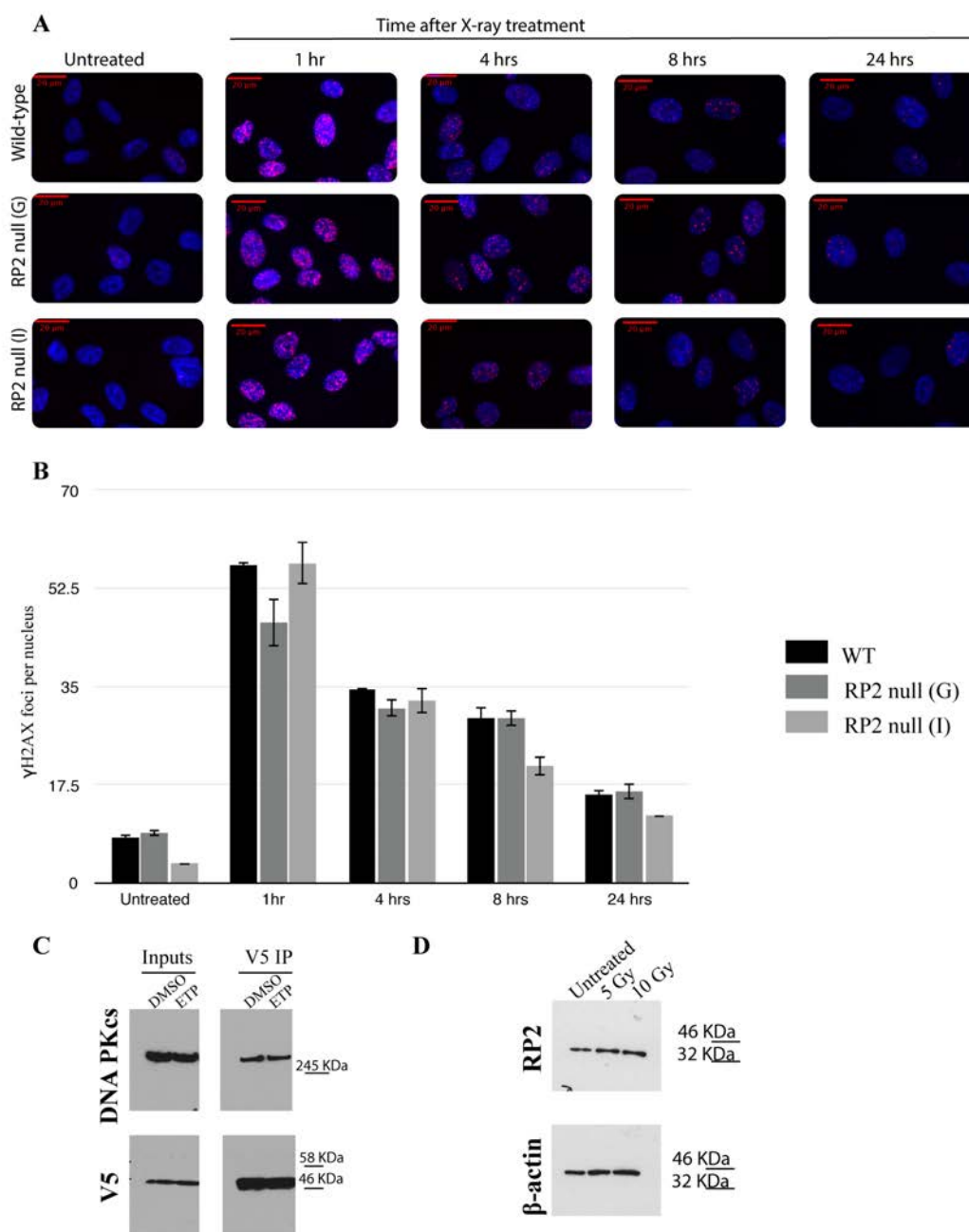


Figure 4.8. *RP2* knockout does not result in defects in H2AX activation and repair of double stranded breaks induced by X-rays.

A) Parental WT and two clones of *RP2* null hTERT-RPE1 cells were subjected to X-ray treatment (2 Gy) and  $\gamma$ H2AX immunofluorescence staining was conducted at different time-points after treatment. Red=  $\gamma$ H2AX, blue=DAPI. B) Quantification of  $\gamma$ H2AX foci in the nuclei of untreated and X-ray treated cells shows no differences in the activation and deactivation pattern of  $\gamma$ H2AX among the different cell lines that can be attributed to absence of *RP2* (mean  $\pm$  SEM for 3 technical repeats, n=50 cells each repeat). C) In order to test if the DNA PKcs-*RP2* interaction is regulated in response to DNA damage, *RP2*-V5 was immunoprecipitated from hTERT-RPE1 cells' lysates expressing the corresponding construct after treatment with 50  $\mu$ M

etoposide for 4 hrs or DMSO as negative control. The IPs and the inputs were analysed by SDS-PAGE and western blot using anti-DNA PKcs and anti-V5 antibodies. D) To test if the expression of endogenous RP2 is regulated in response to DNA damage, lysates from hTERT-RPE1 cells were analysed 1 hr after treatment of the cells with 5 Gy and 10 Gy X-rays and compared to untreated cells as negative control.

## **4.3 Discussion**

### **4.3.1 Characterisation of the RP2-DNA PKcs interaction**

In this chapter, I demonstrated that the catalytic subunit of the DNA-dependent protein kinase (DNA PKcs) was among the proteins that qualified as potential interaction partners of RP2 in the LC-MS/MS analysis after affinity purification of RP2-V5 from HEK293T cells. Subsequently, I confirmed by western blotting that DNA PKcs efficiently co-precipitates with transiently expressed RP2 from HEK293T and hTERT-RPE1 cells and, reciprocally, that RP2 co-precipitates with endogenous DNA PKcs from HEK293T cells. Further, I also showed that the missense pathogenic RP2 mutation C3S renders the protein unable to interact with DNA PKcs. This result is important because it provides a useful negative control to support my hypothesis that the interaction is authentic and specific. In order to test if this interaction is important for retinal biology, it is necessary to show if it occurs in the retina. This could be achieved by endogenous co-IP of the two proteins from bovine retinal extracts.

To form a hypothesis about the potential function of the RP2-DNA PKcs complex, I investigated where the proteins co-localise within the cell. I conducted biochemical fractionations of hTERT-RPE1 cells and showed that both DNA PKcs and RP2 can be detected in all three generated fractions (cytoplasmic fractions, membranes and nucleus). Although DNA PKcs is predominantly known as a nuclear protein whereas RP2 is known to be plasma-membrane bound, my results generally agree with the existing bibliography, as alternative localisations have been reported for both proteins. DNA PKcs has been shown to be involved in active shuttling between the cytoplasm and the nucleus (Huston et al. 2008) and to undergo microtubule-mediated trafficking (Poruchynsky et al. 2015). In addition, biochemical methods have been

used to show that DNA PKcs is a component of lipid rafts, where it mediates phosphorylation of many substrates following irradiation (Lucero et al. 2003). On the other hand, this is the first time a nuclear localisation for RP2 is reported, except for one study which claimed RP2 translocates to the nucleus in response to DNA damage (Yoon et al. 2006). Recently, the involvement of its best studied interaction partner ARL3 in STAT3 activation has hinted for a transcriptional role for the two proteins (Togi et al. 2016). Interestingly, the presence in my mass spectrometry data of multiple nuclear transport receptors (Transportin 1, Exportin 7, Exportin 5, Importin 4) might suggest active nuclear transport and export for RP2 (Appendix Table 1).

To pinpoint exactly where the RP2-DNA PKcs interaction occurs, fluorescence resonance energy transfer (FRET) or proximity ligation assay (PLA) could be used, both *in vitro* and on retinal sections. I hypothesise that the proteins interact at the plasma membrane, because C3S RP2, which has lost the ability to localise to the plasma membrane but instead accumulates in intracellular structures, does not interact with DNA PKcs. Based on this, it can also be suggested that the complex is not part of the canonical functions of DNA PKcs in the nucleus; instead, it might serve to relay DNA damage signalling to the plasma membrane. Both G2 and C3, the sites of lipid modifications on RP2 which are responsible for membrane targeting, are strictly conserved residues among vertebrates, suggesting membrane targeting is crucial for the function of RP2 in vertebrates (Chapple et al. 2002). It should be noted that both myristoylation and palmitoylation of RP2 are also necessary for its targeting to cilia (Hurd et al. 2010), and G2A or C3S mutants do not interact with Importin  $\beta$ 2 (Hurd et al. 2011). Given the centrosomal localisation of DNA PKcs that has been observed during mitosis (Douglas et al. 2014), a potential co-localisation of the two proteins at the basal body should be investigated in the future.

In addition, I showed that the interaction between the two proteins potentially results in S/T phosphorylation of RP2 by DNA PKcs at S213/T214. My study further highlights the flexibility of DNA PKcs-mediated phosphorylation regarding targeted motifs. The development of a phospho-specific antibody for this site will make it possible to investigate if phosphorylation is induced after DNA damage and,



importantly, where this phosphorylation occurs in the cells or in retinal sections; these experiments will be highly informative about the function of the interaction. Interestingly, a large-scale study of the neurite phosphoproteome in mice recently identified this site on RP2 as phosphorylated under neurite growth conditions (Wang et al. 2011). Given the importance of DNA PKcs in mouse retinal development, but also the extensive neurodevelopmental and neurodegenerative defects of a patient with very little residual DNA PKcs activity (Woodbine et al. 2013), it will be interesting to investigate a function for the complex in neuronal development.

#### **4.3.2 Potential roles of the RP2-DNA PKcs complex**

Because its function in NHEJ is the most well-described role for DNA PKcs, it is natural to begin the search for a common role of DNA PKcs and RP2 from DSB repair pathways. My studies have shown that hTERT-RPE1 cells that lack RP2 expression completely can still efficiently repair DSBs caused by a low dose of IR. On the same note, RP2 expression does not appear to be induced by IR. Further, I showed that the RP2-DNA PKcs is independent of DNA damage and is not affected by treatment with etoposide, a DSB-causing chemotherapeutic drug. Taken together, these results suggest that the RP2-DNA PKcs complex is not involved in DSB repair. Nevertheless, it should not be excluded that it participates in another pathway of repairing different kinds of DNA lesions, which are perhaps more physiologically relevant to the retina, such as the BER pathway for repairing DNA oxidative damage or the NER pathway for repairing UV-induced lesions. It is intriguing that (Yoon et al. 2006) described RP2 as having DNA-binding and 3' to 5' exonuclease activity *in vitro*, and suggested it participates in the BER pathway. For these reasons, one of the key future experiments should be to examine the response of *RP2* null cells to H<sub>2</sub>O<sub>2</sub> treatment and UV irradiation, for example by performing clonogenic assays (to assess survival) or alkaline electrophoresis-comet assay (to assess DNA damage repair).

Finally, according to the existing bibliography, it is tempting to link the RP2-DNA PKcs to Golgi cohesion. As already mentioned above, DNA PKcs was recently

shown to be critical for Golgi shape reorganisation as a response to DNA damage, via phosphorylation of GOLPH3 (Farber-Katz et al. 2014). Cells that have reduced RP2 levels due to shRNA-mediated knockdown, as well as reprogrammed fibroblasts from an RP2 patient, have been reported to have markedly dispersed Golgi (Evans et al. 2010, Schwarz et al. 2015). Does this mean that the DNA PK/GOLPH3 pathway is hyperactive in cells that lack RP2 activity? One way to answer this question is by examining phosphorylation levels of GOLPH3 in cells lacking RP2 compared to wild-type cells, under normal or DDR conditions.

### 4.3.3 Conclusions and future directions

In conclusion, I have shown that RP2 binds to DNA PKcs in HEK293T and RPE1 cells, and proposed that this interaction is likely taking place at the plasma membrane and is characterised by a kinase-substrate relationship. I suggest that the RP2-DNA complex might be functioning at the plasma membrane, possibly in a non-canonical DNA PKcs pathway that is independent of DSB induction. Since more experiments are necessary to elucidate this, it is still possible that the complex is part of the DDR response, more likely in a DDR pathway other than DSB repair. In any case, I assume that the DNA PKcs-RP2 complex participates in a neuronal-specific or even photoreceptor-specific pathway, given the absence of any clinical features associated with DNA PK dysfunction in RP patients. Although DNA PKcs is present in the retina at protein level (Proteomic DB, <http://www.proteomicsdb.org>), it would be interesting to investigate specifically which retinal cell types express this protein. Interestingly, the only reported case of almost complete lack of DNA PKcs activity presented with marked neurological abnormalities, including post-natal neuronal atrophy, sensorineural hearing loss and marked visual impairment (Woodbine et al. 2013). This has already led scientist to suggest the existence of important roles for DNA PKcs in neuronal maintenance that are not shared by other NHEJ components. To answer these questions, it will be important to bypass the restrictions of *in vitro* work and cell culture by using animal models. For this purpose, the next chapter will focus on the generation of a vertebrate *RP2* null model of RP type 2.

## **Chapter 5: Generation of a zebrafish model for the genetic loss-of-function of *rp2* and examination of its effect on retinal lamination**

### **5.1 Introduction**

#### **5.1.1 The use of zebrafish in retinal research**

In order to better understand the biological processes described in the previous chapters, namely the function of the RP2-OSTF1 interaction and the potential role of RP2 in DNA damage repair pathways, studies must be conducted in a whole organism context. Therefore, animal models for RP type 2 are needed. Two mouse models of *Rp2* knockout have been generated (Li et al. 2013a, Zhang et al. 2015) which both model the late-onset, slowly progressive retinal degeneration observed in patients with *RP2* mutations. However, there are disadvantages of mouse models when studying visual disorders. For example, mice have a rod-dominant retina, with cones accounting for only 3% of total photoreceptor number (Goldsmith and Harris 2003). This could potentially constitute a drawback in RP2 research, given that the clinical image of patients with *RP2* mutations is characterised by high involvement of cone degeneration from early stages (Jayasundera et al. 2010), contrary to typical RP where cone loss is only secondary to the primary death of rod photoreceptors.

Zebrafish (*Danio rerio*) embryos have several characteristics that make them good models for biological research. They are a genetically tractable model system and combine ease of embryological manipulation with optical clarity during embryogenesis, offering the ability to examine the onset and course of a pathological process in real time *in vivo*. Importantly, they offer the possibility of whole-animal, high-throughput screenings for small molecule chemical modifiers of disease pathogenesis and severity, which is especially useful in pharmacology and the identification of new therapies (Lieschke and Currie 2007, Kitambi et al. 2009). For these reasons, zebrafish have been widely used not only as a model for studying vertebrate development, but also to study the mechanisms of visual disorders, due to the similarities between their retinal structure and lamination with that of the human

retina, and the fact that they possess a cone-dense retina (Goldsmith and Harris 2003). However, one major difference that sets zebrafish and human physiology apart is their unique ability to regenerate tissues and organs including the fin, heart, and retina. In mature zebrafish, new retinal neurons, including photoreceptors, are continuously generated from a population of mitotic progenitor cells at the retinal periphery, as well as a population of rod progenitor cells in the central retina (Marcus, Delaney and Easter 1999). In addition, the regeneration of photoreceptors can be stimulated in response to injury (for example, mechanical damage, chemical toxicity, phototoxicity and inherited retinal degeneration) and it has been shown that the mechanisms that mediate regeneration in response to rod or cone degeneration are distinct and involve increased proliferation progenitor cells in the outer nuclear layer (ONL) or the inner nuclear layer (INL), respectively (Morris et al. 2008, Brockerhoff and Fadool 2011).

Despite the regeneration capacity, mutations in plenty of genes have been identified to cause retinal degeneration in zebrafish adults or embryos and they participate in the same pathways that are important for retinal integrity in humans (Brockerhoff and Fadool 2011, Tsujikawa and Malicki 2004a). One prominent example is ciliary transport. For instance, zebrafish larvae with null mutations in *ift122*, encoding a component of the IFT-A complex, and *kif3a*, encoding a kinesin II family member, exhibit photoreceptor degeneration characterised by disorganised or absent outer segment (OS) discs and opsin mislocalisation (Raghupathy et al. 2016, Boubakri et al. 2016). In another study, *kif3a* mutant zebrafish embryos also display absence of connecting cilia and mislocalisation of basal bodies away from the apical surface of the photoreceptor inner segments (Pooranachandran and Malicki 2016). Another example is phototransduction; a mutation in the cone-specific *pde6c* gene leads to rapid degeneration of cone photoreceptors in larvae (Stearns et al. 2007). Finally, as an example of an adult zebrafish model for retinal disease, heterozygous carriers of *sonic hedgehog* (*shh*) null alleles, display cone loss and abnormal morphology (Stenkamp et al. 2008).

### 5.1.2 Zebrafish Rp2

In the zebrafish, there is only one copy of the *rp2* gene on chromosome 6 which encodes a protein of 376 residues, sharing 65% sequence similarity with human RP2 and the same protein domains (Figure 5.1) (Shu et al. 2011). The expression of *rp2* mRNA and protein in the embryo has been studied extensively. Different studies agree that *rp2* expression can be detected at the time of fertilisation (0 hours post fertilisation-hpf) and persists through hatching and larval stages (5 days post fertilisation-dpf) (Hurd et al. 2010, Shu et al. 2011, Desvignes et al. 2015). Interestingly, because *rp2* mRNA is detected during all stages of oogenesis and in the unfertilised egg, it is considered a maternally inherited mRNA suggesting an important role in the embryo's early development (Desvignes et al. 2015). In adult zebrafish, *rp2* appears widely expressed in many tissues including the eyes and the brain, like human RP2 (Shu et al. 2011). In the adult retina, Rp2 is detected by immunofluorescence at the outer plexiform layer (OPL), ONL, inner segment (IS), OS and appears to be mainly plasma membrane localised (Liu et al. 2015).

The function of Rp2 in zebrafish embryos has been examined by knockdown approaches. Knockdown of both zygotic and maternal *rp2* by translation-blocking morpholinos causes multiple developmental defects many of which are reminiscent of ciliary gene mutants (Omori et al. 2008, Raghupathy et al. 2016), including body curvature, hydrocephalus, pericardial effusion, heart looping inversion (a left-right symmetry defect) and cysts in the pronephric duct (Hurd et al. 2010). More relevant to my subject of study are the ocular phenotypic manifestations of the morphants: by 72 hpf, these embryos display microphthalmia (small eyes) and abnormal retina, well documented by histology showing disorganised lamination and increased cell death in the retina (Hurd et al. 2010, Shu et al. 2011, Desvignes et al. 2015). However, knockdown on zygotic *rp2* only by splicing-blocking morpholinos causes much milder effects (Desvignes et al. 2015). Taken together, these studies argue for an essential role of maternally inherited *rp2* mRNA in the early development of zebrafish embryos as well as in retinal maintenance. Several of these defects (body curvature, small eyes, heart looping defects) can be at least partially rescued by zebrafish or human RP2 mRNA (Shu et al. 2011). However, this phenotypic rescue

is incomplete and often quite weak (Shu et al. 2011, Hurd et al. 2010), while several of the reported phenotypes are common non-specific effects of morpholino injections. For these reasons, the phenotypes resulting from *rp2* knockdown must be interpreted cautiously and it is necessary to confirm them in *rp2* mutant embryos.

Based on the similarity between zebrafish and human RP2, highlighted by the discovery that human *RP2* mRNA can rescue defects in zebrafish morphants of *rp2* knockdown, and the evidence that they participate in the same pathways, I aimed to generate an *rp2* knockout zebrafish model, using the recently emerged CRISPR/Cas9 technology (Hwang et al. 2013). If the knockdown phenotypes that are easy to score by simple macroscopic observation, like the body curvature, could be recapitulated in the knockout model, this would provide an excellent platform to screen for small molecules that counteract *rp2* loss and open the way for new therapies. In this chapter, I describe the generation of zebrafish lines with three different deleterious mutations early in *rp2* exon 2 and I provide evidence that they probably lead to null alleles. Interestingly, none of these lines display any fertility defects or embryonic morphological defects. At least two of the lines with frameshifting mutations present with mild retinal degeneration characterised by shortening of the OS at 9 months.

## **5.2 Results**

### **5.2.1 Generation of *rp2* null zebrafish lines via the CRISPR/Cas9 method**

In order to generate a genetic knockout zebrafish model for RP type 2, I used the CRISPR/Cas9 method for genome editing, the gold standard in reverse genetics in recent years for a wide variety of biological models including the zebrafish (Liu et al. 2017b). I tried to target *rp2* gene with three different guide RNA sequences (gRNA) all targeting the beginning of exon 2 which is homologous to exon 2 of the human *RP2* gene and encodes the GAP catalytic domain of RP2 (Figure 5.1). Exon 2 is a mutational hotspot in the human protein since it contains about half of reported pathogenic mutations (Jayasundera et al. 2010). gRNA oligonucleotides and the mRNA encoding for nCas9 endonuclease (a modified version of Cas9 endonuclease that is codon-optimised especially for genome targeting in zebrafish (Jao et al.

2013)) were *in vitro* transcribed, and a mix of those two components was injected into 1-cell stage AB zebrafish embryos. Genomic DNA was extracted from 10-20 pooled injected embryos at 3 dpf and was used to estimate the efficiency of *rp2* targeting using a PCR-based genotyping strategy (see Chapter 2 for genotyping primer sequences). Because of the potential existence of multiple different mutations in these embryos, the PCR products were cloned into pGEM vectors and used to transform competent *E. coli* cells. While no insertions/deletions were found in the targeted sequence after genotyping ~40 individual transformed colonies for gRNA 2 and 3, gRNA 1 proved very efficient, with mutations found in ~60% of colonies sequenced. Although the existence of two different targeting sites was desirable, as it would permit me to eliminate any potential off-target effects by outcrossing fish with different target sites, I had to continue with one targeting site only.

Embryos injected with gRNA 1 and Cas9 were grown to ~3 months of age when they could be genotyped individually to identify founders (F0). Because all potential founder fish carrying *rp2* mutations were female, they were crossed with male AB fish and their progeny were screened for mutations. Two of the females were found to transmit *rp2* mutations through the germline and were named founder 4 and founder 7. All progeny from F0 x AB crosses were grown to ~3 months and genotyped. Among the progeny, three types of deleterious mutations were found heterozygously: a 4 bp deletion (del4) and a 8 bp deletion (del8) among the progeny of founder 4, and a 1 bp insertion (ins1) among the progeny of founder 7. Heterozygous fish (F1) carrying the same *rp2* mutation were crossed (F1 x F1) and their progeny genotyped when they reached ~3 months. Among their progeny (F2), WT, heterozygous and homozygous *rp2* mutants were found in numbers that approximated Mendelian inheritance (Figure 5.2A shows Sanger sequencing of homozygous mutant fish). Knockdown of *rp2* by morpholino injections has been reported to lead to obvious developmental phenotypes such as curved tail, hydrocephalus, small eyes and heart looping, that do not require histological observation or crossing to a reporter line to detect (Hurd et al. 2010, Shu et al. 2011). Interestingly, the *rp2* mutants did not exhibit any embryonic phenotypes or lethality, reached adulthood and were fertile (data not shown). Because of this, I was able to maintain and breed *rp2* mutant lines in homozygosity. This showed that genetic

inactivation of *rp2* does not lead to the same phenotype as embryonic knockdown strategies.

All identified mutations are predicted to be frameshifting, leading to premature stop codons. The del8 *rp2* allele is predicted to encode a truncated polypeptide containing a stretch of 20 incorrect amino acids, starting with a Glu to Gly substitution at position 73 (pGlu73Glyfs\*20). The ins1 allele is also predicted to encode a truncated polypeptide, containing a stretch of 21 incorrect residues starting with a Val to Gly substitution at position 75 (pVal75Glyfs\*21). On the other hand, the del4 allele is predicted to encode a somewhat longer truncated polypeptide with 37 incorrect amino acids, starting with a Thr to Trp substitution at position 74 (pThr74Trpfs\*37) (Appendix figure 5). To investigate the severity of these mutant alleles, I examined the levels of *rp2* transcript in 3 dpf-old pooled embryos that were either wild-type AB, del8 or ins1 homozygous mutants by real-time qPCR and normalised against the zebrafish  $\beta$ -actin gene *actb1*, a housekeeping gene used routinely in the lab which shows consistent levels of expression (Figure 5.2B). To test for any alternative transcripts that might remain unaffected by the mutations I generated, I used three different sets of primers encompassing different exon-exon junctions across the transcript (Exons 1-2 pair which encompasses the mutations and exons 3-4 and 4-5 pairs which are found downstream of the mutations). The primer pairs in relation to the transcript are shown as arrows in Figure 5.1. Both del8 and ins1 mutations lead to a decrease in transcript levels of approximately 70% compared to the wild-type transcript, indicating increased mRNA degradation possibly due to nonsense-mediated decay. The existence of one unique qPCR product in each case was confirmed by melting curve analysis and agarose gel analysis (Appendix figure 6A). Alignment of Sanger-sequenced cDNA molecules used as templates for qPCR did not reveal any alternative splicing events in the mutants compared to WT embryos (Appendix figure 6B). To test for expression at the protein level, I conducted western blotting in whole eye lysates from adult (7 months) F3 homozygous mutant and wild-type (derived from the progeny of founder 4) fish, using an anti-human RP2 antibody previously used to detect the zebrafish protein (Shu et al. 2011) (Figure 5.2C). I previously confirmed that this antibody can detect zebrafish Rp2-GFP when expressed in HEK293T cells (Appendix figure 7). Taken together, these results



suggest that the del8 and ins1 mutations at least are severe and lead to null alleles. However, it should be noted that there is an apparently non-specific band which is detected by the anti-RP2 antibody at a much higher molecular weight than wild-type RP2 protein only in the del4 and del8 mutant eyes (indicated by a red asterisk in Figure 5.2C). Because this band appears in two lines only and is stronger in the del4 fish that do not display a retinal degeneration phenotype, as it will be discussed later in the chapter, future research should be conducted to exclude any possibility that the del4 and del8 lines are hypomorphic (for example, if the unspecific band corresponds to a mutant form of RP2 arising from splicing changes caused by the mutations).

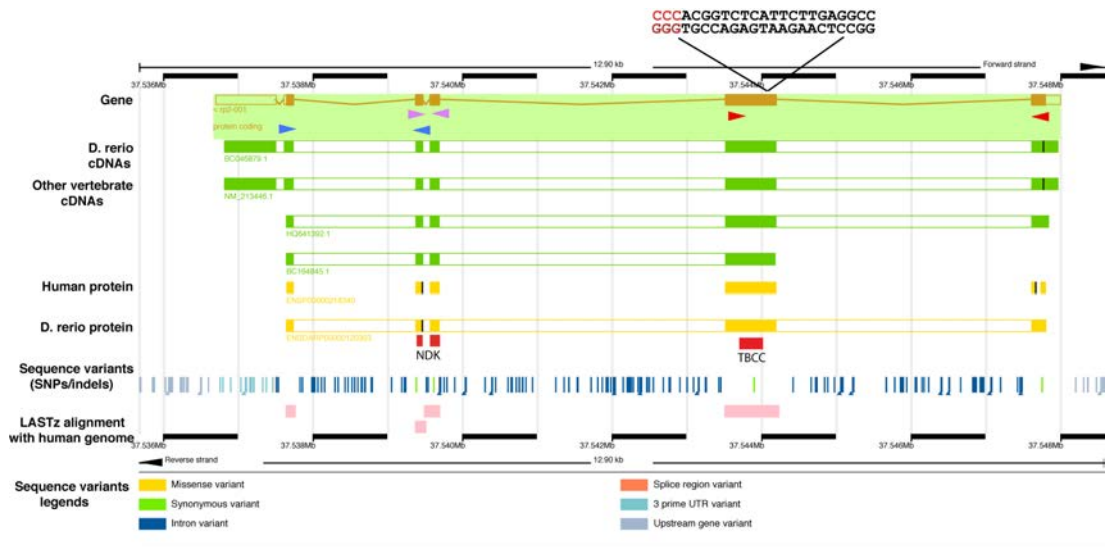


Figure 5.1. Ensembl annotation of the *rp2* gene in zebrafish and the position of CRISPR- induced mutations.

An Ensembl-based annotation of *Danio rerio*'s *rp2* gene is shown in orange colour where introns, exons, and untranslated regions are depicted as lines, filled boxes, and empty boxes, respectively. The genomic sequence targeted by gRNA1 is located close to the beginning of exon 2, with the PAM sequence highlighted in red. Primers used for real-time PCR are shown in red (pair 1), purple (pair 2) and blue (pair 3) arrows. Below the gene structure, an Ensembl representation of zebrafish and other vertebrate *RP2* cDNA molecules (from NCBI RefSeq and ENA databases) aligned to the genome is shown in green. The alignment of the zebrafish Rp2 protein's Ensembl sequence, as well as that of the human orthologous RP2 protein, to the genome, are shown in yellow colour. Below the zebrafish protein's alignment, the position of the main domains of the protein, TBCC-like, and NDK-like, are shown in red. These are encoded by genomic sequences downstream of the disruptions caused by CRISPR/Cas9. In addition, known sequence variants in the zebrafish gene are included in the diagram with the explanation of their nature found below in the "legend" section. Finally, the Ensembl LASTz analysis uses pink colour to show blocks of synteny in the aligned genomic sequences of zebrafish and human genes. These mostly overlap with the coding areas of the gene.

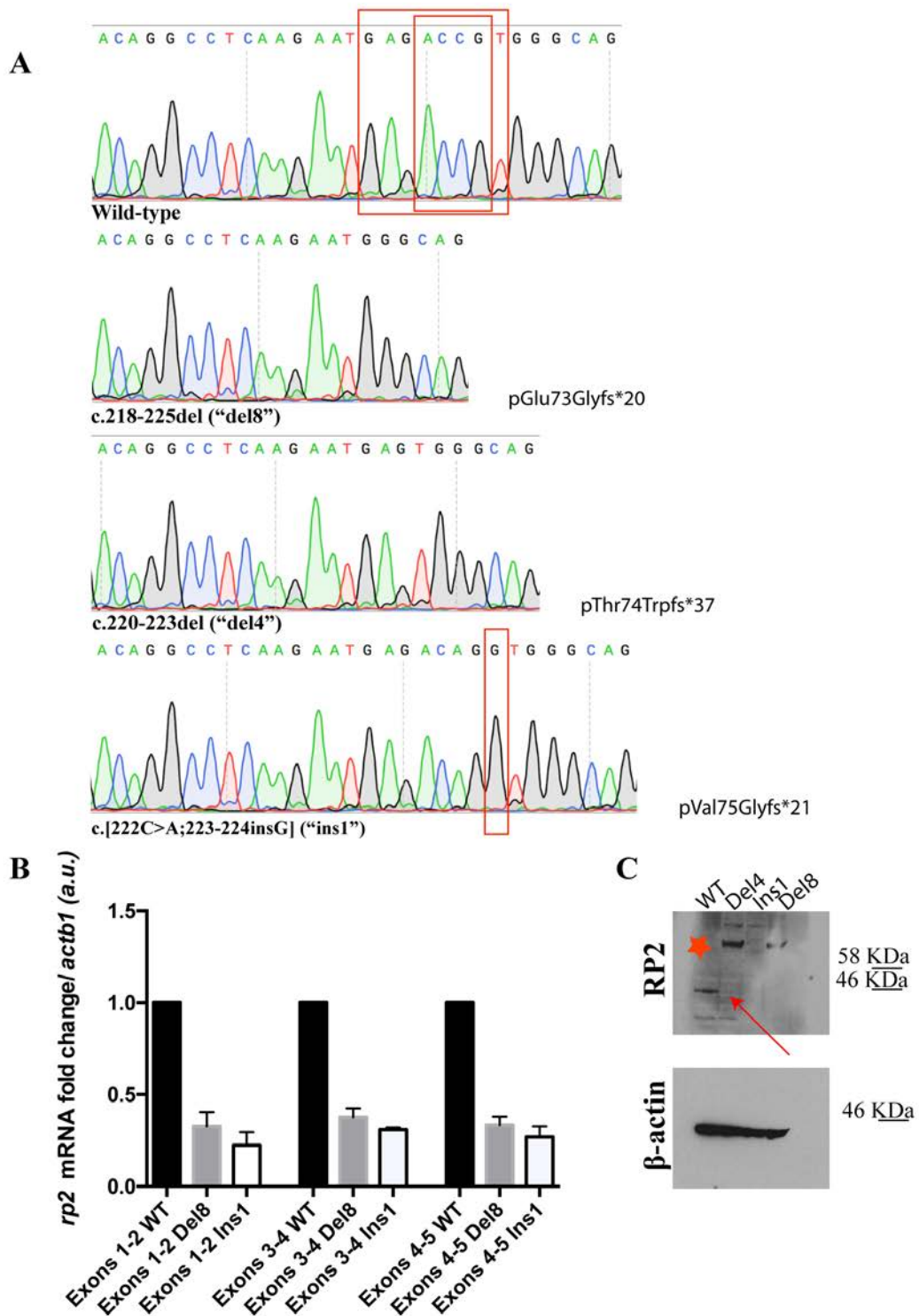


Figure 5.2. Induction of deleterious mutations in the zebrafish *rp2* gene.

A) Sanger sequencing on DNA isolated from homozygous mutant adult fish verified the existence of mutations in the 3 main lines that were created by targeting *rp2* gene with gRNA1. The 8 residues that are deleted from the del8 mutant, 4 residues deleted

from the del4 mutant (big and small box, respectively, on WT sequence) and the extra residue that is inserted in the ins1 mutant are enclosed in red boxes. B) *rp2* transcript levels (normalised to  $\beta 1$  *actin* transcript levels) are reduced in 3 dpf embryos that are homozygous for the del8 and ins1 mutations, compared to WT embryos. This reduction implies that nonsense-mediated decay of the transcripts is taking place. Levels of expression were estimated by real-time qPCR using three sets of primers encompassing the exon-exon junctions between exons 1 and 2, 3 and 4 and 4 and 5 (error bars correspond to S.E.M. from 3 biological repeats of the real-time qPCR experiment,  $p < 0.005$  for all WT vs mutant values assessed by one-sample t-test). Au=arbitrary units C) In order to confirm the absence of full-length Rp2 from the mutant lines, protein was extracted from whole adult eyes and subjected to SDS-PAGE and western blotting using an antibody raised against a human RP2 peptide. The red arrow points to the band on the predicted molecular weight for Rp2. The red asterisk points to apparently non-specific bands (discussed in further detail in the main text). The blotted membrane was subsequently stripped and re-probed with an anti- $\beta 1$  actin antibody as a loading control.

### **5.2.2 Characterisation of retinal structure in adult *rp2* mutant fish by histology**

Since the *rp2* mutant zebrafish did not display any externally obvious embryonic defects, I decided to investigate the integrity of the retinal structure in adult fish by histology. In several mouse models of RP (Thompson et al. 2012, Li et al. 2013a, Sun et al. 2016), retinal degeneration manifests as a decline in the thickness of the OS and the ONL, where the photoreceptor nuclei are found, due to cell death. To test if this is the case in my zebrafish models, I generated 7  $\mu\text{m}$ -thick paraffin retinal sections cut orthogonally to the vertical meridian of the eye from homozygous mutant F2 fish and wild-type siblings and used H&E stain to visualise the different layers of the retina. Subsequently, I measured the thickness of the photoreceptor layer (PL) (combined ONL and OS), and the INL, where bipolar, horizontal and amacrine cells reside (Figures 5.4-5.7). Homozygous fish for the ins1 mutation were examined at 9 months and displayed thinning of the PL compared to their wild-type siblings; this defect seems to be primarily due to the thinning of the OS rather than the nuclear layer (Figure 5.3). The difference occurs mainly at the nasal side and the central retina (near the optic nerve).

The observation that not all parts of the retina degenerate at the same rate has been reported before for other zebrafish models of retinal degeneration, both during

development and in adulthood. For example, cones degenerate in the central one-half of the retina at 4 dpf in *pde6c* mutant zebrafish embryos; because this pattern occurs during development, it is explained by the fact that central photoreceptors are more mature than peripheral ones (Stearns et al. 2007). In the *nba* zebrafish mutant, rod and cone degeneration is observed only in the central-most regions of the retina during adulthood (Li and Dowling 1997). This phenomenon is probably attributed to the fact that the zebrafish retina continues to grow beyond larval stages via the continuous addition of new cells at the peripheral region of the retina called the “ciliary marginal zone”. As a result, the retina that was generated in the embryonic and larval stages is found at the centre of the retina near the optic nerve head, while more recently generated retina is found near the tissue periphery (Hoon et al. 2014). Interestingly, the remnant of the larval retina in the adult fish retains a different, less organised distribution pattern of cone photoreceptors compared to the rest of the retina (Allison et al. 2010). These differences might account for my observation that thinning of the PL is more pronounced at the central retina in the *ins1 rp2* mutant zebrafish.

The INL remains unaffected in *Ins1* homozygous fish; because RP in humans and in animal models is known to specifically affect the photoreceptors and to spare other retinal cell types, the INL provides a good control to ensure that any observed difference is not an unspecific result of the histological processing (Figure 5.3D).

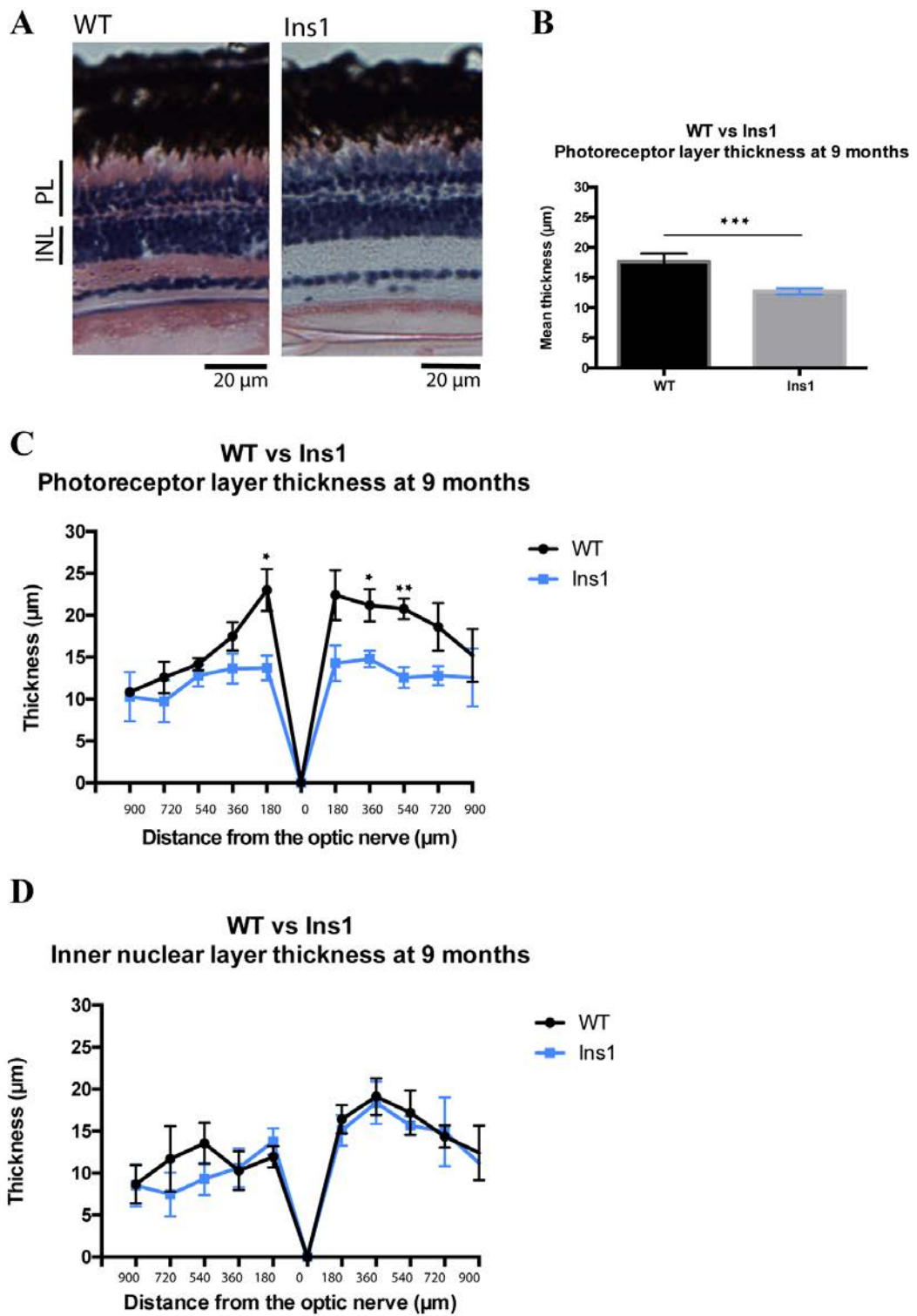


Figure 5.3. Ins1 homozygous fish show mild thinning of the photoreceptor layer compared to their wild-type siblings at 9 months.

A) H&E staining and light microscopy of 7  $\mu$ m retinal sections cut orthogonally to the vertical meridian of the eye. B) Ins1 mutant zebrafish display thinner

photoreceptor layer (PL), including both nuclei and OS, compared to their WT siblings at 9 months.  $P < 0.001$  according to paired two-tailed t-test<sup>6</sup>. C, D) Morphometric analysis showing PL thickness (C) and inner nuclear layer (INL) thickness (D) at different distances from the optic nerve head (point 0 on the x-axis) to the far peripheral retinae. Overall, although the mean thickness of the PL was significantly reduced in the *ins1* homozygous fish compared to their wild-type siblings, this is not the case for the INL ( $P = 0.1159$  according to two-tailed t-test). Asterisks on the graph indicate significance when the thicknesses at different distances on the retina were compared individually and assessed by multiple t-tests (\*:  $p \leq 0.05$ , \*\*:  $p \leq 0.01$ ). Error bars represent S.E.M for  $n = 3$  fish.

9 month-old zebrafish harbouring the *del8* mutation also display a decrease of the mean PL thickness across the whole retina, although the difference is less pronounced compared to the fish with the *ins1* mutation (Figure 5.4A, C-left graph). Because retinal degeneration in the *ins1* fish was more pronounced at the nasal retina, I carried out a closer analysis of the nasal retina of *del8* fish. When taking measurements from the nasal side of the retina specifically, the difference in PL thickness between WT and *del8* fish appears more pronounced (Figure 5.4B, C-right graph). Again, INL thickness remains identical between wild-type and mutant fish along the length of the retina (Figure 5.4D). However, any differences in PL thickness are lost when examining 12 month-old fish (Figure 5.5). At this older age, although the overall mean thickness of the PL in the *del8* fish appears mildly reduced compared to their WT siblings, no specific area of the retina appears much thinner. Therefore, any photoreceptor loss might be replaced by retinal regeneration as the fish get older. More experiments will be required to clarify this question. Finally, retinal sections from *del4* homozygous fish were examined at 7 months and no statistically significant differences were found in terms of PL thickness between *del4* homozygous fish and their wild-type siblings (Figure 5.6).

---

<sup>6</sup> Mean difference of PL thickness (WT vs *Ins1* at 9 months):  $4.907 \mu\text{m}$ , with 95% confidence interval:  $7.111$  to  $2.703 \mu\text{m}$ .

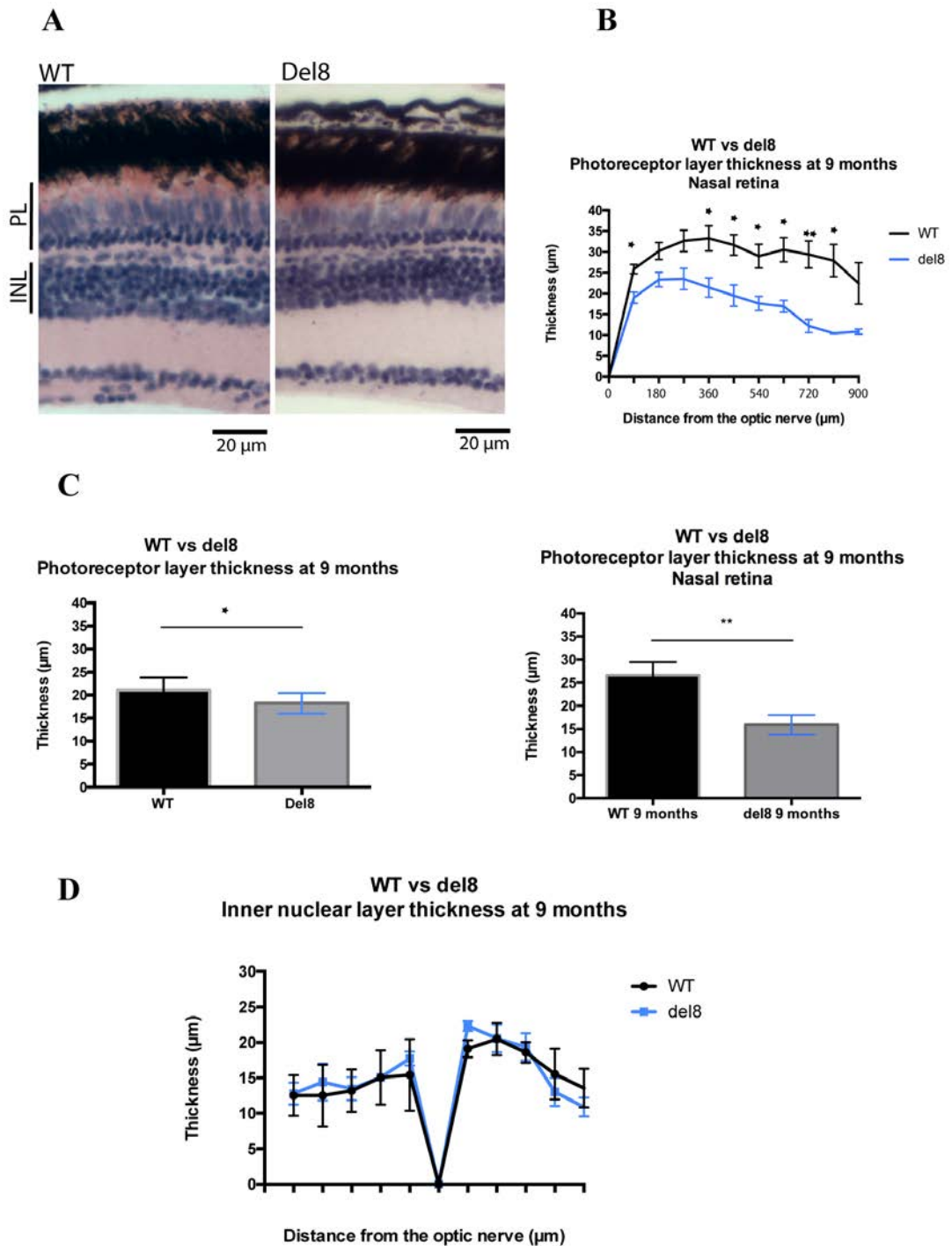


Figure 5.4. **Del8** homozygous fish show very mild thinning of the photoreceptor layer compared to their wild-type siblings at 9 months.

A) H&E staining and light microscopy of 7 μm retinal sections cut orthogonally to the vertical meridian of the eye. B) Morphometric analysis showing the thickness of the PL at the nasal retina and at different distances from the optic nerve head (point 0 of the x-axis). Asterisks on the graph indicate significance when the thicknesses at different distances on the retina were compared individually and assessed by multiple t-tests (\*:  $p \leq 0.05$ , \*\*:  $p \leq 0.01$ ). C) Del8 mutant zebrafish display thinner



photoreceptor layer (PL), including both nuclei and OS, compared to their WT siblings at 9 months. This difference is more pronounced when assessing the nasal side of the retina only.  $P=0.039$  (whole retina),  $p = 0.0020$  (nasal retina) according to two-tailed Wilcoxon matched-pairs signed rank test. D) Morphometric analysis showing the thickness of the inner nuclear layer (INL) at different distances from the optic nerve head (point 0 on the x-axis) to the far peripheral retinae. Mean thickness of the INL is not significantly different between WT and mutant retinae ( $P=0.3223$  according to two-tailed Wilcoxon matched-pairs signed rank test). Error bars represent S.E.M for  $n=3$  fish.

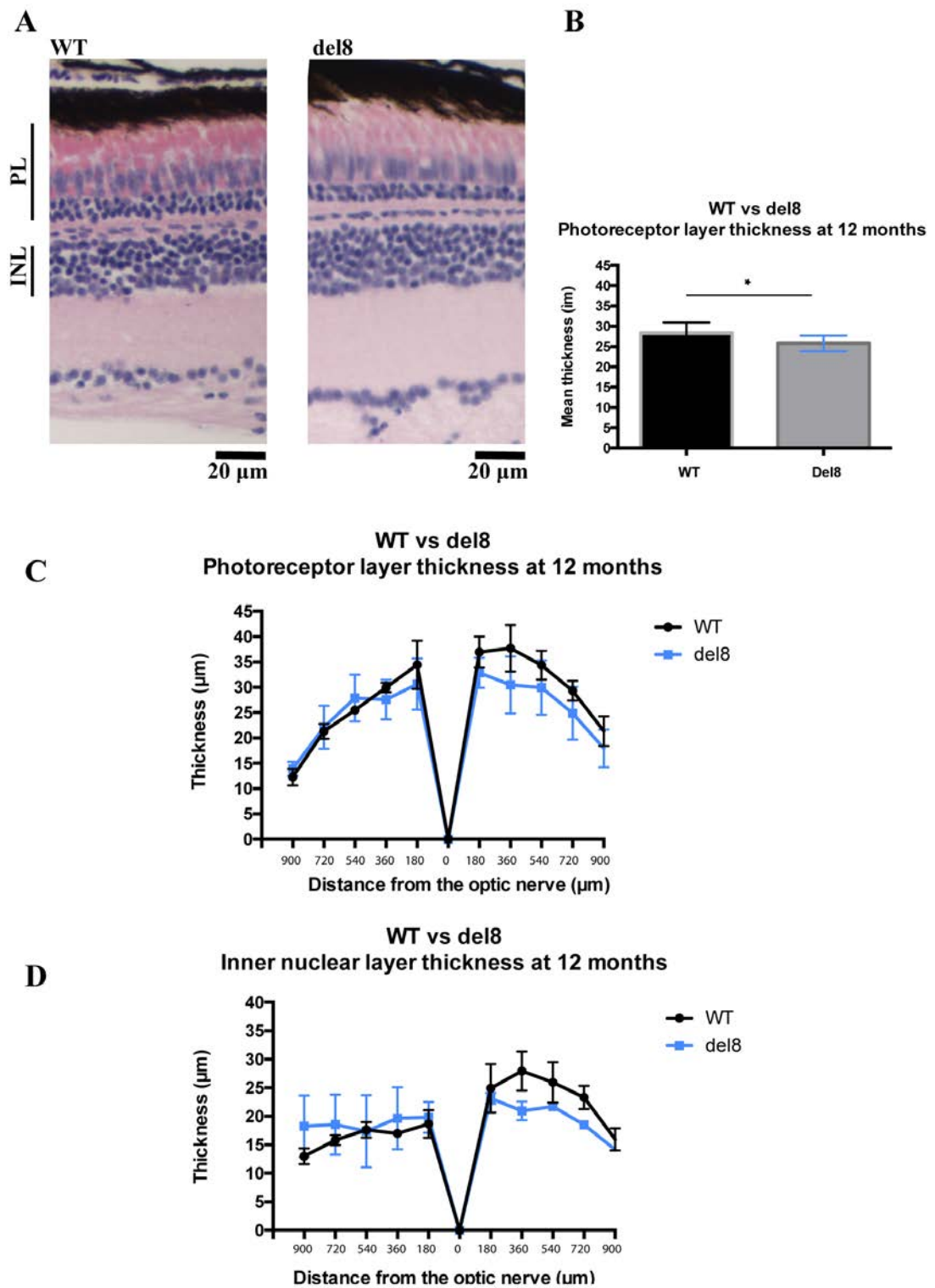


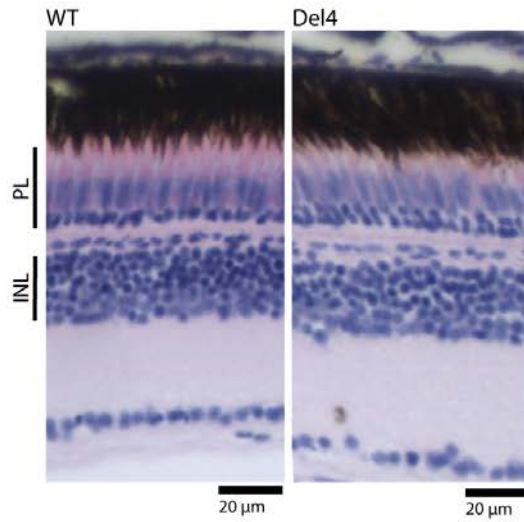
Figure 5.5. Del8 homozygous fish show only very mild thinning of the photoreceptor layer compared to their wild-type siblings at 12 months.

A) H&E staining and light microscopy of 7  $\mu\text{m}$  retinal sections cut orthogonally to the vertical meridian of the eye. B) Del8 mutant zebrafish display marginally thinner

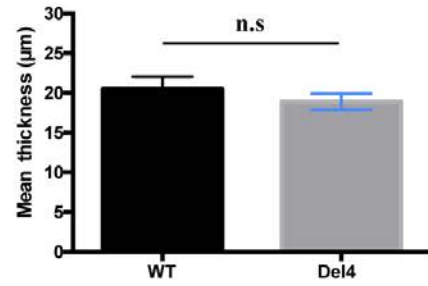
photoreceptor layer (PL), including both nuclei and OS, compared to their WT siblings at 12 months.  $P=0.0309$  according to two-tailed paired t-test<sup>7</sup>. C, D) Morphometric analysis showing the thickness of the PL (C) and the inner nuclear layer (INL) (D) at different distances from the optic nerve head (point 0 on the x-axis) to the far peripheral retinae. Overall, although the mean thickness of the PL was marginally reduced in the del8 homozygous fish compared to their wild-type siblings, none specific area of the retina appeared significantly thinner when values for different distances from the optic nerve were compared individually and assessed by multiple t-tests. The mean thickness of the INL was not significantly thinner between the two groups ( $P=0.5264$  according to two-tailed paired t-test) and no individual point displayed statistically significant difference between the INL of WT and mutant fish. Error bars represent S.E.M for  $n=3$  fish.

---

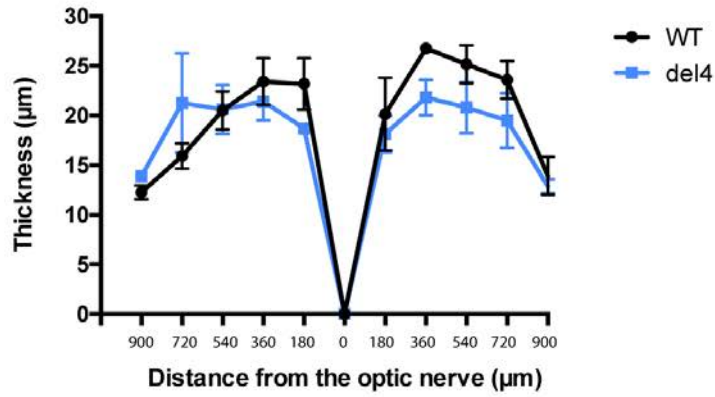
<sup>7</sup> Mean difference of PL thickness (WT vs Del8 at 12 months):  $2.501 \mu\text{m}$ , with 95% confidence interval:  $4.715$  to  $0.2869 \mu\text{m}$ .

**A****B**

WT vs del4  
Photoreceptor layer thickness at 7 months



WT vs del4  
Photoreceptor layer thickness at 7 months

**C****D**

WT vs del4  
Inner nuclear layer thickness at 7 months

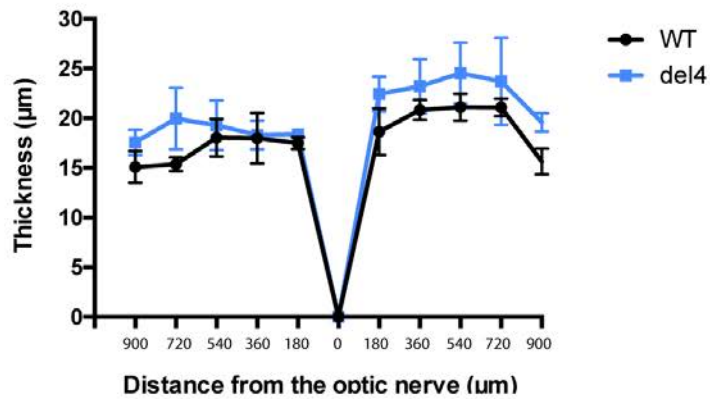


**Figure 5.6. Del4 homozygous fish do not show thinning of the photoreceptor layer compared to their wild-type siblings at 7 months.**

A) H&E staining and light microscopy of 7  $\mu\text{m}$  retinal sections cut orthogonally to the vertical meridian of the eye. B) Del4 mutant zebrafish do not display thinner photoreceptor layer (PL), including both nuclei and OS, compared to their WT siblings at 7 months.  $P=0.1571$  according to two-tailed paired t-test. C) Morphometric analysis showing the thickness of the PL (C) and the inner nuclear layer (INL) (D) at different distances from the optic nerve head (point 0 on the x-axis) to the far peripheral retinae. Overall, the mean thickness of the PL was not significantly reduced in the del4 homozygous fish compared to their wild-type siblings, and none specific area of the retina appeared significantly thinner when values or different distances from the optic nerve were compared individually and assessed by multiple t-tests. Error bars represent S.E.M for  $n=3$  fish.

### **5.2.3 Generation of *rp2* knockout/eGFP knock-in zebrafish model**

When I started my project, it was not known yet whether *rp2* knock-out would cause embryonic lethality in homozygosity. If the mutant adult fish had to be kept in heterozygosity, I had to find a way to isolate homozygous mutant embryos to use in the small-molecule screen. For this reason, I planned to engineer fluorescent reporter-encoding sequences in the zebrafish genome and in particular at the Cas9 endonuclease target site in the *rp2* gene. This approach would have a double purpose: 1) to easily isolate *rp2* homozygous mutants based on fluorescence (especially if I generated two heterozygous lines encoding different fluorescent reporters that I could intercross) 2) to express fluorescent reporters under the control of *rp2* promoter sequences, offering the ability to study Rp2 expression. Knock-in of fluorescent reporters has been achieved before by homologous recombination in endogenous zebrafish loci where double-stranded breaks have been induced by TALENs (Zu et al. 2013). On the other hand, a simpler approach has also been reported where large DNA cassettes were injected into sites of Cas9 targeting in exogenous loci in the zebrafish genome via non-homologous end joining, with three times higher efficiency (Auer et al. 2014). Their simple technique includes co-injecting the embryo with a vector containing the DNA cassette downstream of a sequence identical to the gRNA target sequence in the genome. Since gRNA would guide Cas9 to cleave both the genomic site and the vector, the latter would then integrate into the genome as a linear DNA piece.

To achieve this, I generated the relevant constructs using pEntr plasmid as a template. Into this vector, I cloned eGFP and mKate2 coding sequences downstream of a “bait” sequence which is identical to the gRNA 1 target sequence in the *rp2* gene, and a P2A self-cleaving peptide sequence between them (Figure 5.7). Subsequently, I injected the modified vector into 1-cell stage zebrafish embryos together with nCas9 mRNA and gRNA1. However, co-injecting the constructs proved toxic for the embryos and this impeded the continuation of the project. However, this preliminary work can provide the basis for a future project with the aim to ameliorate the efficiency of the injections and produce the desired zebrafish lines.

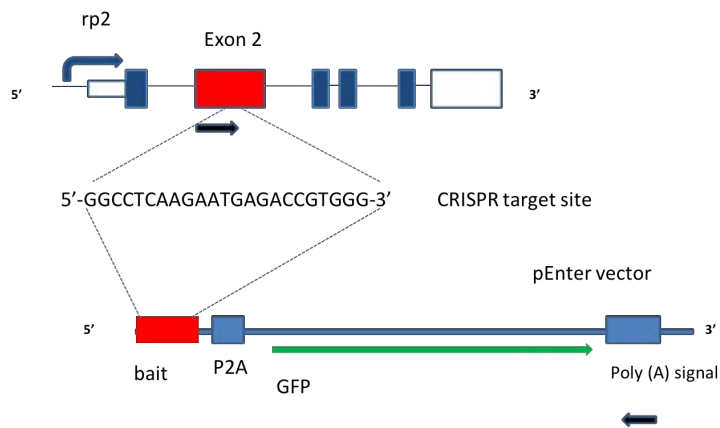


Figure 5.7. **Description of the experimental design for the generation of an *rp2* knockout/eGFP knock-in zebrafish model.**

The following components were injected into 1-cell stage zebrafish embryos: gRNA against the target site on *rp2* exon2, WT Cas9 mRNA and a pEnter vector containing eGFP coding sequence downstream of a 'bait' sequence which is identical to the gRNA target sequence. Cas9 is expected to cleave both the plasmid and the genomic site. The linearised plasmid should then integrate into the genomic site by NHEJ.

## 5.3 Discussion

### 5.3.1 The discrepancy between gene editing approaches for targeting *rp2* in zebrafish and morpholino-mediated knockdown

Morpholino-mediated knockdown of zebrafish *rp2*, a method which has been the gold standard in zebrafish reverse genetics for years, leads to severe developmental defects that are easily detected, according to more than one studies (Hurd et al. 2010, Shu et al. 2011, Desvignes et al. 2015). However, *rp2* morphants are not a good platform for conducting chemical screens because of the variability of the phenotypes and the difficulty in controlling toxicity arising from morpholino injections. On the other hand, if *rp2* mutants presented with developmental phenotypes, they would provide an ideal platform for a high-throughput small molecule screen to identify substances that can rescue or modify the phenotype caused by the loss of Rp2 function. To create a uniform population of mutant

embryos and to avoid the variabilities in phenotype severity and knockdown efficiency, which are often observed in a population of morpholino-injected embryos, I aimed to generate stable genetic mutations in *rp2*. I generated F2 fish homozygous for frameshifting mutations in *rp2* exon 2 which are predicted to generate premature stop codons, namely del8, del4, and ins1. Truncation mutations, due to deletions or premature stop codons, are the most common type of RP2 pathogenic mutations and lead to complete protein degradation (as in the case of the common p. R120X mutation) (Schwarz et al. 2015) or aggregation in insoluble fractions when expressed in mammalian cells (Schwahn et al. 2001). I found that the mutations I generated caused increased rate of mRNA degradation in 3 dpf embryos and absence of protein in the adult eyeballs- the tissue I focused my experiments on. Therefore, the *rp2* mutants I generated should be good models for RP2 disease in humans.

However, it soon became apparent that the homozygous mutant embryos did not present with any externally obvious developmental malformations. Moreover, F2 homozygous fish could be intercrossed to produce viable embryos. Interestingly, while this project was ongoing, a study was published where the authors used TALENs to generate zebrafish that are homozygous for a 5 base-pair deletion in *rp2* exon 2 (Liu et al. 2015) (“del5”). Similarly to my observations, (Liu et al. 2015) report the absence of any developmental phenotype and the ability of adult homozygous fish to breed normally despite the complete absence of *rp2* expression and reduced *rp2* transcript levels. This latest study combined with my results put a question mark over the conclusions drawn by morpholino-mediated knockdown experiments. In fact, since the emergence of genome editing strategies in zebrafish, finding that the knockout embryos do not display the same phenotypes as the morphants is a very common occurrence. It has even been claimed that, most of the time, zebrafish mutants generated by targeted genome editing exhibit no obvious phenotype (Kok et al. 2015). These findings highlight the off-target effects morpholinos often produce in zebrafish embryos, even when the morphants’ phenotype can be rescued by co-injection with the wild-type mRNA, and the need to find more stringent controls for this type of experiments. However, other studies indicate that morpholino-mediated knockdown should not be rejected too easily as



different reasons might be responsible for the discrepancy in phenotypes caused by the two experimental approaches, like the generation of hypomorphic alleles and the induction of genetic compensation by knockout approaches. For example, a recent study found that genetic lesions lead to specific upregulation of proteins in two genetic knockout zebrafish lines, a phenomenon which can account for the phenotypical rescue and does not occur after knockdown (Rossi et al. 2015).

That said, it still cannot be ruled out that *Rp2* has a role in the zebrafish embryo's early development, especially since it is a maternally inherited mRNA, even though I observed that progeny of homozygous mutant mothers were viable and developed normally. To solve this question in my mutant lines, I would first have to investigate *rp2* expression in the ovaries of mutant female fish and in very early embryos, as specific alternative *rp2* transcripts might be expressed in these tissues that are not affected by the mutations I generated. In addition, morpholino-mediated knockdown of *rp2* to study developmental phenotypes can still be used if the morpholinos are titrated on *rp2* null embryos to find an appropriate concentration that does not lead to any developmental phenotypes on this background. Another approach to investigating the validity of morpholinos is to examine if there is p53 mRNA induction after injections, as this often hints at non-specific effects (Robu et al. 2007). However, solving this problem was not a central aim in my Ph.D.

### **5.3.2 Comparing the phenotype of adult zebrafish *rp2* mutants to other reported animal models of RP2 disease**

According to the other study describing targeting zebrafish *rp2* by gene editing methods, *Del5 rp2* null zebrafish display late-onset retinal degeneration (which starts at ~4 months and is very pronounced by ~7 months); this affects both rods and cones and manifests mainly as shorter and aberrant OS layers (Liu et al. 2015). This phenotype is comparable to *Rp2* knockout mouse models, although thinning of the ONL due to the loss of photoreceptor nuclei, one of the main manifestations of retinal degeneration in the mouse models, is not observed in zebrafish. Moreover, degeneration in the *del5* zebrafish model is characterised by slightly decreased

protein levels and/or impaired trafficking of lipid-modified phototransduction proteins Grk1 (rhodopsin kinase), Gnat1 and Gnb1 (alpha and beta subunits of rod transducin), as well as total prenylated proteins in the retina (Liu et al. 2015). In that aspect, the del5 zebrafish model agrees with the gene trap mouse model (Zhang et al. 2015) more than with the exon2 deletion mouse model (Li et al. 2013a) (the phenotypes of these two mouse models are described in detail in Chapter 1.3.3).

Ins1 *rp2* null zebrafish which are described here display mild late onset thinning of the PL at ~9 months, manifesting mainly as shorter OS, which is the same histological observation that was reported in the del5 zebrafish study (Liu et al. 2015). Importantly, histopathological examination of eyes from RP patients have also reported the existence of poorly organised, shorter or absent OS (Ben-Arie-Weintrob, Berson and Dryja 2005). Protein levels of phototransduction proteins were not assessed in my thesis, as in previous studies (Liu et al. 2015, Liu et al. 2017a). However, I provide here the complete histological analysis of the thickness of retinal layers across the whole length of the retina, which is not reported in the other study. My analysis reveals that thinning of the PL at the ins1 model is more pronounced at the central area of the nasal retina. Given the polarity of the zebrafish retina and because OS thickness is not consistent across the length of the tissue, I show here that is important to report which exact area of the retina a picture has been taken from.

Ins1 zebrafish seem to display a more late-onset and milder phenotype compared to del5 zebrafish, as reported in the other study (Liu et al. 2015). It is not clear why this discrepancy occurs, but it is possible that it is a result of inconsistency in light exposure levels between the different fish rooms. In addition, it is surprising that the del4 mutant fish do not display any retinal degeneration, despite the absence of Rp2 protein from their eye lysates (Figure 5.2C). It is possible that the age when the del4 animals were tested (7 months) was too early for any degeneration to show. Because Ins1 fish originate from a different founder female (no 7) than del4 and del8 (no 4), another explanation could be that modifier genes are expressed in one background and not the other and manage to rescue the degeneration phenotype. This situation might reflect the extreme phenotypic variability observed among RP2 patients, even

within the same family. More experiments will be needed to clarify this question. For example, backcrossing *rp2* homozygous null fish from the founder 4 background to fish from the founder 7 background and examining retinal lamination in the progeny could help clarify if modifier genes play a role in the emergence of retinal degeneration.

Moreover, retinal degeneration should be confirmed in the *Ins1* fish by further analysis, for example histological examination of a bigger animal sample and in older ages, assessing visual function by examining ERG or optokinetic response (OKR), and examining cone and rod cell death more closely by immunofluorescence. Finally, the localisation and expression levels of lipid-modified phototransduction proteins Grk1 and Pde6 in retinae from the *ins1* fish should be examined in the future in order to verify the conclusion of the other study that Rp2 participates in the trafficking of these proteins (Liu et al. 2015).

Finally, it will be important to determine whether thinning of the photoreceptor layer is due to cell loss or defective growth of the retina. As mentioned before, cell proliferation continues throughout the lifetime of zebrafish in the ciliary marginal zone (Malicki et al. 2016). To test if cell proliferation is affected in the *rp2* mutant retinae, 5-bromo-2-deoxyuridine (BrdU) incorporation and staining can be used, as well as staining for proliferating cell nuclear antigen (PCNA), a marker of proliferation expressed in the retinal mitotic progenitor cells (Morris et al. 2008, Malicki et al. 2016).

### **5.3.3 Potential use of *rp2* null embryos for studying the role of Rp2 in DNA damage repair**

Because of the lack of developmental phenotypes at the embryonic level, the *rp2* mutant lines are in the end not appropriate for a phenotype-based screening of small molecules, as it was originally designed. However, the embryos of these fish could provide a whole organism platform to test if the RP2-DNA PK complex plays a role in DNA damage repair, expanding on cell culture studies by taking advantage of the benefits of the zebrafish embryos as an experimental model. Zebrafish are a valid

model for investigating DNA repair deficiencies in humans because they have orthologues of genes involved in all known DNA damage pathways of mammals (Pei and Strauss 2013). *Prkdc* null zebrafish have been already generated by genome editing technologies. Their main characteristic is severe combined immunodeficiency (scid), as is the case with DNA PKcs deficiency in mice and human patients (Mathieu et al. 2015), characterised by the absence of functional T/B lymphocytes, growth delay and susceptibility to infections (Jung et al. 2016). Although the authors of this study did not specifically look for neuronal phenotypes or retinal manifestations, it appears that DNA PKcs in zebrafish has the same functional roles as in humans, at least in the maturation of the immune system. Additionally, the genes encoding for Ku70 and Ku80 zebrafish orthologues have been cloned and it has been found that both these proteins originate from maternally inherited transcripts and are strongly expressed in the embryonic brain and retina. For both these proteins, it was proved that knockdown results in radiosensitivity of the embryos (Bladen et al. 2005, Bladen et al. 2007).

It is, therefore, apparent that zebrafish embryos possess a functional DNA PK holoenzyme and are appropriate for studying the consequences of RP2 loss of function in DNA repair. An experiment that could be readily performed is to treat the embryos with increasing doses of ionising radiation and perform TUNEL assay to assess cell death in the retina or the whole embryo. If cell death is more pronounced in the *rp2* null embryos after radiation compared to WT embryos, it is an indication that they are more sensitive to this type of DNA insult.

## Chapter 6. Conclusions and future directions

### 6.1 The importance of basic research for the identification of novel therapies for RP

Today, no widely available treatment exists that can prevent or reverse vision loss in patients with inherited retinal degenerations. The disease can at best be managed or slowed down via the treatment of specific symptoms, nutritional supplements such as lutein/zeaxanthin macular pigments, avoidance of sunlight, and supportive equipment (Sahel et al. 2014). Research has so far focused on two different strategies to treat inherited retinal degenerations: 1) gene-independent therapies and 2) gene- and mutation-specific therapies. The first group includes therapeutic approaches which can apply to many different types of RP and other retinal degenerations because they focus on pro-survival signalling, cell restoration or preventing the secondary death of cones. For example, the administration of neurotrophic factors and other pharmacological approaches have shown efficacy in animal models, and some have been assessed in clinical trials with results which have been limited but existent nonetheless (e.g., regarding calcium channel blockers (Nakazawa et al. 2011, Sacchetti et al. 2015)). Moreover, cell replacement therapy, i.e. the integration and differentiation of retinal precursor cells in the diseased retina, is a very promising strategy for degenerative diseases that lead in cell death and altered retinal morphology, and it has been successfully tried in several rodent models. The sources of those cells are either embryonic stem cells (ESCs) or induced pluripotent stem cells (iPSCs) (reviewed in (Zarbin 2016)). Recently, human ESC-derived RPE cells were implanted in age-related macular degeneration (AMD) and Stargardt's disease patients in a clinical trial with no significant adverse effects (Schwartz et al. 2015). One must not overlook advances in a different field, the field of retinal prosthetics devices, which have acquired commercial use approval in the USA and function in activating the inner retinal network in the place of lost photoreceptors (Sahel et al. 2014).

Among the category of gene-specific prospective therapies, gene therapy is perhaps the most promising approach, aiming to augment or replace the improperly functioning genes with wild-type genes via adeno-associated or lentiviral vector

delivery. Clinical trials for *RPE65* gene replacement in canine models and patients with LCA are safe and resulted in improvement of visual functions for at least three years (Cideciyan 2010, Sharif and Sharif 2017). Today, gene replacement clinical trials are ongoing in patients with Stargardt's disease, *MERTK*-associated RP, choroideremia and AMD (Sahel et al. 2014). RP type 2 is an appropriate candidate for this kind of therapeutic intervention because it is a monogenic disease, it is caused by loss-of-function mutations, and wild-type gene delivery has already been tested in rodent models and showed rescue of retinal degeneration (Mookherjee et al. 2015).

Another promising aspect of gene therapy is the use of CRISPR/Cas9 gene editing techniques to correct genetic defects in the retina. Because photoreceptors are nondividing cells and primarily use NHEJ to correct DNA breaks such as the ones induced by the CRISPR system, this therapeutic development is closer to actual application in diseases caused by dominant negative alleles. For example, disruption of a dominant negative rhodopsin allele (S334Ter) by CRISPR-based knockout has been recently tried *in vivo* in a rat model and led to photoreceptor rescue (Bakondi et al. 2016). In cases of loss-of-function mutations, on the other hand, the potential to correct endogenous genes via HR-based repair of CRISPR DNA lesions using a donor template, while successful in cell culture, still needs a lot of study and improvement before it can be applied to animal models of photoreceptor degeneration [reviewed by (Chrenek, Nickerson and Boatright 2016)].

Despite the success of LCA trials in restoring visual function, a subsequent study showed that transgene expression failed to halt retinal degeneration in treated patients, possibly because a significant portion of the photoreceptors had already "committed" to cell death at the time of administration. This study also suggested the combination of different therapeutic strategies as the way to achieve treatment of retinal degeneration (Cideciyan et al. 2013). Furthermore, studies in mouse models for the loss of *RPGR* function, the other major gene for X-linked RP, showed that the overexpression of the *Rpgr*<sup>Ex1-19</sup> isoform on the *Rpgr*-null background led to a more severe phenotype than the one caused by the loss of *Rpgr* alone (Wright, Hong and Perkins 2011). *Rp2* null mouse studies also report retinal toxicity resulting from high

doses of the exogenous gene (Mookherjee et al. 2015). Therefore, the experience of gene therapy clinical trials for retinal diseases has highlighted the importance of a thorough knowledge of the natural history of the disease and the functions of the transgene product, in order to predict any potential toxic effects of overexpression in the retina.

The work presented here is important because it suggests previously unknown functions of RP2 in the retina and can thus promote future research on the pathways implicated in disease and the identification of novel therapies. It can also enhance the safety of future clinical trials by pointing pathways in the cell that can be affected by the protein's overexpression. For example, if it is proved that RP2 is indeed a positive regulator of cell motility by modulating the interaction between OSTF1 and MYO1E, as it is suggested in Chapter 3, then future research must investigate any potential unwanted side-effect of transgene overexpression to stimulate the migratory capacity of the RPE layer.

## **6.2 Studying the RP2-OSTF1 interaction: future directions**

In Chapter 3, I showed that the C-terminus of RP2 participates in the interaction with OSTF1 and that this function is evolutionarily conserved in vertebrates since the residues identified as belonging to the interaction interface are strictly conserved in all the species tested. Because OSTF1 is an adaptor for c-SRC kinase (Szymkiewicz et al. 2004), I tested the hypothesis that c-SRC phosphorylates RP2 via the interaction with OSTF1. Despite showing that c-SRC can directly phosphorylate RP2 *in vitro* and that overexpression of c-SRC leads to phosphorylation of RP2 at Y27, my experiments were inconclusive about the existence of endogenous c-SRC-mediated RP2 phosphorylation. This pitfall points out that the use of antibodies against global tyrosine phosphorylation was not the best tool for answering this question and that phospho-specific antibodies need to be developed.

Secondly, I examined if *RP2* null cells display abnormal migratory behaviour in culture, following previous suggestions that OSTF1 is a negative regulator of cell motility (Tanimura et al. 2011, Tanimura et al. 2016), and observed reduced

migration capacity compared to wild-type cells. Many questions stem from this observation. Firstly, my results suggest that RP2 has a positive effect on cell motility. One interesting hypothesis that should be tested in the future is that RP2 exerts this effect by modulating the OSTF1-MYO1E interaction. In fact, a study from our group that was recently published and includes part of the work presented here in Chapter 3 suggests that RP2 negatively regulates the OSTF1-MYO1E interaction by recruiting OSTF1 to the cell membrane (Lyraki et al. 2018). This hypothesis is presented schematically in Figure 6.1A. Another important question that follows my experiments is after what trigger/under what conditions the RP2-OSTF1 interaction occurs. It could be that RP2 has two separate functions, the regulation of ciliary protein transport in ciliated cells and the regulation of cell migration via the interaction with OSTF1 in dividing, non-ciliated cells.

Finally, it will be interesting to examine how this effect might be translated in impaired cytoskeletal rearrangements in the diseased retina. Interestingly, the other major XLRP protein, RPGR, has been suggested before to influence actin dynamics by several studies. One study showed that actin turnover and interact with the scaffold protein Whirlin which participates in the cytoskeletal assembly in photoreceptors (Lyraki et al. 2016, Wright, Hong and Perkins 2012). Recently, RPGR was also found to mediate actin disassembly in the photoreceptor CC and, consequently, rhodopsin transport, via its interaction with the actin-severing protein Gelsolin (Megaw et al. 2017). To further understand if loss of RP2 also leads to defective cytoskeletal rearrangements *in vivo*, photoreceptors and RPE cells from *Rp2* null mice could be subjected to cytoskeletal staining and tested for OS phagocytosis.

### **6.3 A potential role of DNA damage-associated signalling in RP type 2: future directions**

Another outcome of the work presented here is the identification of DNA PKcs as an interaction partner of RP2, based on MS/MS analysis of the complexes that co-precipitate with RP2 from HEK293T cells. One of the key functions of DNA PKcs is



in the NHEJ pathway for the repair of DNA DSBs. DSB repair is of particular importance for the viability of neurons in the central nervous system, both during neuronal development and in mature neurons, considering their high metabolic activity and post-mitotic status (Borges, Linden and Wang 2007). It is important to note that because neurons are non-dividing, they lack replication-dependent DNA repair mechanisms such as HR, and must solely depend on NHEJ for the repair of DSBs. These characteristics are also true for the photoreceptors, with the added factor of high PUFA content and constant light exposure which renders them even more susceptible to DNA damage, especially ROS-mediated damage. For this reason, future experiments should focus on elucidating if the lack of RP2 function leads to accumulation of unrepaired DNA damage underlying photoreceptor degeneration. Since my work showed that *RP2* null cells repair X-ray-induced DSBs normally, and because of the photoreceptor's physiology, I suggest that future research should focus on ROS-induced DNA lesions, rather than "clean" DSBs induced by radiation or topoisomerase inhibitors. On the other hand, it is important to note that my experimental setup did not distinguish HR from NHEJ modes of DSB repair, and therefore it might not have detected subtle defects in one or the other pathway.

Two existing *in vivo* systems can be ideally used for these types of experiments. Firstly, levels of DNA damage accumulated physiologically pre- and during retinal degeneration can be compared in *Rp2* null vs. WT mice. For the visualisation of DNA damage, antibodies can be used which detect different kinds of DNA damage, such as 8-hydroxyguanosine, 53BP1 and  $\gamma$ H2AX. Secondly, the response of the retina when challenged with excessive amounts of DNA damage, for example after treatment with H<sub>2</sub>O<sub>2</sub> or cytotoxic drugs, can be compared in *rp2* null vs. WT zebrafish embryos. The effect on these processes of modulating DNA PKcs activity, for example using specific DNA PKcs inhibitors, should also be examined.

On the other hand, it is important to note that in my MS/MS analysis, RP2 did not co-precipitate with other DDR proteins, such as ATM, ATR, or other NHEJ components (Appendix Table 1). This observation suggests that RP2 is not a part of classical DNA repair pathways in the nucleus, but might instead interact with DNA

PKcs in a non-canonical context. The idea that DNA PKcs has specific functions that are not shared by other NHEJ components has been suggested before. Studies have shown a specific requirement for DNA PKcs during neural development in general and retinal development in particular (Woodbine et al. 2013, Baleriola et al. 2010). Interestingly, my work suggested that a kinase from the DNA PK complex can phosphorylate RP2 *in vitro* at a site which has already been identified as phosphorylated under neurite growth conditions (Wang et al. 2011) (Figure 6.1B).

Some of the specific functions of DNA PKcs might even take place outside the nuclear compartment, and my work already suggested that the protein might interact with RP2 in the plasma membrane (Figure 6.1B). Other studies previously suggested that DNA PKcs acts in relaying DNA damage signal to the cytoplasm and the cytoskeleton (Kotula et al. 2013, Farber-Katz et al. 2014). Therefore, it will be useful to study if modulation of the DNA PKcs function can affect RP2-dependent processes such as RP2-regulated protein trafficking. Another interesting subject of future study is the regulation of Golgi cohesion which has been attributed to DNA PKcs, especially since patient-derived RP2 null cells display abnormal Golgi fragmentation, according to an earlier study (Schwarz et al. 2015). Moreover, it should be investigated if DNA PKcs localises to primary cilia, the cilium-associated centrioles, or the photoreceptor CC, similarly to RP2.

Importantly, following up the experiments presented in Chapter 5 could lead to clinical benefits. Because DNA PK has emerged as an attractive target for cancer therapy, several series of selective and potent inhibitors have been designed (Ihmaid et al. 2017). These could be repurposed for the treatment of RP if future research shows that suppressing DNA PKcs activity can modulate retinal degeneration. Moreover, it is important to note that antioxidant therapy might present a promising approach to manage XLRP in the future if further research shows that excessive oxidative stress-induced DNA damage underlies photoreceptor loss due to RP2 mutations. One example of a component that has been administered in RP patients in clinical trials is docosahexaenoic acid (DHA), an omega-3 fatty acid with neuroprotective and free-radical scavenging properties through its derivative NPD1 (Bazan 2006). DHA administration has so far shown a poor capacity to ameliorate

visual acuity or fundus appearance but has slowed down the rate of progression of visual field sensitivity (Hoffman et al. 2015). However, if future research shows that ROS-induced DNA damage underlies retinal degeneration specifically in patients with *RP2* mutations, DHA administration might show better results in these cases.

Lastly, it is essential that future research establishes if there is a relationship between *RP2* mutations and sensitivity to cytotoxic drugs and other DNA-damaging components. This information will be especially important for RP patients who need to undergo some form of anti-tumour therapy. Some studies have reported a link between retinal toxicity and cytotoxic chemotherapy (Blanchet, Wellemeyer and Burton 1992, Tang et al. 2017).

#### **6.4 Convergence of the OSTF1- and DNA PKcs-associated pathways**

The two ways for *RP2* phosphorylation discussed in this thesis, i.e. c-SRC-mediated and DNA PKcs-mediated, might not be separate but belong in interdependent pathways. It has been shown before that c-SRC is activated by ionising radiation and has a role in relaying DNA damage signalling from the plasma membrane to the nucleus, via phosphorylation of EGFR and subsequent translocation to the nucleus and DNA PK activation. Suppression of c-SRC activation is associated with radiosensitivity (Dittmann et al. 2008). In addition, c-SRC phosphorylates the Ku70 subunit of the DNA PK holoenzyme, and this phosphorylation has a protective role against hyperactive apoptosis (Morii et al. 2017). The development of phospho-specific antibodies to Y27 and S213/T214 phosphorylation will aid in examining if the two modes of phosphorylation participate in the same pathway. Future studies should examine if phosphorylation in those two separate sites is induced after DNA damage and if suppressing phosphorylation in one site affects the other site, and vice versa.

#### **6.5 *rp2* null zebrafish as models of retinal degeneration**

The necessary next step is to transfer *in vitro* studies on *RP2* function to a more

physiological context, such as animal models. For this purpose, Chapter 5 of the thesis was dedicated to the generation of a zebrafish model for RP2 type 2 using the CRISPR/Cas9 method. At least two (*ins1*, *del8*) of the *rp2* null zebrafish lines that I generated present with late-onset retinal degeneration characterised by thinning of the OS layer, similarly to human disease where the retina is properly formed and starts to degenerate later in life. Another study which reports the same phenotype in adult zebrafish with *rp2* loss-of-function mutations (Liu et al. 2015) corroborates my results.

My work showed that loss of *Rp2* in zebrafish does not lead to developmental defects and embryonic phenotypes. Nonetheless, this observation will require further clarification, as it is not sure why *rp2* is a maternally provided transcript if it has no role in early development (Desvignes et al. 2015). The data presented in my thesis refute previous studies using morpholino injections to knock-down *rp2* expression in zebrafish embryos, which describe a variety of embryonic phenotypes including small eyes (microphthalmia) and disorganised retina, pericardial oedema, laterality defects, body curvature and hydrocephaly (Desvignes et al. 2015, Hurd et al. 2010, Shu et al. 2011). Although these studies report rescuing the phenotypes by co-injecting the embryos with WT *rp2* mRNA, the specificity of the phenotypes is questionable because the rescue is only partial. Many other zebrafish mutants do not display the phenotypes reported by morpholino-mediated knockdown, even though these have been partially rescued by WT mRNAs (Kok et al. 2015). One useful way to identify non-specific phenotypes, a common occurrence following injections with morpholinos, is to test if the phenotypes arise when the injections take place in embryos that are null for the gene in question (Rossi et al. 2015). As a conclusion, it seems that the generation of knockout fish lines will be essential for all zebrafish research from now on.

The *rp2* null zebrafish represent important assets in the research for the molecular mechanisms that underlie RP, as they can be used to test hypotheses arising from biochemical approaches and to identify the functional relevance of RP2 interactions described in Chapters 3 and 4 of the present thesis. For example, I suggested in Chapter 3 that the involvement of RPE dysfunction in RP type 2 must be carefully

examined, as both RP2 and OSTF1 are expressed in the RPE, and the regulation of cell motility is related to important RPE functions *in vivo*. One way to examine this question would be to conduct mosaic analysis in the zebrafish model. It has been shown before that the transplantation of donor cells to a host embryo during the blastomere stage will result in a chimeric retina, where at least some donor cells will contribute to the neuroepithelium (Goldsmith et al. 2003, Tsujikawa and Malicki 2004a). Using the mosaic analysis approach, it could be tested if mutant photoreceptors survive when they are in contact with WT RPE cells, or if WT photoreceptors degenerate when their environment is composed of mutant RPE cells. This experiment will show if the photoreceptor degeneration observed in RP is a cell-autonomous process and will reveal the exact site where RP2 exerts its role.

Moreover, the *rp2* null zebrafish embryos could be used to test whether RP2 mutations confer sensitivity to DNA damage, as I have proposed in Chapter 4. This could be achieved by comparing the viability of WT and mutant embryos, as well as the amount of cell death in the retina and other tissues following exposure to DNA damage-causing drugs or ionising radiation [an approach which has been used before by (Bladen et al. 2005, Bladen et al. 2007)]. As a whole-organism platform, zebrafish embryos are far superior to cultured cells for this type of assays. If *rp2* null zebrafish embryos display sensitivity to DNA damage, then they can be used for a small-molecule screen looking for chemical compounds that alleviate or rescue this sensitivity. Finally, it should be examined whether any link of RP2 mutations to increased sensitivity to DNA damage is because of increased apoptosis due to the inability to repair DNA damage or cell cycle arrest due to the inability to resume proliferation after replication stress caused by DNA damage. This possibility can be examined in zebrafish retinæ, taking advantage of the fact that proliferating cells exist throughout the animals' lifetimes in the ciliary marginal zone (Hoon et al. 2014). The amount of cell proliferation in WT and *rp2* null retinæ can be compared via staining for cell proliferation markers such as PCNA, or BrdU incorporation (Morris et al. 2008).

Finally, zebrafish genetics can be leveraged to identify potential functional interactions between the two different RP2 interaction partners studied in the present

thesis, OSTF1 and DNA PKcs. For example, RP2/OSTF1, RP2/DNA PK and OSTF1/DNA PK double mutants could be generated to examine if mutations in both genes exacerbate or rescue the phenotypes caused by mutations in one of the genes only. Thus, it can be determined if the proteins act in the same pathway and whether they act upstream or downstream of RP2.

As a conclusion, it seems that both mouse and zebrafish can successfully model late-onset retinal degeneration caused by *RP2* mutations (Liu et al. 2015, Zhang et al. 2015, Li et al. 2013a) and will complement each other in future research.

## **6.6 Final remark**

By demonstrating that RP2 participates in novel complexes, my work suggests that it is a multifunctional protein with more than one roles in cellular biology and that it might not be correct to view RP type 2 as a disease of exclusively ciliary pathology. This finding might benefit retinal research in general, as other forms of retinal degeneration might share the same pathogenic mechanisms, as well as ciliopathy research, by adding one more piece of evidence to the emerging paradigm of ciliary genes participating in DNA-related processes.

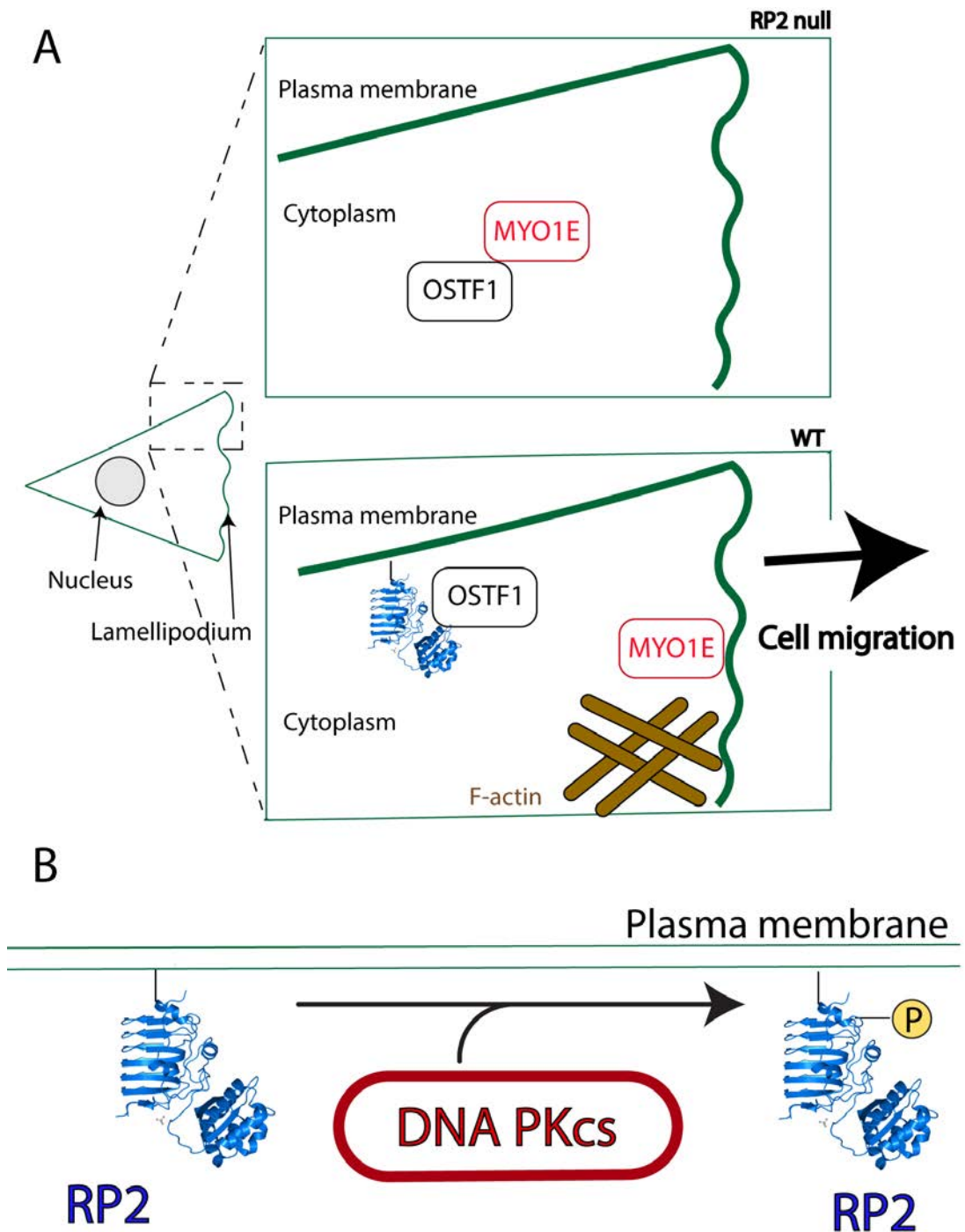


Figure 6.1. Schematic representation of suggested roles for the RP2-OSTF1 and RP2-DNA PKcs interactions.

A) RP2 might be a positive regulator of cell motility by downregulating the OSTF1-MYO1E interaction. According to (Tanimura et al. 2016), OSTF1 inhibits cell motility by acting as a cytoplasmic “anchor” for MYO1E with whom it directly interacts. I suggest that this is the case in the absence of RP2 (right, top panel). In the presence of RP2 (right, bottom panel), the RP2-OSTF1 interaction might lead to reduced OSTF1-MYO1E interaction (for example, via recruitment of OSTF1 to the

plasma membrane). This allows MYO1E to translocate to sites of actin nucleation, permitting lamellipodia formation and cell motility to occur. B) RP2 might interact with DNA PKcs at the plasma membrane, leading to phosphorylation of RP2 at S213 or T214. I suggest that this interaction is part of a “non-canonical” role of DNA PKcs in relaying DNA damage signalling to cellular locations outside the nucleus.

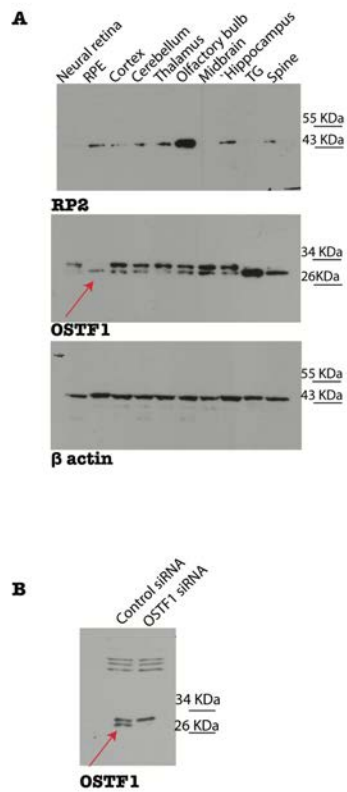




MGCFFSKRRKADKESRPENEEERPKQ<sup>30</sup>YSWDQREKVDPKDYMFSGLKDETVGRLPGTVAGQ<sup>60</sup>  
 QFLIQDCENCNIYIFDHSATVTIDDCTNCIIIFLGPVKGSVFFRNCRDCKCTLACQQFRVR<sup>120</sup>  
 DCRKLEVFLCCATQPIIESSSNIKFGCFQWYYPELAFQFKDAGLSIFNNTWSNIHDFTPV<sup>180</sup>  
 SGELNWSLLPEDAVVQDY<sup>210</sup>VPIPTTEELKAVRVSTEANRSIVPISRQQRQKSSDESCLVVL<sup>240</sup>  
 FAGDY<sup>270</sup>TIANARKLIDEMVGKGFLLVQTKEVSMKAEDAQRVFREKAPDFLPLLNKGPVIAL<sup>300</sup>  
 EFNGDGAVEVCQLIVNEIFNGTKMFVSESKETASGDVDSFY<sup>330</sup>NFADIQMG I

**Appendix figure 2. Peptide coverage of RP2 in MS/MS analysis used to identify sites of tyrosine phosphorylation.**

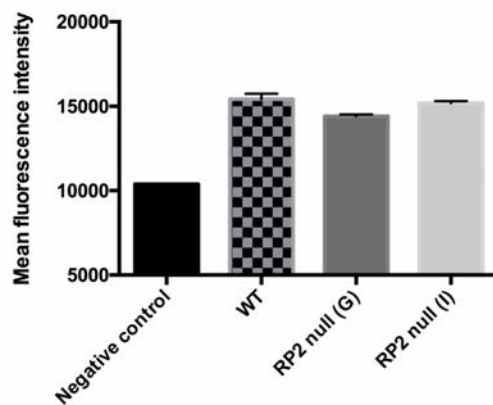
Sequence of human RP2 protein where the unique peptides detected during the MS/MS analysis (Figure 3.5) are highlighted in red. Blue boxes enclose tyrosine residues that are either predicted to be phosphorylated by computational tools or identified in large-scale proteomic studies (Figure 3.6).



Appendix figure 3. **Expression pattern of RP2 and OSTF1 in the mouse central nervous system by western blot.**

A) Mouse neural tissues were lysed in mild (Triton-containing) lysis buffer and subjected to SDS-PAGE and western blot using anti-RP2 and anti-OSTF1 antibodies (n=1 mouse tested). Anti-β actin blot was used to ensure equal loading. RPE: retinal pigment epithelium, TG: trigeminal ganglion. The neural retina was crudely separated from the RPE during dissection. Evidence of RP2 expression at protein level exist in the RPE, cortex, cerebellum, thalamus, hippocampus and spine while it is exceptionally high in the olfactory bulb. Note that there is no detectable RP2 signal in the neural retina, contrary to the RPE; RP2 expression in mouse photoreceptors has been shown before by electron microscopy and therefore it is assumed that it is too low to be detected by the present method (Evans et al. 2010). OSTF1 is present in all tissues tested except for the neural retina and it is highly expressed in the TG. It is therefore assumed that, regarding ocular tissues, RP2 and OSTF1 are co-expressed in the RPE, at least in mice. However, the trustworthiness of the anti-OSTF1 antibody is ambiguous as it detects two bands around the predicted molecular weight for OSTF1. It is assumed that the lower band (red arrow) is the correct one because it disappears after OSTF1 knockdown by siRNA in HEK293T cells (B)

Detection of endogenous oxidative stress in RPE1 cells using CellRox Green reagent



Appendix figure 4. *RP2* null cells do not have altered reactive oxygen species (ROS) balance compared to wild-type cells in culture.

The CellRox Green reagent (Molecular Probes) was used for oxidative stress detection in live hTERT-RPE1 cells, either wild-type or *RP2* null (G,I clones). This dye emits bright green fluorescence upon oxidation by ROS. Here, fluorescence intensity was measured by flow cytometry. “Negative control” corresponds to background fluorescence in cells that have not been incubated with the CellRox dye.

```

Homo      MGCFFSKRRKADKES-----RPENEEERPKQYSWDQREKV
Danio     MGCFFSKRSRRKSPKKDAALPTGDESATGNDLAETNNTALGSNSNQEAPKQYSWDKREKV
Del4      MGCFFSKRSRRKSPKKDAALPTGDESATGNDLAETNNTALGSNSNQEAPKQYSWDKREKV
Ins1      MGCFFSKRSRRKSPKKDAALPTGDESATGNDLAETNNTALGSNSNQEAPKQYSWDKREKV
Del8      MGCFFSKRSRRKSPKKDAALPTGDESATGNDLAETNNTALGSNSNQEAPKQYSWDKREKV
          *****: : . . .                               :.:* *****:****

Homo      DPKDFMFSGLKDETVGRLPGTVAGQQFLIQDCENCNIYIFDHSATVTIDDCTNCIIFLGP
Danio     DPKDFMLTGLKNETVGRLPGKLNQQFVIQDCENCNIFVLDHSATITIDDCVNCRIVLGP
Del4      DPKDFMLTGLKNEWAGYQASSTVSSLS----FRTA-----KTVTYLCWTIRQLLPS
Ins1      DPKDFMLTGLKNETGGQVTRQAQRSAV----CHSG-----LRKL*--
Del8      DPKDFMLTGLKN---GQVTRQAQRSAV----CHSG-----LRKL*--
          ****:*:****: * . . .                               .

Homo      VKGSVFFRNCRDCKCTLACQQFRVRDCRKLEVFLLCCATQPIIESSSNIKFGCFQWYYPEL [155]
Danio     VKGSVFFRDCKDIKCVVACQQFRTRDCKKMDVFLCCATQPIIESSGMKFGCFQYYYPEL
Del4      MTV*-----
Ins1      -----
Del8      -----

Homo      AFQFKDAGLSIFNNTWSNIHDFTPVSGELNWSLLPEDAVVQDYVPIPTTE-ELKAVRVST [214]
Danio     AFHFKDAGLSIFNNNWSNIHDFTPVSGETNWSLLPEDAVVLDHVLPDPPESEFKSVRIAT
Del4      -----
Ins1      -----
Del8      -----

Homo      EANRSIVPISRGRQKSSDESCLVVLFAGDYTTANARKLIDEMVGKGFLLVQTKEVSMKA
Danio     EAGRSIVPLTKGSRRTSEESCLFVFFAGDYTTANARKLIDEATAKGFVLIQTKEVSMRP
Del4      -----
Ins1      -----
Del8      -----

Homo      EDAQRVFREKAPDFLPLLKGPVIALEFNGDGAVEVCQLIVNEIFNGTKMFVSESKETAS
Danio     EDVSRVVFQNAESLTEWITKGPVVALELNGDGVVEACRSFANEVFNQTQLFVSESKNTSS
Del4      -----
Ins1      -----
Del8      -----

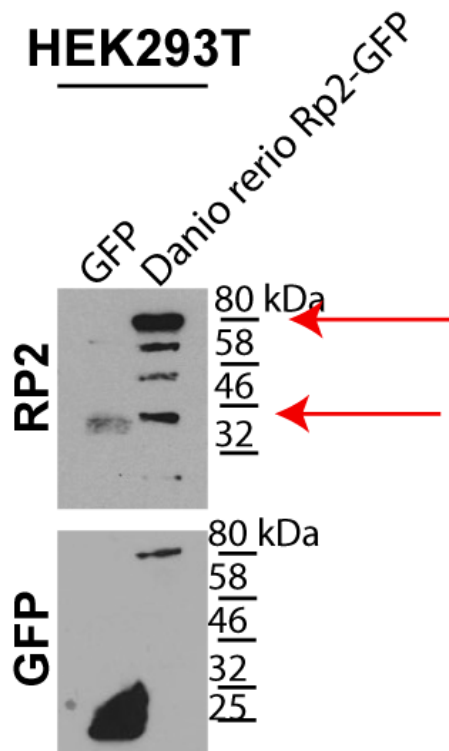
Homo      GDVDSFYNFADIQMG I
Danio     RDVDNFFNFADMQMGL
Del4      -----
Ins1      -----
Del8      -----

```

Appendix figure 5. **Multiple sequence alignment of human, zebrafish wild-type and zebrafish mutant RP2.**

Multiple sequence alignment of human RP2 (“Homo”), zebrafish wild-type Rp2 (“Danio”) and the predicted truncated peptides that would theoretically be expressed from the mutated *rp2* gene in the lines generated by CRISPR/Cas9 genome editing. Important residues R118, E138 and R211 (shown in red) on the human protein which are sites of missense pathogenic mutations and conserved on the zebrafish protein would be absent from these truncated peptides. R118H and E138G (in the catalytic core of the protein) abolish the GAP activity of RP2 and the RP2-ARL3 interaction, while R211L abolishes the RP2-OSTF1 interaction.





Appendix figure 7. **Western blotting detection of exogenously expressed zebrafish Rp2-GFP by the anti-RP2 antibody used in Chapter 6.**

To test if the anti-RP2 antibody used for western blotting on zebrafish eyeballs (Chapter 5: Figure 5.2C) can recognise zebrafish Rp2, zebrafish Rp2-GFP and GFP alone (as a negative control) were transiently expressed in HEK293T cells and the lysates were used for western blotting using anti-RP2 and anti-GFP antibodies. Red arrows point to endogenous RP2, recognised by the antibody in both cell lysates, and exogenous zebrafish Rp2-GFP, recognised by the antibody only in the Rp2-GFP – transfected lysates.

Appendix Table 1. **List of proteins identified by MS/MS in RP2-V5 IPs.**

Ratio represents fold enrichment in RP2-V5 IPs vs. negative control (IPs from empty-vector transfected cells). P- value represents significance and is estimated using unpaired two-tailed t-tests based on three biological replicates. Only proteins with  $p < 0.1$  are shown.

<b>PROTEIN NAMES</b>	<b>GENE NAMES</b>	<b>RATIO</b>	<b>P- VALUE</b>
<b>Protein XRP2</b>	<b>RP2</b>	<b>12.9961056</b>	<b>0.01091767</b>
Signal recognition particle receptor subunit beta	SRPRB	6.64169678	0.0172088
<b>Osteoclast-stimulating factor 1</b>	<b>OSTF1</b>	<b>6.31091699</b>	<b>0.00037541</b>
Exportin-7	XPO7	5.99848853	0.01862622
Membrane-associated progesterone receptor component 1	PGRMC1	5.95995821	0.00622987
Exportin-5	XPO5	5.94028863	0.02001779
Cullin-associated NEDD8-dissociated protein 1	CAND1	5.73851598	0.04820888
26S proteasome non-ATPase regulatory subunit 13	PSMD13	5.26688901	0.00501358
SRA stem-loop-interacting RNA-binding protein, mitochondrial	SLIRP	5.19970632	0.05151275
Sarcoplasmic/endoplasmic reticulum calcium ATPase 2	ATP2A2	5.14348908	0.06921151
Voltage-dependent anion-selective channel protein 2	VDAC2	5.13163859	0.01292253
Leucine-rich PPR motif-containing protein, mitochondrial	LRPPRC	5.02057991	0.02757329
MICOS complex subunit MIC19	CHCHD3	4.82963271	0.04965206



Trafficking protein particle complex subunit 3	TRAPPC3	4.75336925	0.0017578
Serine/threonine-protein kinase mTOR	MTOR	4.71363582	0.01205821
Stomatin-like protein 2, mitochondrial	STOML2	4.67384297	0.05995246
Sodium/potassium-transporting ATPase subunit alpha-1	ATP1A1	4.64828	0.01031532
Membrane-associated progesterone receptor component 2	PGRMC2	4.64552553	0.0053892
Transportin-1	TNPO1	4.38670885	0.0176949
Importin-4	IPO4	4.24765752	0.06078979
26S protease regulatory subunit 4	PSMC1	4.18162594	0.0495033
Protein unc-45 homolog A	UNC45A	4.1082625	0.08899154
Importin subunit beta-1	KPNB1	4.0303007	0.02633798
V-type proton ATPase subunit H	ATP6V1H	4.01426437	0.06693755
Uncharacterized protein C19orf43	C19orf43	3.91551744	0.00311376
Coatomer subunit alpha;Xenin;Proxenin	COPA	3.91363061	0.04869633
Proteasome-associated protein ECM29 homolog	ECM29	3.85356057	0.09807692
Exocyst complex component 7	EXOC7	3.84508421	0.06550598
Wolframin	WFS1	3.78188627	0.00254774
Probable ubiquitin carboxyl-terminal hydrolase FAF-X;Probable ubiquitin carboxyl-terminal hydrolase FAF-Y	USP9X;USP9Y	3.77167126	0.0957394

Lamin-B receptor	LBR	3.65550145	0.0958337
Translational activator GCN1	GCN1L1	3.5656167	0.06320478
Nuclear autoantigenic sperm protein	NASP	3.55868492	0.09971216
Gem-associated protein 2	GEMIN2	3.51443752	0.08090646
RNA-binding protein 26	RBM26	3.47584639	0.00361256
Protein transport protein Sec61 subunit beta	SEC61B	3.19949487	0.06655518
T-complex protein 1 subunit delta	CCT4	3.00994036	0.05778609
Transmembrane protein 194A	TMEM194A	3.00897411	0.01802931
<b>DNA-dependent protein kinase catalytic subunit</b>	<b>PRKDC</b>	<b>3.00214485</b>	<b>0.07931247</b>
Dolichol-phosphate mannosyltransferase subunit 3	DPM3	2.96870761	0.06986405
MICOS complex subunit MIC60	IMMT	2.96309514	0.03614755
D-3-phosphoglycerate dehydrogenase	PHGDH	2.75431643	0.05261122
FAST kinase domain- containing protein 5	FASTKD5	2.72236827	0.08381522
Proteasomal ubiquitin receptor ADRM1	ADRM1	2.66563899	0.008217
T-complex protein 1 subunit eta	CCT7	2.53475966	0.04880528
Nascent polypeptide- associated complex subunit alpha, muscle-specific form	NACA	2.44676709	0.08967704
Far upstream element- binding protein 2	KHSRP	1.99539916	0.09425262
60 kDa heat shock protein,	HSPD1	1.73579564	0.05853484

mitochondrial			
Serine/threonine-protein phosphatase 4 regulatory subunit 3A;Serine/threonine-protein phosphatase 4 regulatory subunit 3B	SMEK1;SMEK2	1.68458981	0.04695093
G2/mitotic-specific cyclin-B1	CCNB1	1.5924915	0.0961335
14-3-3 protein theta	YWHAQ	1.26822145	0.02338302
Ubiquitin-associated domain-containing protein 2	UBAC2	0.85978568	0.03735788

## References

- Adijanto, J., T. Banzon, S. Jalickee, N. S. Wang & S. S. Miller (2009) CO<sub>2</sub>-induced ion and fluid transport in human retinal pigment epithelium. *J Gen Physiol*, 133, 603-22.
- Aicart-Ramos, C., R. A. Valero & I. Rodriguez-Crespo (2011) Protein palmitoylation and subcellular trafficking. *Biochim Biophys Acta*, 1808, 2981-94.
- Airik, R., G. G. Slaats, Z. Guo, A. C. Weiss, N. Khan, A. Ghosh, T. W. Hurd, S. Bekker-Jensen, J. M. Schroder, S. J. Elledge, J. S. Andersen, A. Kispert, M. Castelli, A. Boletta, R. H. Giles & F. Hildebrandt (2014) Renal-Retinal Ciliopathy Gene Sdccag8 Regulates DNA Damage Response Signaling. *Journal of the American Society of Nephrology*, 25, 2573-2583.
- Allison, W. T., L. K. Barthel, K. M. Skebo, M. Takechi, S. Kawamura & P. A. Raymond (2010) Ontogeny of cone photoreceptor mosaics in zebrafish. *J Comp Neurol*, 518, 4182-95.
- An, J., T. Yang, Y. Huang, F. Liu, J. Sun, Y. Wang, Q. Xu, D. Wu & P. Zhou. 2011. Strand-specific PCR of UV radiation-damaged genomic DNA revealed an essential role of DNA-PKcs in the transcription-coupled repair. In *BMC Biochem*, 2.
- Arshavsky, V. Y. & T. G. Wensel (2013) Timing Is Everything: GTPase Regulation in Phototransduction. *Invest Ophthalmol Vis Sci*, 54, 7725-33.
- Ashkenazy, H., S. Abadi, E. Martz, O. Chay, I. Mayrose, T. Pupko & N. Ben-Tal (2016) ConSurf 2016: an improved methodology to estimate and visualize evolutionary conservation in macromolecules. *Nucleic Acids Res*, 44, W344-50.
- Audo, I., K. Bujakowska, S. Mohand-Saïd, M. E. Lancelot, V. Moskova-Doumanova, N. H. Waseem, A. Antonio, J. A. Sahel, S. S. Bhattacharya & C. Zeitz. 2010. Prevalence and novelty of PRPF31 mutations in French autosomal dominant rod-cone dystrophy patients and a review of published reports. In *BMC Med Genet*, 145.
- Auer, T. O., K. Duroure, A. De Cian, J. P. Concordet & F. Del Bene (2014) Highly efficient CRISPR/Cas9-mediated knock-in in zebrafish by homology-independent DNA repair. *Genome Res*, 24, 142-53.
- Bakondi, B., W. Lv, B. Lu, M. K. Jones, Y. Tsai, K. J. Kim, R. Levy, A. A. Akhtar, J. J. Breunig, C. N. Svendsen & S. Wang (2016) In Vivo CRISPR/Cas9 Gene Editing Corrects Retinal Dystrophy in the S334ter-3 Rat Model of Autosomal Dominant Retinitis Pigmentosa. *Mol Ther*, 24, 556-63.
- Baleriola, J., T. Suarez & E. J. de la Rosa (2010) DNA-PK promotes the survival of young neurons in the embryonic mouse retina. *Cell Death Differ*, 17, 1697-706.
- Barsoum, I. B. & C. King-Smith (2007) Myosin II and Rho kinase activity are required for melanosome aggregation in fish retinal pigment epithelial cells. *Cell Motil Cytoskeleton*, 64, 868-79.

- Bartolini, F., A. Bhamidipati, S. Thomas, U. Schwahn, S. A. Lewis & N. J. Cowan (2002) Functional overlap between retinitis pigmentosa 2 protein and the tubulin-specific chaperone cofactor C. *J Biol Chem*, 277, 14629-34.
- Basinger, S., D. Bok & M. Hall (1976) Rhodopsin in the rod outer segment plasma membrane.
- Bazan, N. G. (2006) Cell survival matters: docosahexaenoic acid signaling, neuroprotection and photoreceptors. *Trends Neurosci*, 29, 263-71.
- Ben-Arie-Weintrob, Y., E. L. Berson & T. P. Dryja (2005) Histopathologic-genotypic correlations in retinitis pigmentosa and allied diseases. *Ophthalmic Genet*, 26, 91-100.
- Bershteyn, M., S. X. Atwood, W. M. Woo, M. Li & A. E. Oro (2010) MIM and cortactin antagonism regulates ciliogenesis and hedgehog signaling. *Dev Cell*, 19, 270-83.
- Berta, A. I., K. Boesze-Battaglia, A. Magyar, A. Szel & A. L. Kiss (2011) Localization of caveolin-1 and c-src in mature and differentiating photoreceptors: raft proteins co-distribute with rhodopsin during development. *J Mol Histol*, 42, 523-33.
- Bhargava, R., D. O. Onyango & J. M. Stark (2016) Regulation of Single-Strand Annealing and its Role in Genome Maintenance. *Trends Genet*, 32, 566-75.
- Bilotta, J., S. Saszik & S. E. Sutherland (2001) Rod contributions to the electroretinogram of the dark-adapted developing zebrafish. *Dev Dyn*, 222, 564-70.
- Bladen, C. L., W. K. Lam, W. S. Dynan & D. J. Kozlowski (2005) DNA damage response and Ku80 function in the vertebrate embryo. *Nucleic Acids Res*, 33, 3002-10.
- Bladen, C. L., S. Navarre, W. S. Dynan & D. J. Kozlowski (2007) Expression of the Ku70 subunit (XRCC6) and protection from low dose ionizing radiation during zebrafish embryogenesis. *Neurosci Lett*, 422, 97-102.
- Blanchet, P., M. L. Wellemeyer & G. V. Burton (1992) Case report: retinitis pigmentosa following cytotoxic chemotherapy in Usher's syndrome. *Am J Med Sci*, 303, 319-20.
- Bonilha, V. L. (2014) Retinal pigment epithelium (RPE) cytoskeleton in vivo and in vitro. *Experimental Eye Research*, 126, 38-45.
- Borges, H. L., R. Linden & J. Y. Wang (2007) DNA damage-induced cell death: lessons from the central nervous system. *Cell Research*, 18, 17-26.
- Bottero, V., V. Busuttil, A. Loubat, N. Magne, J. L. Fischel, G. Milano & J. F. Peyron (2001) Activation of nuclear factor kappaB through the IKK complex by the topoisomerase poisons SN38 and doxorubicin: a brake to apoptosis in HeLa human carcinoma cells. *Cancer Res*, 61, 7785-91.
- Boubakri, M., T. Chaya, H. Hirata, N. Kajimura, R. Kuwahara, A. Ueno, J. Malicki, T. Furukawa & Y. Omori (2016) Loss of ift122, a Retrograde Intraflagellar Transport (IFT) Complex Component, Leads to Slow, Progressive Photoreceptor Degeneration Due to Inefficient Opsin Transport. *J Biol Chem*, 291, 24465-24474.

- Boudry-Labis, E., B. Demeer, C. Le Caignec, B. Isidor, M. Mathieu-Dramard, G. Plessis, A. M. George, J. Taylor, S. Aftimos, A. Wiemer-Kruel, J. Kohlhase, G. Anneren, H. Firth, I. Simonic, J. Vermeesch, A. C. Thuresson, H. Copin, D. R. Love & J. Andrieux (2013) A novel microdeletion syndrome at 9q21.13 characterised by mental retardation, speech delay, epilepsy and characteristic facial features. *Eur J Med Genet*, 56, 163-70.
- Boya, P. & E. J. de la Rosa (2005) Cell death in early neural life. *Birth Defects Res C Embryo Today*, 75, 281-93.
- Bramall, A. N., A. F. Wright, S. G. Jacobson & R. R. McInnes (2010) The genomic, biochemical, and cellular responses of the retina in inherited photoreceptor degenerations and prospects for the treatment of these disorders. *Annu Rev Neurosci*, 33, 441-72.
- Branham, K., M. Othman, M. Brumm, A. J. Karoukis, P. Atmaca-Sonmez, B. M. Yashar, S. B. Schwartz, N. B. Stover, K. Trzupsek, D. Wheaton, B. Jennings, M. L. Ciccarelli, K. T. Jayasundera, R. A. Lewis, D. Birch, J. Bennett, P. A. Sieving, S. Andreasson, J. L. Duncan, G. A. Fishman, A. Iannaccone, R. G. Weleber, S. G. Jacobson, J. R. Heckenlively & A. Swaroop (2012) Mutations in RPGR and RP2 account for 15% of males with simplex retinal degenerative disease. *Invest Ophthalmol Vis Sci*, 53, 8232-7.
- Bravo-Gil, N., M. G.-d. Pozo, M. Martín-Sánchez, C. Méndez-Vidal, E. R.-d. I. Rúa, S. Borrego & G. Antiñolo (2017) Unravelling the genetic basis of simplex Retinitis Pigmentosa cases. *Scientific Reports, Published online: 3 February 2017; | doi:10.1038/srep41937*.
- Breuer, D. K., B. M. Yashar, E. Filippova, S. Hiriyan, R. H. Lyons, A. J. Mears, B. Asaye, C. Acar, R. Vervoort, A. F. Wright, M. A. Musarella, P. Wheeler, I. MacDonald, A. Iannaccone, D. Birch, D. R. Hoffman, G. A. Fishman, J. R. Heckenlively, S. G. Jacobson, P. A. Sieving & A. Swaroop. 2002. A Comprehensive Mutation Analysis of RP2 and RPGR in a North American Cohort of Families with X-Linked Retinitis Pigmentosa. In *Am J Hum Genet*, 1545-54.
- Brockerhoff, S. E. & J. M. Fadool (2011) Genetics of photoreceptor degeneration and regeneration in zebrafish. *Cell Mol Life Sci*, 68, 651-9.
- Brooks, B. P., A. H. Thompson, R. J. Bishop, J. A. Clayton, C. C. Chan, E. T. Tsilou, W. M. Zein, D. Tamura, S. G. Khan, T. Ueda, J. Boyle, K. S. Oh, K. Imoto, H. Inui, S. I. Moriwaki, S. Emmert, N. T. Iliff, P. Bradford, J. J. DiGiovanna & K. H. Kraemer (2013) Ocular manifestations of xeroderma pigmentosum: long term follow-up highlights the role of DNA repair in protection from sun damage. *Ophthalmology*, 120, 1324-36.
- Cantagrel, V., J. L. Silhavy, S. L. Bielas, D. Swistun, S. E. Marsh, J. Y. Bertrand, S. Audollent, T. Attie-Bitach, K. R. Holden, W. B. Dobyns, D. Traver, L. Al-Gazali, B. R. Ali, T. H. Lindner, T. Caspary, E. A. Otto, F. Hildebrandt, I. A. Glass, C. V. Logan, C. A. Johnson, C. Bennett, F. Brancati, E. M. Valente, C. G. Woods & J. G. Gleeson (2008) Mutations in the cilia gene ARL13B lead to the classical form of Joubert syndrome. *Am J Hum Genet*, 83, 170-9.

- Chakarova, C., M. Papaioannou, H. Khanna, I. Lopez, N. Waseem, A. Shah, T. Theis, J. Friedman, C. Maubaret, K. Bujakowska, B. Veraitch, M. El-Aziz, D. Prescott, S. Parapuram, W. Bickmore, P. Munro, A. Gal, C. Hamel, V. Marigo, C. Ponting, B. Wissinger, E. Zrenner, K. Matter, A. Swaroop, R. Koenekoop & S. Bhattacharya. 2007. Mutations in TOPORS Cause Autosomal Dominant Retinitis Pigmentosa with Perivascular Retinal Pigment Epithelium Atrophy. In *Am J Hum Genet*, 1098-103.
- Chakarova, C. F., H. Khanna, A. Z. Shah, S. B. Patil, T. Sedmak, C. A. Murga-Zamalloa, M. G. Papaioannou, K. Nagel-Wolfrum, I. Lopez, P. Munro, M. Cheetham, R. K. Koenekoop, R. M. Rios, K. Matter, U. Wolfrum, A. Swaroop & S. S. Bhattacharya (2011) TOPORS, implicated in retinal degeneration, is a cilia-centrosomal protein. *Hum Mol Genet*, 20, 975-87.
- Chaki, M., R. Airik, A. K. Ghosh, R. H. Giles, R. Chen, G. G. Slaats, H. Wang, T. W. Hurd, W. Zhou, A. Cluckey, H. Y. Gee, G. Ramaswami, C. J. Hong, B. A. Hamilton, I. Cervenka, R. S. Ganji, V. Bryja, H. H. Arts, J. van Reeuwijk, M. M. Oud, S. J. Letteboer, R. Roepman, H. Husson, O. Ibraghimov-Beskrovnya, T. Yasunaga, G. Walz, L. Eley, J. A. Sayer, B. Schermer, M. C. Liebau, T. Benzing, S. Le Corre, I. Drummond, S. Janssen, S. J. Allen, S. Natarajan, J. F. O'Toole, M. Attanasio, S. Saunier, C. Antignac, R. K. Koenekoop, H. Ren, I. Lopez, A. Nayir, C. Stoetzel, H. Dollfus, R. Massoudi, J. G. Gleeson, S. P. Andreoli, D. G. Doherty, A. Lindstrad, C. Golzio, N. Katsanis, L. Pape, E. B. Abboud, A. A. Al-Rajhi, R. A. Lewis, H. Omran, E. Y. Lee, S. Wang, J. M. Sekiguchi, R. Saunders, C. A. Johnson, E. Garner, K. Vanselow, J. S. Andersen, J. Shlomag, G. Nurnberg, P. Nurnberg, S. Levy, A. Smogorzewska, E. A. Otto & F. Hildebrandt (2012) Exome capture reveals ZNF423 and CEP164 mutations, linking renal ciliopathies to DNA damage response signaling. *Cell*, 150, 533-48.
- Chapple, J. P., A. J. Hardcastle, C. Grayson, L. A. Spackman, K. R. Willison & M. E. Cheetham (2000) Mutations in the N-terminus of the X-linked retinitis pigmentosa protein RP2 interfere with the normal targeting of the protein to the plasma membrane. *Hum Mol Genet*, 9, 1919-26.
- Chapple, J. P., A. J. Hardcastle, C. Grayson, K. R. Willison & M. E. Cheetham (2002) Delineation of the plasma membrane targeting domain of the X-linked retinitis pigmentosa protein RP2. *Invest Ophthalmol Vis Sci*, 43, 2015-20.
- Chen, B. P. C., N. Uematsu, J. Kobayashi, Y. Lerenthal, A. Krempler, H. Yajima, M. Löbrich, Y. Shiloh & D. J. Chen (2007) Ataxia Telangiectasia Mutated (ATM) Is Essential for DNA-PKcs Phosphorylations at the Thr-2609 Cluster upon DNA Double Strand Break.
- Chiang, A. P., D. Nishimura, C. Searby, K. Elbedour, R. Carmi, A. L. Ferguson, J. Secrist, T. Braun, T. Casavant, E. M. Stone & V. C. Sheffield (2004) Comparative genomic analysis identifies an ADP-ribosylation factor-like gene as the cause of Bardet-Biedl syndrome (BBS3). *Am J Hum Genet*, 75, 475-84.
- Chowdhury, D., M. C. Keogh, H. Ishii, C. L. Peterson, S. Buratowski & J. Lieberman (2005) gamma-H2AX dephosphorylation by protein phosphatase 2A facilitates DNA double-strand break repair. *Mol Cell*, 20, 801-9.

- Chrenek, M. A., J. M. Nickerson & J. H. Boatright (2016) CRISPR challenges in treating retinal disease. *Asia Pac J Ophthalmol (Phila)*, 5, 304-8.
- Cideciyan, A. V. (2010) Leber congenital amaurosis due to RPE65 mutations and its treatment with gene therapy. *Prog Retin Eye Res*, 29, 398-427.
- Cideciyan, A. V., S. G. Jacobson, W. A. Beltran, A. Sumaroka, M. Swider, S. Iwabe, A. J. Roman, M. B. Olivares, S. B. Schwartz, A. M. Komaromy, W. W. Hauswirth & G. D. Aguirre (2013) Human retinal gene therapy for Leber congenital amaurosis shows advancing retinal degeneration despite enduring visual improvement. *Proc Natl Acad Sci U S A*, 110, E517-25.
- Cortina, M. S., W. C. Gordon, W. J. Lukiw & N. G. Bazan (2003) DNA repair in photoreceptor survival. *Mol Neurobiol*, 28, 111-22.
- Cox, J. & M. Mann (2008) MaxQuant enables high peptide identification rates, individualized p.p.b.-range mass accuracies and proteome-wide protein quantification. *Nat Biotechnol*, 26, 1367-72.
- Cuvillier, A., F. Redon, J. C. Antoine, P. Chardin, T. DeVos & G. Merlin (2000) LdARL-3A, a Leishmania promastigote-specific ADP-ribosylation factor-like protein, is essential for flagellum integrity. *J Cell Sci*, 113 ( Pt 11), 2065-74.
- Dandekar, S. S., N. D. Ebenezer, C. Grayson, J. P. Chapple, C. A. Egan, G. E. Holder, S. A. Jenkins, F. W. Fitzke, M. E. Cheetham, A. R. Webster & A. J. Hardcastle (2004) An atypical phenotype of macular and peripapillary retinal atrophy caused by a mutation in the RP2 gene. *Br J Ophthalmol*, 88, 528-32.
- Davis, A. J. & D. J. Chen (2013) DNA double strand break repair via non-homologous end-joining. *Transl Cancer Res*, 2, 130-43.
- den Hollander, A. I., R. Roepman, R. K. Koenekoop & F. P. Cremers (2008) Leber congenital amaurosis: genes, proteins and disease mechanisms. *Prog Retin Eye Res*, 27, 391-419.
- Deretic, D., L. A. Huber, N. Ransom, M. Mancini, K. Simons & D. S. Papermaster (1995) rab8 in retinal photoreceptors may participate in rhodopsin transport and in rod outer segment disk morphogenesis. *J Cell Sci*, 108 ( Pt 1), 215-24.
- Deretic, D. & J. Wang (2012) Molecular assemblies that control rhodopsin transport to the cilia. *Vision Res*, 75, 5-10.
- Desvignes, T., T. Nguyen, F. Chesnel, A. Bouleau, C. Fauvel & J. Bobe (2015) X-Linked Retinitis Pigmentosa 2 Is a Novel Maternal-Effect Gene Required for Left-Right Asymmetry in Zebrafish. *Biol Reprod*, 93, 42.
- Dittmann, K., C. Mayer, R. Kehlbach & H. P. Rodemann. 2008. Radiation-induced caveolin-1 associated EGFR internalization is linked with nuclear EGFR transport and activation of DNA-PK. In *Mol Cancer*, 69.
- Donaldson, J. G. & C. L. Jackson (2011) ARF family G proteins and their regulators: roles in membrane transport, development and disease. *Nat Rev Mol Cell Biol*, 12, 362-75.
- Douglas, P., G. P. Sapkota, N. Morrice, Y. Yu, A. A. Goodarzi, D. Merkle, K. Meek, D. R. Alessi & S. P. Lees-Miller (2002) Identification of in vitro and in vivo phosphorylation sites in the catalytic subunit of the DNA-dependent protein kinase. *Biochem J*, 368, 243-51.



- Douglas, P., R. Ye, L. Trinkle-Mulcahy, J. A. Neal, V. De Wever, N. A. Morrice, K. Meek & S. P. Lees-Miller (2014) Polo-like kinase 1 (PLK1) and protein phosphatase 6 (PP6) regulate DNA-dependent protein kinase catalytic subunit (DNA-PKcs) phosphorylation in mitosis. *Biosci Rep*, 34.
- Dun, Y., J. Vargas, N. Brot & S. C. Finnemann (2013) Independent roles of methionine sulfoxide reductase A in mitochondrial ATP synthesis and as antioxidant in retinal pigment epithelial cells. *Free Radic Biol Med*, 65, 1340-51.
- Edgar, R. C. (2004) MUSCLE: a multiple sequence alignment method with reduced time and space complexity. *BMC Bioinformatics*, 5, 113.
- Evans, R. J., N. Schwarz, K. Nagel-Wolfrum, U. Wolfrum, A. J. Hardcastle & M. E. Cheetham (2010) The retinitis pigmentosa protein RP2 links pericentriolar vesicle transport between the Golgi and the primary cilium. *Hum Mol Genet*, 19, 1358-67.
- Faghiri, Z. & N. G. Bazan (2010) PI3K/Akt and mTOR/p70S6K pathways mediate neuroprotectin D1-induced retinal pigment epithelial cell survival during oxidative stress-induced apoptosis. *Exp Eye Res*, 90, 718-25.
- Farber-Katz, S. E., H. C. Dippold, M. D. Buschman, M. C. Peterman, M. Xing, C. J. Noakes, J. Tat, M. M. Ng, J. Rahajeng, D. M. Cowan, G. J. Fuchs, H. Zhou & S. J. Field (2014) DNA damage triggers Golgi dispersal via DNA-PK and GOLPH3. *Cell*, 156, 413-27.
- Ferrari, S., E. Di Iorio, V. Barbaro, D. Ponzin, F. S. Sorrentino & F. Parmeggiani. 2011. Retinitis Pigmentosa: Genes and Disease Mechanisms. In *Curr Genomics*, 238-49.
- Fraser, C., J. C. Dawson, R. Dowling, D. R. Houston, J. T. Weiss, A. F. Munro, M. Muir, L. Harrington, S. P. Webster, M. C. Frame, V. G. Brunton, E. E. Patton, N. O. Carragher & A. Unciti-Broceta (2016) Rapid Discovery and Structure-Activity Relationships of Pyrazolopyrimidines That Potently Suppress Breast Cancer Cell Growth via SRC Kinase Inhibition with Exceptional Selectivity over ABL Kinase. *J Med Chem*, 59, 4697-710.
- Galluzzi, L., S. Aaronson, J. Abrams, E. Alnemri, D. Andrews, E. Baehrecke, N. Bazan, M. Blagosklonny, K. Blomgren, C. Borner, D. Bredesen, C. Brenner, M. Castedo, J. Cidlowski, A. Ciechanover, G. Cohen, V. De Laurenzi, R. De Maria, M. Deshmukh, B. Dynlacht, W. El-Deiry, R. Flavell, S. Fulda, C. Garrido, P. Golstein, M. L. Gougeon, D. Green, H. Gronemeyer, G. Hajnóczky, J. Hardwick, M. Hengartner, H. Ichijo, M. Jäättelä, O. Kepp, A. Kimchi, D. Klionsky, R. Knight, S. Kornbluth, S. Kumar, B. Levine, S. Lipton, E. Lugli, F. Madeo, W. Malorni, J. C. Marine, S. Martin, J. Medema, P. Mehlen, G. Melino, U. Moll, E. Morselli, S. Nagata, D. Nicholson, P. Nicotera, G. Nuñez, M. Oren, J. Penninger, S. Pervaiz, M. Peter, M. Piacentini, J. Prehn, H. Puthalakath, G. Rabinovich, R. Rizzuto, C. Rodrigues, D. Rubinsztein, T. Rudel, L. Scorrano, H. U. Simon, H. Steller, J. Tschopp, Y. Tsujimoto, P. Vandenabeele, I. Vitale, K. Vousden, R. Youle, J. Yuan, B. Zhivotovsky & G. Kroemer (2009) Guidelines for the use and interpretation of assays for monitoring cell death in higher eukaryotes. *Cell Death Differ*, 16, 1093-107.

- Ghalayini, A. J., N. Desai, K. R. Smith, R. M. Holbrook, M. H. Elliott & H. Kawakatsu (2002) Light-dependent association of Src with photoreceptor rod outer segment membrane proteins in vivo. *J Biol Chem*, 277, 1469-76.
- Ghosh, D., D. Lippert, O. Krokhin, J. P. Cortens & J. A. Wilkins (2010) Defining the membrane proteome of NK cells. *J Mass Spectrom*, 45, 1-25.
- Goldsmith, P., H. Baier & W. A. Harris (2003) Two zebrafish mutants, ebony and ivory, uncover benefits of neighborhood on photoreceptor survival. *J Neurobiol*, 57, 235-45.
- Goldsmith, P. & W. A. Harris (2003) The zebrafish as a tool for understanding the biology of visual disorders. *Semin Cell Dev Biol*, 14, 11-8.
- Goodwin, J. F. & K. E. Knudsen (2014) Beyond DNA repair: DNA-PK function in cancer. *Cancer Discov*, 4, 1126-39.
- Gordon, W. C., D. M. Casey, W. J. Lukiw & N. G. Bazan (2002) DNA damage and repair in light-induced photoreceptor degeneration. *Invest Ophthalmol Vis Sci*, 43, 3511-21.
- Gordon, W. C., D. o. O. a. N. C. From the Louisiana State University Health Sciences Center, New Orleans, Louisiana., D. M. Casey, D. o. O. a. N. C. From the Louisiana State University Health Sciences Center, New Orleans, Louisiana., W. J. Lukiw, D. o. O. a. N. C. From the Louisiana State University Health Sciences Center, New Orleans, Louisiana., N. G. Bazan & D. o. O. a. N. C. From the Louisiana State University Health Sciences Center, New Orleans, Louisiana. (2016) DNA Damage and Repair in Light-Induced Photoreceptor Degeneration. *Investigative Ophthalmology & Visual Science*, 43, 3511-3521.
- Gorgels, T. G. M. F., I. v. d. Pluijm, R. M. C. Brandt, G. A. Garinis, H. v. Steeg, G. v. d. Aardweg, G. H. Jansen, J. M. Ruijter, A. A. B. Bergen, D. v. Norren, J. H. J. Hoeijmakers & G. T. J. v. d. Horst (2007) Retinal Degeneration and Ionizing Radiation Hypersensitivity in a Mouse Model for Cockayne Syndrome.
- Gotthardt, K., M. Lokaj, C. Koerner, N. Falk, A. Giessler & A. Wittinghofer (2015) A G-protein activation cascade from Arl13B to Arl3 and implications for ciliary targeting of lipidated proteins. *Elife*, 4.
- Grayson, C., F. Bartolini, J. P. Chapple, K. R. Willison, A. Bhamidipati, S. A. Lewis, P. J. Luthert, A. J. Hardcastle, N. J. Cowan & M. E. Cheetham (2002) Localization in the human retina of the X-linked retinitis pigmentosa protein RP2, its homologue cofactor C and the RP2 interacting protein Arl3. *Hum Mol Genet*, 11, 3065-74.
- Gregory-Evans, C. Y. (2012) Zebrafish: a model system for the investigation of novel treatments for retinal disease. *Adv Exp Med Biol*, 723, 399-405.
- Gu, X., N. J. Neric, J. S. Crabb, J. W. Crabb, S. K. Bhattacharya, M. E. Rayborn, J. G. Hollyfield & V. L. Bonilha (2012) Age-related changes in the retinal pigment epithelium (RPE). *PLoS One*, 7, e38673.
- Han, S., Q. Liu, F. Wang & Z. Yuan (2016) Targeting the SH3 domain of human osteoclast-stimulating factor with rationally designed peptoid inhibitors. *J Pept Sci*, 22, 533-9.

- Hanke-Gogokhia, C., Z. Wu, C. D. Gerstner, J. M. Frederick, H. Zhang & W. Baehr (2016) Arf-like Protein 3 (ARL3) Regulates Protein Trafficking and Ciliogenesis in Mouse Photoreceptors. *J Biol Chem*, 291, 7142-55.
- Hartong, D. T., E. L. Berson & T. P. Dryja (2006) Retinitis pigmentosa. *Lancet*, 368, 1795-809.
- Hendrickson, A. 2005. Organization of the Adult Primate Fovea. In *Macular Degeneration*, ed. P. L. Penfold, Provis J.M., 1-23. Springer Berlin Heidelberg.
- Hill, J. T., B. L. Demarest, B. W. Bisgrove, Y. C. Su, M. Smith & H. J. Yost (2014) Poly peak parser: Method and software for identification of unknown indels using sanger sequencing of polymerase chain reaction products. *Dev Dyn*, 243, 1632-6.
- Hoffman, D. R., D. K. Hughbanks-Wheaton, R. Spencer, G. E. Fish, N. S. Pearson, Y. Z. Wang, M. Klein, A. Takacs, K. G. Locke & D. G. Birch (2015) Docosahexaenoic Acid Slows Visual Field Progression in X-Linked Retinitis Pigmentosa: Ancillary Outcomes of the DHAX Trial. *Invest Ophthalmol Vis Sci*, 56, 6646-53.
- Holden, P. & W. A. Horton (2009) Crude subcellular fractionation of cultured mammalian cell lines. *BMC Res Notes*, 2, 243.
- Hollyfield, J. G., V. L. Bonilha, M. E. Rayborn, X. Yang, K. G. Shadrach, L. Lu, R. L. Ufret, R. G. Salomon & V. L. Perez (2008) Oxidative damage-induced inflammation initiates age-related macular degeneration. *Nat Med*, 14, 194-8.
- Honig, B. & A. Nicholls (1995) Classical electrostatics in biology and chemistry. *Science*, 268, 1144-9.
- Hoon, M., H. Okawa, L. D. Santina & R. O. Wong (2014) Functional Architecture of the Retina: Development and Disease. *Prog Retin Eye Res*, 42, 44-84.
- Humphrey, S. J., G. Yang, P. Yang, D. J. Fazakerley, J. Stockli, J. Y. Yang & D. E. James (2013) Dynamic adipocyte phosphoproteome reveals that Akt directly regulates mTORC2. *Cell Metab*, 17, 1009-20.
- Hurd, T., W. Zhou, P. Jenkins, C. J. Liu, A. Swaroop, H. Khanna, J. Martens, F. Hildebrandt & B. Margolis (2010) The retinitis pigmentosa protein RP2 interacts with polycystin 2 and regulates cilia-mediated vertebrate development. *Hum Mol Genet*, 19, 4330-44.
- Hurd, T. W., S. Fan & B. L. Margolis (2011) Localization of retinitis pigmentosa 2 to cilia is regulated by Importin beta2. *J Cell Sci*, 124, 718-26.
- Huston, E., M. J. Lynch, A. Mohamed, D. M. Collins, E. V. Hill, R. MacLeod, E. Krause, G. S. Baillie & M. D. Houslay (2008) EPAC and PKA allow cAMP dual control over DNA-PK nuclear translocation. *Proc Natl Acad Sci U S A*, 105, 12791-6.
- Huttlin, E. L., L. Ting, R. J. Bruckner, F. Gebreab, M. P. Gygi, J. Szpyt, S. Tam, G. Zarraga, G. Colby, K. Baltier, R. Dong, V. Guarani, L. P. Vaites, A. Ordureau, R. Rad, B. K. Erickson, M. Wuhr, J. Chick, B. Zhai, D. Kolippakkam, J. Mintseris, R. A. Obar, T. Harris, S. Artavanis-Tsakonas, M. E. Sowa, P. De Camilli, J. A. Paulo, J. W. Harper & S. P. Gygi (2015) The BioPlex Network: A Systematic Exploration of the Human Interactome. *Cell*, 162, 425-40.

- Hwang, W. Y., Y. Fu, D. Reyon, M. L. Maeder, S. Q. Tsai, J. D. Sander, R. T. Peterson, J. R. Yeh & J. K. Joung (2013) Efficient genome editing in zebrafish using a CRISPR-Cas system. *Nat Biotechnol*, 31, 227-9.
- Ihmaid, S., H. E. A. Ahmed, A. Al-Sheikh Ali, Y. E. Sherif, H. M. Tarazi, S. M. Riyadh, M. F. Zayed, H. S. Abulkhair & H. S. Rateb (2017) Rational design, synthesis, pharmacophore modeling, and docking studies for identification of novel potent DNA-PK inhibitors. *Bioorg Chem*, 72, 234-247.
- Ismail, S. A., Y. X. Chen, M. Miertzschke, I. R. Vetter, C. Koerner & A. Wittinghofer (2012) Structural basis for Arl3-specific release of myristoylated ciliary cargo from UNC119. *Embo j*, 31, 4085-94.
- Ismail, S. A., Y. X. Chen, A. Rusinova, A. Chandra, M. Bierbaum, L. Gremer, G. Triola, H. Waldmann, P. I. Bastiaens & A. Wittinghofer (2011) Arl2-GTP and Arl3-GTP regulate a GDI-like transport system for farnesylated cargo. *Nat Chem Biol*, 7, 942-9.
- Jackson, S. P. & J. Bartek (2009) The DNA-damage response in human biology and disease. *Nature*, 461, 1071-1078.
- Jaliffa, C., I. Ameqrane, A. Dansault, J. Leemput, V. Vieira, E. Lacassagne, A. Provost, K. Bigot, C. Masson, M. Menasche & M. Abitbol (2009) Sirt1 involvement in rd10 mouse retinal degeneration. *Invest Ophthalmol Vis Sci*, 50, 3562-72.
- Jao, L. E., S. R. Wentz & W. Chen (2013) Efficient multiplex biallelic zebrafish genome editing using a CRISPR nuclease system. *Proc Natl Acad Sci U S A*, 110, 13904-9.
- Jayasundera, T., K. E. Branham, M. Othman, W. R. Rhoades, A. J. Karoukis, H. Khanna, A. Swaroop & J. R. Heckenlively (2010) THE RP2 PHENOTYPE AND PATHOGENETIC CORRELATIONS IN X-LINKED RETINITIS PIGMENTOSA. *Arch Ophthalmol*, 128, 915-23.
- Jette, N. & S. P. Lees-Miller (2015) The DNA-dependent protein kinase: A multifunctional protein kinase with roles in DNA double strand break repair and mitosis. *Prog Biophys Mol Biol*, 117, 194-205.
- Jiang, K., K. L. Wright, P. Zhu, M. J. Szego, A. N. Bramall, W. W. Hauswirth, Q. Li, S. E. Egan & R. R. McInnes (2014) STAT3 promotes survival of mutant photoreceptors in inherited photoreceptor degeneration models. *Proc Natl Acad Sci U S A*, 111, E5716-23.
- Jin, M., S. Li, W. N. Moghrabi, H. Sun & G. H. Travis (2005) Rpe65 is the retinoid isomerase in bovine retinal pigment epithelium. *Cell*, 122, 449-59.
- Jin, M., M. Yamada, Y. Arai, T. Nagai & S. Hirotsune (2014) Arl3 and LC8 regulate dissociation of dynactin from dynein. *Nat Commun*, 5, 5295.
- Jung, I. H., Y. Y. Chung, D. E. Jung, Y. J. Kim, D. H. Kim, K. S. Kim & S. W. Park (2016) Impaired Lymphocytes Development and Xenotransplantation of Gastrointestinal Tumor Cells in Prkdc-Null SCID Zebrafish Model1. *Neoplasia*, 18, 468-79.
- Kajiwara, K., E. L. Berson & T. P. Dryja (1994) Digenic retinitis pigmentosa due to mutations at the unlinked peripherin/RDS and ROM1 loci. *Science*, 264, 1604-8.

- Kanungo, J. (2016) DNA-PK Deficiency in Alzheimer's Disease. *J Neurol Neuromedicine*, 1, 17-22.
- Kettenbach, A. N., D. K. Schweppe, B. K. Faherty, D. Pechenick, A. A. Pletnev & S. A. Gerber Quantitative Phosphoproteomics Identifies Substrates and Functional Modules of Aurora and Polo-Like Kinase Activities in Mitotic Cells. *Sci Signal*, 4.
- Kevany, B. M. & K. Palczewski (2010) Phagocytosis of Retinal Rod and Cone Photoreceptors. *Physiology (Bethesda)*, 25, 8-15.
- Kinner, A., W. Wu, C. Staudt & G. Iliakis (2008) Gamma-H2AX in recognition and signaling of DNA double-strand breaks in the context of chromatin. *Nucleic Acids Res*, 36, 5678-94.
- Kitambi, S. S., K. J. McCulloch, R. T. Peterson & J. J. Malicki (2009) Small molecule screen for compounds that affect vascular development in the zebrafish retina. *Mech Dev*, 126, 464-77.
- Kitamoto, J., R. T. Libby, D. Gibbs, K. P. Steel & D. S. Williams (2005) Myosin VI is required for normal retinal function. *Exp Eye Res*, 81, 116-20.
- Koike, M., J. Sugasawa, M. Yasuda & A. Koike (2008) Tissue-specific DNA-PK-dependent H2AX phosphorylation and gamma-H2AX elimination after X-irradiation in vivo. *Biochem Biophys Res Commun*, 376, 52-5.
- Kok, F. O., M. Shin, C. W. Ni, A. Gupta, A. S. Grosse, A. van Impel, B. C. Kirchmaier, J. Peterson-Maduro, G. Kourkoulis, I. Male, D. F. DeSantis, S. Sheppard-Tindell, L. Ebarasi, C. Betsholtz, S. Schulte-Merker, S. A. Wolfe & N. D. Lawson (2015) Reverse genetic screening reveals poor correlation between morpholino-induced and mutant phenotypes in zebrafish. *Dev Cell*, 32, 97-108.
- Kong, X., Y. Shen, N. Jiang, X. Fei & J. Mi (2011) Emerging roles of DNA-PK besides DNA repair. *Cell Signal*, 23, 1273-80.
- Kotula, E., W. Faigle, N. Berthault, F. Dingli, D. Loew, J. S. Sun, M. Dutreix & M. Quanz. 2013. DNA-PK Target Identification Reveals Novel Links between DNA Repair Signaling and Cytoskeletal Regulation. In *PLoS One*.
- Krock, B. L., I. Mills-Henry & B. D. Perkins (2009) Retrograde intraflagellar transport by cytoplasmic dynein-2 is required for outer segment extension in vertebrate photoreceptors but not arrestin translocation. *Invest Ophthalmol Vis Sci*, 50, 5463-71.
- Kuhnel, K., S. Veltel, I. Schlichting & A. Wittinghofer (2006) Crystal structure of the human retinitis pigmentosa 2 protein and its interaction with Arl3. *Structure*, 14, 367-78.
- Kunte, M. M., S. Choudhury, J. F. Manheim, V. M. Shinde, M. Miura, V. A. Chiodo, W. W. Hauswirth, O. S. Gorbatyuk & M. S. Gorbatyuk (2012) ER stress is involved in T17M rhodopsin-induced retinal degeneration. *Invest Ophthalmol Vis Sci*, 53, 3792-800.
- Kurihara, N., C. Mena, H. Maeda, D. J. Haile & S. V. Reddy (2001) Osteoclast-stimulating Factor Interacts with the Spinal Muscular Atrophy Gene Product to Stimulate Osteoclast Formation.
- Kurimasa, A., S. Kumano, N. V. Boubnov, M. D. Story, C. S. Tung, S. R. Peterson & D. J. Chen (1999) Requirement for the kinase activity of human DNA-dependent

- protein kinase catalytic subunit in DNA strand break rejoining. *Mol Cell Biol*, 19, 3877-84.
- Lamb, T. D. & E. N. Pugh, Jr. (2004) Dark adaptation and the retinoid cycle of vision. *Prog Retin Eye Res*, 23, 307-80.
- Law, A.-L., Q. Ling, K. A. Hajjar, C. E. Futter, J. Greenwood, P. Adamson, S. T. Wavre-Shapton, S. E. Moss & M. J. Hayes (2009) Annexin A2 Regulates Phagocytosis of Photoreceptor Outer Segments in the Mouse Retina.
- Le, P. N., D. G. Maranon, N. H. Altina, C. L. Battaglia & S. M. Bailey (2013) TERRA, hnRNP A1, and DNA-PKcs Interactions at Human Telomeres. *Front Oncol*, 3, 91.
- Lee, K. J., Y. F. Lin, H. Y. Chou, H. Yajima, K. R. Fattah, S. C. Lee & B. P. Chen (2011) Involvement of DNA-dependent protein kinase in normal cell cycle progression through mitosis. *J Biol Chem*, 286, 12796-802.
- Lee, Y. H., H. T. Tan & M. C. Chung (2010) Subcellular fractionation methods and strategies for proteomics. *Proteomics*, 10, 3935-56.
- Levy, N., A. Martz, A. Bresson, C. Spenlehauer, G. de Murcia & J. Menissier-de Murcia (2006) XRCC1 is phosphorylated by DNA-dependent protein kinase in response to DNA damage. *Nucleic Acids Res*, 34, 32-41.
- Li, L. & J. E. Dowling. 1997. A dominant form of inherited retinal degeneration caused by a non-photoreceptor cell-specific mutation. In *Proc Natl Acad Sci U S A*, 11645-50.
- Li, L., N. Khan, T. Hurd, A. K. Ghosh, C. Cheng, R. Molday, J. R. Heckenlively, A. Swaroop & H. Khanna (2013a) Ablation of the X-linked retinitis pigmentosa 2 (Rp2) gene in mice results in opsin mislocalization and photoreceptor degeneration. *Invest Ophthalmol Vis Sci*, 54, 4503-11.
- Li, L., K. N. Rao, Y. Zheng-Le, T. W. Hurd, C. Lillo & H. Khanna (2015) Loss of Retinitis Pigmentosa 2 (RP2) protein affects cone photoreceptor sensory cilium elongation in mice. *Cytoskeleton (Hoboken)*, 72, 447-54.
- Li, M., Y. F. Lin, G. A. Palchik, S. Matsunaga, D. Wang & B. P. Chen (2014) The catalytic subunit of DNA-dependent protein kinase is required for cellular resistance to oxidative stress independent of DNA double-strand break repair. *Free Radic Biol Med*, 76, 278-85.
- Li, Y., X. Wang, P. Yue, H. Tao, S. S. Ramalingam, T. K. Owonikoko, X. Deng, Y. Wang, H. Fu, F. R. Khuri & S. Y. Sun. 2013b. Protein Phosphatase 2A and DNA-dependent Protein Kinase Are Involved in Mediating Rapamycin-induced Akt Phosphorylation\*. In *J Biol Chem*, 13215-24.
- Lieschke, G. J. & P. D. Currie (2007) Animal models of human disease: zebrafish swim into view. *Nat Rev Genet*, 8, 353-67.
- Liu, F., J. Chen, S. Yu, R. K. Raghupathy, X. Liu, Y. Qin, C. Li, M. Huang, S. Liao, J. Wang, J. Zou, X. Shu, Z. Tang & M. Liu (2015) Knockout of RP2 decreases GRK1 and rod transducin subunits and leads to photoreceptor degeneration in zebrafish. *Hum Mol Genet*, 24, 4648-59.
- Liu, F., Y. Qin, S. Yu, D. C. Soares, L. Yang, J. Weng, C. Li, M. Gao, Z. Lu, X. Hu, X. Liu, T. Jiang, J. Y. Liu, X. Shu, Z. Tang & M. Liu (2017a) Pathogenic Mutations in

- Retinitis Pigmentosa 2 Predominantly Result in Loss of RP2 Protein Stability in Human and Zebrafish. *J Biol Chem*.
- Liu, J., Y. Zhou, X. Qi, J. Chen, W. Chen, G. Qiu, Z. Wu & N. Wu (2017b) CRISPR/Cas9 in zebrafish: an efficient combination for human genetic diseases modeling. *Hum Genet*, 136, 1-12.
- Loewen, C. J., O. L. Moritz & R. S. Molday (2001) Molecular characterization of peripherin-2 and rom-1 mutants responsible for digenic retinitis pigmentosa. *J Biol Chem*, 276, 22388-96.
- Lucero, H., D. Gae & G. E. Taccioli (2003) Novel localization of the DNA-PK complex in lipid rafts: a putative role in the signal transduction pathway of the ionizing radiation response. *J Biol Chem*, 278, 22136-43.
- Lyraki, R., M. Lokaj, D. C. Soares, A. Little, M. Vermeren, J. A. Marsh, A. Wittinghofer & T. Hurd (2018) Characterization of a novel RP2-OSTF1 interaction and its implication for actin remodeling. *J Cell Sci*.
- Lyraki, R., R. Megaw & T. Hurd (2016) Disease mechanisms of X-linked retinitis pigmentosa due to RP2 and RPGR mutations. *Biochem Soc Trans*, 44, 1235-1244.
- Ma, Y., U. Pannicke, H. Lu, D. Niewolik, K. Schwarz & M. R. Lieber (2005) The DNA-dependent Protein Kinase Catalytic Subunit Phosphorylation Sites in Human Artemis.
- Malanson, K. M. & J. Lem (2009) Rhodopsin-mediated retinitis pigmentosa. *Prog Mol Biol Transl Sci*, 88, 1-31.
- Malicki, J., N. Pooranachandran, A. Nikolaev, X. Fang & A. Avanesov (2016) Analysis of the retina in the zebrafish model. *Methods Cell Biol*, 134, 257-334.
- Malu, S., V. Malshetty, D. Francis & P. Cortes (2012) Role of non-homologous end joining in V(D)J recombination. *Immunol Res*, 54, 233-46.
- Marcus, R. C., C. L. Delaney & S. S. Easter, Jr. (1999) Neurogenesis in the visual system of embryonic and adult zebrafish (*Danio rerio*). *off. Vis Neurosci*, 16, 417-24.
- Marszalek, J. R., X. Liu, E. A. Roberts, D. Chui, J. D. Marth, D. S. Williams & L. S. Goldstein (2000) Genetic evidence for selective transport of opsin and arrestin by kinesin-II in mammalian photoreceptors. *Cell*, 102, 175-87.
- Mathieu, A. L., E. Verronese, G. I. Rice, F. Fouyssac, Y. Bertrand, C. Picard, M. Chansel, J. E. Walter, L. D. Notarangelo, M. J. Butte, K. C. Nadeau, K. Csomos, D. J. Chen, K. Chen, A. Delgado, C. Rigal, C. Bardin, C. Schuetz, D. Moshous, H. Reumaux, F. Plenat, A. Phan, M. T. Zobot, B. Balme, S. Viel, J. Bienvenu, P. Cochat, M. van der Burg, C. Caux, E. H. Kemp, I. Rouvet, C. Malcus, J. F. Meritet, A. Lim, Y. J. Crow, N. Fabien, C. Menetrier-Caux, J. P. De Villartay, T. Walzer & A. Belot (2015) PRKDC mutations associated with immunodeficiency, granuloma, and autoimmune regulator-dependent autoimmunity. *J Allergy Clin Immunol*, 135, 1578-88.e5.
- Mazelova, J., L. Astuto-Gribble, H. Inoue, B. M. Tam, E. Schonteich, R. Prekeris, O. L. Moritz, P. A. Randazzo & D. Deretic (2009) Ciliary targeting motif VxPx directs assembly of a trafficking module through Arf4. *Embo j*, 28, 183-92.

- McCabe, J. B. & L. G. Berthiaume. 1999. Functional Roles for Fatty Acylated Amino-terminal Domains in Subcellular Localization. In *Mol Biol Cell*, 3771-86.
- Mears, A. J., L. Gieser, D. Yan, C. Chen, S. Fahrner, S. Hiriyanna, R. Fujita, S. G. Jacobson, P. A. Sieving & A. Swaroop. 1999. Protein-truncation mutations in the RP2 gene in a North American cohort of families with X-linked retinitis pigmentosa. In *Am J Hum Genet*, 897-900. United States.
- Megaw, R., H. Abu-Arafeh, M. Jungnickel, C. Mellough, C. Gurniak, W. Witke, W. Zhang, H. Khanna, P. Mill, B. Dhillon, A. F. Wright, M. Lako & C. Ffrench-Constant (2017) Gelsolin dysfunction causes photoreceptor loss in induced pluripotent cell and animal retinitis pigmentosa models. *Nat Commun*, 8, 271.
- Miano, M. G., F. Testa, F. Filippini, M. Trujillo, I. Conte, C. Lanzara, J. M. Millan, C. De Bernardo, B. Grammatico, M. Mangino, I. Torrente, R. Carrozzo, F. Simonelli, E. Rinaldi, V. Ventruto, M. D'Urso, C. Ayuso & A. Ciccodicola (2001) Identification of novel RP2 mutations in a subset of X-linked retinitis pigmentosa families and prediction of new domains. *Hum Mutat*, 18, 109-19.
- Michaelides, M., A. J. Hardcastle, D. M. Hunt & A. T. Moore (2006) Progressive cone and cone-rod dystrophies: phenotypes and underlying molecular genetic basis. *Surv Ophthalmol*, 51, 232-58.
- Moiseyev, G., Y. Chen, Y. Takahashi, B. X. Wu & J. X. Ma (2005) RPE65 is the isomerohydrolase in the retinoid visual cycle. *Proc Natl Acad Sci U S A*, 102, 12413-8.
- Molday, R. S., U. Kellner & B. H. Weber (2012) X-linked juvenile retinoschisis: clinical diagnosis, genetic analysis, and molecular mechanisms. *Prog Retin Eye Res*, 31, 195-212.
- Mookherjee, S., S. Hiriyanna, K. Kaneshiro, L. Li, Y. Li, W. Li, H. Qian, T. Li, H. Khanna, P. Colosi, A. Swaroop & Z. Wu (2015) Long-term rescue of cone photoreceptor degeneration in retinitis pigmentosa 2 (RP2)-knockout mice by gene replacement therapy. *Hum Mol Genet*, 24, 6446-58.
- Morii, M., S. Kubota, T. Honda, R. Yuki, T. Morinaga, T. Kuga, T. Tomonaga, N. Yamaguchi & N. Yamaguchi (2017) Src Acts as an Effector for Ku70-dependent Suppression of Apoptosis through Phosphorylation of Ku70 at Tyr-530.
- Moritz, A., Y. Li, A. Guo, J. Villen, Y. Wang, J. MacNeill, J. Kornhauser, K. Sprott, J. Zhou, A. Possemato, J. M. Ren, P. Hornbeck, L. C. Cantley, S. P. Gygi, J. Rush & M. J. Comb (2010) Akt-RSK-S6 kinase signaling networks activated by oncogenic receptor tyrosine kinases. *Sci Signal*, 3, ra64.
- Moritz, A., Y. Li, A. Guo, J. Villén, Y. Wang, J. MacNeill, J. Kornhauser, K. Sprott, J. Zhou, A. Possemato, J. M. Ren, P. Hornbeck, L. C. Cantley, S. P. Gygi, J. Rush & M. J. Comb Akt-RSK-S6-kinase Signaling Networks Activated by Oncogenic Receptor Tyrosine Kinases. *Sci Signal*, 3, ra64.
- Morris, A. C., T. L. Scholz, S. E. Brockerhoff & J. M. Fadool (2008) Genetic dissection reveals two separate pathways for rod and cone regeneration in the teleost retina. *Dev Neurobiol*, 68, 605-19.



- Nagahara, H. L., Robert R. Ezhevsky, Sergei A. Dowdy, Steven F. (2016) Two-Dimensional Phosphopeptide Mapping.
- Nakazawa, M., H. Ohguro, K. Takeuchi, Y. Miyagawa, T. Ito & T. Metoki (2011) Effect of nilvadipine on central visual field in retinitis pigmentosa: a 30-month clinical trial. *Ophthalmologica*, 225, 120-6.
- Neal, J. A., V. Dang, P. Douglas, M. S. Wold, S. P. Lees-Miller & K. Meek (2011) Inhibition of homologous recombination by DNA-dependent protein kinase requires kinase activity, is titratable, and is modulated by autophosphorylation. *Mol Cell Biol*, 31, 1719-33.
- Neidhardt, J., E. Glaus, B. Lorenz, C. Netzer, Y. Li, M. Schambeck, M. Wittmer, S. Feil, R. Kirschner-Schwabe, T. Rosenberg, F. P. Cremers, A. A. Bergen, D. Barthelmes, H. Baraki, F. Schmid, G. Tanner, J. Fleischhauer, U. Orth, C. Becker, E. Wegscheider, G. Nurnberg, P. Nurnberg, H. J. Bolz, A. Gal & W. Berger (2008) Identification of novel mutations in X-linked retinitis pigmentosa families and implications for diagnostic testing. *Mol Vis*, 14, 1081-93.
- Newsome, D. A., M. V. Miceli, M. R. Liles, D. J. Tate & P. D. Oliver (1994) Antioxidants in the retinal pigment epithelium. *Progress in Retinal and Eye Research*, 13, 101-123.
- Nowak, J. Z. (2006) Age-related macular degeneration (AMD): pathogenesis and therapy. *Pharmacol Rep*, 58, 353-63.
- O'Neill, T., A. J. Dwyer, Y. Ziv, D. W. Chan, S. P. Lees-Miller, R. H. Abraham, J. H. Lai, D. Hill, Y. Shiloh, L. C. Cantley & G. A. Rathbun (2000) Utilization of Oriented Peptide Libraries to Identify Substrate Motifs Selected by ATM.
- Omori, Y., C. Zhao, A. Saras, S. Mukhopadhyay, W. Kim, T. Furukawa, P. Sengupta, A. Veraksa & J. Malicki (2008) Elipsa is an early determinant of ciliogenesis that links the IFT particle to membrane-associated small GTPase Rab8. *Nat Cell Biol*, 10, 437-44.
- Organisciak, D. T. & D. K. Vaughan (2010) Retinal light damage: mechanisms and protection. *Prog Retin Eye Res*, 29, 113-34.
- Otto, E. A., T. W. Hurd, R. Airik, M. Chaki, W. Zhou, C. Stoetzel, S. B. Patil, S. Levy, A. K. Ghosh, C. A. Murga-Zamalloa, J. van Reeuwijk, S. J. Letteboer, L. Sang, R. H. Giles, Q. Liu, K. L. Coene, A. Estrada-Cuzcano, R. W. Collin, H. M. McLaughlin, S. Held, J. M. Kasanuki, G. Ramaswami, J. Conte, I. Lopez, J. Washburn, J. Macdonald, J. Hu, Y. Yamashita, E. R. Maher, L. M. Guay-Woodford, H. P. Neumann, N. Obermuller, R. K. Koenekoop, C. Bergmann, X. Bei, R. A. Lewis, N. Katsanis, V. Lopes, D. S. Williams, R. H. Lyons, C. V. Dang, D. A. Brito, M. B. Dias, X. Zhang, J. D. Cavalcoli, G. Nurnberg, P. Nurnberg, E. A. Pierce, P. K. Jackson, C. Antignac, S. Saunier, R. Roepman, H. Dollfus, H. Khanna & F. Hildebrandt (2010) Candidate exome capture identifies mutation of SDCCAG8 as the cause of a retinal-renal ciliopathy. *Nat Genet*, 42, 840-50.
- Pan, Y. R. & E. Y. Lee (2009) UV-dependent interaction between Cep164 and XPA mediates localization of Cep164 at sites of DNA damage and UV sensitivity. *Cell Cycle*, 8, 655-64.

- Parlanti, E., G. Locatelli, G. Maga & E. Dogliotti (2007) Human base excision repair complex is physically associated to DNA replication and cell cycle regulatory proteins. *Nucleic Acids Res*, 35, 1569-77.
- Pazour, G. J., S. A. Baker, J. A. Deane, D. G. Cole, B. L. Dickert, J. L. Rosenbaum, G. B. Witman & J. C. Besharse (2002) The intraflagellar transport protein, IFT88, is essential for vertebrate photoreceptor assembly and maintenance. *J Cell Biol*, 157, 103-13.
- Pearring, J. N., R. Y. Salinas, S. A. Baker & V. Y. Arshavsky (2013) Protein sorting, targeting and trafficking in photoreceptor cells. *Prog Retin Eye Res*, 0, 24-51.
- Peddi, P., C. W. Loftin, J. S. Dickey, J. M. Hair, K. J. Burns, K. Aziz, D. C. Francisco, M. I. Panayiotidis, O. A. Sedelnikova, W. M. Bonner, T. A. Winters & A. G. Georgakilas (2010) DNA-PKcs deficiency leads to persistence of oxidatively-induced clustered DNA lesions in human tumor cells. *Free Radic Biol Med*, 48, 1435-43.
- Pei, D. S. & P. R. Strauss (2013) Zebrafish as a model system to study DNA damage and repair. *Mutat Res*, 743-744, 151-9.
- Pelletier, V., M. Jambou, N. Delphin, E. Zinovieva, M. Stum, N. Gigarel, H. Dollfus, C. Hamel, A. Toutain, J. L. Dufier, O. Roche, A. Munnich, J. P. Bonnefont, J. Kaplan & J. M. Rozet (2007) Comprehensive survey of mutations in RP2 and RPGR in patients affected with distinct retinal dystrophies: genotype-phenotype correlations and impact on genetic counseling. *Hum Mutat*, 28, 81-91.
- Pooranachandran, N. & J. J. Malicki (2016) Unexpected Roles for Ciliary Kinesins and Intraflagellar Transport Proteins. *Genetics*, 203, 771-85.
- Poruchynsky, M. S., E. Komlodi-Pasztor, S. Trostel, J. Wilkerson, M. Regairaz, Y. Pommier, X. Zhang, T. Kumar Maity, R. Robey, M. Burotto, D. Sackett, U. Guha & A. T. Fojo (2015) Microtubule-targeting agents augment the toxicity of DNA-damaging agents by disrupting intracellular trafficking of DNA repair proteins. *Proc Natl Acad Sci U S A*, 112, 1571-6.
- Prokisch, H., M. Hartig, R. Hellinger, T. Meitinger & T. Rosenberg (2007) A population-based epidemiological and genetic study of X-linked retinitis pigmentosa. *Invest Ophthalmol Vis Sci*, 48, 4012-8.
- Pujic, Z. & J. Malicki (2001) Mutation of the zebrafish glass onion locus causes early cell-nonautonomous loss of neuroepithelial integrity followed by severe neuronal patterning defects in the retina. *Dev Biol*, 234, 454-69.
- Quanz, M., A. Herbette, M. Sayarath, L. de Koning, T. Dubois, J. S. Sun & M. Dutreix. 2012. Heat Shock Protein 90 $\alpha$  (Hsp90 $\alpha$ ) Is Phosphorylated in Response to DNA Damage and Accumulates in Repair Foci\*. In *J Biol Chem*, 8803-15.
- Raghupathy, R. K., X. Zhang, R. H. Alhasani, X. Zhou, M. Mullin, J. Reilly, W. Li, M. Liu & X. Shu (2016) Abnormal photoreceptor outer segment development and early retinal degeneration in kif3a mutant zebrafish. *Cell Biochem Funct*, 34, 429-40.
- Rakoczy, E. P., C. Kiel, R. McKeone, F. Stricher & L. Serrano (2011) Analysis of disease-linked rhodopsin mutations based on structure, function, and protein stability calculations. *J Mol Biol*, 405, 584-606.

- Ramkumar, H. L., B. P. Brooks, X. Cao, D. Tamura, J. J. Digiovanna, K. H. Kraemer & C. C. Chan (2011) Ophthalmic manifestations and histopathology of xeroderma pigmentosum: two clinicopathological cases and a review of the literature. *Surv Ophthalmol*, 56, 348-61.
- Reddy, S., t. V. A. M. C. a. T. U. o. T. H. S. C. Department of Medicine/Hematology/Endocrinology, San Antonio, Texas, R. Devlin, t. V. A. M. C. a. T. U. o. T. H. S. C. Department of Medicine/Hematology/Endocrinology, San Antonio, Texas, C. Mena, t. V. A. M. C. a. T. U. o. T. H. S. C. Department of Medicine/Hematology/Endocrinology, San Antonio, Texas, R. Nishimura, O. U. Department of Biochemistry, Osaka, Japan, S. J. Choi, t. V. A. M. C. a. T. U. o. T. H. S. C. Department of Medicine/Hematology/Endocrinology, San Antonio, Texas, M. Dallas, t. V. A. M. C. a. T. U. o. T. H. S. C. Department of Medicine/Hematology/Endocrinology, San Antonio, Texas, T. Yoneda, t. V. A. M. C. a. T. U. o. T. H. S. C. Department of Medicine/Hematology/Endocrinology, San Antonio, Texas, G. D. Roodman, t. V. A. M. C. a. T. U. o. T. H. S. C. Department of Medicine/Hematology/Endocrinology, San Antonio, Texas & A. M. V. A. H. Research Service (151), 7400 Merton Minter Boulevard, San Antonio, TX 78284 (1998) Isolation and characterization of a cDNA clone encoding a novel peptide (OSF) that enhances osteoclast formation and bone resorption. *Journal of Cellular Physiology*, 177, 636-645.
- Resh, M. D. (2016) Chapter 13 – Lipid Modification of Proteins. 391–414.
- Robu, M. E., J. D. Larson, A. Nasevicius, S. Beiraghi, C. Brenner, S. A. Farber & S. C. Ekker (2007) p53 activation by knockdown technologies. *PLoS Genet*, 3, e78.
- Roepman, R., G. van Duijnhoven, T. Rosenberg, A. J. Pinckers, L. M. Bleeker-Wagemakers, A. A. Bergen, J. Post, A. Beck, R. Reinhardt, H. H. Ropers, F. P. Cremers & W. Berger (1996) Positional cloning of the gene for X-linked retinitis pigmentosa 3: homology with the guanine-nucleotide-exchange factor RCC1. *Hum Mol Genet*, 5, 1035-41.
- Rohrer, B., K. Kunchithapautham, A. Genewsky & O. Strauss (2014) Prolonged SRC kinase activation, a mechanism to turn transient, sublytic complement activation into a sustained pathological condition in retinal pigment epithelium cells. *Adv Exp Med Biol*, 801, 221-7.
- Rosidi, B., M. Wang, W. Wu, A. Sharma, H. Wang & G. Iliakis (2008) Histone H1 functions as a stimulatory factor in backup pathways of NHEJ. *Nucleic Acids Res*, 36, 1610-23.
- Rossi, A., Z. Kontarakis, C. Gerri, H. Nolte, S. Holper, M. Kruger & D. Y. Stainier (2015) Genetic compensation induced by deleterious mutations but not gene knockdowns. *Nature*, 524, 230-3.
- Ruiz-Loredo, A. Y. & A. M. Lopez-Colome (2012) New insights into the regulation of myosin light chain phosphorylation in retinal pigment epithelial cells. *Int Rev Cell Mol Biol*, 293, 85-121.
- Sacchetti, M., F. Mantelli, D. Merlo & A. Lambiase (2015) Systematic Review of Randomized Clinical Trials on Safety and Efficacy of Pharmacological and

- Nonpharmacological Treatments for Retinitis Pigmentosa. *J Ophthalmol*, 2015.
- Sahel, J. A., K. Marazova & I. Audo (2014) Clinical characteristics and current therapies for inherited retinal degenerations. *Cold Spring Harb Perspect Med*, 5, a017111.
- Samardzija, M., J. von Lintig, N. Tanimoto, V. Oberhauser, M. Thiersch, C. E. Reme, M. Seeliger, C. Grimm & A. Wenzel (2008) R91W mutation in Rpe65 leads to milder early-onset retinal dystrophy due to the generation of low levels of 11-cis-retinal. *Hum Mol Genet*, 17, 281-92.
- Schrack, J. J., P. Vogel, A. Abuin, B. Hampton & D. S. Rice (2006) ADP-ribosylation factor-like 3 is involved in kidney and photoreceptor development. *Am J Pathol*, 168, 1288-98.
- Schwahn, U., S. Lenzner, J. Dong, S. Feil, B. Hinzmann, G. van Duijnhoven, R. Kirschner, M. Hemberger, A. A. Bergen, T. Rosenberg, A. J. Pinckers, R. Fundele, A. Rosenthal, F. P. Cremers, H. H. Ropers & W. Berger (1998) Positional cloning of the gene for X-linked retinitis pigmentosa 2. *Nat Genet*, 19, 327-32.
- Schwahn, U., N. Paland, S. Techritz, S. Lenzner & W. Berger (2001) Mutations in the X-linked RP2 gene cause intracellular misrouting and loss of the protein. *Hum Mol Genet*, 10, 1177-83.
- Schwartz, S. D., C. D. Regillo, B. L. Lam, D. Elliott, P. J. Rosenfeld, N. Z. Gregori, J. P. Hubschman, J. L. Davis, G. Heilwell, M. Spirn, J. Maguire, R. Gay, J. Bateman, R. M. Ostrick, D. Morris, M. Vincent, E. Anglade, L. V. Del Priore & R. Lanza (2015) Human embryonic stem cell-derived retinal pigment epithelium in patients with age-related macular degeneration and Stargardt's macular dystrophy: follow-up of two open-label phase 1/2 studies. *Lancet*, 385, 509-16.
- Schwarz, N., A. J. Carr, A. Lane, F. Moeller, L. L. Chen, M. Aguila, B. Nommiste, M. N. Muthiah, N. Kanuga, U. Wolfrum, K. Nagel-Wolfrum, L. da Cruz, P. J. Coffey, M. E. Cheetham & A. J. Hardcastle (2015) Translational read-through of the RP2 Arg120stop mutation in patient iPSC-derived retinal pigment epithelium cells. *Hum Mol Genet*, 24, 972-86.
- Schwarz, N., A. Lane, K. Jovanovic, D. A. Parfitt, M. Aguila, C. L. Thompson, L. da Cruz, P. J. Coffey, J. P. Chapple, A. J. Hardcastle & M. E. Cheetham (2017) Arl3 and RP2 regulate the trafficking of ciliary tip kinesins. *Hum Mol Genet*, 26, 2480-2492.
- Schwarz, N., T. V. Novoselova, R. Wait, A. J. Hardcastle & M. E. Cheetham (2012) The X-linked retinitis pigmentosa protein RP2 facilitates G protein traffic. *Hum Mol Genet*, 21, 863-73.
- Schymkowitz, J., J. Borg, F. Stricher, R. Nys, F. Rousseau & L. Serrano (2005) The FoldX web server: an online force field. *Nucleic Acids Res*, 33, W382-8.
- Serrano, M. A., Z. Li, M. Dangeti, P. R. Musich, S. Patrick, M. Roginskaya, B. Cartwright & Y. Zou (2013) DNA-PK, ATM and ATR collaboratively regulate p53-RPA interaction to facilitate homologous recombination DNA repair. *Oncogene*, 32, 2452-62.

- Sharif, W. & Z. Sharif (2017) Leber's congenital amaurosis and the role of gene therapy in congenital retinal disorders. *Int J Ophthalmol*, 10, 480-484.
- Sharma, K., R. C. D'Souza, S. Tyanova, C. Schaab, J. R. Wisniewski, J. Cox & M. Mann (2014) Ultradeep human phosphoproteome reveals a distinct regulatory nature of Tyr and Ser/Thr-based signaling. *Cell Rep*, 8, 1583-94.
- Sharon, D., M. A. Sandberg, V. W. Rabe, M. Stillberger, T. P. Dryja & E. L. Berson (2003) RP2 and RPGR mutations and clinical correlations in patients with X-linked retinitis pigmentosa. *Am J Hum Genet*, 73, 1131-46.
- Shrivastav, M., L. P. De Haro & J. A. Nickoloff (2008) Regulation of DNA double-strand break repair pathway choice. *Cell Res*, 18, 134-47.
- Shu, X., Z. Zeng, P. Gautier, A. Lennon, M. Gakovic, M. E. Cheetham, E. E. Patton & A. F. Wright (2011) Knockdown of the zebrafish ortholog of the retinitis pigmentosa 2 (RP2) gene results in retinal degeneration. *Invest Ophthalmol Vis Sci*, 52, 2960-6.
- Sibanda, B. L., D. Y. Chirgadze & T. L. Blundell (2010) Crystal structure of DNA-PKcs reveals a large open-ring cradle comprised of HEAT repeats. *Nature*, 463, 118-21.
- Sivasubramaniam, S., X. Sun, Y. R. Pan, S. Wang & E. Y. Lee (2008) Cep164 is a mediator protein required for the maintenance of genomic stability through modulation of MDC1, RPA, and CHK1. *Genes Dev*, 22, 587-600.
- Stearns, G., M. Evangelista, J. M. Fadool & S. E. Brockerhoff (2007) A mutation in the cone-specific pde6 gene causes rapid cone photoreceptor degeneration in zebrafish. *J Neurosci*, 27, 13866-74.
- Stenkamp, D. L., R. Satterfield, K. Muhunthan, T. Sherpa, T. S. Vihtelic & D. A. Cameron (2008) Age-related cone abnormalities in zebrafish with genetic lesions in sonic hedgehog. *Invest Ophthalmol Vis Sci*, 49, 4631-40.
- Strom, S. P., M. J. Clark, A. Martinez, S. Garcia, A. A. Abelazeem, A. Matynia, S. Parikh, L. S. Sullivan, S. J. Bowne, S. P. Daiger & M. B. Gorin (2016) De Novo Occurrence of a Variant in ARL3 and Apparent Autosomal Dominant Transmission of Retinitis Pigmentosa. *PLoS One*, 11, e0150944.
- Stuart, S. A., S. Houel, T. Lee, N. Wang, W. M. Old & N. G. Ahn (2015) A Phosphoproteomic Comparison of B-RAFV600E and MKK1/2 Inhibitors in Melanoma Cells. *Mol Cell Proteomics*, 14, 1599-615.
- Sun, H. & J. Nathans (2001) ABCR, the ATP-binding cassette transporter responsible for Stargardt macular dystrophy, is an efficient target of all-trans-retinal-mediated photooxidative damage in vitro. Implications for retinal disease. *J Biol Chem*, 276, 11766-74.
- Sun, X., J. H. Park, J. Gumerson, Z. Wu, A. Swaroop, H. Qian, A. Roll-Mecak & T. Li (2016) Loss of RPGR glutamylation underlies the pathogenic mechanism of retinal dystrophy caused by TTLL5 mutations. *Proc Natl Acad Sci U S A*, 113, E2925-34.
- Sung, C. H. & J. Z. Chuang. 2010. The cell biology of vision. In *J Cell Biol*, 953-63.
- Szymkiewicz, I., O. Destaing, P. Jurdic & I. Dikic (2004) SH3P2 in complex with Cbl and Src. *FEBS Lett*, 565, 33-8.

- Tang, Q. L., J. Liu, L. Zuo, C. Chi, H. Y. Dong, X. X. Jiang & X. F. Jiang (2017) Bilateral blindness with secondary retinitis pigmentosa following postoperative docetaxel and platinum combination chemotherapy in primary small-cell carcinoma of the endometrium: An unusual case report and review of the literature. *Mol Clin Oncol*, 6, 477-482.
- Tanimura, S., J. Hashizume, N. Arichika, K. Watanabe, K. Ohyama, K. Takeda & M. Kohno (2016) ERK signaling promotes cell motility by inducing the localization of myosin 1E to lamellipodial tips.
- Tanimura, S., J. Hashizume, Y. Kurosaki, K. Sei, A. Gotoh, R. Ohtake, M. Kawano, K. Watanabe & M. Kohno (2011) SH3P2 is a negative regulator of cell motility whose function is inhibited by ribosomal S6 kinase-mediated phosphorylation. *Genes Cells*, 16, 514-26.
- Tanna, P., R. W. Strauss, K. Fujinami & M. Michaelides (2017) Stargardt disease: clinical features, molecular genetics, animal models and therapeutic options. *Br J Ophthalmol*, 101, 25-30.
- Tawara, A., H. H. Varner & J. G. Hollyfield (1989) Proteoglycans in the mouse interphotoreceptor matrix. II. Origin and development of proteoglycans. *Exp Eye Res*, 48, 815-39.
- Thompson, D. A., N. W. Khan, M. I. Othman, B. Chang, L. Jia, G. Grahek, Z. Wu, S. Hiriyanna, J. Nellissery, T. Li, H. Khanna, P. Colosi, A. Swaroop & J. R. Heckenlively (2012) Rd9 is a naturally occurring mouse model of a common form of retinitis pigmentosa caused by mutations in RPGR-ORF15. *PLoS One*, 7, e35865.
- Tian, G., S. A. Lewis, B. Feierbach, T. Stearns, H. Rommelaere, C. Ampe & N. J. Cowan (1997) Tubulin subunits exist in an activated conformational state generated and maintained by protein cofactors. *J Cell Biol*, 138, 821-32.
- Togi, S., R. Muromoto, K. Hirashima, Y. Kitai, T. Okayama, O. Ikeda, N. Matsumoto, S. Kon, Y. Sekine, K. Oritani & T. Matsuda (2016) A New STAT3-binding Partner, ARL3, Enhances the Phosphorylation and Nuclear Accumulation of STAT3. *J Biol Chem*, 291, 11161-71.
- Tsang, S. H., I. Tsui, C. L. Chou, J. Zernant, E. Haamer, R. Iranmanesh, J. Tosi & R. Allikmets (2008) A novel mutation and phenotypes in phosphodiesterase 6 deficiency. *Am J Ophthalmol*, 146, 780-8.
- Tsujikawa, M. & J. Malicki (2004a) Genetics of photoreceptor development and function in zebrafish. *Int J Dev Biol*, 48, 925-34.
- (2004b) Intraflagellar transport genes are essential for differentiation and survival of vertebrate sensory neurons. *Neuron*, 42, 703-16.
- Tsujikawa, M., Y. Wada, M. Sukegawa, M. Sawa, F. Gomi, K. Nishida & Y. Tano (2008) Age at onset curves of retinitis pigmentosa. *Arch Ophthalmol*, 126, 337-40.
- Tu, W. Z., B. Li, B. Huang, Y. Wang, X. D. Liu, H. Guan, S. M. Zhang, Y. Tang, W. Q. Rang & P. K. Zhou (2013) gammaH2AX foci formation in the absence of DNA damage: mitotic H2AX phosphorylation is mediated by the DNA-PKcs/CHK2 pathway. *FEBS Lett*, 587, 3437-43.

- Ubersax, J. A. & J. E. Ferrell, Jr. (2007) Mechanisms of specificity in protein phosphorylation. *Nat Rev Mol Cell Biol*, 8, 530-41.
- Valdes-Sanchez, L., B. De la Cerda, F. J. Diaz-Corrales, S. Massalini, C. F. Chakarova, A. F. Wright & S. S. Bhattacharya (2013) ATR localizes to the photoreceptor connecting cilium and deficiency leads to severe photoreceptor degeneration in mice. *Hum Mol Genet*, 22, 1507-15.
- van der Burg, M., I. J. H. N. S. Verkaik, T. Turul, W. W. Wiegant, K. Morotomi-Yano, P. O. Mari, I. Tezcan, D. J. Chen, M. Z. Zdzienicka, J. J. van Dongen & D. C. van Gent. 2009. A DNA-PKcs mutation in a radiosensitive T-B- SCID patient inhibits Artemis activation and nonhomologous end-joining. In *J Clin Invest*, 91-8.
- Veleri, S., C. H. Lazar, B. Chang, P. A. Sieving, E. Banin & A. Swaroop (2015) Biology and therapy of inherited retinal degenerative disease: insights from mouse models.
- Veltel, S., R. Gasper, E. Eisenacher & A. Wittinghofer (2008) The retinitis pigmentosa 2 gene product is a GTPase-activating protein for Arf-like 3. *Nat Struct Mol Biol*, 15, 373-80.
- Vermeren, M., R. Lyraki, S. Wani, R. Airik, O. Albagha, R. Mort, F. Hildebrandt & T. Hurd (2017) Osteoclast stimulation factor 1 (Ostf1) KNOCKOUT increases trabecular bone mass in mice. *Mamm Genome*, 28, 498-514.
- Villaverde-Montero, C., M. Garcia-Hoyos, A. Gimenez-Pardo, M. J. Trujillo-Tiebas, M. Baiget & C. Ayuso (2007) Gene symbol: RP2. *Hum Genet*, 121, 289.
- Voss, M., M. Lettau & O. Janssen (2009) Identification of SH3 domain interaction partners of human FasL (CD178) by phage display screening. *BMC Immunology*, 10, 53.
- Wang, Y., F. Yang, Y. Fu, X. Huang, W. Wang, X. Jiang, M. A. Gritsenko, R. Zhao, M. E. Monore, O. C. Pertz, S. O. Purvine, D. J. Orton, J. M. Jacobs, D. G. Camp, 2nd, R. D. Smith & R. L. Klemke (2011) Spatial phosphoprotein profiling reveals a compartmentalized extracellular signal-regulated kinase switch governing neurite growth and retraction. *J Biol Chem*, 286, 18190-201.
- Webb, T. R., D. A. Parfitt, J. C. Gardner, A. Martinez, D. Bevilacqua, A. E. Davidson, I. Zito, D. L. Thiselton, J. H. Ressa, M. Aperi, N. Schwarz, N. Kanuga, M. Michaelides, M. E. Cheetham, M. B. Gorin & A. J. Hardcastle. 2012. Deep intronic mutation in OFD1, identified by targeted genomic next-generation sequencing, causes a severe form of X-linked retinitis pigmentosa (RP23). In *Hum Mol Genet*, 3647-54.
- Williams, D. S. (2002) Transport to the photoreceptor outer segment by myosin VIIa and kinesin II. *Vision Res*, 42, 455-62.
- Woodbine, L., A. R. Gennery & P. A. Jeggo (2014) The clinical impact of deficiency in DNA non-homologous end-joining. *DNA Repair (Amst)*, 16, 84-96.
- Woodbine, L., J. A. Neal, N. K. Sasi, M. Shimada, K. Deem, H. Coleman, W. B. Dobyns, T. Ogi, K. Meek, E. G. Davies & P. A. Jeggo (2013) PRKDC mutations in a SCID patient with profound neurological abnormalities. *J Clin Invest*, 123, 2969-80.

- Wright, A. F., C. F. Chakarova, M. M. Abd El-Aziz & S. S. Bhattacharya (2010) Photoreceptor degeneration: genetic and mechanistic dissection of a complex trait. *Nat Rev Genet*, 11, 273-84.
- Wright, R. N., D. H. Hong & B. Perkins (2011) Misexpression of the constitutive Rprg(ex1-19) variant leads to severe photoreceptor degeneration. *Invest Ophthalmol Vis Sci*, 52, 5189-201.
- (2012) RprgORF15 connects to the usher protein network through direct interactions with multiple whirlin isoforms. *Invest Ophthalmol Vis Sci*, 53, 1519-29.
- Wright, Z. C., R. K. Singh, R. Alpino, A. F. Goldberg, M. Sokolov & V. Ramamurthy (2016) ARL3 regulates trafficking of prenylated phototransduction proteins to the rod outer segment. *Hum Mol Genet*, 25, 2031-2044.
- Xue, Y., Z. Liu, J. Cao, Q. Ma, X. Gao, Q. Wang, C. Jin, Y. Zhou, L. Wen & J. Ren (2011) GPS 2.1: enhanced prediction of kinase-specific phosphorylation sites with an algorithm of motif length selection.
- Xue, Y., J. Ren, X. Gao, C. Jin, L. Wen & X. Yao (2008) GPS 2.0, a Tool to Predict Kinase-specific Phosphorylation Sites in Hierarchy.
- Yoon, J. H., J. Qiu, S. Cai, Y. Chen, M. E. Cheetham, B. Shen & G. P. Pfeifer (2006) The retinitis pigmentosa-mutated RP2 protein exhibits exonuclease activity and translocates to the nucleus in response to DNA damage. *Exp Cell Res*, 312, 1323-34.
- Young, R. W. & D. Bok (1969) Participation of the retinal pigment epithelium in the rod outer segment renewal process. *J Cell Biol*, 42, 392-403.
- Yu, D. Y., S. Cringle, K. Valter, N. Walsh, D. Lee & J. Stone (2004) Photoreceptor death, trophic factor expression, retinal oxygen status, and photoreceptor function in the P23H rat. *Invest Ophthalmol Vis Sci*, 45, 2013-9.
- Zarbin, M. (2016) Cell-Based Therapy for Degenerative Retinal Disease. *Trends Mol Med*, 22, 115-34.
- Zhang, H., R. Constantine, J. M. Frederick & W. Baehr (2012) The prenyl-binding protein PrBP/ $\delta$ : a chaperone participating in intracellular trafficking. *Vision Res*, 75, 19-25.
- Zhang, H., R. Constantine, S. Vorobiev, Y. Chen, J. Seetharaman, Y. J. Huang, R. Xiao, G. T. Montelione, C. D. Gerstner, M. W. Davis, G. Inana, F. G. Whitby, E. M. Jorgensen, C. P. Hill, L. Tong & W. Baehr (2011) UNC119 is required for G protein trafficking in sensory neurons. *Nat Neurosci*, 14, 874-80.
- Zhang, H., C. Hanke-Gogokhia, L. Jiang, X. Li, P. Wang, C. D. Gerstner, J. M. Frederick, Z. Yang & W. Baehr (2015) Mistrafficking of prenylated proteins causes retinitis pigmentosa 2. *Faseb j*, 29, 932-42.
- Zhao, C., Y. Omori, K. Brodowska, P. Kovach & J. Malicki (2012) Kinesin-2 family in vertebrate ciliogenesis. *Proc Natl Acad Sci U S A*, 109, 2388-93.
- Zhao, Y., H. D. Thomas, M. A. Batey, I. G. Cowell, C. J. Richardson, R. J. Griffin, A. H. Calvert, D. R. Newell, G. C. M. Smith & N. J. Curtin (2006) Preclinical Evaluation of a Potent Novel DNA-Dependent Protein Kinase Inhibitor NU7441.



- Zhou, C., L. Cunningham, A. I. Marcus, Y. Li & R. A. Kahn (2006) Arl2 and Arl3 regulate different microtubule-dependent processes. *Mol Biol Cell*, 17, 2476-87.
- Zu, Y., X. Tong, Z. Wang, D. Liu, R. Pan, Z. Li, Y. Hu, Z. Luo, P. Huang, Q. Wu, Z. Zhu, B. Zhang & S. Lin (2013) TALEN-mediated precise genome modification by homologous recombination in zebrafish. *Nat Methods*, 10, 329-31.